Dissertation submitted to the

Combined Faculty of Natural Sciences and Mathematics of the
Ruperto Carola University Heidelberg, Germany

for the degree of

Doctor of Natural Sciences

Presented by

M.Sc. Anne-Kathrin Schürholz

Born in: Leonberg

Oral examination: 19th July 2019

Spatio-temporal control of cell wall properties and signalling networks in Arabidopsis meristems

Referees: Prof. Dr. Jan Lohmann

Dr. Sebastian Wolf

I sincerely affirm to have composed this thesis work autonomously, to have indicated completely and accurately all aids and sources used and to have marked anything taken from other works, with or without changes. Furthermore, I affirm to have observed the constitution of the University of Heidelberg for the safeguarding of good scientific practice, as amended.

Heidelberg, May 6th 2019

_____

Anne-Kathrin Schürholz

Table of Contents

Abstract

Post-embryonic growth and development tailored to the environmental condition is a distinguishing characteristic of plants imposed by their sessile lifestyle. Lifelong growth from seed to plant death is enabled by pluripotent stem cells encompassed in the meristems, which continuously generate new plant material with high proliferation rates in the periphery, and slowly dividing stem cells in the centre. This gradient of varying proliferation rates is tightly controlled to balance cell proliferation and replenishment with differentiation. A plethora of signalling networks consisting of peptides, phytohormones and transcriptional regulators are crucial to control all these processes in a spatio-temporal manner. Particularly in the shoot apical meristem (SAM), these processes have to be tightly monitored, as cells in the SAM acquire cell identities along their trajectory from the centre of the meristem through the periphery irrespective of clonal lineage. In this study, we attempted to achieve three main aims using genetic characterization, live-cell imaging, and transcriptome profiling. We tried to understand how cell wall properties influence cell identity and differentiation by means of pectin modifications in the shoot apical meristem. We could reveal that imbalancing the pectin modifications in the whole SAM leads to disruption of cell size control, cell shapes, and overall meristem size. Second, we attempted to decipher the role of malectin-like containing RLP4 and its RLP4-like subgroup in cell wall signalling. We show that the evolutionarily conserved RLP4 is specifically located in cell edges. In addition, the extracellular domain of RLP4 associates with th cell wall, suggesting RLP4 could be a novel component of cell wall signalling. Last, we wanted to characterize a newly identified mutant, named *cle signalling component1* (*csc1*) and its function in maintenance of the root and shoot apical meristem. *csc1* displayed an enlarged SAM, defects in flower development and elevated xylem cells in the vasculature. We identified, that CSC1 determines meristem size, excerting negative control over both cytokinine response and the expression of the stem cell fate inducing transcription factor WUSCHEL (WUS) in the SAM. Together, our findings expand the wiring networks in maintaining stem cells by one essential player and elucidate the importance of cell wall signalling and cell wall properties in the meristems of Arabidopsis.

Kurzdarstellung

Postembryonales Wachstum und Entwicklung sind ein charakteristisches Merkmal von Pflanzen, welches ihnen durch ihre ortsgebundene Lebensweise auferlegt wurde, um auf Umwelteinflüsse reagieren zu können. Das lebenslange Wachstum, ausgehend vom Samen bis zum Absterben der Pflanze wird durch pluripotente Stammzellen ermöglicht, die in den Meristemen enthalten sind. Diese erzeugen kontinuierlich neues Pflanzenmaterial mit hohen Proliferationsraten in der Peripherie und sich langsam teilende Stammzellen im Zentrum des Meristems. Dieser Proliferationsratengradient wird durch die Pflanze streng kontrolliert, um die Zellproliferation und -erneuerung mit der notwendigen Differenzierung auszugleichen. Eine Vielzahl von Signalnetzwerken, bestehend aus Peptiden, Phytohormonen und Transkriptionsregulatoren, ist entscheidend, um alle diese Prozesse räumlich und zeitlich zu steuern. Insbesondere im Sprossapikalmeristem (SAM) müssen diese Prozesse streng überwacht werden, da Zellen im SAM ihre Zellidentität während ihres Weges vom Zentrum des Meristems zu den Außengrenzen entwicklen, unabhängig der klonalen Abstammung. In dieser Arbeit haben wir versucht drei Hauptziele unter Anwendung der genetischen Charakterisierung, der Visualisierung von lebenden Zellen und dem Transkriptom-Profiling zu erreichen. Wir haben versucht herauszufinden, wie Pektinmodifikationen im SAM die Zellwandeigenschaften die Zellidentität und –differenzierung beeinflussen. Es konnte gezeigt werden, dass ein Ungleichgewicht der Pektinmodifikationen im SAM zu einer gestörten Entwicklung der Zellgröße, Zellformen und der Gesamtgröße des Meristems führt. Desweiteren wollten wir die Funktion von malectinähnlichen Domänstrukturen in RLP4 und der RLP4-ähnlichen Untergruppe in Zellwandsignalwegen entschlüsseln. Wir identifizierten das evolutionär konservierte RLP4, das spezifisch in Zellecken der Zelle lokalisiert ist. Zusätzlich bindet die extrazelluläre Domäne von RLP4 an die Zellwand, was darauf hindeutet, dass RLP4 eine neue Komponente in Zellwandsignalwegen sein könnte. Zuletzt konnte eine neu identifizierte Mutante namens *cle signalling component1* (*csc1*) charakterist werden, sowie deren Funktion im Wurzel- und Sprossapikalmeristem. *csc1* zeigte ein vergrößertes SAM, Defekte in der Blütenentwicklung und eine erhöhte Xylemzellanzahl im Gefäßsystem der Wurzel. So konnten wir feststellen, dass CSC1 die Meristemgröße beeinflusst und sowohl die Cytokinin als auch die Expression des Transkriptionsfaktors WUSCHEL (WUS) negativ reguliert. Unsere Ergebnisse konnten daher das verflochtene Netz um einen weiteren Akteur zur Aufrechterhaltung der Stammzellen vergrößern und verdeutlichen die Bedeutung von Zellwandsignalwegen und Zellwandeigenschaften in den Meristemen von Arabidopsis.

1 General introduction

The following introduction is a general introduction leading to the three main chapters: 2. The role of pectin methyl esterases (PMEs) in the shoot apical meristem, 3. RLP4 and subfamily RLP4-like (R4L) as putative cell wall binding proteins and 4. Unravelling the function of *CSC1* – The *CLE SIGNALLING COMPONENT1.*

1.1 Plant cell wall composition and synthesis

Plant cell walls are a characteristic feature of multicellular plants and played a crucial role in the colonization of terrestrial ecosystems, enabling upright growth and the development of a vascular tissue system (Sorensen et al., 2010). Cell walls are characterized by a heterogeneous network of polysaccharides and structural proteins (Cosgrove, 2005; Somssich et al., 2016). The main load-bearing elements in the cell wall are the insoluble cellulose microfibrils which are organized in parallel and thereby contribute to mechanical properties of the cell wall (Li et al., 2014). They are embedded in a matrix of hemicellulose and pectins to which they are interconnected via various linkages (Cosgrove, 2016). Cellulose microfibrils are directly synthesized at the plasma membrane by cellulose synthase complexes (CSCs), forming β-1,4-linked glucan chains (McFarlane et al., 2014). CSCs are comprised of six subunits, whereby each subunit contains six cellulose synthase (CESA) proteins (Cosgrove, 2014). Plasma membrane underlying cortical microtubules are guiding CESAs movements and thus define the orientation of the microfibrils (Gu et al., 2010). Because microtubules are often oriented in parallel, they can influence the orientation of the microfibrils and therefore interfere with cell wall properties. (Gutierrez et al., 2009; McFarlane et al., 2014).

Hemicelluloses are classified into xylans, mannans, glucomannans and xyloglucans (Scheller and Ulvskov, 2010). Xyloglucans are the most abundant hemicelluloses in primary cell walls of Arabidopsis and have a linear β-1,4-linked glucan chain as backbone, similar to cellulose (Cosgrove, 2005). Hemicelluloses have been reported to tether cellulose microfibrils, contributing to cell wall rigidity and being involved in the response to pathogens (Cosgrove, 2005; Xiao et al., 2016).

Considered as the most complex class of polysaccharides in the plant cell wall, pectins contain the four mayor groups: rhamnogalacturonan I and II (RGI and RG II), xylogalacturonan (XGA), and homogalacturonan (HG), of which HG is the most abundant in primary cell walls (Cosgrove, 2005; Caffall et al., 2009). Most of the pectins share a α-1,4-linked galacturonic acid (GalA) backbone and different side chains classifying the pectins in the aforementioned groups.

In contrast to cellulose, hemicelluloses and pectins are synthesised in the Golgi apparatus by membrane bound glycosyltransferases (GTs) and secreted to the apoplast via small secretory vesicles (Wolf et al., 2009). Pectins are transported highly methyl esterified to the apoplast, where pectin modifying enzymes such as pectin methyl esterases (PMEs) and their inhibitors (PMEIs), pectate lyases (PLs), polygalacturonases (PGs) or pectin acetyl esterases (PAEs) can have an impact on the cell wall properties (see also 2.1.1) (Wang et al., 2013; Hocq et al., 2017).

All these polysaccharides and structural proteins are part of the primary cell wall, which is deposited between the plasma membrane and the pectin-rich middle lamella, the shared border of two neighbouring cells and important for cell adhesion (Zamil and Geitmann, 2017). Secondary cell walls can form in specific cell types and incorporate between primary cell wall and plasma membrane (Kumar et al., 2016). They are mainly composed of cellulose, hemicellulose (xylan) and hydrophobic, phenolic lignin (Caffall and Mohnen, 2009). Differentiation towards the synthesis of a secondary cell wall often initialize progressive cell death to form for instance the water conducting xylem tracheary elements (Schuetz et al., 2013).

Based on the complexity of cell wall components and their modifications, identification of genes or enzymes involved in cell wall biosynthesis or modifications and their function in cell wall properties is not straightforward. For example, the *cesa6*/*prc1-1* mutant, that depicts stunted growth, presumably due to a deficiency of cellulose. Further investigations revealed that the *theseus1* (*the1*) mutant could restore the *cesa6*/*prc1-1* mutant phenotype, but not the cellulose deficiency (Hématy et al., 2007). Thus, the stunted growth in the *cesa6*/*prc1-1* mutant was not directly caused by a reduction in cellulose content, but due to a compensatory mechanism mediated by THE1 (Hématy et al., 2007). Likewise, these compensatory effects were also observed in plants overexpressing PMEI5, which showed a severe phenotype with root-waving and convoluted stems (Wolf et al., 2012a). These compensatory mechanisms are due to cell wall signalling, which will be illustrated in the next paragraph (Figure 1).

1.2 Cell wall signalling

Plant cell walls are facing a predicament: “Too soft, or not too soft, that is the question”. On the one hand, cell walls need to be rigid to enable upright growth, counteract the turgor pressure from inside the cell, and are a barrier for extrinsic cues such as abiotic and biotic stresses. On the other hand, cell walls need to be dynamic to respond to intrinsic cues such as plant growth, development and physiological processes (Cosgrove, 2005).

To convey extrinsic signals to the cell interior and *vice versa*, signals have to pass through the plasma membrane. In recent years, many studies were focusing on these signalling pathways, termed “cell wall signalling” (CWS), in cell wall containing organisms such as yeast (*Saccharomyces cerevisiae,* referred to as Saccharomyces) and plants (*Arabidopsis thaliana;* referred to as Arabidopsis) (Klis et al., 2006; Wolf et al., 2012b). In Saccharomyces, many plasma membrane receptors involved in CWS and the downstream signalling pathways could be identified (Wolf et al., 2012b). Recently various kinds of new plasma membrane proteins were identified in Arabidopsis, that are conveying numerous signals from the cell wall via the plasma membrane to the cell interior and might be putative members for CWS (Figure 1). For instance, stretch-activated channels, Integrin/Formin-like proteins, LRR-RLKs/RLPs, WAK1 and CrRLK1L (Wolf, 2017) (Figure 1). Here, we want to focus mainly on the last three classes of plasma membrane proteins in Arabidopsis, that are members of the receptor-like kinase (RLK) protein family.

Many different signals are assumed to activate CWS via binding to their receptors in the plasma membrane, that convey them. Plasma membrane proteins can either directly bind to cell wall components such as the LRR-RLP44 to pectate (Holzwart, 2018) or the WALL-ASSOCIATED KINASE1 (WAK1), that binds directly to pectin or pectin break down products, the oligogalacturonic acids (OGs) (Kohorn and Kohorn, 2012). Cell wall break down products can be “plant derived” due to the activity of cell wall degrading enzymes or “pathogen-derived”. Pathogens as bacteria or fungi often contain their own cocktail of cell wall degrading enzymes to facilitate the entry to the cell interior (Kubicek et al., 2014). These derived cell wall products (DAMPs) can activate the plant immunity system (Savatin et al., 2014). In addition, mechanical stresses or tension can be sensed and conveyed by members of the CrRLK1L family, stretch-activated ion channels or Integrin/Formin-like proteins. For instance, Formin1 (AtFH1) spans the plasma membrane and binds intracellularly to the actin cytoskeleton and extracellularly it anchors to cell wall components (Martinière et al., 2011; Feng et al., 2018) (Figure 1). Downstream of the receptors, signalling cascades are activated upon the ligand-receptor binding and lead to changes in transcription or post-translational modifications. The transcriptional machineries that are activated upon cell wall signalling are more or less well studied, albeit the different signalling components from the plasma membrane to transcription factors are often elusive. Signalling cascades that could be unravelled are for instance members of the receptor-like cytoplasmic kinases (RLCKs), Ca^{2+}-dependent kinases (CPKs), mitogen-activated kinases (MAPKs) and small GTPase protein families (Vernoud et al., 2003; Hamel et al., 2012; Schulz et al., 2013; Bi et al., 2018) (Figure 1).

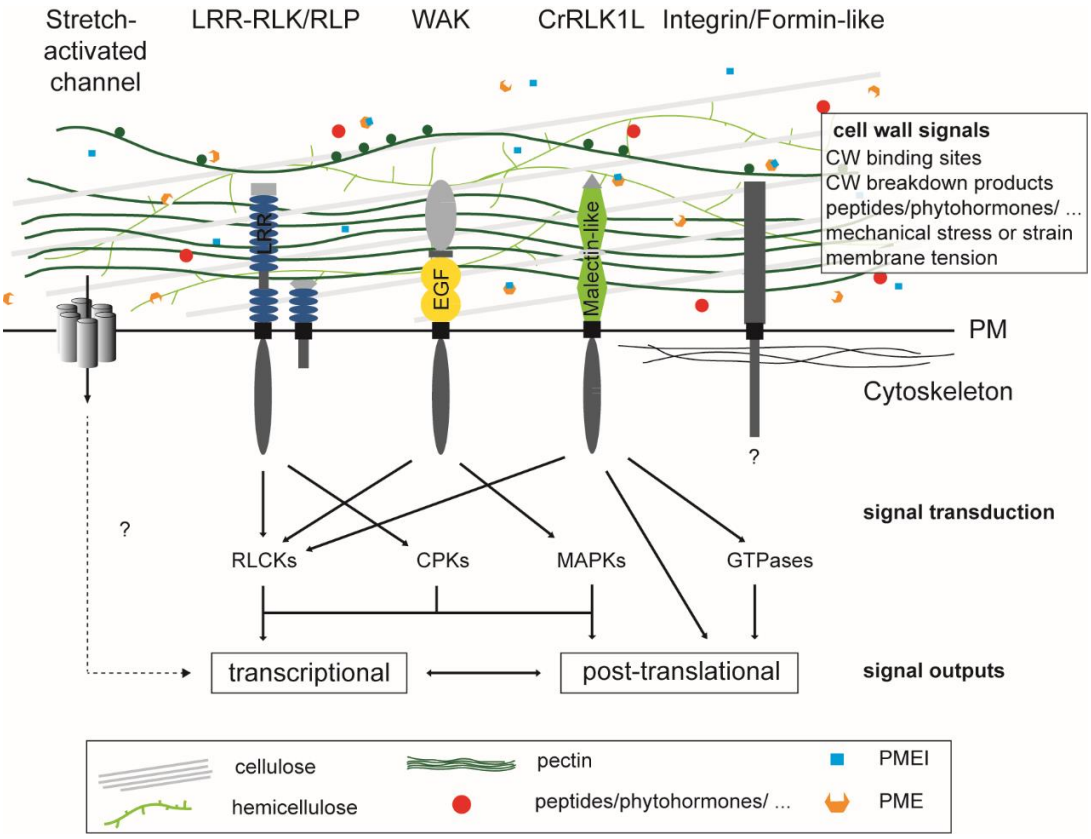

Figure 1. Overview of putative cell wall signalling receptors, cell wall-derived signals and downstream signalling pathways. Five classes of plasma membrane proteins that are involved in conveying cell wall signals to the cell interior: Stretch-activated ion channels, Integrin/Formin-like, and the main group of Receptor-like kinases (RLKs) containing of LRR-RLKs, WAKs and CrRLK1L. Putative cell wall signals that are recognized by these proteins are: Cell wall binding sites or break down products, peptides and phytohormones, mechanical stresses and membrane tension. Activated receptors convey the signal downstream via intracellular receptor-like cytoplasmic kinases (RLCKs), calcium-dependent protein kinases (CPKs), mitogen-activated protein kinases (MAPKs) or small GTPase protein families (GTPases) and alter gene transcription or post-translational modifications. Modified after (Wolf, 2017).

1.3 Receptor-like kinases

The class of receptor-like kinases (RLKs) contains more than 600 proteins in Arabidopsis (Shiu et al., 2002; Tör et al., 2009), of these the group of leucine-rich repeat (LRR) RLKs are the most abundant ones (Li et al., 1997; Clark et al., 1997; Gómez-Gómez et al., 2000; Li et al., 2002; Zipfel et al., 2006). They exhibit LRRs in their extracellular domain (ECD) which are often involved in protein-protein interactions and serve as ligand binding domains (Smakowska-Luzan et al., 2018). Protein-protein interactions were for example identified with the SOMATIC EMBRYOGENESIS RECEPTOR KINASEs (SERKs) that form heteromeric complexes with other LRR-RLKs and often function as co-receptors in the presence of a bound ligand. Upon ligand binding, auto- and trans-phosphorylation of the intracellular protein kinases activates the downstream signalling cascades, altering transcription or post-translational modifications (Figure 1). One well studied LRR-RLK is BRASSINOSTEROID INSENSITIVE1 (BRI1), the BRASSINOSTEROID (BR) receptor, that interacts with SERK3, better known as BRASSINOSTEROID ASSOCIATED KINASE1 (BAK1), in the presence of the BR phytohormone, leading to the activation of the BR signalling pathway (Nam and Li, 2002). PHYTOSULFOKINE RECEPTOR1 and 2 (PSKR1/PSKR2) are two LRR-RLKs, that also interact with BAK1 after perception of the ligand, PHYTOSULFOKINE (PSK). Downstream PSK signalling is involved in cell elongation, QC divisions, procambial identity and defence (Igarashi et al., 2012; Sauter, 2015; Holzwart et al., 2018). Two other well-studied LRR-RLKs are involved in plant defence, ELONGATING FACTOR-TU RECEPTOR (EFR) and FLAGELLIN-SENSING 2 (FLS2), which are activated upon the binding of their ligands, the bacterial EF-TU and flagellin, respectively (Gómez-Gómez et al., 2000; Zipfel et al., 2006). In the shoot apical meristem (SAM), the LRR-RLK CLAVATA1 (CLV1) is involved in stem cell maintenance. The transcription factor *WUSCHEL* (*WUS*) is expressed in the underlying tissues of the stem cells in the centre of the meristem. WUS migrates into the stem cell region and activates the expression of the small secreted peptide CLV3, which in turn diffuses into the WUS domain, where it represses the expression of WUS. By this negative feedback loop, stem cells are maintained in the SAM (Brand et al., 2000; Schoof et al., 2000).

A second subgroup of RLKs are the WALL ASSOCIATED KINASEs (WAKs), which contain characteristic epidermal growth factor (EGF) like repeats in their ECD. WAK1 was identified as a receptor for OGs and can also bind to pectin in the cell wall (Decreux and Messiaen, 2005; Brutus et al., 2010; Kohorn and Kohorn, 2012). The group of *Catharanthus roseus* receptor-like kinase1-like (CrRLK1L) proteins contains 17 members in Arabidopsis, that are characterized by an extracellular malectin-like domain (Boisson-Dernier et al., 2011). This malectin-like domain is similar to the malectin protein, which was identified as a carbohydrate binding site in Xenopus (Schallus et al., 2008). Thus, the malectin-like domain might be a binding site for carbohydrates

in plants. A well-studied CrRLK1L in Arabidopsis is FERONIA (FER). FER is involved in numerous developmental processes such as female fertility, cell wall composition and hormone- and pathogen-induced responses (Li et al., 2016a). Recent studies identified, that RAPID ALKALIZATION FACTOR1 (RALF1) is a ligand of FER and the loss of FER in *fer* mutants alters the cell wall and cell wall perturbations induced by salt stress, lead to cell swelling and bursting in *fer* mutants (Feng et al., 2018). Recently, it was shown, that FER can bind to pectin in cell walls (Feng et al., 2018; Lin et al., 2018), and THE1 is also presumably associating with pectin (Hermann Höfte, personal communication). THE1 is a CrRLK1L member and was, as aforementioned, identified as the causative protein, for the stunted growth of the *cesa6*/*pcr1-1* mutant (Hématy et al., 2007). Recently, RALF34 was identified as THE1 ligand (Gonneau et al., 2018), see also chapter 3.1.1.

1.4 Receptor-like proteins

The characteristic of the plasma membrane receptor-like proteins (RLPs) is the missing intracellular protein kinase domain. Therefore, many RLPs are interacting with RLKs, as phosphorylation is an important post-translational modification (Gust and Felix, 2014). The Arabidopsis RLP family includes 57 members, that are plasma membrane proteins and characterized by LRRs in their extracellular domain, a transmembrane domain and a short cytosolic domain, which lacks a protein kinase domain (Wang et al., 2008). Several RLPs are involved in plant pathogen recognition. For instance, RLP18 and RLP30 are involved in plant resistance against *Pseudomonas syringae* pv *phaseolicola* (*Psp*), because *rlp18* and *rlp30* mutants were more susceptible to the pathogen-associated molecular pattern (PAMP) flg22, the flagellin peptide from *Psp* (Wang et al., 2008). RLP23 was also recently identified being involved in plant immunity. A recently identified RLK, SUPPRESOR OF BIR1-1 (SOBIR1) is interacting with various RLPs, among them RLP23 and RLP30, and positively regulates defence signalling in Arabidopdis (Bi et al., 2014). In addition, several RLPs were described to be involved in plant development, for example RLP17/TMM, RLP10/CLV2, RLP4 and RLP44. The first three RLPs will be described in more detail in the chapter 3.1.2. Recently, RLP44 was identified as a member of CWS in a suppressor screen of the *PECTIN METHYLESTERASE INHIBITOR5* over-expressor (referred to as PMEIox) (Wolf et al., 2014). PMEIox plants showed a characteristic root-waving and convoluted stems as a response to interference with pectin modifications. These phenotypes were suppressed by mutations in RLP44 or in BRI1 (Wolf et al., 2012a; Wolf et al., 2014b). PMEI5 over-expression modifies pectin strands and thereby alters cell wall properties, which is sensed by RLP44. Association of the RLP44-ECD to the cell wall was observed *in vivo* and association

of RLP44 to pectate was shown *in vitro* (Holzwart, 2018). It is assumed that upon RLP44 activation by cell wall signals or its over-expression, RLP44 interacts with BAK1 and BRI1, to activate BR signalling. This restores structural integrity of the cell wall, but leads to the severe PMEIox phenotype as an indirect consequence (Wolf et al., 2012c; Wolf et al., 2014; Holzwart et al., 2018). Furthermore, RLP44 can also interact with PSKR1, activating the PSK signalling pathway, which is important for procambial identity (Holzwart et al., 2018).

1.5 Meristems in Arabidopsis

Root apical meristem (RAM) and shoot apical meristem (SAM) are primary meristems, located at the apices of root and shoot, respectively. They harbour stem cells, which give rise to on the one hand all below ground tissues and on the other hand, to all above ground tissues, driving longitudinal growth in plants (Gaillochet and Lohmann, 2015). A third meristem, the cambium is a secondary meristem, situated inside stems and roots and harbours stem cells for the vascular tissues, xylem and phloem, driving the radial growth of plants (Tonn and Greb, 2017).

Although the three meristems are differently arranged in their shape and how cells acquire cell identities, they have in common that the stem cell pool is maintained by a negative feedback loop of one member of the WUSCHEL RELATED HOMEOBOX (WOX) proteins (Dolzblasz et al., 2016). The transcription factor family comprises 15 members, with WUSCHEL (WUS) as founding member (Lian et al., 2014). In the SAM, WUS and CLV3 form a negative feedback loop to maintain stem cells (Schoof et al., 2000; Brand et al., 2000). Likewise, a negative feedback loop also maintains the stem cells in the RAM, here the players are CLE40-ARABIDOPSIS CRINKLY4 (ACR4)-WOX5 and CLE41/44-PHLOEM INTERCALATED WITH XYLEM (PXY)-WOX4 in the cambium (Stahl et al., 2009; Etchells et al., 2010; Dolzblasz et al., 2012). Furthermore, phytohormones such as auxin and cytokinin (CK) are involved in stem cell maintenance and cell differentiation in the meristems. In the SAM, CK signalling activates WUS expression and supports stem cell maintenance, whereas auxin signalling promotes differentiation and initiating of leave or flower primordia (Gordon et al., 2009; Vernoux et al., 2010). In the RAM, the two phytohormones acquire opposing functions (Liu et al., 2017). In the cambium, cytokinin is crucial for stem cell maintenance and auxin drives xylem and phloem differentiation (De Rybel et al., 2016), see also chapter 4.1.8.

1.6 Cell division, growth, and identities

Morphogenesis defines the biological processes, that are involved in shaping organisms, for example cell division, elongation, differentiation, migration and apoptosis. Since plant cells are encompassed by a cell wall and are glued together, migration as in animal cells can be excluded. Apoptosis, the programmed cell death, is taken place only in specific plant cells for example as a consequence of differentiation in xylem cells, that incorporate a secondary cell wall which leads to the formation of tracheary elements to form water-conducting tubes (Schuetz et al., 2013). In plants, morphogenesis is therefore largely driven by cell division, elongation and differentiation, to all of which the cell wall contributes in important ways (Cosgrove, 2005; Wolf and Höfte, 2014a; Wolf, 2017). Here, we will focus on cell division and the specification of cell identity.

Cell division mainly takes place in the three meristems, SAM, RAM and cambium, which harbour the stem cells that give rise to the post-embryonically derived plant tissues. Since all cells are interconnected via their cell walls and cells undergo elongation, cell division has to be coordinated. Cell division is spatio-temporally controlled by the position of the cell plate which marks the plane of division (Gutierrez, 2009; Rasmussen et al., 2013; Louveaux et al., 2016). During the cell cycle, mainly in G_1 and G_2 phases, cells grow and expand their volume which leads to mechanical stress in the surrounding cells and altered cell wall properties and enhanced cell wall biosynthesis in the growing cell (Cosgrove, 2005; Mirabet et al., 2011; Braidwood et al., 2014; Lipka et al., 2015; Cosgrove, 2016). In meristematic cells, which display an isotropic cell growth, Errera's rule can be applied (Errera, 1888), stating that cells divide along the shortest paths. Recently, the contribution of molecular players, such as microtubules (MTs), have been addressed to the implementation of Errera's rule (Besson and Dumais, 2011; Lipka et al., 2015). Position and orientation of the site, where the cell plate fuses with the parental walls, is marked by the preprophase band (PPB), formed in the preprophase of early mitosis (Rasmussen et al., 2013). It is established by cortical MT strands, that condense in the cell periphery close to the cell wall and form a ring-like structure (Smith, 2001; Rasmussen et al., 2013).

The RAM is a rewarding meristematic organ to study cell division, elongation and differentiation at once. Because of the concentric design of cell tissues surrounding the stem cell niche in the root tip, the early identification of cell identities for almost all early root tissues is possible by genetically encoded reporters. Cells in different cell tissues can be visualized and traced through the high proliferation rate in the meristematic zone, the elongation zone and finally the differentiation zone. For instance, cells can differentiate and form root hairs in the epidermis, embed suberin in their cell walls in the endodermis and lignin in the casparian strip, or lignin in

xylem cells to differentiate into xylem tracheary elements (Singh et al., 2008; Grebe, 2011; Schuetz et al., 2013).

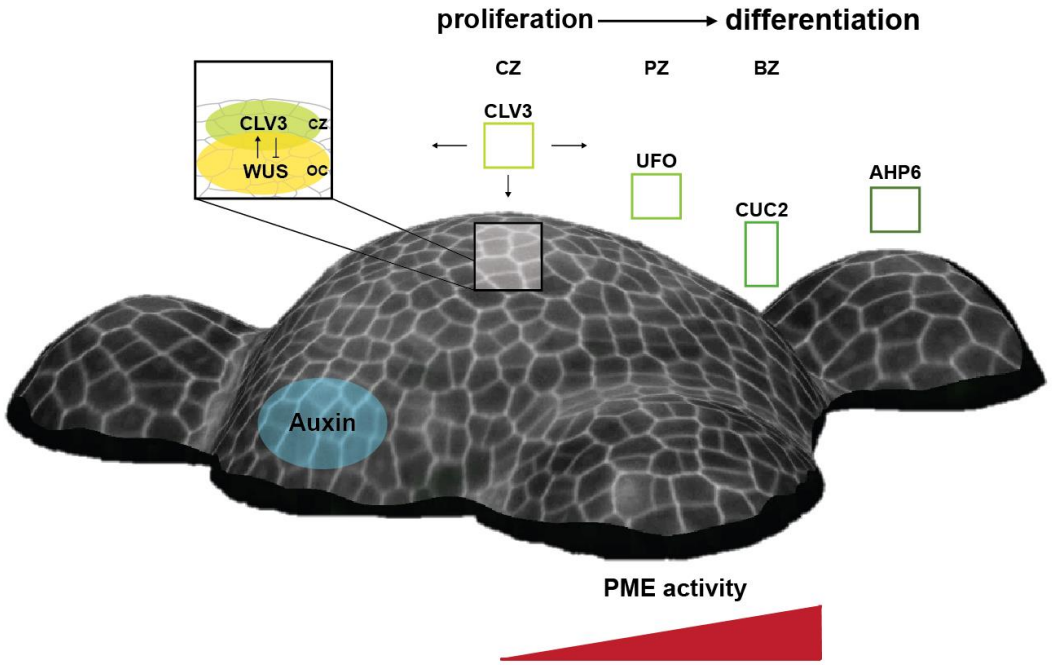

Figure 2. Overview of factors determining cell identities in the SAM. Stem cells are located in the central zone (CZ) and are maintained by the negative feedback loop between CLAVATA3 (CLV3) and WUSCHEL (WUS) in the organizing centre (OC). Cell growth and divisions push the cells located in the epidermis and the underlying cell layer (L2) through the peripheral zone (PZ) to the boundary zone (BZ), accompanied by alterations in gene transcription. During this trajectory, they acquire cell identities by altered cell wall properties, for instance increased PME activity in the boundaries or phytohormone signals. Elevated auxin levels in the PZ prime cells for primordia initiation.

In contrast to the RAM, cell identities in the SAM are not defined from early stages on, they are acquired during their trajectory from the meristematic centre, the central zone (CZ), through the peripheral zone (PZ) to the boundary zone (BZ) (Figure 2). Cell differentiation is rather dependent on the spatio-temporal position and positional information of the cell in the meristem than being primed for a cell fate/identity by its lineage (van den Berg et al., 1995; Reinhardt et al., 2003a; Reinhardt et al., 2003b; Gaillochet and Lohmann, 2015). During their journey from the centre to boundary, cells undergo molecular transitions. Some of the cells could be identified and utilized for cell identity reporters in the shoot apical meristem, such as *CLV3* for stem cells, *WUS* for the stem cell underlying organizing centre (OC), *UNUSUAL FLORAL ORGANS* (*UFO*) expressed in the PZ or *CUP SHAPED COTELYDONS2* (*CUC2*) for the BZ (Schürholz et al., 2018; see chapter

2.2.3). However, these domains are coarse in contrast to tissue specific markers that exist for the RAM. Furthermore, these markers are based on gene expression profiles, whereas changes in cell wall composition of modifications are neglected. As aforementioned, especially in the active proliferating meristems, it is assumed that cell wall biosynthesis rates are high and cell wall properties are challenged by cell growth and expansion and have to adopt to mechanical stresses due to cell divisions and cell expansions (Cosgrove, 2005 and 2015;(Cosgrove, 2015) Louveaux et al., 2016; Kierzkowski et al., 2019). Thus, cell wall properties and cell wall signalling are likely additional factors in determining cell identities in the SAM (Fleming et al., 1997; Peaucelle et al., 2008 and 2011; Milani et al., 2011; Sassi et al., 2014; Landrein et al., 2015a; Yang et al., 2016). In addition, the two cross-talking phytohormone signalling pathways auxin and CK are involved in cell proliferation and differentiation in the SAM. Here, cytokinin is essential for WUS expression and maintaining stem cell activity (Leibfried et al., 2005; Gordon et al., 2009; Xie et al., 2018), whereas auxin triggers cells to differentiate into leaf or flower primordia (Vernoux et al., 2010; Besnard et al., 2014a; Schaller et al., 2015; Qi et al., 2017). Thus, cells in the SAM are facing many factors, that are spatio-temporally determining their cell identities.

2 The role of pectin methyl esterases (PMEs) in the SAM

2.1 Introduction

The plant cell wall is a complex structure, mainly composed of cellulose, hemicelluloses, pectins and structural proteins. Depending on the developmental demands of the plant, the cell wall has to adopt its mechanical properties to enable cell proliferation and differentiation, while at the same time serving as an exoskeleton necessary for upright growth and additionally, as a barrier against abiotic and biotic stresses (Cosgrove, 2005). In the introduction, we will focus on the function of pectin modifying enzymes, the pectin methyl esterases (PMEs), in the shoot apical meristem (SAM) of Arabidopsis.

2.1.1 PMEs and pectin-modifying enzymes in the cell wall

The heteropolysaccharide pectin is a major component of primary cell walls in plants (Caffall and Mohnen, 2009). It includes four classes of different pectins: rhamnogalacturonan I and II (RGI and RGII), xylogalacturonan (XG) and homogalacturonan (HG), of which HG comprises the major component of plant cell walls (Caffall and Mohnen, 2009). Pectins are synthesized in the Golgi apparatus and linear HG can be acetylated (5-10 %) or methyl esterified (up to 80 %) (Wolf et al., 2014a; Gou et al., 2012). Once methyl esterified, pectins are transported to the apoplast, where they can be further modified by a variety of pectin modifying enzymes like pectin methyl esterases (PMEs), pectate lyases (PL), polygalacturonases (PG) and pectin acetyl esterases (PAEs) (Cosgrove, 2016; Hocq et al., 2017). PAEs remove acetyl groups of pectins in the cell wall (Gou et al., 2012), while PLs are considered responsible for the degradation of methyl esterified pectins (Yadav et al., 2009b). Furthermore, PGs have been describe as the enzymes involved in the degradation of pectins with low degrees of methyl groups, implying prior activity of pectin methyl esterases (PMEs) (Daher and Braybrook, 2015). PMEs catalyze the hydrolysis of methyl groups from pectin producing de-methyl esterified pectin, methanol and protons (Sénéchal et al., 2014a) and are regulated by pectin methyl esterase inhibitors (PMEIs). The gene family of PMEs in Arabidopsis is comprised of 66 members and can be divided into two types. Type I PMEs include 43 members, and proteins contain a pro-region at their N-terminus, which is similar to PMEIs and is assumed to have an inhibitory function (Bosch et al., 2005; Wolf et al., 2009b). For a functional PME, this pro-region has to be processed, which presumably happens in the Golgi apparatus, for example through subtilisin-like proteases (SBTs), which recognize the conserved amino acid region RR(K)LL (Wolf et al., 2009; Sénéchal et al., 2014b). It is assumed that the pro-region in type I PMEs enables better post-translational control, as unprocessed proPMEs are retained in the Golgi (Wolf et al., 2009; Wang et al., 2013). In contrast, type II PMEs do not contain the

inhibitory pro-region at their N-terminus and are comprised of 23 members. Increased activity of either type of PMEs in the cell wall leads to de-methyl esterification of pectin chains, called pectate. Block-wise de-methyl esterification produces pectate chains that can form egg-box-like structures together with other pectate chains upon covalent binding to Ca^{2+} (Grant et al., 1973; Peaucelle et al., 2012). *In vitro* and in pollen tubes it has been shown, that block wise de-methyl esterification results in increased cell wall stiffening, whereas patchy de-methyl esterification softens the cell wall, but it does not hold true for multicellular plants (Willats et al., 2001; Cosgrove, 2016). Additionally, RG II can also form covalent bonds, not only with Ca^{2+}, but also with borate, and therefore strengthen pectin cross-linkage (O'Neill et al., 2004). These modifications can change the mechanical properties of the cell wall. However, reports are inconclusive whether enhanced PME activity leads to cell wall loosening or cell wall stiffening. A variety of processes such as degree of de-methyl esterified pectins, apoplastic pH, availability of divalent cations, cell type and tissue, and compensatory mechanisms seem to play a major role in determining the rigidity of plant cell walls (Pelletier et al., 2004; Peaucelle et al., 2008; Peaucelle et al., 2011; Wolf et al., 2012a; Dünser et al., 2015). In addition, the PME and PMEI gene families are comprised of numerous members and are expressed throughout the whole plant with overlapping expression patterns, therefore impeding the generation of gain- and loss-of-function mutants. Functional redundancy and compensatory mechanism further result in shading phenotypes.

In our group, we generated plants overexpressing the Arabidopsis *PMEI5* (referred to as PMEIox), which displayed a number of phenotypes including root-waving, convoluted stems and organ fusion. Previous publications have attributed, this severe phenotype was a secondary effect, due to enhanced brassinosteroid signalling triggered by signals from the cell wall (Wolf et al., 2012b; Wolf et al., 2014). The over-expression of the pollen-specific PME *VANGUARD1* (*VGD1*), exhibited stunted growth and a high extend of de-methyl esterified pectin in cell walls of the stem (Wolf et al., 2012a). Mutations of VGD1 in Arabidopsis resulted in defects in pollen tube growth and constrained fertility (Jiang et al., 2005). This suggests that VGD1 is indeed active in pectin modifications and together with PMEIox a suitable candidate to study the function of cell wall modifications.

2.1.2 PMEs and PMEIs in the shoot apical meristem

SAM, RAM and the cambium harbour stem cells which give rise to all above-ground, below-ground and vascular tissues in plants, respectively. In all three meristems these stem cells are located in stem cell niches. Via asymmetric division and subsequent cell growth, daughter cells

are pushed out of the niche, where they acquire specific cell fates dependent on their position. In the RAM, the quiescent centre (QC) is surrounded by one layer of initial cells, each containing a characteristic pattern of transcription factors dependent on their position with regards to the QC and giving rise to one distinct tissue in the root (van den Berg et al., 1995; Drisch and Stahl, 2015). Here, the cell fate is directly set with the first asymmetric stem cell division. Contrary to the RAM, stem cells in the SAM are generalists, as they do not include initial cells for different cell tissues. The resulting cells acquire their cell fates/identities dependent on their position in the meristem, which needs to be adjusted during their route from central zone (CZ) through the peripheral zone (PZ) to the boundaries. In addition, cell-to-cell signalling, organ patterning and mechanical forces drive cell fate in the meristem (Efroni, 2018). The positional information of cell types can be analysed by differential expression of transcription factors or altered cell wall composition. The latter, is assumed to play a crucial role when defining cell identities in the SAM, as high cell division rates in the proliferating surrounding of the stem cells are in contrast to differentiating cells in the periphery, which presumably have different cell wall contents and cell wall rigidities, as they are receiving various positional signals and are facing different stresses due to cell division and elongation. Due to the dome-shaped structure of the SAM, the mechanical forces increase towards the meristem boundary and cells in the meristem centre are, for instance, more rigid compared to walls in the periphery (Peaucelle et al., 2011). In the SAM, enhanced activity of PME5 results in softer cell walls and emergence of a higher number of primordia, whereas overexpression of PMEI3 increases cell wall rigidity and inhibits primordia outgrowth (Peaucelle et al., 2008 and 2011). Here, the state of the cell wall either enables or inhibits outgrowth of primordia, but it remains to be elucidated, if changes in the mechanical properties are primary or secondary effects. Combining the acid growth theory with enhanced auxin signalling might establish a potential connection between auxin-mediated alterations in the cell wall pH and its effect on PME/PMEI activity, which in turn has consequences for the cell wall state (Sassi et al., 2014; Hocq et al., 2017).

Almost 50 years ago, the acid growth theory was formulated and is based on experiments, which investigated cell elongation and growth upon acidification of the apoplast (Rayle and Cleland., 1970). Additionally, the application of auxin obtained similar results (Rayle, 1973). Recent studies can now support this theory by means of genetically encoded markers to visualize phytohormone levels or signalling such as cytokinin and auxin (Zurcher et al., 2013; Liao et al., 2015) or cell wall rigidity measurements by applying atomic force microscopy (AFM) (Peaucelle et al., 2011; Braybrook et al., 2013; Qi et al., 2014; Peaucelle et al., 2015). Research has shown, that the apoplastic pH can be decreased by the activity of H^+-ATPases, which in turn are phosphorylated through auxin signalling (Takahashi et al., 2012; Haruta et al., 2016). Auxin accumulates in distinct

domains in the periphery, which then leads to pectin de-methyl esterification, softer cells and primordia outgrowth, suggesting further a role for auxin in controlling the activity of PMEs (Braybrook et al., 2013).

In our research, attempts to express PME and PMEI-fluorophore fusions in the apoplast were unsuccessful, possibly because the proteins were not secreted to the apoplast or, similar to type I PMEs, were processed. Therefore, the generation of PME transcriptional reporters presented itself as essential and, we generated a unique inducible cell type-specific two component tool, which enables the expression of *PME* or *PMEI* genes in defined tissues.

2.1.3 Aims

Cell wall properties are determined on the cellular level and have to be tightly coordinated between neighbouring cells, thereby affecting cell types, tissues and the whole organism. As an abundant polysaccharide in primary cell walls, pectins and pectin modifications are mainly influencing cell wall properties and might mediate cell identities in the meristems. As cells in the shoot apical meristem are generalists, meaning they are missing initial cells for specific cell types, it is assumed that cell identities are accomplished through a network of distinct signals, one might be the state of pectin in the cell walls. Hence, we aimed to achieve the following goals:

A) Elucidate the role of pectin modification in the shoot apical meristem

B) Reveal the function of PMEs in differentiation in the shoot apical meristem

C) Generate inducible, cell type-specific trans-activation/reporter lines in Arabidopsis to study pectin modifying genes in specific cell types in the shoot apical meristem

2.2 Results

Postembryonic plant growth is driven predominantly by high proliferation rates in stem cell-harbouring meristems. Cell proliferation is accompanied by cell expansion mainly driven by turgor pressure from the cell interior (Cosgrove, 2005; Braidwood et al., 2014). For cell expansion, cell wall properties are rearranged, leading to softer cell walls and induces stress relaxation, which facilitates water uptake and enables plant growth (Cosgrove, 2016). Cell wall rearrangements are either achieved by cell wall biosynthesis or modifications of the cell wall components by structural proteins. Through cell wall signalling, signals from the cell wall are conveyed over the plasma membrane and activate downstream signalling cascade, leading to transcriptional changes, which can trigger synthesis of cell wall components or structural proteins. For instance, the severe phenotypes in the PMEIox plants were identified as secondary and compensatory effects due to enhanced cell wall signalling through the activation of the BR signalling pathway (Wolf et al., 2012b). Here, we want to study how the activity of PMEs and PMEIs in the SAM, and thereby the modification of pectins, might influence cell wall properties, up- and down-stream associated signalling processes and potentially cell fate.

2.2.1 Overexpression of VGD1 and PMEI5 leads to a severe decrease in the size of the SAM

In this study, we focused on the above-ground phenotypes in Arabidopsis plants over-expressing PMEs and PMEIs, represented by the VGD1ox (AT2G47040) and PMEIox (PMEI5; AT2G31430) plants. All above-ground tissues derivefrom stem cells embedded in the SAM. Thus, alterations in the size of the SAM or its cells, or different mechanics in the SAM, maybe due to changes in the cell wall state, often have significant consequences for plant phyllotaxis and normal growth and development (Peaucelle et al., 2008 and 2011; Wolf et al., 2012a, c; Landrein et al., 2015 b; Jones et al., 2017).

Phenotypic characterization of PMEIox and VGD1ox seedlings showed a strong root-waving phenotype in PMEIox, whereas VGD1ox did not feature an obvious phenotype when compared to Col-0 wild type (Figure 3A). VGD1ox had a dwarfed phenotype in the vegetative stage in 28-day-old plants compared to Col-0 (Figure 3B). PMEIox exhibited curled rosette leaves in 28-day-old plants compared to Col-0 (Figure 3B). Phenotypes of VGD1ox and PMEIox were even more prominent in the reproductive stage of 48-day-old plants, depicting stunted growth, an altered shoot development and impaired silique development compared to Col-0 (Figure 3C). In detail,

SAM inflorescences of VGD1ox plants were bigger, exhibiting pre-opened flower buds and enhanced elongated gynoecia, which could attenuate self-fertilization and could explain the many observed seedless siliques (Figure 3D). Furthermore, VGD1ox shoots were more brittle compared to Col-0 which might be a result of altered cell wall composition and modifications caused by a reduction of pectin methyl esterification due to VGD1 overexpression (Wolf et al., 2012a). PMEIox plants exhibited curled and fused cauline leaves and stems, as well as small misshapen siliques (Figure 3E). Previous studies have shown that alterations in pectin methyl esterifications can be sensed by RLP44 which in turn activates the BR signalling pathway (Wolf et al., 2012b; Wolf et al., 2014). Enhanced BR signalling leads to up-regulation of cell wall modifying genes, which antagonize the alteration of the cell wall composition, but are inducing in a compensatory effect depicted by PMEIox phenotypes (Wolf et al., 2012b; Wolf et al., 2014). Therefore, the phenotypes in PMEIox plants are most likely the result of secondary effects, initiated by enhanced BR signalling due to loss of cell wall integrity (CWI), and not direct effects of overexpression of this particular PMEI (Wolf et al., 2012b; Wolf et al., 2014).

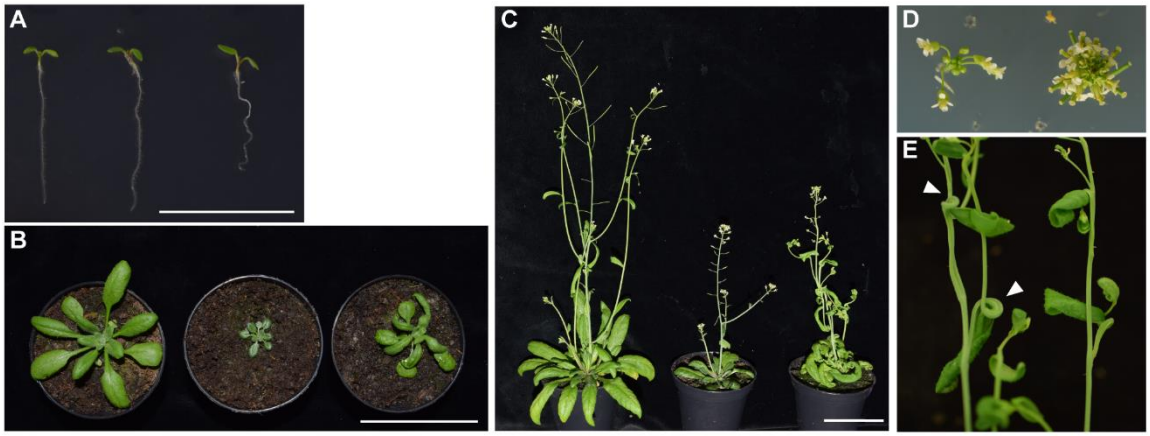

Figure 3. Over-expression of *VGD1* and *PMEI5* leads to severe developmental phenotypes. Phenotypic characterization of *p35S:VGD1* and *p35S:PMEI5* expressed in Col-0 backgrounds compared to Col-0. (A) Col-0, VGD1ox and PMEIox six-day-old seedlings (left to right). Note the root-waving phenotype in PMEIox. Scale bar: 10 mm. (B) Above-ground phenotypes of 28-day-old Col-0, VGD1ox and PMEIox plants (left to right). Scale bar: 50 mm. (C) Above ground phenotypes of 48-day-old Col-0, VGD1ox and PMEIox plants (left to right) with inflorescences. Note the stunted growth of VGD1ox and PMEIox. Scale bar: 50 mm. (D) Inflorescences of Col-0 and VGD1ox (left to right). Note the pre-opened buds and elongated gynoecia. (E) PMEIox inflorescences with typical curled stems and organ fusion of cauline leaves (white arrow heads).

For quantification of epidermal cell numbers and meristem size, shoot apices of Col-0, VGD1ox and PMEIox plants were dissected and cell walls were counterstained with propidium iodide (PI) for subsequent imaging using CLSM. Analysis of VGD1ox and PMEI5ox inflorescence shoot apical meristems revealed a decrease in meristem size compared to Col-0 (Figure 4A).

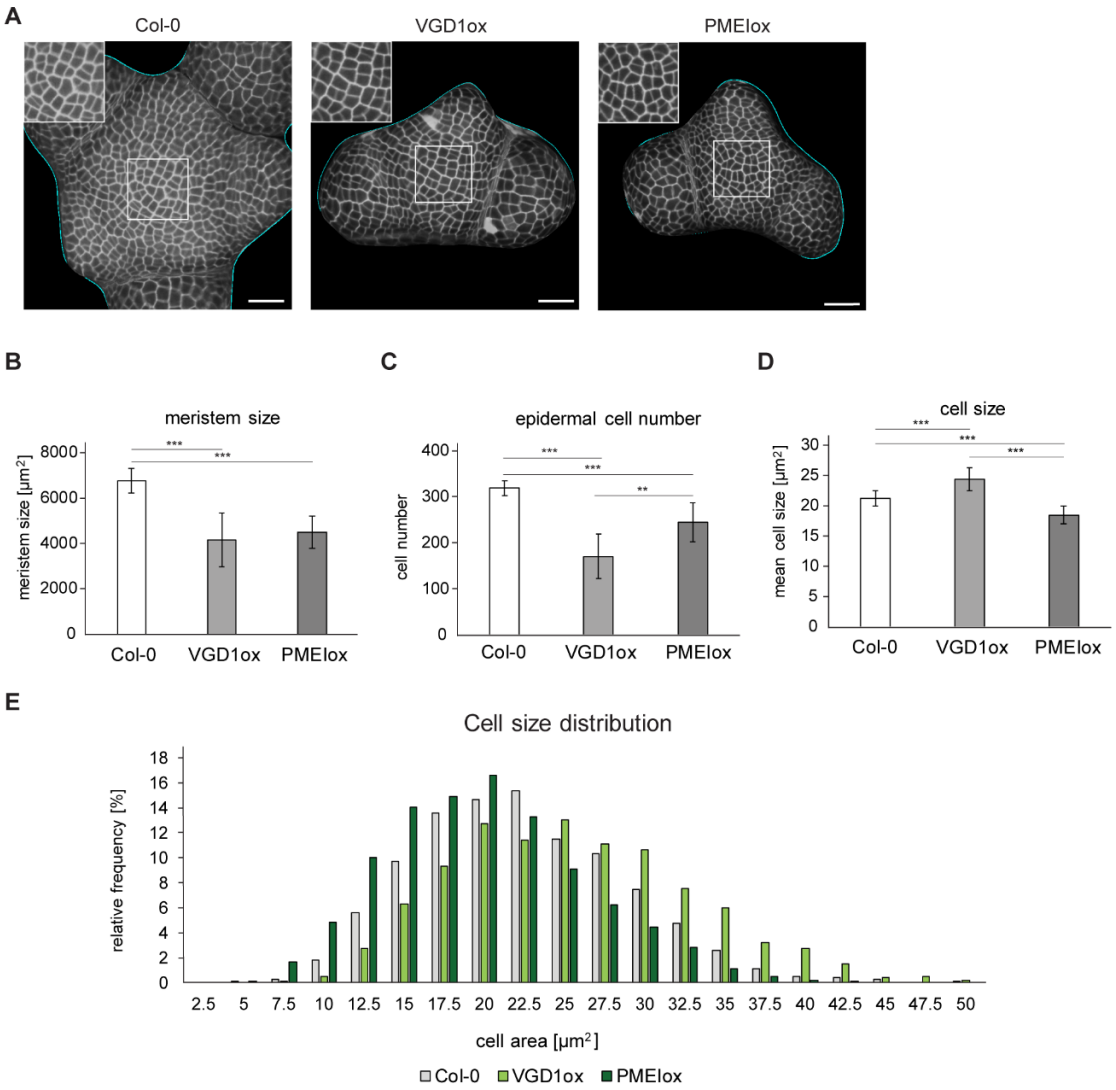

Figure 4. Overexpression of *VGD1* and *PMEI5* reduces the meristem size in the SAM. (A) Representative 3D views of inflorescence SAMs of Col-0 (38 day-old plants), VGD1ox (45 day-old plants) and PMEIox (45 day-old plants) (left to right). Note the zoom in of the central zone area and the more squared cells in VGD1ox compared to Col-0 and PMEIox. Scale bar: 20 µm. (B-E) Quantification of (B) meristem size, (C) epidermal cell number, (D) mean cell size and (E) cell size distribution in Col-0 (n=14), VGD1ox (n=10) and PMEIox (n=10) shoot apical meristems (35-45 day-old plants). Statistically significant difference from Col-0 and VGD1ox/PMEIox based on two tailed t-test (** p<0.01, *** p<0.001). (E) Cell size distribution in Col-0, VGD1ox and PMEIox.

Noticeable were the squared and symmetrical cells with four cell walls in the central zone of VGD1ox meristems, reminiscent of a chess board (Figure 4A). In contrast, Col-0 and PMEIox meristems depicted more often asymmetric cell shapes with more than four cell walls. Quantification of meristem size and epidermal cell number using the image analysis tool MorphoGraphX (Barbier de Reuille et al., 2015) exhibited a significant reduction in meristem size in VGD1ox and PMEIox compared to Col-0 (Figure 4B). Additionally, the meristems of the two over-expressing lines contained fewer cells, with VGD1ox displaying a more dramatic reduction of cells in the meristem in comparison to PMEIox (Figure 4C). The analysis of mean cell sizes revealed that VGD1ox plants have fewer epidermal cells, however increased overall cell size compensated for the number of meristematic cells, resulting in comparable meristem size to the PMEIox (Figure 4B-D). The mean cell size in PMEIox meristems was determined to be significantly decreased when compared to Col-0 (Figure 4D). In addition, the calculation of cell size distribution showed that most epidermal cells in PMEIox had a cell size of 15-20 μm^2, thereby smaller as most cells in Col-0 with 17.5 to 22.5 μm^2 (Figure 4E). In comparison, VGD1ox epidermal cells had a size of 20-25 μm^2 and more cells than in PMEIox and Col-0 exhibited larger sizes of 30 to 40 μm^2 (Figure 4E). Over-expression of PMEI5 and VGD1 resulted in either overall smaller or bigger cells compared to Col-0, so it is reasonable to argue that the activity of both proteins in the cell wall has an impact on cell division and growth.

Taken together, the over-expression of the pollen-specific *PME VGD1* and *PMEI5* resulted in severe above-ground phenotypes, presumably due to the decreased size of the SAM in both lines over-expressing VGD1 and PMEI5. Furthermore, PMEIox exhibited overall smaller and VGD1ox larger cells in comparison to Col-0, suggesting an altered cell cycle or defects in cell expansion.

2.2.2 PMEs are downregulated in the central zone of the SAM

The gene families of PMEs and PMEIs in *Arabidopsis thaliana* include 66 PMEs and 71 PMEIs, and are expressed in various tissues throughout the whole plant (Wang et al., 2013). We focused mainly on PMEs and PMEIs that were expressed in the SAM. Here, publicly available microarray data, using protoplasts (Yadav et al., 2014), was combined and analysed in combination with ChIP-Seq and RNA-Seq experiments performed by Andrej Miotk, using WUS-GR plant samples (Andrej Miotk, PhD Thesis 2015, Jan Lohmann Lab). These data showed that a number of *PME*s is differentially expressed in the SAM, whereas *PMEI*s are uniformly expressed throughout the apical meristem. Therefore, we assumed a specific role of PMEs in the SAM in development and focused on the expression and function of PMEs in the SAM.

Table 1. Differentially expressed *PME*s in the SAM. Combined ChIP-Seq, RNA-Seq and microarray data from Miotk 2015 and Yadav et al., 2014, respectively. Red bars represent high *PME* expression levels in the specific domain, relative to all values. Grey labelled boxes depict PMEs used for further analysis.

Accession number [TAIR]	name	regulated via WUS	WUS peak	WUS	CLV3	KAN1	FIL	LAS	HMG	AtML1
AT2G26440	PME12	down	1	71.0919643	15.2036692	471.457283	752.352983	105.751233	42.9448409	40.0352248
AT2G26450	pectinesterase family protein	-	0	36.1199125	64.178034	77.7947987	128.697146	69.8678297	57.9518513	85.323438
AT5G19730	pectinesterase family protein	up	1	195.099255	13.6471591	150.535783	400.556258	156.99578	13.3216645	50.3368668
AT5G20740	invertase/pectin methylesterase inhibitor family protein	up	0	261.321472	197.689857	361.275455	327.401423	174.858432	243.441806	615.907129
AT5G64640	pectinesterase family protein	-	0	451.237983	250.414051	269.187953	417.538361	340.074883	306.635645	303.92917
AT5G53370	PMEPCRF (PECTIN METHYLESTERASE PCR FRAGMENT F); pectinesterase	-	1	1105.8145	44.425237	563.047077	1315.8382	165.658428	49.7759625	57.6007088
AT5G50030	invertase/pectin methylesterase inhibitor family protein	-	0	50.3228766	107.452332	67.5796364	75.7239968	70.208998	85.0601505	73.9866921
AT5G47500	PME5	-	1	446.554295	159.953157	1821.76641	1661.52918	515.275989	197.963453	300.013251
AT5G09760	pectinesterase family protein	-	0	1615.64177	843.744776	1396.61863	1591.7148	1151.90109	935.238993	1017.65783
AT3G59010	pectinesterase family protein	-	0	34.0199493	28.1793444	33.7621886	31.2184438	42.4464836	37.8119263	60.2941947
AT3G49220	PME34	down	1	1753.3385	1203.06427	1779.96072	2043.86553	1548.71959	1525.38507	2256.71589
AT3G47670	enzyme inhibitor/ pectinesterase/ pectinesterase inhibitor	-	0	86.7464662	120.537644	111.532776	103.602841	92.0119284	107.106663	104.540204
AT3G43270	pectinesterase family protein	-	0	50.5181827	36.8125069	212.890585	75.107998	71.3190932	52.2473242	106.894038
AT4G33220	PME44	down	1	39.4476376	105.019308	1491.31894	471.560059	188.960929	709.465251	1187.4907
AT4G25260	invertase/pectin methylesterase inhibitor family protein	down	1	91.3405369	135.502261	136.716664	144.960636	115.489999	170.55362	152.645002
AT4G12390	PME1	-	0	174.246352	91.8875162	149.442926	146.529063	74.212174	60.4777122	67.709284
AT4G02330	PME41	up	0	526.300642	157.76032	2075.34612	625.229979	1226.78443	727.228342	1437.60551
AT3G29090	pectinesterase family protein	slightly up	0	1246.77239	874.894071	1139.84395	1456.7628	1280.00638	955.213036	1229.20516
AT3G14310	PME3	down	1	648.517939	496.151475	367.751803	1815.07149	350.432467	275.95341	621.242969
AT3G06830	pectinesterase family protein	-	0	29.6576589	59.8828637	53.3307373	41.9626611	55.7126739	68.1747701	77.3008873
AT3G10720	pectinesterase, putative	down	2	201.549939	67.7219766	187.16201	38.7144743	129.076135	288.207422	302.676565
AT1G11580	PMEPCRA (METHYLESTERASE PCR A); enzyme inhibitor/ pectinesterase	down	0	31.0643745	33.3307171	60.0450393	8.90371932	11.8414584	44.1321033	15.12952
AT1G02810	pectinesterase family protein	-	0	89.1697168	94.8802931	590.209781	122.293576	424.566848	323.512014	383.599145
AT1G53840	ATPME1; pectinesterase	-	1	1720.24293	1578.24429	1988.18181	1257.65561	1581.18769	3131.61851	1993.39223
AT1G14890	enzyme inhibitor/ pectinesterase/ pectinesterase inhibitor	-	1	156.558819	4.84522006	189.209206	287.93891	57.7472426	18.6992148	18.2703879
AT1G23200	pectinesterase family protein	-	0	47.3087803	64.6182867	64.4964333	61.3812963	39.9791504	41.5777819	57.2934012
AT2G01610	invertase/pectin methylesterase inhibitor family protein	-	0	36.7831186	10.5723101	60.6933589	80.7427457	57.1890103	24.5340332	66.6411133

For further analysis, we chose seven PMEs (highlighted in grey,Table 1), that were strongly expressed in specific domains of the SAM (Table 1). Distinct expression domains are represented by expression of *WUSCHEL (WUS)* in the organizing centre (OC) and *CLAVATA3* (*CLV3)* for the central zone (CZ) of the SAM. *KANADI1* (*KAN1*) and *FILAMENTOUS FLOWER* (*FIL1*) represent boundaries and abaxial domains in forming primordia, respectively. *LATERAL SUPPRESSOR* (*LAS*) defines adaxial domain in developing primordia. *HIGH MOBILITY GROUP* (HMG) marks expression in the whole meristem and *MERISTEM LAYER1* (*ML1*) in the epidermal layer (L1). Analysis of the ChIP-Seq data revealed WUS binding peaks in PME promoters expressed in the SAM (Miotk, 2015). For *AT5G53370*, *PME3*, *PME12*, *PME34* and *PME44* a WUS binding peak was identified and, except of *AT5G53370*, down-regulation of *PME*s was determined using the microarray data, suggesting a direct repression of these *PME*s through WUS (Table 1). Six of the seven *PME*s also showed weak expression in the *CLV3* domain, except *PME34* which was highly expressed throughout the whole meristem (Table 1). Based on the microarray data, *PME41* appears to be positively regulated by WUS, however, thiscould be an indirect effect, as no WUS peak was found. In addition, for *AT5G53370* no regulation via WUS could be assigned, although a WUS peak was identified (Table 1). *AT5G53370* and *PME5* showed elevated expression in the *WUS*, *KAN1* and *FIL* domains, while *PME3* was also expressed at low levels in the *WUS* domain, but only exhibited elevated expression levels in the *FIL* domain. *PME12* was higher expressed in the *KAN1* and *FIL* domains. *PME44* depicted elevated expression in the *KAN1*, *FIL* and *ML1* domains and *PME41* was similar expressed, with additional enhanced expression in the *WUS* and *LAS* domains (Table 1).

In summary, the analysis of *PME* expression in the SAM revealed that many SAM-expressed *PME*s had higher expression levels in the periphery of the meristem, where differentiation takes place, and could be repressed by WUS in the central zone.

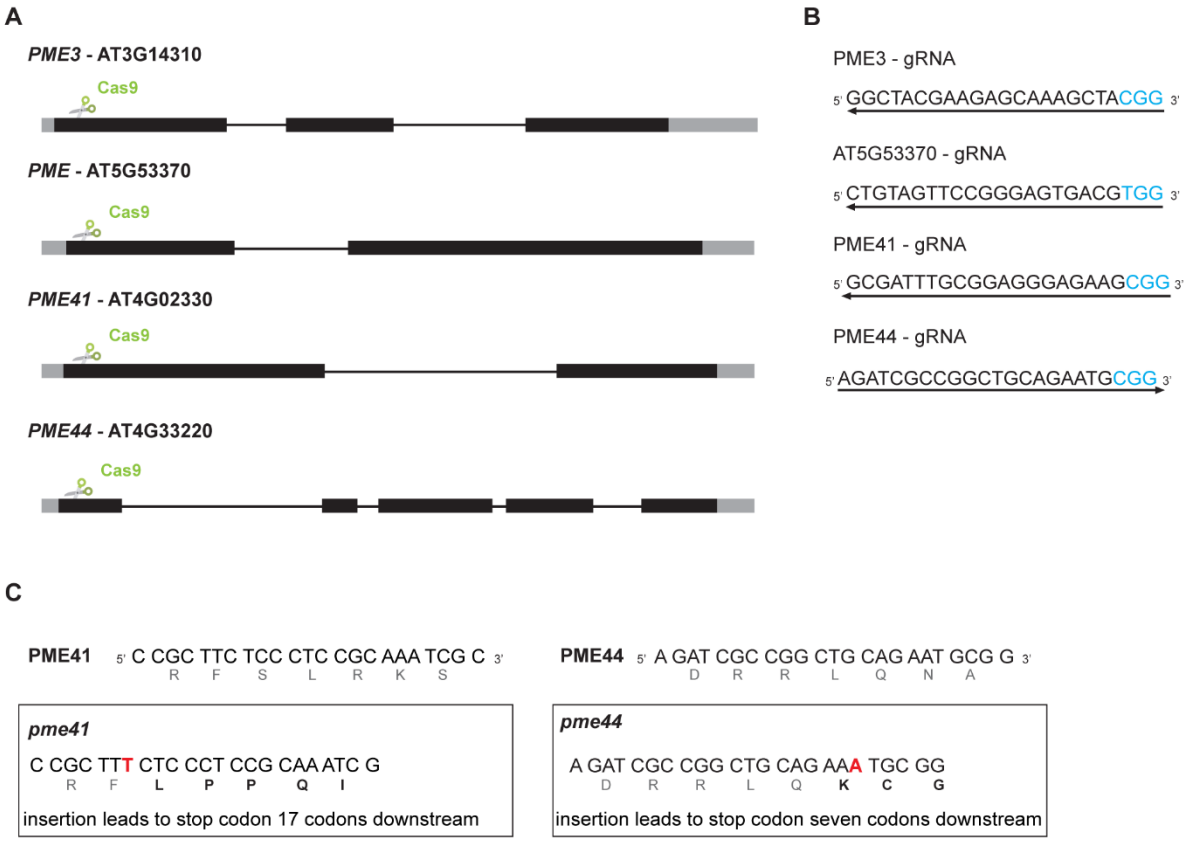

Figure 5. Design of *pme* CRISPR/Cas9 double mutants. (A) Overview of UTRs (grey boxes), exons (black boxes) and introns (black lines) in *PME3, AT5G53370, PME41 and PME44.* Cas9 recognition site is depicted in green. (B) gRNA sequences and orientation for *PME3, AT5G53370, PME41 and PME44* used in the CRISPR/Cas9 approach with PAM sequence indicated in blue. (C) *PME41 and PME44* wild type CRISPR/Cas9 target sites together with corresponding amino acids. Both gRNAs were combined in one plasmid to generate a *pme41 pme44* double mutant. Identified mutations in *PME41* and *PME44* are depicted in the boxes below, together with the nucleotide insertion (red) and changed amino acid sequences (bold and black).

To study the role of the pectin modification state in cells of the SAM in a more genetically natural condition, we next wanted to generate PME double mutants using the CRISPR/Cas9 genome-editing technique. Due to functional redundancy of many PMEs, we chose two PMEs for knock-down that had similar expression levels in the SAM. The first combination was *PME3* (AT3G14310) and *AT5G53370* which showed both elevated expression in the *FIL* domain, with

AT5G53370 also being higher expressed in the *WUS* domain. The second combination was *PME41* (AT4G02330) and *PME44* (AT4G33220), which both displaying elevated expression levels in the *KAN1* domain. Suitable gRNAs for the four target genes were designed by using the ChopChop webpage, targeting the beginning of the first exon (Figure 5A,B). Additionally, no off-targets and no self-complementation was predicted for the designed gRNAs. In the T_2 generation, only plants without the Cas9 containing T-DNA were propagated to the next generation. Unfortunately, we were not able to identify any mutations neither for *PME3*, nor for *AT5G53370*. For the second double mutant line, *pme41 pme44*, an insertion of a thymidine (t) was identified in *PME41* after position 185 downstream of the ATG in the gDNA sequence (Figure 5C).

The insertion generated an amino acid exchange from serine to leucine at position S63L, introducing a stop codon 17 codons downstream from the insertion (Figure 5C). In *PME44*, an adenosine (a) insertion after position 200 downstream of the ATG in the gDNA sequence was identified (Figure 5C). The insertion generated an amino acid exchange from asparagine to lysine at position N67K and introduced a stop codon seven codons downstream (Figure 5C). However, first phenotypic analysis in the T_2 did not result in a strong phenotype of the *pme41 pme44* double mutants compared to Col-0, presumably due to functional redundancy (data not shown).

Next, we generated PME promoter reporter lines to verify the PME expression based on the microarray data in the different domains of the SAM. Promoters of the following PMEs were generated: *PME5*, *PME12*, *AT5G53370*, *PME34* and *PME44*, which were driving the expression of a nucleus-targeted triple GFP fusion protein (*pPME:3xGFP-NLS:tUBQ10*). Inflorescence shoot apical meristems of T_2 plants were dissected and imaged using CLSM.

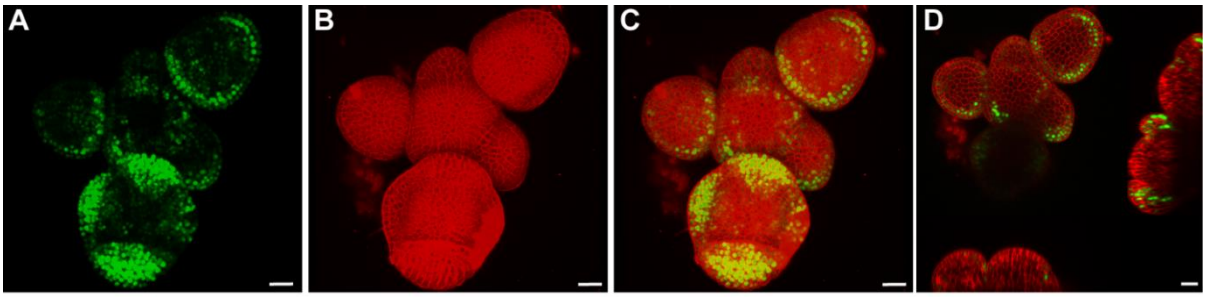

Figure 6. *PME5* expression seems to be repressed in the central zone of the SAM. (A-D) Expression of *pPME5:3xGFP-NLS* in the shoot apical meristem inflorescences of 40-day old plants. SAMs are stained with PI to label cell walls. Scale bars: 20 µm. (A) GFP signal in the nuclei, (B) PI signal of cell walls (C) merge and (D) XZ and YZ cross sections.

However, GFP fluorescence was only detected in plants expressing *pPME5:3xGFP-NLS:tUBQ10* (Figure 6). Here, *pPME5* was active in the boundaries of the SAM and young primordia. Flower primordia in stage 3 showed *pPME5* expression in sepal buds (Figure 6A, C, D). Thus, visualized *pPME5* expression in the shoot apical meristem confirmed expression in *KAN1* and *FIL* domains as suggested by microarray and RNA-Seq data (Yadav et al., 2014; Miotk, 2015).

Taken together, *pme41 pme44* double mutants did not exhibit a striking phenotype, probably due to functional redundancy, so it would be advised to generate plants with a larger number of mutant *pmes*. Furthermore, a *PME5* reporter line confirmed the observed microarray expression data, showing expression in the boundaries of the SAM with no expression in the central zone.

2.2.3 Inducible cell type-specific gene expression

As previously mentioned, PMEs are hardly expressed in the centre of the SAM. To investigate how and why they are not or only weakly expressed, we generated a tool, to induce the expression of PMEs in tissue-specific domains, for example in the SAM.

Our approach included the generate of Arabidopsis driver lines, containing a tissue specific promoter driving a fluorescent reporter, whose transcription is spatially and temporally controlled, and responder lines carrying the effector construct. By crossing these two transgenic plant lines and upon induction, the phenotypes of the effector in a specific tissue type can be studied (Figure 7) (Schürholz et al., 2018).

To generate inducible tissue-specific driver lines, we made use of the modular Golden Gate-based Green Gate cloning system. This technique enabled us to assemble different tissue specific promoters together with the Dex-inducible GR-LhG4 system and the mTurquoise2 reporter into one construct (Lampropoulos et al., 2013). The T-DNA was composed as followed: a tissue specific promoter driving the expression of the chimeric glucocorticoid/transcription factor GR-LhG4, followed by the *Rbcs* terminator, the *pOp6* promoter, the endoplasmatic reticulum (ER) signal peptide (SP), the reporter mTurquoise2 (Goedhart et al., 2012), the ER retention motif His-Asp-Glu-Leu (HDEL), the *UBQ10* terminator and a sulfadiazine resistance cassette ($Sulf^R$) (Lampropoulos et al., 2013). Upon Dex-induction, Dex binds to GR, which leads to nuclear import and binding of LhG4 to the *pOp6* element in combination with a minimal *35S* promoter. LhG4 binding to *pOp6* initiates transcription of ER(SP)-mTurquoise2-HDEL.

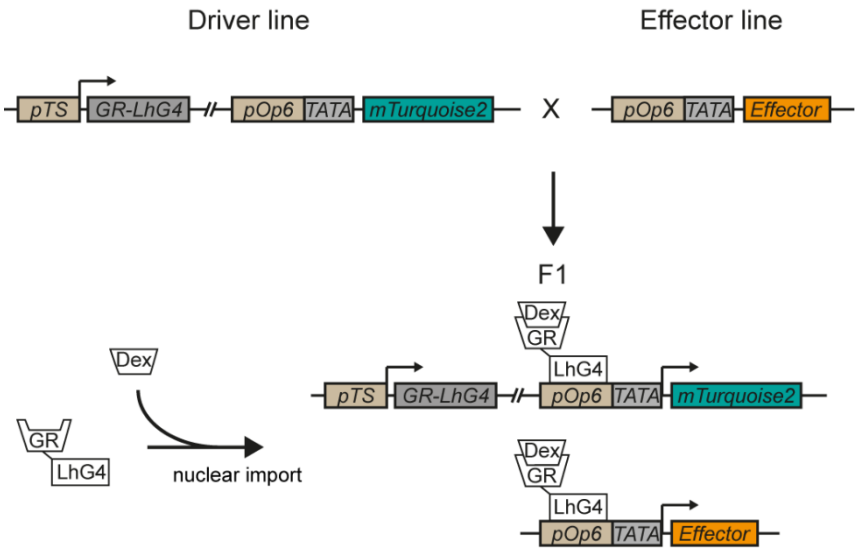

Figure 7. Overview of the Dex-inducible GR-LhG4/pOp system. Driver lines contain the synthetic transcription factor LhG4, the *Op6* promoter and the mTurquoise2 fluorophore, which is expressed upon Dex-induction in defined tissues, specified by the tissue specific promoter (*pTS*). By crossing the driver line with an effector line, containing the *Op6* promoter and the "effector", Dex-induction leads to binding of the GR-LhG4 transcription factor to the pOP6 promoter and activates simultaneously expression of the mTurquoise2 reporter and the effector, but only in certain cell types, determined by the tissue specific promoter in the driver line. (Schürholz et al., 2018).

Due to the ER signal peptide and the ER retention signal, mTurquoise2 fluorescence is only detected in the ER (*pOp6:SP-mTurquoise2-HDEL*) (Figure 7). As GR-LhG4 is expressed under the control of the tissue specific promoter (*pTS*), the expression of mTurquoise2 is also dependent on the activity of the *pTS.* In combination with an effector line, which also harbours the *pOp6* element, the driver line expresses the "effector of interest" in a specific tissue together with the mTurquoise2 reporter.

For the comprehensive tissue-specific driver lines, we chose tissue-specific promoters based on our own expression data and previously published literature (Table 2). All together, 19 promoters were selected covering most cell types in the SAM, the RAM and the cambium. The generated constructs were transformed into Arabidopsis Col-0 wild type plants and experiments were performed with stable, homozygous, single insertion T_3 plants.

Driver lines expressing root tissue specific promoters, were directly induced on plate by media containing 30 µM Dex for five days. Cell walls in seedling roots were counterstained with PI and fluorescent signals of PI and the mTurquoise2 fluorophore were imaged in five-day-old seedlings using CLSM. We detected tissue-specific expression of the mTurquoise2 reporter in the following

driver lines: *pCASP1*, *pAHP6*, *pTMO5*, *pXPP*, *pATHB-8* (Figure 8). Their expression pattern was corresponding to data from literature (Table 2). To analyse the expression in the SAM-specific driver lines, inflorescence meristems were sprayed with 10 µM Dex 48 h before imaging. The SAMs were dissected, cell walls were counter stained with PI and fluorescent signals of PI and mTurquoise2 were imaged with CLSM. The following driver lines, which showed expression in the SAM, were generated: *pML1*, *pCLV3*, *pREV*, *pUFO*, *pCUC2* and *pAHP6 (*Figure 9). Their expression pattern was corresponding to the data from literature (Table 2).

Table 2. Overview of promoters selected for driver lines.

promoter	expression
pATHB-8	procambium, xylem precursors and columella in RAM
pXPP	xylem pole pericycle
pAHP6	protoxylem precursor, pericycle, organ primordia in the SAM
pTMO5	xylem precursors
pCASP1	endodermis
pML1	L1 layer, epidermis
pCLV3	SAM stem cells
pREV	SAM rib meristem
pUFO	SAM peripheral zone
pCUC2	boundaries in SAM and leaf

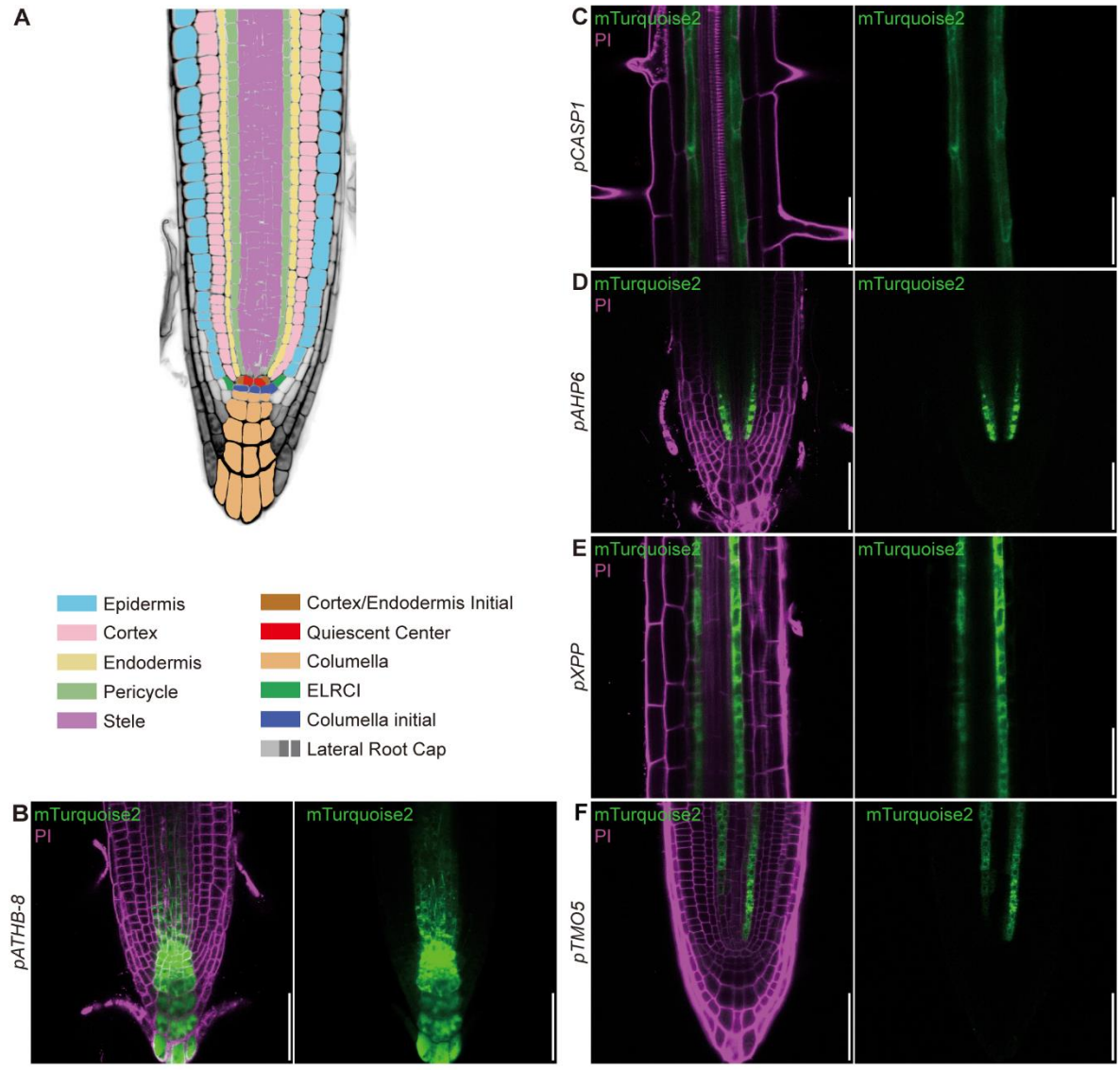

Figure 8. Dex-induced driver lines depict tissue specific expression in seedling roots. (A) Schematic overview of root tissue layers. (B-F) Induced tissue specific driver lines with PI-stained cell walls and mTurquoise2 reporter expression in the root. Scale bars: 50 µm. (B) *pHOMEOBOX GENE-8* (*pATHB-8*) expressed in stele initials, cortex/endodermis initial (CEI) and columella initials, (C) *pCASPARIAN STRIP MEMBRANE DOMAIN PROTEIN1* (*pCASP1*) expressed in the differentiating endodermis, (D) *pHISTIDINE PHOSPHOTRANSFER PROTEIN6* (*pAHP6*) expressed in phloem precursor cells and adjacent pericycle cells, (E) *pXYLEM POLE PERICYLE* (*pXPP*) expressed in xylem pole pericycle cells, (F) *pTARGET OF MONOPTEROS5* (*pTMO5*) expressed in xylem precursor cells. PI is false coloured in magenta, mTurquoise2 is false coloured in green. Figure done by Zhenni Li, modified after Schürholz et al., 2018.

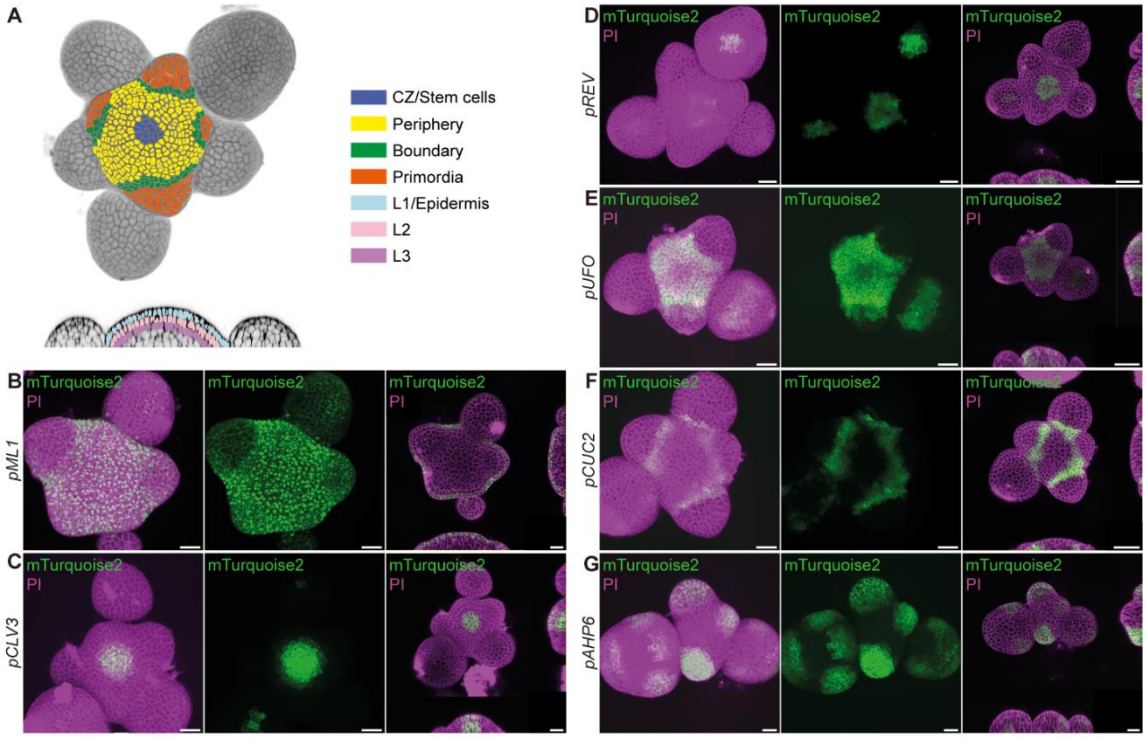

Figure 9. Dex-induced driver lines depict tissue specific expression in the inflorescence shoot apical meristem. (A) Schematic overview of tissue layers in the inflorescence stem. (B-I) Induced tissue specific driver lines with PI-stained cell walls and mTurquoise2 reporter expression in the shoot apical meristem. Scale bars: 50 µm. (B) *pMERISTEM LAYER1* (*pML1*) expressed in the L1 layer/epidermis, (C) *pCLAVATA3* (*pCLV3*) expressed in the stem cell domain, (D) *pREVOLUTA* (*pREV*) expressed in the central zone, (E) *pUNUSUAL FLOWER ORGANS* (*pUFO*) expressed in the peripheral zone, (F) *pCUP-SHAPED COTYLEDON2* (*pCUC2*) expressed in the boundary domain and (G) (*pAHP6*) expressed in organ primordia. PI is false coloured in magenta, mTurquoise2 is false coloured in green (Schürholz et al., 2018).

We generated several inducible, tissue-specific driver lines in the three main meristems in Arabidopsis and showed, that Dex-induction is functional (Schürholz et al., 2018). We could further show with Dex dose-response experiments, that fluorescent intensity seemed to be saturated at Dex concentrations from 10-100 µM (Schürholz et al., 2018). In addition, time-course analysis of Dex-induction revealed that after six hours the first mTurquoise2 fluorescence was detectable in the RAM (Schürholz et al., 2018).

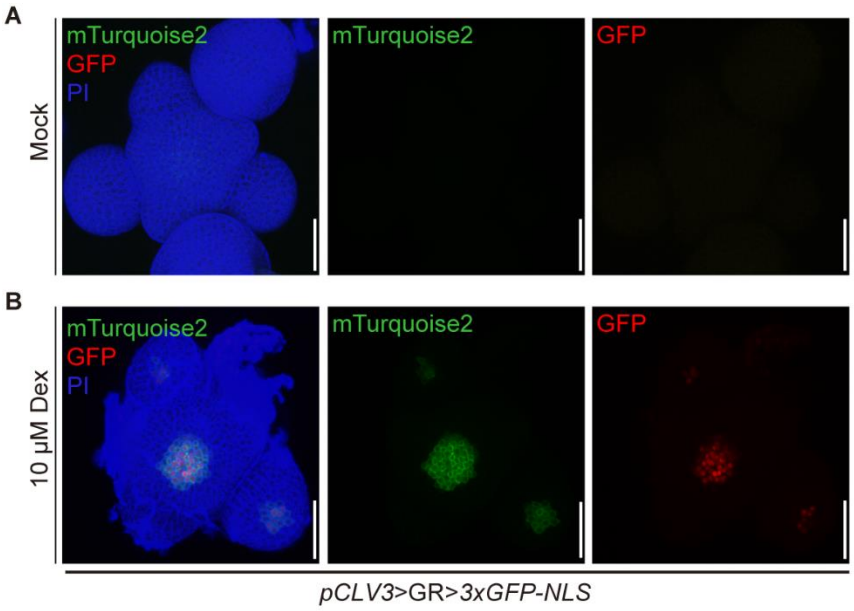

Figure 10. Co-expression of mTurquoise2 and triple GFP in the SAM. *pCLV3* driver line was crossed with *3xGFP-NLS* plants and Dex-induced/mock treated F_1 plants were imaged in the SAM. Scale bar: 40 µm. PI is false coloured in blue, mTurquoise2 in green and GFP in red. Modified after Schürholz et al., 2018.

We further tested, if Dex-induction can activate expression of an independent T-DNA insertion, which is also carrying a *pOp* element in trans, in our driver lines. For the SAM, the *pCLV3* driver line was crossed with a nucleus-targeted triple GFP driven by the *pOP6* promoter (*pOp6:3xGFP-NLS*). F_1 plants of the cross were mock treated and Dex-induced and subsequently imaged by CLSM. Mock treatment did not exhibit any fluorescence of mTurquoise2 or GFP (Figure 10A). Dex-induced plants depicted mTurquoise2 and GFP fluorescence in the *pCLV3* domain (Figure 10B). These findings confirmed the specific transactivation of transgenes in F_1 plants. Furthermore, it could be shown that Dex-induction of F_1 crosses of the *pSCR* driver line and the *VND7-VP16* effector line led to the differentiation into vessel-like elements in endodermal cells, due to the pSCR activity (Schürholz et al., 2018).

Taken together, we generated 19 inducible, cell type-specific driver lines for the main cell types and tissues in Arabidopsis, focusing on the SAM, being able study gene function in tissue specific context with a high spatiotemporal resolution.

2.3 Discussion

2.3.1 Overexpression of VGD1 and PMEI5 reduced SAM size

The SAM is a suitable tool to investigate the spatio and temporal preparation of individual cells for their future cell fate. Here, we investigated the activity of PMEs in the SAM and their function in defining cell identities. For our analysis, we selected stable lines overexpressing plant lines, VGD1ox and PMEIox, that presented severe phenotypes (Wolf et al., 2012a; Wolf et al., 2012b). Analysis of the size of their SAMs revealed a dramatically reduction in meristem size, fewer cells, and altered cell size and shape (Figure 4). Phenotypic characterization of VGD1ox further revealed a dwarfed phenotype, brittle side shoots, reduced fertility, elongated gynoecia and a small SAM. Further, previous immunolabelling of the pectin state in VGD1ox revealed a strong decrease in the methyl esterification state of pectin in the stem (Wolf et al., 2012a). The very brittle side shoots that easily break off the main shoot, would suggest that enhanced PME activity leads to stiffer cell walls.

For many years, it has been proposed that enhanced PME activity and the resulting de-methyl esterification of pectin forms egg-box-like structures with other pectate chains via covalent binding with Ca^{2+}, result in stiffer cell walls (Willats et al., 2001; Wolf et al., 2009a and b). However, a number of studies showed the opposite results for PME/PMEI activities and their effects on cell wall properties, based on atomic force microscopy (AFM) or immunolabelling (Pattathil et al., 2010; Peaucelle et al., 2011). Overexpression of the co-expressed PME5 and PMEI3 in the SAM resulted in less rigid cells and enhanced primordia outgrowth in PME5ox, whereas PMEI3ox exhibited more rigid cell walls and no emerging primordia (Peaucelle et al., 2011). PME5 and PMEI3 overexpression also resulted in softer and more rigid cell walls in seedling's hypocotyls, respectively (Peaucelle et al., 2015). These results are contrary to the phenotypes we observed in VGD1ox plants. One possible explanation can be that overexpression might activate compensatory effects leading to alterations of other cell wall components (Zabotina et al., 2012; Xiao et al., 2016) or PMEs might have specific functions dependent on the tissues where they are expressed, leading to the observed results. Furthermore, it is possible that PMEs acquire various types of de-methyl esterification, either block wise or non-blockwise leading to discrete cell wall states (Willats et al., 2001; Hocq et al., 2017).

As of now, we do not provide supporting AFM or immunolabelling data for our PMEIox plants, however, based on the observed results and literature, it is reasonable to argue that enhanced PMEI activity in the SAM leads to stiffer cell walls. PMEIox plants still produce primordia, although their meristems are very small and the cell size distribution is skewed towards smaller cells

compared to Col-0. AFM analysis of dark-grown hypocotyls revealed, that slow growing cells had reduced PME activity grew isotropically, similar to cells in the central zone, which are still proliferating and repress differentiation processes such as elongation (Peaucelle et al., 2015). Hence, enhanced activity of PMEI5 might lead to stiffer cells and thereby smaller cells.

Interestingly, the cells in the SAM of VGD1ox were larger in relation to Col-0 and PMEIox and more often presented a symmetric, square shape when compared to Col-0 (Figure 4). These phenotypes might be caused by a different cell wall state or altered cell division patterns. It was reported, that the cell size is controlled by cell cycle length, which is mainly regulated by cyclin-dependent kinases (CDKs) and CDK-specific cyclins, between G_1/S and G_2/M phase (Jones et al., 2017). A reduction in cyclins or CDKs, for example, led to cells, since each cell remained longer in the corresponding cell cycle phases and therefore increased in size (Jones et al., 2017). Although at the moment we do not have supporting data for this hypothesis, it is feasible, that VGD1ox cells are larger because of less rigid cell walls due to enhanced PME activity. In future experiments it would be important to analyse mitotically active cells by EdU staining in VGD1ox and PMEIox in comparison to Col-0.

In contrast to Col-0 cells, which often have more than four cell walls and asymmetric cell shapes, VGD1ox cells in the central zone of the SAM often only contain four cell walls and are symmetrically shaped. Based on the Errera's rule or the adjusted Besson Dumais rule, cells in the centre of the meristem divide along the shortest path (Besson and Dumais, 2011). However, in a square, all paths have the same length except for the diagonal, so this rule cannot explain why the cells might be symmetrical. Therefore, it would be crucial to identify how and when cells divide in VGD1ox and, more importantly, if cells in *pme* mutants present aberrant cell shapes in the SAM.

2.3.2 PME expression in the central zone might be regulated by WUS

Based on a large number of studies on the methyl esterification state of pectins and their influence on cell wall mechanics in different tissues, we wanted to identify the function of PMEs in the shoot apical meristem. Analysis of microarray, RNA-Seq and ChIP-Seq data of protoplasts or WUS-GR inflorescence meristems revealed a suppression of expression of several PMEs in the central zone (Table 1) (Yadav et al., 2009a; Yadav et al., 2014; Miotk, 2015). We hypothesized that PMEs are necessary for cell differentiation in the SAM periphery and therefore their expression in the central zone must be suppressed, presumably indirectly or directly by WUS. In our focus were seven *PME*s (*PME12*, *AT5G53370*, *PME5*, *PME34*, *PME44*, *PME41* and *PME3*) which were

strongly expressed in the *KAN1*, *FIL* or *LAS* domains and showed a weak expression in the *CLV3* domain, with an exception of *PME34*, which was highly expressed throughout the whole SAM. Interestingly, for six of the *PME*s other than, *PME41*, a WUS binding peak was identified, further supporting our hypothesis, that WUS acts directly on *PME*s (Miotk, 2015). Based on the expression data, most *PME*s with a WUS binding peak also showed repression in the *CLV3* domain, presumably due to binding of WUS. The homeodomain transcription factor WUS is known to repress genes in the central zone associated with differentiation for stem cells maintenance. Other WUS negatively regulated genes are for instance *KAN1*, *KAN2*, *AS2* and *YAB3* (Yadav et al., 2013).

To further substantiate our hypothesis, we tried to generate promoter reporters of five of the seven PMEs, but only for PME5 we wanted to generate promoter reporter constructs of five of the seven PMEs, but were only able to generate a stable Arabidopsis line for *PME5*. The PME5 reporter line showed no activity in the central zone, but fluorescence in the periphery and on the abaxial side of the emerging primordia reflecting the expression data (Figure 6). We also tried to generate two *pme* double mutants for four of the seven PMEs. The double mutant *pme41 pme44* was analyzed in the T_2 generation, but unfortunately, no morphological phenotype was observed, which might be due to functional redundancy of the other five PMEs, which showed similar expression patterns in the SAM (Figure 5). The generation of higher number *pme* mutants is therefore highly recommended.

Our hypothesis that PME activity must be repressed in the central zone of the meristem is further supported by the well-established acid growth theory and more recent studies linking auxin signalling to the de-methyl esterification state of pectins (Braybrook et al., 2013; Qi et al., 2014; Qi et al., 2017). In the SAM, peripheral cells are primed for primordia initiation by high auxin levels. Recent publications also showed that an increase in auxin signalling can lead to cell wall acidification and thus increased cell growth. On the other hand, this led to an increased PME activity in addition to less rigid cell walls and presumably to an easier emergence of primordia outgrowth. PME activity and increased auxin signalling appear to have the same effect, namely softening of the cell wall, however, it is not known whether they are interdependent or parallel. It has also been shown that an auxin-mediated decrease of pH in the apoplast inhibits PME activity either by inhibition of PMEIs or optimal conditions with higher pH values (enzyme activity). Studies on auxin signalling and the methyl esterification state of pectin in young primordia (P1) identified high auxin levels in the abaxial side of the primordia, concurrent with higher PME activity, resulting in softer cell walls (Qi et al., 2014; Qi et al., 2017). In contrary, on the adaxial side, decreased auxin levels and reduced PME activity resulted in stiffer cell walls (Qi et al., 2014; Qi et al., 2017).

Although we are lacking data about the cell wall extensibility in the VGD1ox and PMEIox SAMs as well as more PME reporter lines and characterization of higher number *pme* mutants, the mentioned studies about the connection of auxin and PME activity support our hypothesis, that PME activity is correlated with differentiation in the periphery of the SAM. Thereby, it has to be controlled and is presumably repressed by WUS in the central zone. Mutation of WUS binding cassettes in PME promoters in the SAM would be a crucial future experiments, to identify the regulation of PMEs by WUS.

2.3.3 Inducible, cell type-specific expression

The introduction of new techniques and methods for molecular biologists, such as the genome editing tool CRISPR/Cas9 (Xing et al., 2014; Wang et al., 2015) or the modular cloning system GoldenGate/Greengate (Lampropoulos et al., 2013), enable the comparatively fast generation of mutants or combinations of different DNA sequences for the easy production of long DNA constructs.

Here, we were able to obtain an inducible, cell type-specific two component system for driver and effector lines in Arabidopsis (Schürholz et al., 2018). We were able to show that the induction system works for driver lines and in combination with effector lines for transactivation Figure 8, Figure 9, Figure 10). The system is not leaky and various promoters can be activated in different tissues and their activity can be adjusted by Dex concentrations or the duration of induction. Furthermore, the system can be applied not only for Arabidopsis, but also to other plant species suitable for transformation. Additionally, thanks to the modular Green Gate cloning system, users can easily and quickly generate their own driver or effector lines. Moreover, effector cassettes can also be used for cell type-specific complementation, artificial microRNA induced domain-specific knockdown or tissue-specific expression of CRISPR/Cas9 modules. Thus, this system provides an extensive spectrum for applications ranging from the investigation of gene expression in tissue-specific context to the generation of inducible genetic perturbations. We are gaining in importance to use this system to better analyse the functions of PMEs and PMEIs in specific tissues in the SAM for example by expressing PMEs or PMEIs in the *CLV3* or *UFO* domain.

3 RLP4 and RLP4-like as putative cell wall binding proteins

3.1 Introduction

Plant cells are surrounded by the cell wall, a stiff compartment to enable mechanical support, counteract the intracellular turgor to prevent cell bursting, and to serve as a physiological barrier against biotic and abiotic stress. On the other hand, the cell wall is pliable to allow normal plant growth like cell division and elongation (Cosgrove, 2005). To adopt to these varying needs, signals from the outside to the inside of the cell and *vice versa* have to be conveyed. For this process, plasma membrane proteins and associated signalling cascades referred to as cell wall signalling, are crucial for plant development like cell division, elongation and differentiation (Wolf et al., 2012b; Wolf, 2017). To date several cell wall receptors were identified that might be putative candidates for members of cell wall signalling.

3.1.1 Malectin-like proteins

Recently, a group of plasma membrane proteins have been discussed as putative cell wall binding proteins, because they contain a malectin-like (Mal-like) domain (Franck et al., 2018). This domain is structurally related to the malectin domain, which was identified in an ER-membrane localized protein with the potential of binding di-glucose motifs in *Xenopus laevis* (Schallus et al., 2008 and 2010). Malectin-containing proteins build a subgroup of the well-studied lectin proteins, that are present in all kingdoms of life (Van Holle et al., 2019). Their ligands are polysaccharides or proteoglycans localized either in the cell interior or at the cell surface (Van Holle et al., 2019). In the plant kingdom, the Mal-like domain is often appended to LRRs in the extracellular domain and an intracellular protein kinase domain or a short intracellular tail. Additionally, the Mal-like domain often appears in two divergent tandem domains, assuming that their binding functions and their ligands might be dfferent compared to the bacteria or animal kingdom (Bellande et al., 2017). In *A. thaliana*, approximately 70 Mal-like containing proteins have been identified. They can be divided into two main groups, the *Catharanthus roseus* receptor kinase 1-like (CrRLK1L) proteins without LRRs, and Mal-LRRs, which contain LRRs and are comprising Mal-LRR-RLKs and -RLPs (Schulze-Muth et al., 1996) (Figure 11).

3.1.1.1 CrRLK1L

This group of malectin-like domain proteins, was named after the first identified plant-specific member in *Catharanthus roseus* RLK1-like from *C. roseus* cell cultures (Schulze-Muth et al.,

1996). Ten of 17 members of the CrRLKL1 group are characterized and mainly function in cell expansion and cell wall sensing and signalling (Figure 11), namely: FERONIA (FER), ANXUR1 and 2 (ANX1/2), BUDDHA PAPER SEAL 1/2 (BUPS1/2), HERKULES 1 and 2 (HERK1/2), THESEUS1 (THE1), [Ca^{2+}]CYT-ASSOCIATED PROTEIN KINASE 1 (CAP1/ERULUS) and CURVY1 (CVY1) (Hématy et al., 2007; Guo et al., 2009a; Miyazaki et al., 2009; Keinath et al., 2010; Nissen et al., 2016; Ge et al., 2017; Stegmann et al., 2017). All members are plasma membrane localised proteins with an intracellular kinase domain and an extracellular Mal-like domain (Boisson-Dernier et al., 2011). Although the downstream signalling cascades of many CrRLKL1 members are still elusive, some peptides have been proposed as ligands for CrRLKL1 proteins. Several small peptides, known as RAPID ALKALINIZATION FACTORs (RALFs) were identified and proposed as ligands for CrRLK1Ls, but also carbohydrates were considered as putative binding factors for CrRLK1Ls (Haruta et al., 2014; Nissen et al., 2016; Stegmann et al., 2017).

THE1 and FER contain two extracellular tandem Mal-like domains and both appeared to function in cell wall signalling (Hématy et al., 2007; Feng et al., 2018). THE1 was identified in a suppressor screen of the mutant *cesa6*/*procruste1-1* (*prc1-1*), that shows a reduction in cellulose content and exhibits a short hypocotyl phenotype in dark-grown conditions (Hématy et al., 2007). Mutation of THE1 rescued the *cesa6*/*prc1-1* hypocotyl phenotype, albeit cellulose deficiency was not restored, suggesting a role of THE1 in cell wall monitoring and signalling. Therefore, it is assumed, that the short hypocotyl phenotype of *cesa6*/*prc1-1* is a secondary effect due to enhanced THE1 mediated signalling, consistent with large THE1-dependent transcriptional rearrangements in the mutant (Hématy et al., 2007). Recently, the secreted peptide RALF34 was identified as ligand of THE1 (Gonneau et al., 2018). Similarly, FER functions as a receptor for RALF1 and RALF23 (Haruta et al., 2014; Stegmann et al., 2017). FER is involved in plant immunity, in the response to several hormones such as ethylene, abscisic acid and BR as well as in the recognition of pollen tubes by the female gametophyte (Keinath et al., 2010; Ngo et al., 2014; Li et al., 2016; Liao et al., 2017). Furthermore, FER is considered as mechano-sensor (Shih et al., 2014) and is involved in cell expansion in the female gametophyte, acting as putative co-receptor of THE1 and HERK1 and 2 (Guo et al., 2009; Guo et al., 2009b; Höfte et al., 2015). Opposite to FER, ANX1 and 2, the closest FER-homologues, are important for mechano-sensing and cell wall integrity in the pollen tubes (Boisson-Dernier et al., 2009; Ge et al., 2017). It was recently identified, that the FER extracellular domain containing Mal-like domains I and II can bind to pectins (polygalacturonic acid (PGA)) *in vitro* (Lin et al., 2018; Feng et al., 2018). Up to date, studies with ANX1 could not reveal a putative ligand since candidates of a variety of glucose-derived disaccharides such as maltose, cellobiose, mannose or PGA did not bind to ANX1 (Moussu et al., 2018).

3.1.1.2 Mal-LRR-RLKs

The Mal-LRR-RLK group comprises 42 proteins in Arabidopsis, that differ from their protein structure from the CrRLK1L group by having additional LRRs and a conserved amino acid motif, Gly-Asp-Pro-Cys (GDPC), in the extracellular domain (Osička et al., 2004; Lidell et al., 2006; Hok et al., 2011; Kosuta et al., 2011). The GDPC motif is located between the LRRs and the Mal domain and was identified as processing motif, cleaved either auto-catalytically or by a yet unidentified protease in plants (Kosuta et al., 2011; Antolín-Llovera et al., 2014) (Figure 11).

From the Mal-LRR-RLK group in Arabidopsis, only SENESCENCE-INDUCED RECEPTOR KINASE 1 (SIRK1, AT2G19190), IMPAIRED OOMYCETE SUSCEPTIBILITY 1 (IOS1, AT1G51800) and MATERNAL EFFECT EMBRYO 39 (MEE39, AT3G46330) have been functionally characterized so far (Robatzek et al., 2002; Pagnussat et al., 2005; Hok et al., 2014). SIRK1 is involved in defence and senescence–related processes, IOS1 is involved in ABA fungal pathogen responses, and MEE39 is involved in embryo development (Robatzek et al., 2002; Pagnussat et al., 2005; Hok et al., 2014). Apart of these three Mal-LRR-RLKs in Arabidopsis, the best-studied Mal-LRR-RLK in plants is SYMBIOSIS RECEPTOR-LIKE KINASE (SYMRK) from *Lotus japonicus* (*L. japonicus*, Lj) (Stracke et al., 2002). In terms of protein domain structure SYMRK is very similar to RLP4 and R4L1, with the exception of the presence of a protein kinase domain in SYMRK. It is required for symbiosis with arbuscular mycorrhiza rhizobia in legumes (Antolín-Llovera et al., 2014; Stracke et al., 2002). Like the Arabidopsis Mal-LRR-RLKs, SYMRK comprises a Mal-like-, a LRR-, a transmembrane and an intracellular protein kinase domain (Antolín-Llovera et al., 2014). In the extracellular domain, LjSYMRK also harbours a conserved GDPC motif between the Mal-like domain and the LRRs that is either cleaved by proteases or by autocatalytic self-processing. Upon cleavage of the Mal-like domain in *L. japonicus*, the processed SYMRK can interact with NOD FACTOR RECEPTOR (NFR5), which is important for symbiosis (Antolín-Llovera et al., 2014).

3.1.1.3 Mal-LRR-RLPs

In a phylogenetic analysis of malectin-like proteins in Arabidopsis, several un-characterized Mal-LRR-RLPs were identified (Bellande et al., 2017). This group comprises nine proteins that divide into two subgroups. The first subgroup contains five members which harbour a transmembrane- and a cytosolic domain. RLP4 (AT1G28340) and R4L1 (AT1G25570) cluster into this group together with three uncharacterized proteins AT1G24485, AT3G46270 and AT3G46280. The smallest subgroup comprises four proteins, that are lacking the transmembrane and cytosolic domain. These proteins are R4L2 (AT3G05990), R4L3 (AT3G19230) and AT3G46250 and AT1G51840 (Bellande et al., 2017) (Figure 11).

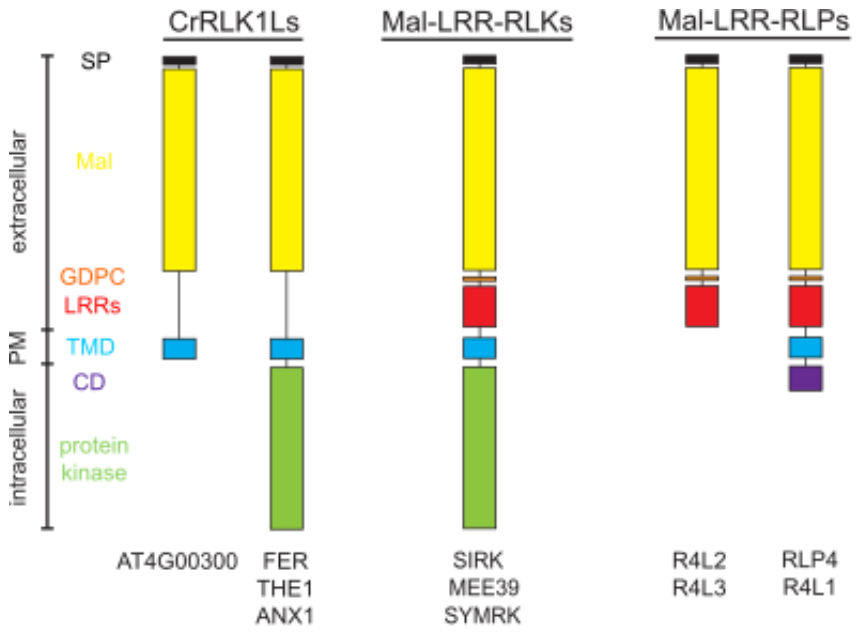

Figure 11. Overview of domain structures of CrRLK1Ls, Mal-LRR-RLKs and Mal-LRR-RLPs. Different protein domains in the groups of malectin-like containing proteins, CrRLK1L, Mal-LRR-RLKs and Mal-LRR-RLPs, are depicted as followed: Signal peptide (SP) in black, malectin-like domain in yellow, GDPC motif in orange, LRRs in red, transmembrane domain (TMD) in blue, cytoplasmic domain (CD) in purple and protein kinase domain in green. Representative proteins of each protein class are depicted below.

3.1.2 LRR-RLKs/-RLPs in Arabidopsis

The group of leucine-rich repeat (LRR) RLKs are the most abundant ones of the more than 600 RLKs in Arabidopsis (Li et al., 1997; Clark et al., 1997; Gómez-Gómez et al., 2000; Li et al., 2002; Zipfel et al., 2006). They contain an extracellular LRR that is involved in ligand binding or protein-protein interactions (Smakowska-Luzan et al., 2018). Upon binding or interaction, the intracellular protein kinase domain is activated and auto- or transphosphorylations initiate downstream signalling pathways (Figure 1).

So far, 57 proteins in *Arabidopsis thaliana* were annotated as receptor-like proteins (RLPs), but recent studies could identify eight additional proteins, extending the group of RLPs to 65 members in Arabidopsis (Wang et al., 2008; Augustin, 2015; Bellande et al., 2017). RLPs contain an extracellular leucine rich repeat (LRR), a transmembrane- and a short cytoplasmic domain. Of the now 65 RLPs, only a scarce amount are studied and characterized. These are for example

TOO MANY MOUTHS (TMM, AtRLP17; Nadeau et al., 2002), essential in stomata development and CLAVATA2 (CLV2, AtRLP10; Jeong et al., 1999), important for stem cell maintenance in the shoot apical meristem. Several RLPs have been identified in immunity such as RLP1, RLP23 and RLP30 (Wang et al., 2008; Bi et al., 2014). RLP44 was recently identified as a component of cell wall signalling, conveying signals from the cell wall to the cell interior via interacting with BRASSINOSTREROID INSENSITIVE1 (BRI1) and BRI1-ASSOCIATED RECEPTOR KINASE1 (BAK1) (Wolf et al., 2014a; Holzwart et al., 2018). Thereby, the Brassinosteroid (BR) signalling pathway is activated, leading to expression of cell wall biosynthetic and remodelling genes (Wolf et al., 2014a). Additionally, the association of RLP44 to the cell wall was identified *in vitro* and *in vivo* (Holzwart, 2018). However, the function of most of the other RLPs are not yet identified, but they are presumably involved in plant immunity or development (Wang et al., 2010a). Previous studies largely focused on the function of the characteristic LRR domains in RLPs in protein-protein interaction or ligand perceptions (Hazak et al., 2017; Lin et al., 2017).

RLP4, together with its subfamily of R4Ls, form a unique group of annotated RLPs, because they contain a Mal-like domain in their extracellular domain. This Mal-like domain is structurally related to the malectin domain in animals, which is known to bind to carbohydrates (Schallus et al., 2008). In plants, Mal-like domain containing proteins are therefore in focus as putative carbohydrate-binding proteins in the ER or the plasma membrane (Boisson-Dernier et al., 2011; Bellande et al., 2017). Thus, RLP4 could function as a cell wall binding protein and cell wall signalling receptor.

Previous studies of RLP4 in our lab led to the identification of the RLP4-like subgroup (R4L) consisting of R4L1 (AT1G25570), R4L2 (AT3G05990) and R4L3 (AT3G19230) (Augustin, 2015). These R4Ls also contain a Mal-like domain, but R4L2 and R4L3 are lacking a transmembrane and cytosolic domain. The presence of a putative carbohydrate binding site in the Mal-like domain, made these proteins suitable candidates for cell wall binding proteins. RLP4 and R4L1 are expressed throughout most plant tissues, with elevated levels in the shoot apical meristem and the epidermis in root and shoot and both localize to the plasma membrane (eFP Browser, Appendix A3, A4). R4L2 and R4L3 are similarly expressed with high expression levels in the shoot apical meristem, pollen and the vasculature (eFP Browser, Appendix A5, A6). The localization of R4L2 and R4L3 in contrast is not known yet. Previous experiments with RLP4 revealed a strong developmental phenotype of RLP4 overexpressing plants compared to Col-0 wild type. These plants exhibited fasciated stems which was reminiscent of *clv3-10* mutant plants, suggesting a developmental function of RLP4 in the shoot apical meristem (Figure 25G, Figure 39) (Augustin, 2015). Protein sequence comparisons of RLP4 and the structurally similar protein SYMRK from *Lotus japonicus*, identified the GDPC motif also in RLP4. The GDPC motif in SYMRK is important for processing and cleavage of the Mal-like domain (Antolín-Llovera et al., 2014). However,

cleavage of the Mal-like domain could not be identified in RLP4 (Figure 1) (Augustin, 2015). Moreover, the ability of cell wall binding of the extracellular domain of RLP4 was tested in plasmolysis experiments in hypocotyls. Unfortunately, no binding could be revealed (Augustin, 2015).

3.1.3 Aims

RLP4 and the recently identified subgroup of RLP4-like proteins contain a malectin-like domain that is assumed to associate with carbohydrates, similar to Xenopus malectin (Schallus et al., 2008). Therefore, this small group of RLPs in Arabidopsis are putative candidates for cell wall signalling and might associate with cell wall components. Thus, we aimed to achieve the following objectives in this study:

A) Reveal the function of RLP4 and RLP4-like subgroup in cell wall signalling

B) Identify the association of RLP4 to cell wall compartments

3.2 Results

3.2.1 RLP4 forms a distinct clade with the three RLP4-like proteins in a phylogenetic analysis of RLPs in Arabidopsis

Arabidopsis thaliana includes 65 receptor-like proteins (RLPs) that contain an extracellular leucine rich repeat (LRR), a transmembrane domain and a short cytoplasmic domain (Wang et al., 2008). Recently, three additional RLPs were identified in a phylogenetic study, analysing RLP orthologues in representatives of the plant kingdom (Augustin, 2015). A subgroup of the receptor-like protein 4 (RLP4), named RLP4-like (R4L), comprised R4L1 (AT1G25570), R4L2 (AT3G05990) and R4L3 (AT3G19230). The newly discovered R4Ls are structurally similar to RLP4 and also contain a malectin-like domain and LRRs (Augustin, 2015). For the phylogenetic analysis, the 57 annotated RLPs together with the recently identified RLP4-likes were used. RLP4 and its subgroup of RLP4-like cluster together with RLPs from Arabidopsis and form group IV (Figure 12). Within this group, R4L2 and R4L3 form one clade and RLP4 and R4L1 another, which displays a higher similarity in sequences of RLP4-R4L1 and R4L2-R4L3 (Figure 12). R4L2 and R4L3 also contain a malectin-like domain, the GDPC motif and LRRs in the extracellular domain, but are missing the transmembrane- and cytoplasmic domain (Figure 1; Bellande et al., 2017). RLP4 and R4L1 are expressed in the whole plant with high expression levels in the shoot apical meristem (eFP Browser, Appendix A3, A4). R4L2 and R4L3 are also expressed in the shoot apical meristem (SAM), whereas R4L3 is more restricted to the central zone of the SAM and both are highly expressed in pollen. In the root, R4L2 shows increased expression in procambium and phloem cells, whereas R4L3 only has elevated expression levels in the procambium (eFP Browser, Appendix A5, A6).

RLP44 (group III) was recently identified as an interactor of BAK1 and BRI1, conveying signals from the cell exterior to the cell interior upon their interaction (Wolf et al., 2014a). Recent studies could also show, that RLP44 associated to the cell wall *in vivo* and was binding to the cell wall component pectate *in vitro* (Holzwart et al., unpublished). Although RLP44 does not contain a malectin-like domain like RLP4 and the R4L subgroup (group IV), they are the closest relatives compared to other RLPs in Arabidopsis. This might hint to a putative common function in cell wall signalling. RLP proteins in group I have an island domain in their extracellular domain and a N-terminal transmembrane domain, whereas group II RLPs do not contain an island domain Wang et al., 2008). Group V RLPs have a long island domain in the extracellular domain (Wang et al., 2008). In general, many RLPs from groups I, II and V are not well characterized so far.

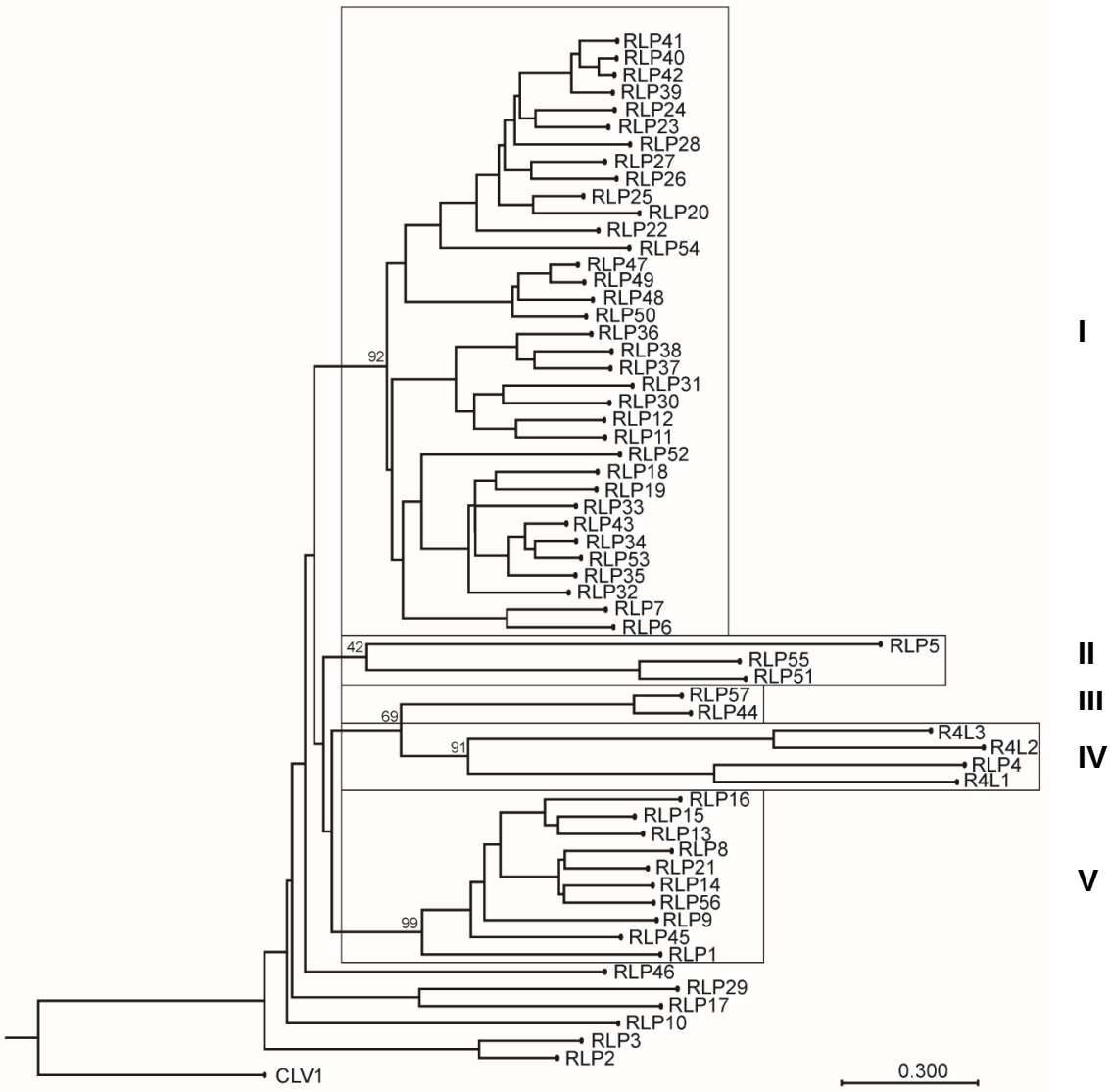

Figure 12. Phylogenetic tree of amino acid sequences of RLPs in Arabidopsis. RLPs clustered in five main groups, group I contains RLPs with an island domain and many of the RLPs have a N-terminal transmembrane domain. Group II comprises RLP5, 51 and 55 without island domain. Group III contains RLP44 and RLP57. RLP4 and the subgroup R4L form group IV with the characteristic malectin-like domain. Group V comprises RLPs with a long island domain. AtCLV1 was used to root the tree. Bar represents the branch length, that corresponds to a genetic change of 0.3. Branch numbers represent the percentage of bootstrap values (1000 replicates). Alignment and phylogenetic tree were performed by CLC Main Workbench 8.1 (Qiagen).

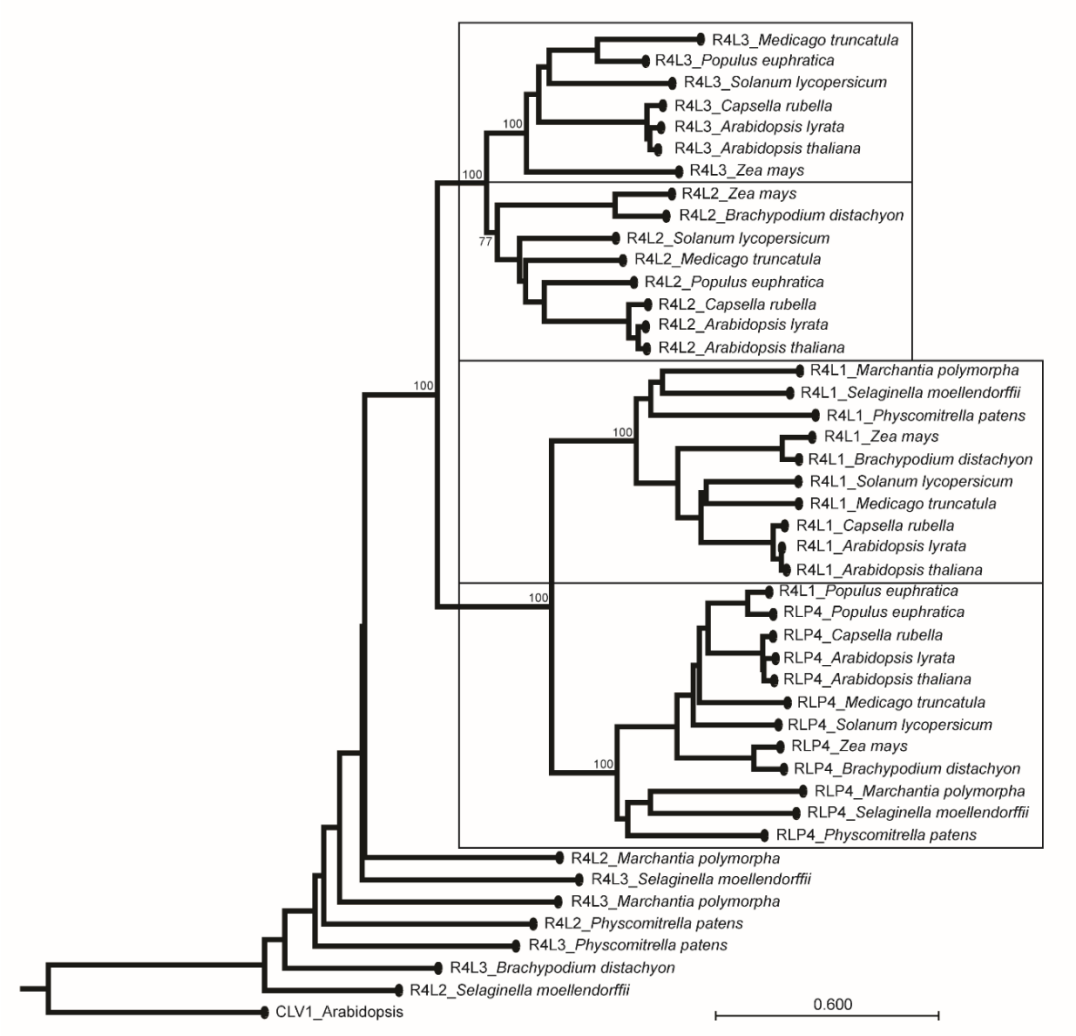

Figure 13. Phylogenetic tree of RLP4 and R4L orthologues. Group I: Orthologues of AtR4L3. Group II: Orthologues of AtR4L2. Group III: Comprises orthologues of AtR4L1, except orthologue in *Populus euphratica*. Group IV: Orthologues of AtRLP4. AtCLV1 was used to root the tree. Bar represents the branch length, that corresponds to a genetic change of 0.6. Branch numbers represent the percentage of bootstrap values (1000 replicates). Alignment and phylogenetic tree were performed by CLC Main Workbench 8.1 (Qiagen).

To further analyse the RLP group IV proteins, we searched for orthologues in several sequenced plant orders from brassicaceas to bryophytes. In particular, we searched for orthologues in *Arabidopsis lyrata* (*Al*), *Capsella rubella* (*Cr*), *Populus euphratica* (*Pe*), *Medicago truncatula* (*Mt*), *Solanum lycopersicum* (*Sl*), *Brachypodium distachyon* (*Bd*), *Zea mays* (*Zm*), *Selaginella moellendorffii* (*Sm*), *Physcomitrella patens* (*Pp*) and *Marchantia polymorpha* (*Mp*). The amino acid sequences of AtRLP4, AtR4L1, AtR4L2 and AtR4L3 were used as bait in protein blast searches for orthologues (NCBI). Sequences with the highest identity and query coverage were included in the phylogenetic tree that was generated by maximum likelihood phylogeny and bootstrapping with 1000 replicates (CLC Main Workbench 8.1, Qiagen). The phylogenetic tree revealed a separation of the four proteins RLP4, R4L1, R4L2 and R4L3 visualized by black outlined boxes (I-IV) (Figure 13). Group I comprises AtR4L3 orthologues of *Al*, *Cr*, *Pe*, *Mt*, *Sl* and *Zm*. Orthologues of *Bd*, *Sm*, *Pp* and *Mp* could not be identified (Figure 13). This might be due to missing amino acid sequences of these proteins in the data bases or AtR4L3 orthologues do not exist in these early land plant species. Selected amino acid sequences of *Bd*, *Sm*, *Pp* and *Mp* with the highest identity and query coverage do not cluster in the four groups (I-IV), but form an outgroup together with CLV1. Similar results were identified for AtR4L2 orthologues in group II. Here, no orthologues for *Sm*, *Pp* and *Mp* could be identified (Figure 13). Amino acid sequences of these R4L2 and R4L3 proteins seem to be more related to CLV1 then to other RLP4 R4L amino acid sequences.

To obtain further information regarding the conservation of the four RLPs, we compared their domain structures (Figure 14) . Annotations of malectin-like domains (yellow), the GDPC motif (orange), LRRs (red), the transmembrane domain (blue) and the cytosolic domain (purple) were annotated according to AtRLP4 as a reference (Uniprot; ID: F4HWL3). The alignment shows, that all of the proteins, except of CLV1, contain a malectin-like domain, depicted by the high conservation of amino acids in the assigned malectin-like domain from AtRLP4 (Figure 14, Appendix A1). Additionally, the alignment clarifies, why R4L2 and R4L3 relative proteins from *S. moellendorffii*, *P. patens* and *M. polymorpha* do not cluster with the R4L2 and R4L3 proteins from the other plant orders. They harbour an intracellular domain, that is longer as the cytoplasmic domain of RLP4 and R4L1 and blast analysis annotated this region as protein kinases. Therefore, they were excluded from groups I-IV and were closer related to the protein kinase containing CLV1.

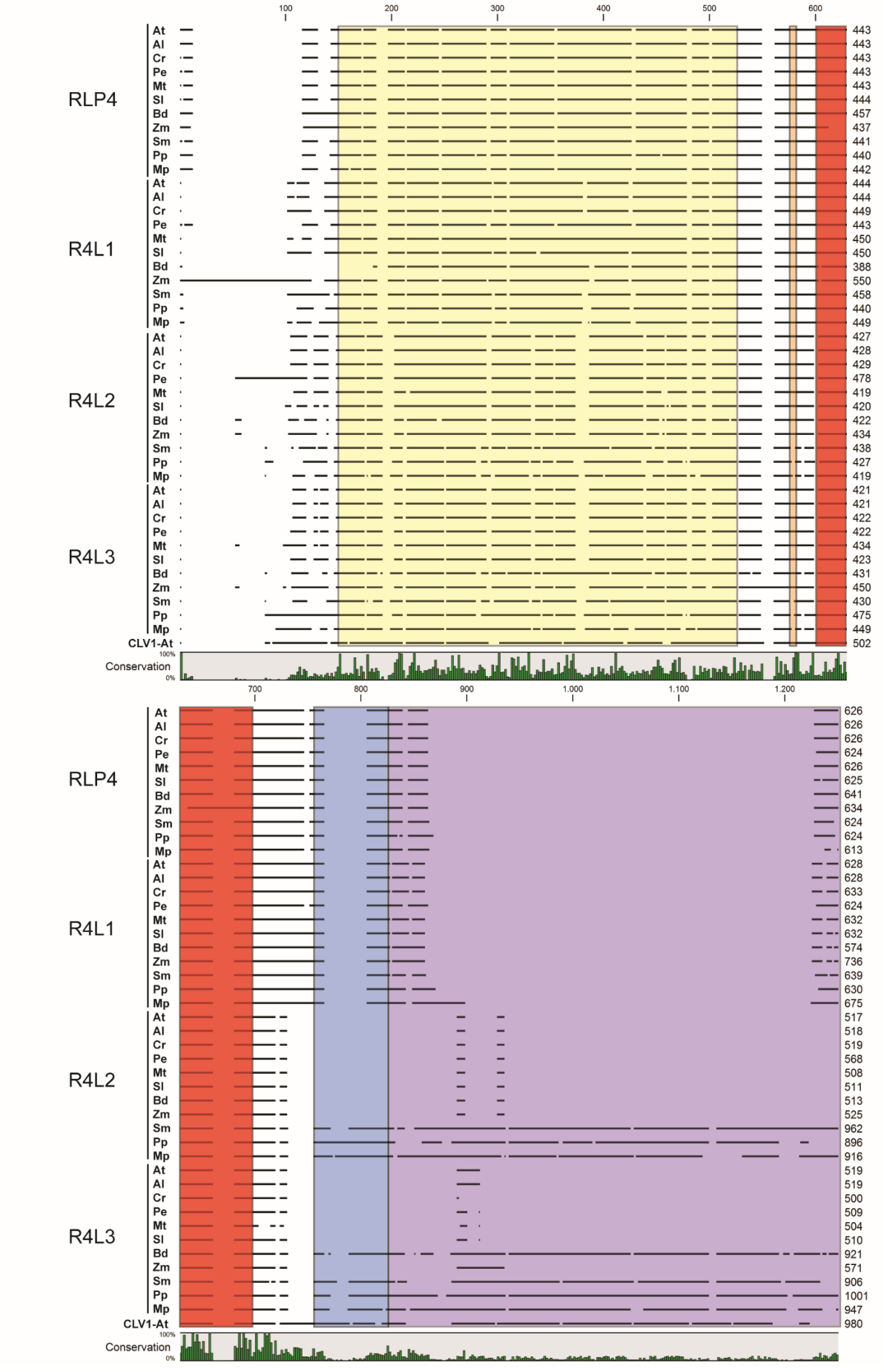
100
200
300
400
500
600
RLP4
R4L1
R4L2
R4L3
At 443
Al 443
Cr 443
Pe 443
Mt 443
Sl 444
Bd 457
Zm 437
Sm 441
Pp 440
Mp 442
At 444
Al 444
Cr 449
Pe 443
Mt 450
Sl 450
Bd 388
Zm 550
Sm 458
Pp 440
Mp 449
At 427
Al 428
Cr 429
Pe 478
Mt 419
Sl 420
Bd 422
Zm 434
Sm 438
Pp 427
Mp 419
At 421
Al 421
Cr 422
Pe 422
Mt 434
Sl 423
Bd 431
Zm 450
Sm 430
Pp 475
Mp 449
CLV1-At 502
100%
Conservation
0%
700
800
900
1.000
1.100
1.200
RLP4
R4L1
R4L2
R4L3
At 626
Al 626
Cr 626
Pe 624
Mt 626
Sl 625
Bd 641
Zm 634
Sm 624
Pp 624
Mp 613
At 628
Al 628
Cr 633
Pe 624
Mt 632
Sl 632
Bd 574
Zm 736
Sm 639
Pp 630
Mp 675
At 517
Al 518
Cr 519
Pe 568
Mt 508
Sl 511
Bd 513
Zm 525
Sm 962
Pp 896
Mp 916
At 519
Al 519
Cr 500
Pe 509
Mt 504
Sl 510
Bd 921
Zm 571
Sm 906
Pp 1001
Mp 947
CLV1-At 980
100%
Conservation
0%

Figure 14. Conservation of protein domains in RLP4, R4L1, R4L2 and R4L3 proteins. Domain structures were assigned according to AtRLP4 protein domains (Uniprot; ID: F4HWL3). Malectin-like domain (yellow), GDPC motif (orange), LRRs 1-4 (red), transmembrane domain (blue), cytoplasmic domain (purple). Putative RLP4, R4L1, R4L2 and R4L3 orthologues of the following plant species were aligned: *Arabidopsis thaliana* (*At*), *Arabidopsis lyrata* (*Al*), *Capsella rubella* (*Cr*), *Populus euphratica* (*Pe*), *Medicago truncatula* (*Mt*), *Solanum lycopersicum* (*Sl*), *Brachypodium distachyon* (*Bd*), *Zea mays* (*Zm*), *Selaginella moellendorffii* (*Sm*), *Physcomitrella patens* (*Pp*) and *Marchantia polymorpha* (*Mp*). Green bars represent conservation of amino acids in percentage. AtCLV1 was used as outgroup. Alignment was performed using CLC Main Workbench 8.1 (Qiagen).

Furthermore, all of the proteins, except CLV1, have a 100 % conserved GDPC motif, which is also present in SYMRK (Antolín-Llovera et al., 2014). In LjSYMRK, this motif is necessary to cleave off the malectin-like domain and enable interaction of LRRs with other proteins. It is assumed, that the GDPC motif is conserved in proteins containing a malectin-like domain and LRRs in their extracellular domain to enable processing and fine tune interaction with different partners. CrRLK1L proteins, which contain a malectin-like domain, but not LRRs, do not contain this GDPC motif. However, processing of AtRLP4 and releasing of the malectin-like domain could not been shown so far (Sebastian Augustin, Master thesis, 2015).

The LRR repeats are as well conserved in all of the proteins with varying numbers of LRRs. For AtRLP4, four LRRs are assigned. The main difference regarding protein sequence conservation is found in the transmembrane domain and the cytosolic domain. Here, R4L2 and R4L3 proteins that cluster to form group I and II are lacking the transmembrane and cytosolic domains. The short sequences that were aligned and annotated to the cytoplasmic domain in the alignment, probably also belong to the extracellular domain (Figure 14, Appendix A1). The alignment also depicts, why R4L2 and R4L3 relative proteins from *S. moellendorffii*, *P. patens* and *M. polymorpha*, are excluded from group I and II. They contain a transmembrane domain and an intracellular domain. These proteins are presumably more related to SYMRKs, which are in terms of protein structure similar to RLP4 but have an additional kinase domain (Figure 11). Thus, R4L2 and R4L3 are maybe not as conserved as RLP4 and R4L1 in the plant kingdom, the orthologue sequences of these proteins were not assigned in the database or were filtered out due to low identity and query cover. It might also be, that these taxa do not encode for R4L2 and R4L3.

In summary, phylogenetic analysis of AtRLP4 and AtR4L subgroup proteins reveal, that AtRLP4 and AtR4L1 are well conserved up to *M. polymorpha*. AtR4L2 and AtR4L3 are also conserved in

the plant kingdom, but presumably evolved more recently as AtRLP4 and AtR4L1, because no orthologues could be identified in *S. moellendorffii, P. patens* and *M. polymorpha.*

3.2.2 RLP4 is expressed in the SAM and localised in cell edges in the root

To elucidate the function of RLP4 in plant development, we expressed RLP4 fused to GFP via a glycine-serine-rich linker (linker-GFP) at the C-terminus under control of its own promoter, and terminator. The *pRLP4:RLP4:linker-GFP* construct was transformed into *A. thaliana* ecotype Columbia (Col-0, referred to as wildtype (WT)). Transformed plants did not exhibit an appreciable growth or developmental phenotype.

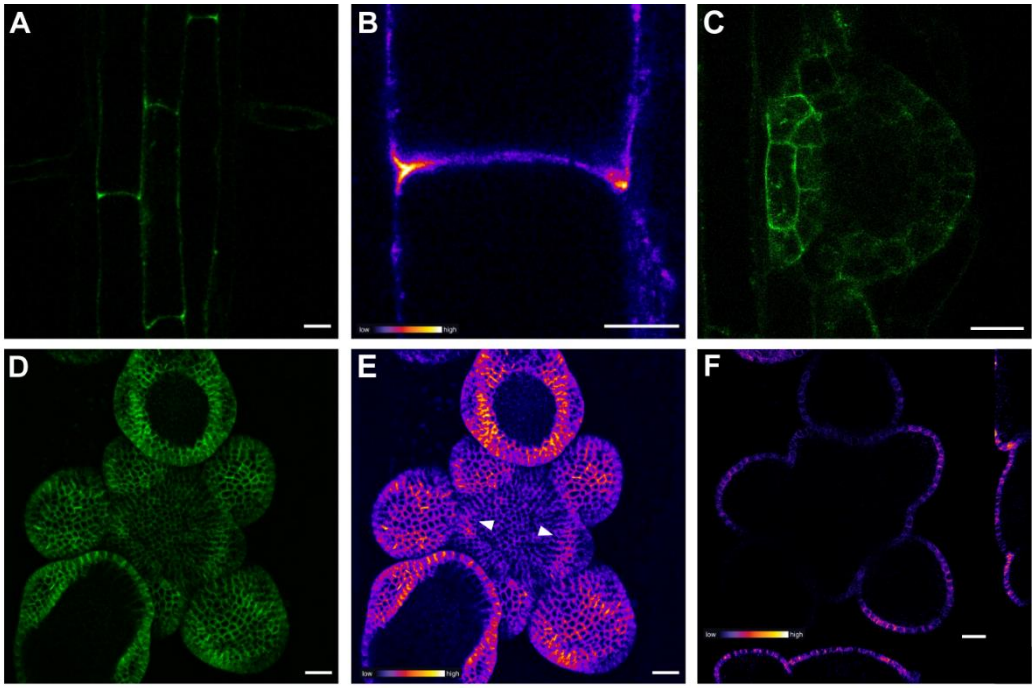

Figure 15. RLP4 is expressed in the root and the shoot apical meristem (SAM). *pRLP4:RLP4:linker-GFP* expression and localization in roots of six-day-old seedlings and in the shoot apical meristem of 40-day-old plants. (A) Expression of RLP4 in the differentiated root. Scale bar: 20 µm. (B) Close up of (A) with polar RLP4 localization in cell edges, fire projection. Scale bar: 10 µm. (C) RLP4 expression in root primordium. Scale bar: 20 µm. (D) Expression of RLP4 in the shoot apical meristem. Maximum projection of GFP signal. Scale bar: 20 µm. (E) Fire projection of (D) with maximum fluorescence intensity in the periphery and early developing primordia. Note maximum fluorescence in the forming crease between meristem and primordia (white arrow heads). Maximum projection, scale bar: 20 µm. (F) Cross section of a SAM depicting expression of RLP4 only in the epidermis (L1) of the meristem and young flower organs.

Referring to publicly available gene expression data (eFP, Genevestigator, Appendix A3-A6), RLP4 is expressed in the whole plant, with elevated levels in the shoot apical meristem and in the epidermis. To corroborate these data, we analysed the expression and subcellular localisation of *pRLP4:RLP4:linker-GFP* in six-day-old-roots and 40-day-old inflorescence meristems. RLP4-GFP fluorescence was detected in differentiated root cells. Here, RLP4 exhibited a polar localization with a maximum fluorescence in cell edges of the epidermis (Figure 15A,B). Furthermore, RLP4 expression was elevated in root primordia and young lateral roots, also depicting polar localization in epidermal cell edges (Figure 15C). Expression in the root vasculature was not visible, in contrast to what was reported for RLP44 in previous studies (Garnelo Gómez, 2017; Holzwart et al., 2018).

Shoot apical meristems of inflorescences were dissected and imaged after 40 days. *pRLP4:RLP4:linker-GFP* expression was observed in the epidermis (L1) of the SAM and the surrounding primordia exhibiting a fluorescence maximum in the periphery of the meristem in early forming creases between the meristem and emerging flower primordia (stage 1) and young primordia (stage 2) (Figure 15D-F) (Smyth et al., 1990). RLP4-GFP was mostly localized to the plasma membrane, but a cell edge localization of RLP4, as it was visible for differentiated epidermis cells in the primary root or in lateral roots, was not detectable in epidermal cells in the SAM. The polar localization of RLP4 in epidermal cell edges of differentiated cells in the root and in young lateral roots, might indicate a specific function of RLP4 in these areas. By overexpressing RLP4 and R4L1, we wanted to analyse, if elevated levels of RLP4 and R4L1 influences the overall plant phenotype.

3.2.3 Overexpression of RLP4 and R4L1 in the SAM did not alter above-ground phenotype

Previous overexpression of RLP4 induced the formation of fasciated stems, but this phenotype was either not due to the RLP4 overexpression or was silenced in the next generation (Sebastian Augustin, Master's thesis, 2015). Therefore, we generated GFP-fusion constructs of RLP4 and R4L1 that were expressed under the control of the ribosomal protein S5a (*pRPS5a*) promoter (*pRPS5a:RLP4:GAGAGA-GFP* and *pRPS5a:R4L1:GAGAGA-GFP*). The *RPS5a* promoter is mainly active in proliferating cells such as the shoot and the root apical meristems (Weijers et al., 2001). We decided to use the GAGAGA-GFP GreenGate module, that uses a short glycine-alanine linker and was kindly provided by Philipp Denninger (Guido Großmann Lab), because the previously used linker-GFP ($(GS)_{11}$-GF) module consisted of a long stretch of eleven Gly-Ser and

it was previously shown that in fusion constructs with RLP44 the serines in the linker region can be phosphorylated (Garnelo Gómez, 2017). Fluorescence microscopy analysis in shoot apical meristems revealed, that both fusion proteins were located at the plasma membrane (Figure 16). In comparison to *pRLP4:RLP4:linker-GFP*, the *pRPS5a*-dependent expression resulted in broader expression patterns with detectable fluorescence in the whole meristem, not only in the epidermis as in plants expressing RLP4 under the endogenous promoter (Figure 15F; Figure 16A,D). However, the overexpressing lines also displayed a maximum fluorescence intensity in young primordia and in the periphery, close to a forming crease which might be due to increased proliferation. Alternatively, post-translational modification could account for this fluorescence distribution. The fluorescence minimum was detected in the centre of the meristem (Figure 16B/E), where the slowly dividing stem cells are located. Moreover, *pRPS5a:R4L1:GAGAGA-GFP* depicts more signal in internal vesicles (Figure 16F), while *pRPS5a:RLP4:GAGAGA-GFP* is only visible at the plasma membrane (Figure 16C).

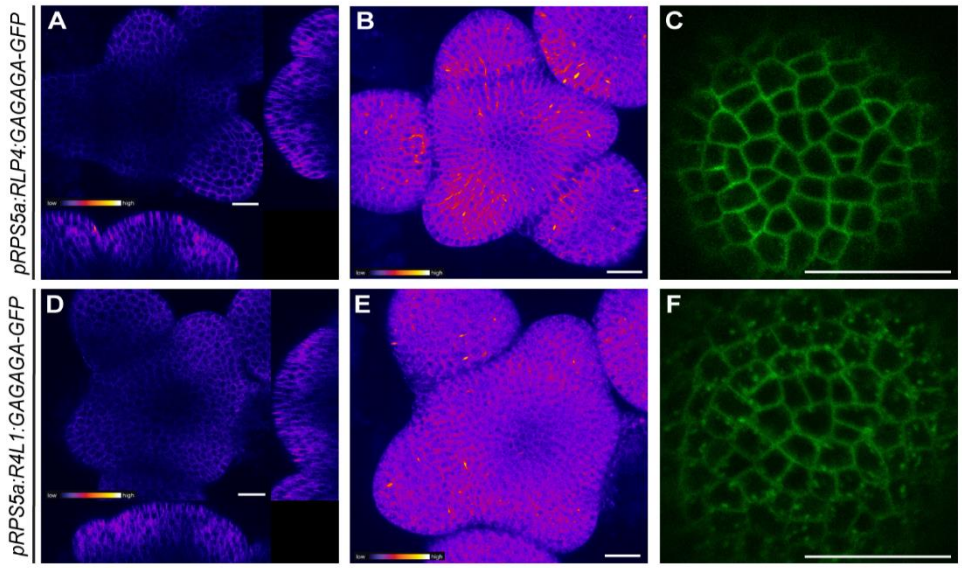

Figure 16. Expression of *pRPS5a:RLP4:GAGAGA-GFP* and *pRPS5a:RL1:GAGAGA-GFP* in the whole shoot apical meristem. (A-C) *pRPS5a:RLP4:GAGAGA-GFP* expression in the SAM. (B) Top view of RLP4 overexpression in the SAM, fire projection. (C) Close up of RLP4 overexpression in the centre of the SAM. (D-F) *pRPS5a:R4L1:GAGAGA-GFP* expression in the SAM. (A,D) Fire projections of cross section and (B,E) top view of the SAM. (C,F) Close ups in the centre of the SAM. Scale bars: 20 µm.

In a previous study, overexpression of *RLP4* under control of the viral *CaMV35S* or the *RPS5a* promoter revealed fasciated shoots in around 50 % T_1 plants (Sebastian Augustin, Master thesis, 2015). However, this strong phenotype was not observed anymore in T_2 plants (Sebastian Augustin, Master thesis, 2015). RLP4 and R4L1 overexpressing plants in this study, did not exhibit developmental phenotypes (data not shown). Taken together, overexpression of RLP4 and R4L1 did lead to an increased expression domain of RLP4 and R4L1 in the SAM also in cell layers below the epidermis (L1). However, RLP4 and R4L1 overexpression in the SAM did not depict an aberrant phenotype compared to Col-0.

3.2.4 CRISPR/Cas9-derived *rlp4 r4l1* double mutants depict altered phenotypes

To further characterise the function of RLP4 and R4L1 in Arabidopsis, single T-DNA lines were analysed (*rlp4-1* (SALK_039264), *rlp4-3* (WiscDsLox_419A01), *rlp4-4* (WiscDsLox_437H02), *r4l1-1* (SALK_147044)). However, no visible growth and developmental phenotype was observed, possibly due to functional overlap of RLP4 and R4L1 (Sebastian Augustin, Master thesis, 2015). Thus, we aimed to generate *rlp4 r4l1* double mutants. Because *RLP4* and *R4L1* genes are located in close proximity on chromosome one (R4L1: 8995600, RLP4: 9940101), recombination and thereby creation of double *rlp4 r4l1* mutants by crossing two single T-DNA lines, is very unlikely. Therefore, we employed the CRISPR/Cas9 technology (Jinek et al., 2012; Xing et al., 2014; Wang et al., 2015). The CRISPR/Cas9 (clustered regularly interspaced short palindromic repeats/CRISPR-associated protein 9) system makes use of a sequence-specific nuclease, the RNA-guided DNA endonuclease zCas9, *Zea mays* codon-optimized *Cas9*. In this system, a target specific guide RNA (gRNA) enables the sequence specific introduction of a DNA double strand break catalysed by Cas9. The DNA double strand break activates the plant DNA repair machinery often leading to an insertion or deletion of one or several nucleotides. These Insertions and deletions alter the amino acid sequence codon and often introduce a premature stop codon resulting in truncation of the gene of interest. With this technique, multiple genome modifications can be created in a fast and easy manner (Xing et al., 2014; Wang et al., 2015; Zhang et al., 2018).

For both, *RLP4* and *R4L1*, a gRNA was designed using the ChopChop webpage (http://chopchop.cbu.uib.no/). To increase the possibilities of creating a knock-out of the genes of interest (GOI), the 5' end of the gene was targeted. In particular, we targeted the beginning of the second exon of both genes (Figure 17A). The suggested gRNAs had an efficiency with values over 70 %, no self-complementary and no off-targets (0-3 nucleotides) (Figure 17B). For cloning,

the GreenGate cloning method (Lampropoulos et al., 2013) was used to either create single mutants or to combine up to three gRNAs in one vector in order to target both genes simultaneously. Arabidopsis T_1 plants were selected on hygromycin containing media and approximately 20 plants were sequenced in order to identify a mutation in *RLP4* and *R4L1*. Three mutant alleles could be identified for *RLP4* and one for *R4L1* (Figure 17C). These mutations were verified in the T_2 generation and only plants without the Cas9 T-DNA were propagated to the next generation and were used for experiments. In *RLP4*, three different alleles were identified. The DNA double strand break led to insertion of either an adenosine (a), a thymidine (t) or a guanosine (g), between guanosine (g) 263 and cytidine (c) 264 in the gDNA sequence of *RLP4*.

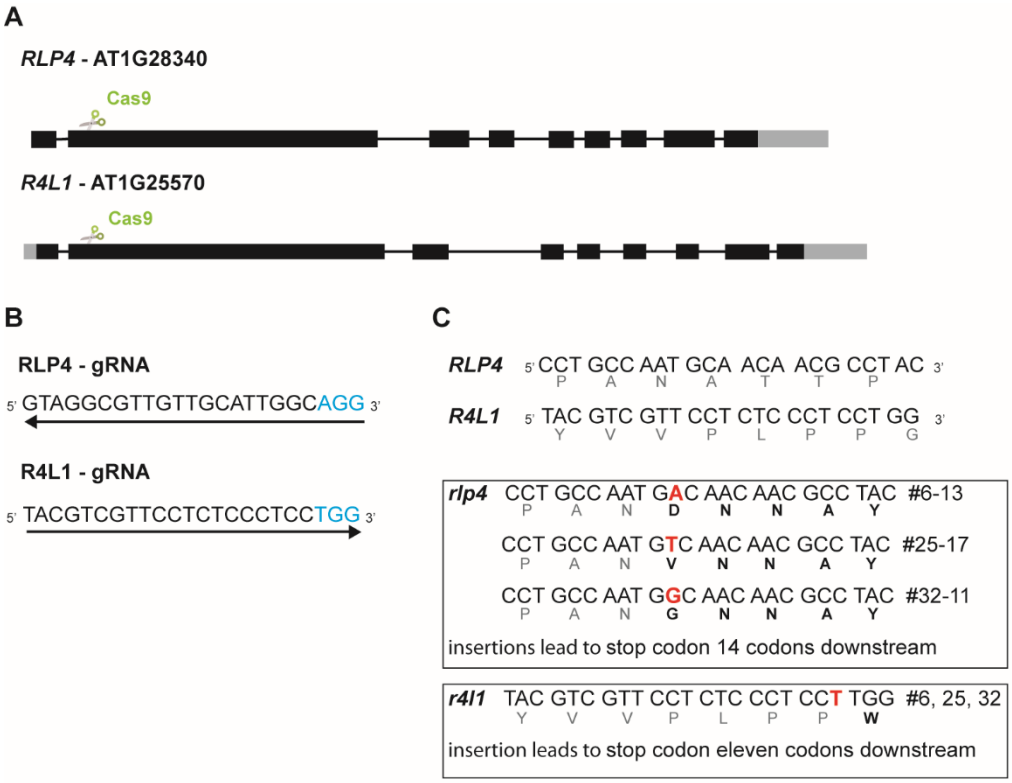

Figure 17. Design of *rlp4 r4l1* CRISPR/Cas9 mutants. (A) Overview of UTRs (grey boxes), exons (black boxes) and introns (black lines) in *RLP4* and *R4L1*, respectively. Cas9 recognition site depicted in green. (B) gRNA sequences and orientation for *RLP4* and *R4L1* used in the CRISPR/Cas9 approach with PAM sequence indicated in blue. (C) *RLP4* and *R4L1* wild type CRISPR/Cas9 target sites together with corresponding amino acids. Mutations for *RLP4* and *R4L1* are depicted in the boxes below, together with the nucleotide insertion (red) and changed amino acid sequences (bold and black).

This resulted in a frame shift in the amino acid sequence at position A62D and a premature stop codon at position 76 of the amino acid sequence. In *R4L1*, only one mutation, the insertion of a thymidine between c362 and t363 in the gDNA was identified. This also led to a frame shift in the amino acid sequence at position G96W and a pre-mature stop codon at position 106 of the amino acid sequence.

Three independent double mutants *rlp4 r4l1* #6-13, #25-17 and #32-11 (referred to as *rlp4 r4l1)* were identified. All three had the same mutation in *R4L1*, but different mutated alleles in *RLP4*. Line #6-13 had an insertion of an “a”, line #25-17 of a “t” and line #32-11 of a “g” (Figure 17C). All three insertions resulted in an amino acid frame shift and pre-mature stop codon. Additionally, *rlp4* and *r4l1* single mutants were also obtained, *rlp4* #30-3 carried the same insertion of an “a” in *RLP4* like double mutant line #6-13. Line *r4l1* #24-13 carried the same “t” insertion in *R4L1* like the double mutant lines. Because single *rlp4* and *r4l1* mutants did not depict a striking phenotype, the double mutant line *rlp4 r4l1* #32-11 was used for further experiments.

3.2.5 *rlp4 r4l1* does not have a shoot apical meristem phenotype

Based on publically available expression data of RLP4 and R4L1 (eFP Browser) and the analysis of *pRLP4:RLP4.linker-GFP* expression in the SAM, we wanted to test, if the loss of *RLP4* and *R4L1* might alter SAM morphologies in *rlp4 r4l1*. We first measured the meristem size, number of cells and cell size in the SAM of the *rlp4 r4l1* double mutant. For quantification, shoot apices of *rlp4 r4l1* and Col-0 inflorescences were dissected and stained with propidium iodide (PI), which presumably stains de-methylesterified pectins in living plant cells. Z-stacks were taken by confocal laser scanning microscopy and were quantified by using MorphoGraphX (Barbier de Reuille et al., 2015). Analysis of *rlp4 r4l1* double mutant and Col-0 in the shoot apical meristem, did not reveal defects in cell division, which would have been depicted by either smaller or bigger cells in comparison to Col-0, or altered shapes of cells (Figure 18A), neither in the periphery where RLP4 exhibited the highest expression, driven by the endogenous promoter (Figure 15E). In addition, *rlp4 r4l1* double mutants did not reveal a significant difference in shoot apical meristem size, number of cells and mean cell size compared to Col-0 (Figure 18B-D).

.

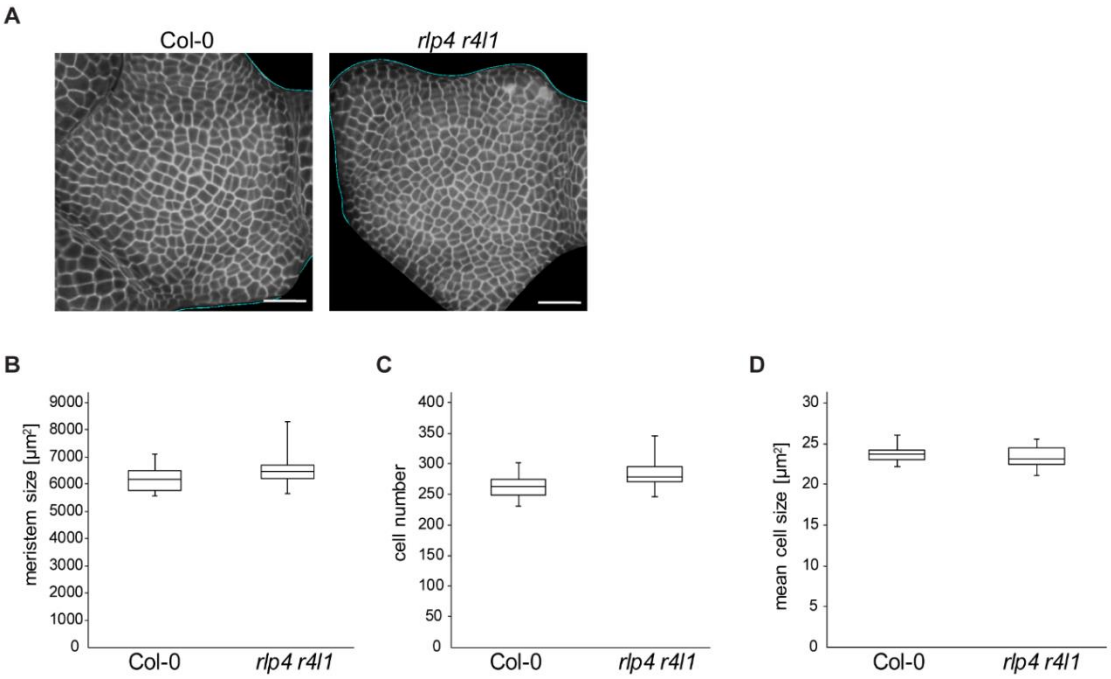

Figure 18. Mutations in *RLP4* and *R4L1* do not change SAM morphology. (A) Representative images of Col-0 and *rlp4 r4l1* shoot apical meristems, top view. SAMs were stained with PI. Scale bar: 20 µm (B) Quantification of shoot apical meristem size (C) cell number and (D) mean cell size in Col-0 and *rlp4 r4l1*. Shoot apices were dissected from primary plant inflorescences, 40-45-day-old plants. Image analysis was performed using MorphoGraphX (mean ± SD, n=11) Student t-test reveal no significance between the two genotypes.

3.2.6 RLP4 and R4L1 do not control vascular cell fate

Studies of RLP44, which is closely related to RLP4 and R4L1 (Figure 12) indicated, that the cell wall signalling mutant *rlp44*^{cnu2} exhibited an increased number of metaxylem cells in the primary root (Holzwart et al., 2018). Although expression of RLP4 under the endogenous promoter only revealed weak expression in the vasculature, we aimed to test whether the *rlp4 rl41* double mutant exhibited a similar phenotype.

The vascular tissues comprise five xylem cells in the centre of the stele, oriented in one longitudinal axis. In the middle of the xylem axis, three metaxylem cells are located and encompassed by one protoxylem cell on each side. Periclinal to the xylem axis are the two phloem poles, comprising of companion cells and sieve elements. The procambium is embedded between xylem and phloem and is the stem cell niche for xylem and phloem cells.

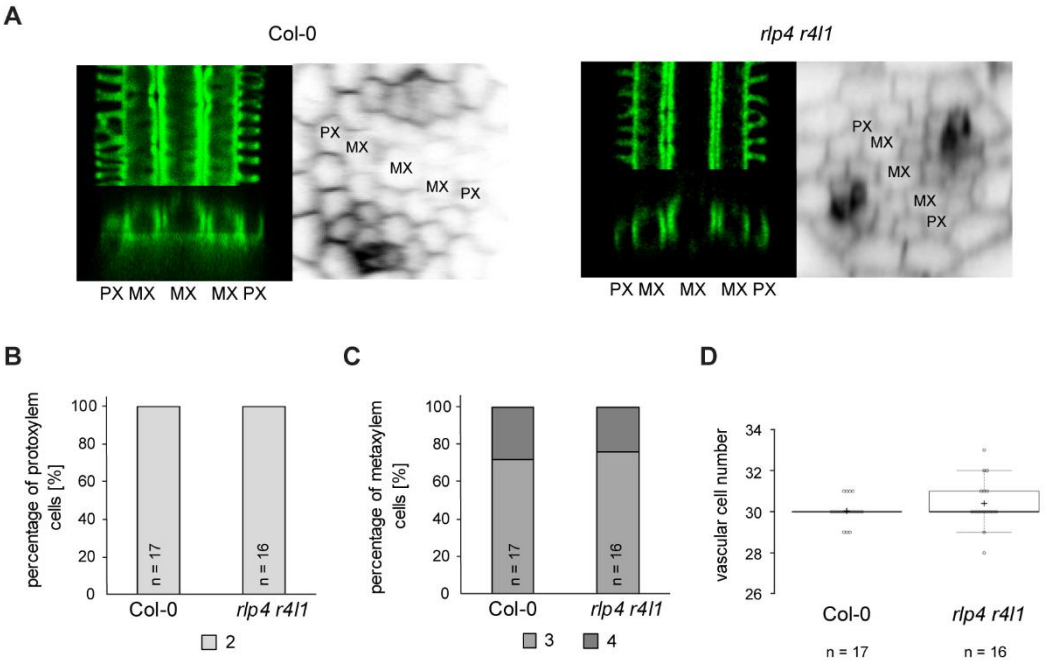

Figure 19. RLP4 and R4L1 might not regulate xylem cell fate in the root. (A) Representative images of longitudinal sections of proto- (PX) and metaxylem (MX) cells, stained with basic fuchsin (left) and cross sections of the vasculature depicting all vascular tissues, that were stained with calcofluor white (right). (B) Percentage of protoxylem cell numbers in Col-0 and *rlp4 r4l1*. Two protoxylem cells were counted in both genotypes (light grey). (C) Percentage of metaxylem cell numbers in Col-0 and *rlp4 r4l1*. Three (middle grey) or four (dark grey) metaxylem cells were counted in both genotypes. (D) Total vascular cell numbers of Col-0 and *rlp4 r4l1*. Col-0 (n=17), *rlp4 r4l1* (n=16). Pairwise t-test revealed no significance between Col-0 and *rlp4 r4l1*.

During vasculature differentiation, xylem cells develop a secondary cell wall that incorporates lignin. In order to investigate a potential function of RLP4 and R4L1 in the root vasculature, we stained lignin using basic fuchsin and stained cellulose using calcofluor white. Root vasculature was analysed in the differentiation zone, depicting fully differentiated proto- and metaxylem cells. Wild type roots always consisted of two protoxylem cells and three to four metaxylem cells in one plane axis (Figure 19A-C). In *rlp4 r4l1* double mutants no difference in protoxylem or metyxylem cell numbers (Figure 19A-C). In addition, cross sections of the root enabled counting of total cell numbers in the vasculature, only counting phloem, xylem and procambium cells. Col-0 wild type plants have in general a consistant number of 30 cells within the vasculature in the early differentitation zone of the root. *rlp4 r4l1* exhibited similar numbers of total vascular cells as Col-0 (Figure 19D).

3.2.7 *rlp4 r4l1* double mutants are hyposensitive towards salt stress

To further shed light on the function of RLP4 and R4L1 in plant development and their putative role in sensing cell wall properties, we treated *rlp4* and *r4l1* single and *rlp4 r4l1* double mutants with different cell wall interferring chemicals and compared root growth or hypocotyl growth to Col-0 wild type. It has been proven, that different chemicals interfere with cell wall homeostasis for instance by imbalancing the ion homeostasis or inhibit the synthesis of cell wall components. All of these effects might have an impact on growth and on root growth in particular.

First, we investigated the growth of Col-0, *rlp4* and *r4l1* single and *rlp4 rl41* double mutants on media containing increasing sodium chloride (NaCl) concentrations, ranging from 50 – 125 mM. Increased concentrations of NaCl in the surrounding environment can cause osmotic and ionic stress, which leads to cellular toxicity and limitations in water uptake (Bohnert et al., 1995; Niu et al., 1995; Feng et al., 2018). In roots, high salt concentrations often lead to altered growth rates and can result in radial cell expansion (Dinneny et al., 2008). Previous studies indicated that several mutants impaired in cell wall development and signalling displayed hypersensitivity to NaCl treatment, including *rlp44*^{cnu2} (Wu et al., 1996; Scheible et al., 2001; Wolf et al., 2014a; Zhao et al., 2018). In control conditions, *rlp4* and *r4l1* single and double mutants already depicted slightly longer roots than Col-0 (Figure 20A,B). At 125 mM NaCl conditions *rlp4* and *r4l1* and corresponding double mutants exhibited a significantly increased root growth compared to Col-0 wild type, indicating that single and double mutants are more tolerant towards higher salt concentrations than Col-0 (Figure 20A). This effect might be due to altered ion concentrations in cell compartments, ion transport, cell wall composition or cell wall signalling in the *rlp4* and *r4l1* single and double mutants. In addition to salt stress, we challenged the growth of *rlp4* and *r4l1* single and double mutants with isoxaben, a cellulose synthase inhibitor (Heim et al., 1990). Because the effect of isoxaben is quite strong on light grown seedlings, already at low concentrations, we performed the experiment in the darkness with four-day-old etiolated seedlings. In control conditions single and double mutants depicted longer hypocotyls compared to Col-0. A similar result was also investigated for the roots. Isoxaben treatment reduced the hypocotyl growth of all mutants and Col-0 wild type at elevated isoxaben concentrations (Figure 20B). Concentrations of 0.01 to 0.5 nM isoxaben had almost no effect on hypocotyl growth in all genotypes, whereas the highest applied concentration of 5 nM almost inhibited completely hypocotyl growth in the mutants and Col-0 (Figure 20B). *rlp4 rl41* double mutants depict a slight insensitivity to isoxaben at 1 nM concentrations, but these data require further validation.

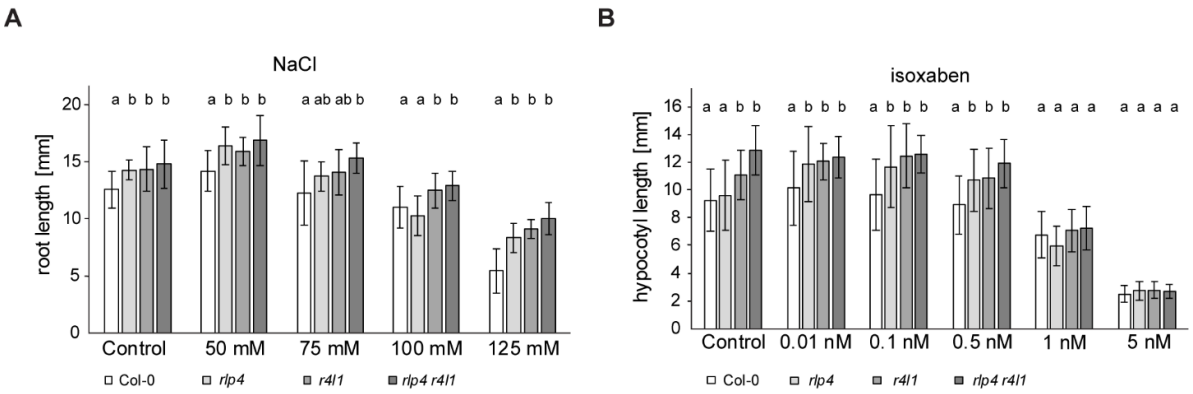

Figure 20. *rlp4 r4l1* single and double mutants are hyposensitive towards salt stress. (A) Absolute root length of six-day-old Col-0 wild type, *rlp4* and *r4l1* single and *rlp4 r4l1* double mutants germinated and grown on media containing indicated NaCl concentrations. Mean ± SD, representative graph of three technical replications, n=15-20. (B) Absolute hypocotyl length of four-day-dark grown Col-0 wild type, *rlp4* and *r4l1* single and *rlp4 r4l1* double mutants on media supplemented with indicated isoxaben concentrations. Mean ± SD, representative graph of three technical replications, n=20-25. Significance was tested by ANOVA with post-hoc tukey. Experiments and data analysis were performed by Enric Bertran Garcia de Olalla, supervised by A.-K. Schürholz.

.

In summary, the *rlp4 r4l1* double mutant exhibited slightly longer roots at standard conditions and hyposensitive root growth in response to 125 mM NaCl concentrations compared to Col-0 wild type. Thereby, *rlp4 r4l1* double mutants depicted an antagonizing phenotype to *rlp44* mutants, which were hypersensitive on elevated NaCl concentrations (Wolf et al., 2014a). It can be presumed, that RLP4 and R4L1 are involved in an RLP44-independent function. On the other hand, inhibition of cellulose synthesis, led to a slight reduction in hypocotyl growth.

3.2.8 *rlp4 r4l1 r4l2 r4l3* quadruple mutants depict elevated root growth

Based on the phylogenetic analysis of RLPs, we speculated that the *RLP4-R4L* clade of RLPs might exhibit some degree of functional overlap among these sub-family members. This might be the reason, why we did not observe severe macroscopic and developmental phenotypes of the *rlp4 r4l1* double mutant. To further investigate the function of the *RLP4-R4L* gene family, we generated *rlp4 r4l1 r4l2 r4l3* quadruple mutants using the CRISPR/Cas9 genome-editing technique. Similar to the generation of the *rlp4 r4l1* double mutant, a suitable gRNA for each target gene, *R4L2* and *R4L3*, was designed by using the ChopChop webpage, targeting the beginning of exon 2 (Figure 21A,B). Several *R4L2* mutant alleles were obtained harbouring a

nucleotide insertion and thereby introducing a frame shift causing a pre-mature stop codon 35 codons downstream of the insertion. Either an adenosine (a), a cytidine (c) or a thymidine (t), was inserted after the nucleoside at position 199 downstream of the ATG in the gDNA sequence. In lines #14-3/14-19, the insertion of "t" introduced an amino acid exchange at position S38F of the amino acid sequence, lines #14-6/26-3 carried a "c" insertion causing the exchange of amino acid at position V39R and the insertion of an "a" in line #26-2 led to the exchange at position S38Y. The insertion caused an exchange of amino acids and a subsequent frame shift in the amino acid sequence in all these lines. As a fourth mutant allele we identified a 30 nucleotide in-frame deletion, resulting in a loss of ten amino acids (CGASSSSVID) in lines #21-7/21-13. The deletion is located after 165 bp downstream of the ATG in the gDNA sequence and at position C32G in the amino acid sequence. For *R4L3*, also three nucleotide insertion alleles were identified leading to a pre-mature stop codon 15 codons downstream of the insertion site. Either an adenosine (a), a cytidine (c) or a thymidine (t), was inserted after the nucleoside at position 189 downstream of the ATG in the gDNA sequence. In line #14-3/14-19, the insertion of "c" led to an amino acid exchange at position P42T of the amino acid sequence, lines #21-7/21-13 carried a "t" insertion leading to the exchange of amino acid at position T41I and the insertion of an "a" in the lines #26-2/26-3 led toan amino acid exchange at position T41N. The insertion led to an exchange of amino acids and a subsequent frame shift in the amino acid sequence in all these lines. As a fourth mutant allele we identified a 21 nucleotide in-frame deletion, resulting in a loss of seven amino acids (NLNEIEY) in the line #14-6. The deletion is located after 268 bp downstream of the ATG in the gDNA sequence and at position N34T in the amino acid sequence.

T_1 lines #14, #21 and #26 were bi-allelic for mutations in *R4L2* as well as for *R4L3*. Thus, for one allele, two different mutations can appear in the next generation (Figure 21C). Several independent quadruple mutant lines were phenotypically analysed in the T_3 generation. All six lines, except line #14-19, exhibited a similar phenotype on soil (Figure 21). However, quadruple mutants appeared to have slightly wider rosette leaves, or leaves are flattened compared to Col-0 wild type (25-day-old plants) (Figure 21D). Line #14-19 was smaller and had wrinkled rosette leaves (Figure 21D). Also the roots of line #14-19 six-day-old seedlings are significantly shorter compared to the other quadruple mutant lines and Col-0 wild type (Figure 21E). Since both lines, #14-3 and #14-19 harbour exactly the same mutations in *R4L2* and *R4L3* and all other quadruple lines exhibit a similar phenotype, line #14-19 most possibly contains an un-specific background mutation introduced by Cas9 in an off-target gene or from the T-DNA insertion (Zhang et al., 2018). Therefore, lines #14-3, #14-6, #21-7, #21-13, #26-2 and #26-3 were kept. As previously discussed, we hypothesised, that *rlp4 r4l1* double mutants did not depict a severe macroscopic or microscopic phenotype, because of a possible functional redundancy of the RLP4 clade.

However, initial macroscopic phenotyping revealed only a mild rosette phenotype (Figure 21D) and slightly longer roots in *rlp4 r4l1 r4l2 r4l3* quadruple mutants compared to Col-0 wild type (Figure 21E).

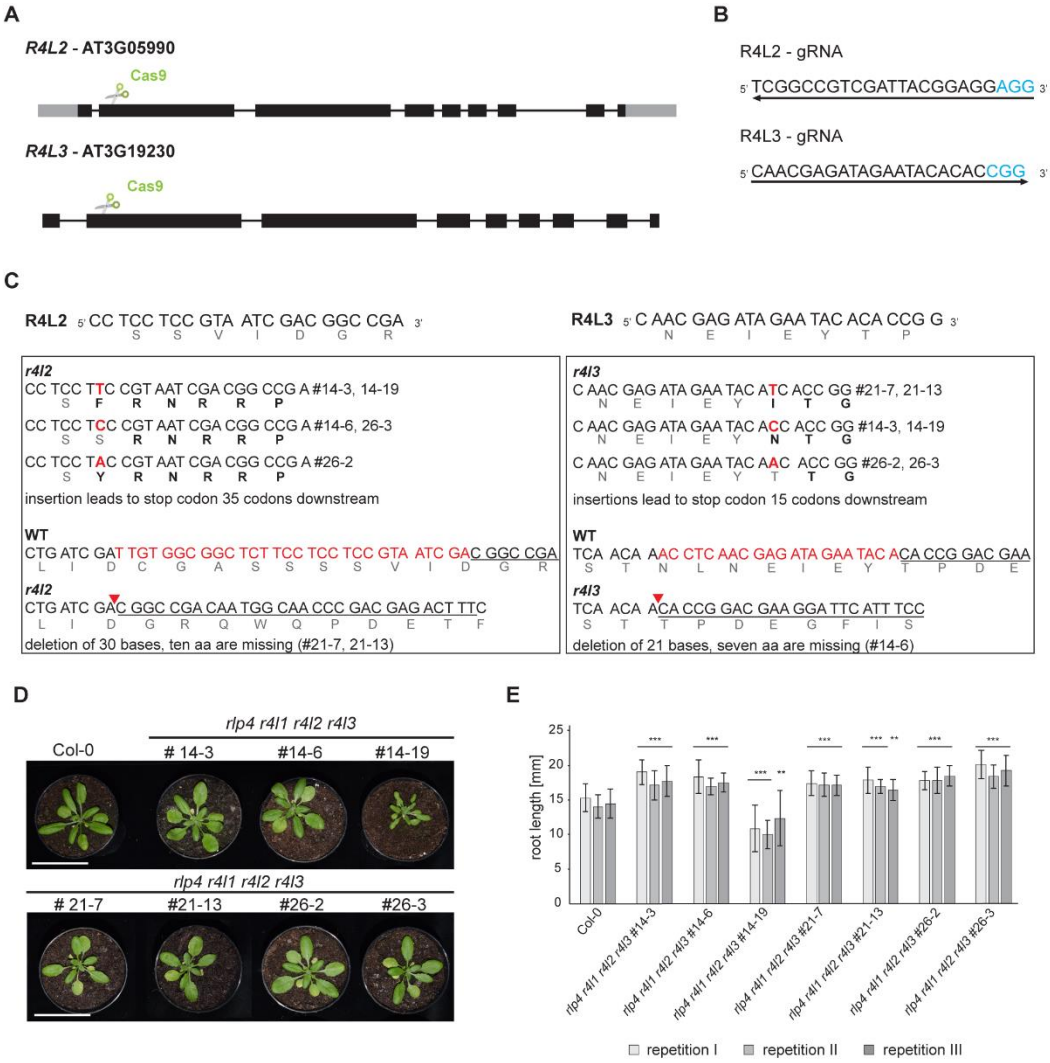

Figure 21. Design and phenotypic analysis of *rlp4 r4l1 r4l2 r4l3* CRISPR/Cas9 mutants. (A) Overview of the two target genes *R4L2* and *R4L3* with 5'- and 3'- UTRs (grey boxes), exons (black boxes) and introns (black lines). Scissors indicate Cas9 target site. (B) gRNA orientation and sequences of the two target genes with PAM sequence indicated in blue. (C) *R4L2* and *R4L3* WT sequences in proximity of the target region. Amino acid sequences are indicated below. Mutant alleles of *R4L2* and *R4L3* are depicted in the boxes below together with the changes in gDNA and amino acid sequences (D). Images of 25-day-old Arabidopsis T_3 plants with indicated genotypes. Scale bar: 5 cm. (E) Root length measurements of six-day-old Col-0 wild type and quadruple mutant alleles (T_3). Statistically significant differences from Col-0 per repetition after pairwise t-test (*p<0.05, **p<0.01, ***p<0.001). Three technical repetitions, n=15-20 per repetition.

3.2.9 RLP4-ECD associates with the cell wall

RLP4 and its subfamily of R4Ls comprise a unique feature in the family of RLPs in *A. thaliana*, the malectin-like (Mal) domain. This extracellular domain (ECD) is known to bind carbohydrates in Xenopus (Schallus et al., 2008). Thus, the malectin-like domain of RLP4 and the R4Ls making them to putative cell wall binding proteins in Arabidopsis.

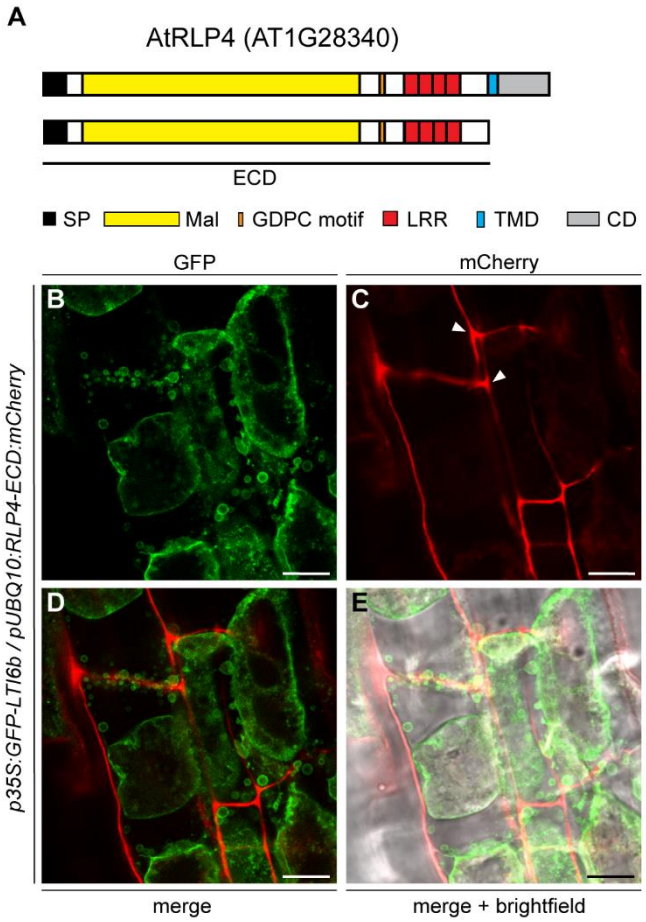

Figure 22: RLP4-ECD associates to the cell wall in lateral roots. (A) Schematic overview of RLP4 full length protein with the signal peptide (SP), malectin-like domain (Mal), GDPC motif, LRRs, the transmembrane domain (TMD) and the cytosolic domain (CD). RLP4 extracellular domain (RLP4-ECD) lacks TMD and CD. (B-E) *pUBQ10:RLP4-ECD:mCherry* and plasma membrane marker *p35S:GFP:LTI6b* in Arabidopsis lateral root cells (seven day-old). For plasmolysis, seedlings were incubated in 0.6 M sorbitol. (B) GFP-LTI6b is localized at the plasma membrane of plasmolysed cells. (C) RLP4-ECD:mCherry attaches to the cell wall with increased signals in cell wall edges (white arrow heads). (D) Merged GFP and mCherry channels. (E) Merged channels of GFP, mCherry and brightfield. Scale bars = 10 µm.

To test this hypothesis, we fused the ECD of RLP4 to mCherry (*pUBQ10:RLP4-ECD:mCherry*) and investigated the localization of this construct in transgenic Arabidopsis plants. The RLP4-ECD construct contains the signal peptide, the malectin-like domain, the GDPC motif and LRRs, which leads to secretion into the apoplast (Figure 22A). The plasma membrane bound GFP-LTI6b cannot associate with the cell wall and served as negative control and plasma membrane marker (Cutler et al., 2000). The *p35S:GFP-LTI6b* construct was stably expressed in Arabidopsis and crossed with the stable Arabidopsis line *pUBQ10:RLP4-ECD:mCherry.* Descendenats of the cross were used for plasmolysis experiments. To study putative cell wall association of RLP4-ECD, we incubated plant tissues in a hypertonic solution, which leads to plasmolysis, meaning the detachment of the plasma membrane from the cell wall. Therefore, plasma membrane binding can be distiniguished from cell wall binding. For plasmolysis analysis seven-day-old seedlings expressing *p35S:GFP-LTI6b* together with *pUBQ10:RLP4-ECD:mCherry* were incubated in 0.6 M sorbitol. After 20 min, plasmolysis was clearly visible for epidermis and cortex cells of lateral roots (Figure 22B,D,E). RLP4-ECD:mCherry exhibited an increased signal at the cell walls with a maximum fluorescence intensity in cell edges (Figure 22C). This accumulation is a clear indication of an association of RLP4-ECD with cell wall components, especially in the cell edges. In contrary, GFP-LTI6b located at the plasma membrane (Figure 22B).

To gain further insights into the function and interaction of proteins with other proteins or ligands, such as hormones or cell wall components, we can make use of crystal structure analysis. Although, the crystal structure of the extracellular domain of RLP4 is not yet explored, we can make use of recent studies of ANX1 and 2, CrRLK1L proteins, that contain malectin-like domains (Moussu et al., 2018).

To predict the crystal structure of RLP4-ECD protein, we used Phyre2 (http://www.sbg.bio.ic.ac.uk/phyre2/html/page.cgi?id=index). The prediction is based on similar amino acid sequences and protein domains. For AtRLP4, the ANX1 crystal structure served as a template (PDB 6fig) 85 % of the RLP4 protein could be predicted and modelled (Figure 23). The ribbon diagram of RLP4 shows the malectin-like (Mal) domain at the N-terminal moiety of the protein (Figure 23A). Due to the similar structure of this domain compared to the ANX1 and 2 malectin-like domains, it is likely, that RLP4 harbours two tandem malectin-like domains, termed mal-N and mal-C (Moussu et al., 2018). The four LRRs are depicted by the parallel β leaflet structure and are followed by the transmembrane domain (green) and the short cytoplasmic tail (red) (Figure 23A). Surface representations of RLP4 reveals a deep cleft in the N-terminal moiety of the malectin-like domain and might be a putative area for binding of cell wall components (Figure 23B,C, black triangles).

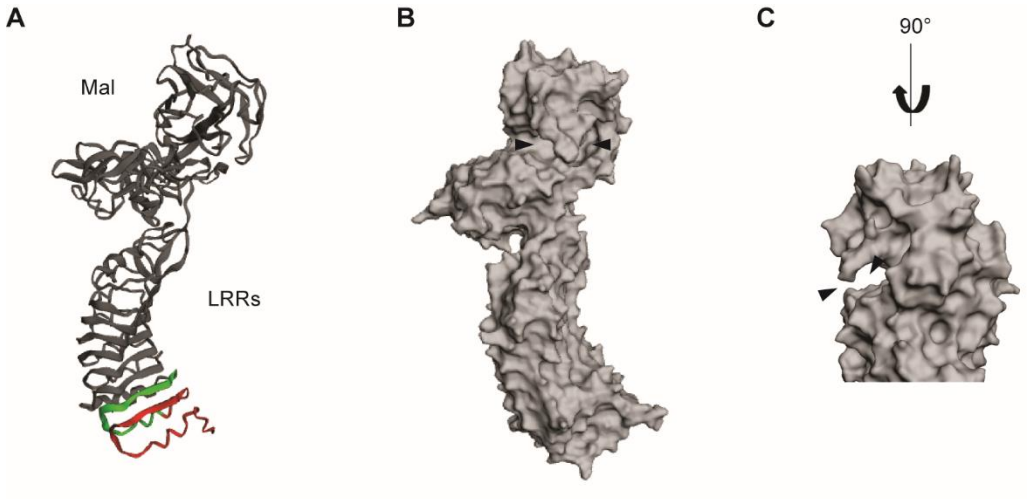

Figure 23. Predicted 3D protein structure of AtRLP4. (A) Ribbon diagram of AtRLP4 depicts the extracellular domain with LRRs and malectin-like domain in gray (Mal), the transmembrane domain (TMD) in green and the cytosolic domain (CD) in red. (B) Surface representation of AtRLP4 reveals a deep cleft in the malectin-like domain (black arrows). (C) Close up and side view of the cleft (black arrows). AtRLP4 strucutre was modeled using Phyre2 and EzMol based on the ANXUR1 structure (PDB 6fig) as a template.

In summary, we could identify, that RLP4-ECD associates with cell wall components in lateral roots. Therefore, RLP4 might be a putative cell wall signalling components. In the future, mutational anaysis of amino acids forming this cleft could help to unravel a potential function of the RLP4 Mal-domain in binding to cell wall components. Furthermore, douple and quadruple RLP4 and RLP4-like mutants displayed slightly longer roots in standard growth conditions, which has to be further analysed by induction of mechanical cell wall stresses and subsequenct CLSM analysis. In addition, immunolabelling of cell wall components in the mutants might reveal further insight into the function of RLP4 in cell edge localisation.

3.3 Discussion

3.3.1 RLP4 and R4L subgroup proteins are highly conserved

Previous phylogenetic analysis of RLPs in *A. thaliana* grouped 57 proteins into the RLP family (Wang et al., 2008). Recently, three un-identified RLPs were discovered that form a subgroup of RLP4 and also contain the malectin-like domain that is unique for RLPs (Sebastian Augustin, Master thesis 2015; this study). The analysis of a phylogenetic tree of 60 RLPs (Figure 12) revealed that RLP4 and the subgroup R4L form one group, which is evolutionary distinct to other RLPs, because of their extracellular malectin-like domain. Within this group, R4L2 and R4L3 form a sub-clade, because they do not contain the transmembrane domain. These proteins are not characterized and their localizations have not been determined yet (Bellande et al., 2017).

Cell wall binding capacities have been proposed for malectin-like containing proteins such as the RLP4-R4L group IV (Figure 12) (Boisson-Dernier et al., 2011). Structurally, RLP4 and R4L1 are similar to the *Lotus japonicus* SYMRK, which has comparable protein domains like the two RLPs, but additionally contains an extracellular kinase domain, which is missing in all RLPs (Antolín-Llovera et al., 2014). The malectin-like domain in SYMRK is cleaved at the conserved GDPC motif, located between the malectin-like domain and LRRs. After processing and cleavage of the malectin-like domain, LRRs can bind to NFR5, necessary for symbiosis (Antolín-Llovera et al., 2014). The GDPC motif is as well present in RLP4 and the R4L subgroup and most of the Mal-LRR-RLKs, such as IOS1 (AT1G51800) and MEE39 (AT3G46330) do contain the GDPC motif. One can speculate, that the processing of the malectin-like domain in LjSYMRK is necessary to enable the interaction of the actual binding domain in the LRRs to obtain protein-protein interaction with NFR5. Therefore, the malectin-like domain could 1) not be involved in association with cell wall components and the actual binding is through LRRs or 2) the malectin-like domain could shield the LRRs and prevent constitutively protein-protein interaction, which might be more likely. It is possible, that the malectin-like domain is only processed upon association with a specific component in the cell wall or the apoplast and due to this binding, the protein is processed, released and downstream signalling is activated.

Processing of RLP4 at the GDPC motif has not been observed yet (Augustin, 2015). It is possible, that RLP4 and R4L1 acquired different functions in non-symbiontic plants like a putative cell wall binding function and cell wall signalling processes. On the other hand, it might be, that processing could not be observed, because specific external stimuli are required or it only occurs in certain tissues. SYMRK-homologous Receptor-like kinase1 (SHRK1, AT1G67720) and SHRK2

(AT2G37050), the closest homolgous of SYMRK in Arabidopsis, do not contain the Mal-domain, but are LRR-RLKs and involved in plant immunity (Ried, 2014).

Our phylogenetic results revealed, that all four RLPs that contain the malectin-like domain are well conserved and RLP4 and R4L1 are even conserved in the evolutionary old plant species *Marchantia polymorpha* (Figure 13). However, the missing intracellular kinase domain would suggest an interaction presumably with a protein kinase domain-containing protein, to convey signals from the apoplast via the plasma membrane to the cell interior and activate downstream signalling cascades, although the missing cytoplasmic protein kinase domain does not exclude the interaction with other proteins via the cytoplasmic domain. To identify putative protein interactors and downstream signalling members of RLP4, crucial future experiments would be to perform IP-MS. Additonally, it would be also appealing to identify the function of R4L2 and R4L3, because they contain the malcetin-like domain, but no transmembrane domain.

3.3.2 RLP4 might be a putative cell wall binding protein in cell wall edges

Malectin-containing proteins in animals are located in the endoplasmatic reticulum and are involved in protein N-glycosylation (Schallus et al., 2008 and 2010). The malectin domain harbours a carbohydrate binding site which allows binding of ligands consisting of di-glucose-high-mannose-N-glycans (Schallus et al., 2008 and 2010). The homologues domain in plants is the malectin-like domain, that is located in the extracellular domain of plasma membrane proteins. Due to the carbohydrate binding capability of malectin domains in animals, it was hypothesised, that malectin-like containing proteins in plants are putative cell wall binding proteins (Boisson-Dernier et al., 2011). The so far best studied groups of malectin-like containing proteins in *A. thaliana*, is the group of CrRLKL1, comprising 17 proteins, consisting for instance of FER, THE1, ANX1 and 2. For FER1, direct association with polygalacturonic acid (PGA) could be identified (Feng et al., 2018) and THE1 can associate with pectate (Herman Höfte, personal communication). Recently, the crystal structures of the malectin-like domains of ANX1 and 2 were revealed, albeit several carbohydrate polymers could not been identified as ligands of ANX1 (Moussu et al., 2018).

Within this study, we identified localization of RLP4 to cell edges in epidermal cells in the differentiation zone of the root. In the SAM, RLP4 is expressed in epidermal cells with a maximum intensity in the periphery, especially in the area of the future forming crease of primordia (Figure 15). This expression pattern is similar to the expression of *SHOOT MERISTEMLESS* (*STM*), a transcription factor involved in regulating meristem functionality by repressing differentiation

(Landrein et al., 2015a). *STM* is upregulated due to mechanical stresses and is required for organ separation (Landrein et al., 2015a). It might be, that STM is a putative negative regulator of RLP4, or the expression of RLP4 and R4L1 could be directly, presumably negatively, controlled by WUS, because two WUS binding peaks were identified in *RLP4* and three in *R4L1* (Miotk, 2015).

As identified in this study, RLP4-ECD can associate to cell wall components in the lateral root (Figure 22). Intriguingly, strong RLP4-ECD signals were, similarly to expression of the full RLP4 protein, associated to cell wall components in cell edges. Hence, RLP4 might be involved in cell wall signalling processes not only in the root, but presumably also in the shoot meristem. Additionally, evidence comes also from collaborative work revealing that RLP4 and R4L1 co-localized in RAB-A5c compartments (Charlotte Kirchhelle, personal communication). RAB-A5c is a GTPase of the RAB (ras-like small GTPases) family of membrane-trafficking regulators and expressed in young lateral roots and young primary leaves (Kirchhelle et al., 2016). On the cellular level, RAB-A5c is localized to cell plates and shuttles from TGN to “RAB-A5c” compartments. These compartments accumulate at the plasma membrane mainly at cell edges in epidermal cells (Kirchhelle et al., 2016). Mutants in RAB-A5c lost the cell edge localization and exhibit a strong mutant phenotype with reduced root length, reduced root hair elongation and lateral roots with irregular cell geometries and incomplete cytokinesis or oblique cell walls compared to Col-0 wild type (Kirchhelle et al., 2016). Therefore, the transport of RAB-A5c compartments to the plasma membrane and the cell plates seems to be pivotal for cell division and cell growth in lateral roots (Kirchhelle et al., 2016). Recent studies could identify RLP4 and R4L1 co-localizing with RAB-A5c within these compartments (Charlotte Kirchhelle, personal communication). Together with our findings, that RLP4 is expressed in the epidermis in the primary root, specifically in cell edges, the shoot apical meristem, the surrounding primordia and the lateral roots, we can suggest that RLP4 and R4L1 are transported within RAB-A5c compartments to the plasma membrane, mainly to cell edges. This hypothesis is supported by experiments with Arabidopsis lines, expressing the RAB-A5c mutant version and *RLP4:GFP* or *R4L1:GFP* driven by the endogenous promoter. Here, RLP4 and R4L1 did not longer localize to the plasma membrane and cell edges (Charlotte Kirchhelle, personal communication). Therefore, the absence of RLP4 and R4L1 at the plasma membrane might cause the severe phenotype in RAB-A5c plants.

The fact, that RLP4-ECD is binding to cell wall components, specifically to cell wall edges in the epidermis of lateral roots, might hint to a function of RLP4 in cell wall signalling in these areas or RLP4 might assist in getting edge cell wall material transported to the plasma membrane. Computational analysis revealed, that reduction in cell wall edge stiffness led to changes in cell geometry resulting in inflated cells in the epidermis (Kirchhelle et al., 2016b). A recent study could demonstrate for epidermal cells in the hypocotyl, that isotropic cells depict the same stiffness in

all cell walls. During anisotropic growth, longitudinal walls are becoming softer then transverse walls to enable cell expansion (Peaucelle et al., 2015).

These findings might support the hypothesis, that RLP4 and R4L1 might be essential for cell wall signalling in the cell edge compartments of epidermal cells, maintaining stiffness during cell elongation to enable cell growth. However, *rlp4 r4l1* double mutants were not analysed in the lateral root regarding these phenotypes. In the future, analysis of a lateral root phenotypes in *rlp4 r4l1* double and *rlp4 r4l1 r4l2 r4l3* quadruple mutants will be crucial experiments. Furthermore, it would be essential to identify how RLP4-ECD is associating to cell wall components. Therefore, mutations in amino acids, that are predicted to be involved in ligand binding, have to be mutated and also different ECD deletion constructs have to be tested to identify, if the association is accomplished by the malectin-like domain.

3.3.3 Phenotypic analysis of *rlp4* and *r4l* mutants

Based on our hypothesis, that RLP4 is a putative cell wall sensor and might convey changes in the cell wall state to the cell interior via cell wall signalling processes, interfering with cell wall composition in the *rlp4 r4l1* double mutant can lead to alterations in plant development. The cell wall signalling mutant *rlp4* is hypersensitive towards elevated NaCl concentrations, whereas *rlp4 rl41* is more resistant to NaCl on high concentrations compared to Col-0 (Figure 20). Isoxaben treatment, a cellulose synthesis inhibitor did not show a significant effect. *rlp4 r4l1* double as well as *rlp4 r4l1 r4l2 r4l3* quadruple mutants depicted under normal conditions longer roots compared to Col-0 (Figure 20, Figure 21). Due to the absence of RLP4-R4L1 in cell edges, it might be possible that reduced cell wall signalling this location leads to softening of cell walls and increased cell elongation, resulting in longer primary roots (Peaucelle et al., 2015). Because *RLP4* is mainly expressed in the epidermis, changes in the epidermis can have effects on the whole plant morphogenesis revealed for the shoot apical meristem (Gruel et al., 2016; Kimura et al., 2018). Additional mutations of *R4L2* and *R4L*3 in the *rlp4 r4l1* double mutant line does not increase the root length phenotype at standard conditions, but it is not known, if the additional mutations in *R4L2* and *R4L3* have an effect on the microscopic phenotype or if they are even present in the RAB-A5c compartments. These would be important future experiments to gain more insights into the function of the RLP4 clade proteins. Furthermore, *rlp4 r4l1* and *rlp4 r4l1 r4l2 r4l3* quadruple mutants can be incubated in hypotonic solutions in comparison to Col-0, to analyse how the cells bulge at the edges.

4 Unravelling the function of *CLE SIGNALLING COMPONENT1* (*CSC1*)

4.1 Introduction

Pluripotent stem cells in the three meristems, shoot and root apical meristem and (pro)cambium, enable developmental plasticity to adapt to extrinsic and intrinsic cues such as light, pathogens, salt stress or cell division, expansion and the sugar state of the cell, respectively (Cosgrove, 2005; Janocha and Lohmann, 2018). To be able to adapt to changing environmental or developmental conditions, all these varieties of signals have to be processed and integrated into responses adequate to the conditions (Janocha and Lohmann, 2018). These mechanisms involve for instance phytohormonal networks, peptides and transcription factors, that have to be spatio-temporally controlled to maintain developmental plasticity in plants (Janocha and Lohmann, 2018).

4.1.1 The auxin signalling pathway

The auxin signalling pathway is besides cytokinins (CK), brassinosteroid (BR), gibberellic acid (GA) and abscisic acid (ABA), one major phytohormone signalling pathway in plants and is well studied in Arabidopsis. It is involved in a plethora of developmental processes such as organ initiation, cell type specification, root stem cell maintenance and stress responses (Weijers and Wagner, 2016). Indole-3-acetic acid, the most active form of auxin, is a tryptophan derivative and synthesized by TRYPTHOPHAN AMINOTRANSFERASE OF ARABIDOPSIS (TAA1) and YUCCA (YUC) family proteins, which are key players in the multiple-step auxin biosynthesis pathway (Cheng, 2006, Stepanova et al., 2008; Mashiguchi et al., 2011). The direct auxin receptor is TRANSPORT INHIBITOR RESPONSE 1 (TIR1), which is together with AUXIN SIGNALING F-BOX (AFB) family members, part of the SKP1-CUL1-F-box (SCF) E3 ubiquitin ligase complex, located in the nucleus (Gray et al., 2001). In conditions with low levels of auxin, the transcriptional repressors of the AUXIN/INDOLE-3-ACETIC ACID (AUX/IAAs) family bind to AUXIN RESPONSE FACTORs (ARFs) (Weijers et al., 2005; Li et al., 2016b). In the presence of auxin, AUX/IAAs are degraded and ARF TFs can bind to auxin-response target genes (Calderón Villalobos et al., 2012). An important transcription factor is for instance ARF5/MONOPTEROS (MP), responsible for vascular development and patterning in the SAM (Hardtke, 1998; Bhatia et al., 2016). A direct target of MP is *TARGET OF MONOPTEROS 5* (*TMO5*), which is crucial to establish vasculature tissues in the early embryo (Ohashi-Ito et al., 2013). Although the auxin signalling pathway does

not consist of many key components or modules, it is highly modular with for instance 29 AUX/IAAs or 22 ARFs in Arabidopsis, allowing dynamic fine tuning of auxin signalling in different developmental processes or tissues (Calderón Villalobos et al., 2012). Auxin often acts away from its side of synthesis and establishes morphogenetic gradients, which are concentration dependently (Vernoux et al., 2010; Tian et al., 2013). To reach cells in which it is not actively synthesised, the protonated form of auxin can cross membranes, but needs to be actively exported (Petrasek and Friml, 2009). Several transporters are involved in auxin transport such as PIN-LIKEs (PILS), AUXIN 1/LIKE AUX1 (AUX1/LAX) and ATP-BINDING CASSETTE SUBFAMILY B (ABCB) proteins (Geisler et al., 2005; Yang et al., 2006; Petrasek and Friml, 2009; Peret et al., 2012; Barbez et al., 2012). Localization of auxin carrier proteins also determine where auxin maxima or minima are established and thereby regulating auxin patterning in the shoot and root apical meristem or the vasculature (Band et al., 2014; Bhatia et al., 2016).

4.1.2 The cytokinin signalling pathway

Cytokinins are N^6-substituted adenine derivatives, that are involved in a plethora of plant developmental processes such as cell proliferation, shoot initiation, stem cell maintenance, flower development, leaf senescence and vascular development (Kieber et al., 2018). Biosynthesis of cytokinin is a multistep process and is catalysed by several enzymes such as ISOPENTENYL-TRANSFERASEs (IPTs) (Miyawaki et al., 2006) or LONELY GUY (LOG), which catalyses the last step of the biosynthesis to active cytokinin (Kuroha et al., 2009). Inactivation of cytokinins can be achieved either by degradation via cytokinin oxidases (CKXs) or conjugation to sugars (Werner, 2003; Kieber et al., 2014). For many years, it was thought that cytokinins are exclusively synthesized in root tissues and are transported to the shoot. However, cytokinins are synthesized in several different tissues in the root and the shoot and are either transporter acropetally (root to shoot) or basipetally (shoot to root) (Park et al., 2017). Recent studies deepened our insight into the mechanistic details of long-distance transport of cytokinins either via influx or efflux transporters, but mainly achieved by xylem and phloem transport. G SUBFAMILY ATP-BINDING CASSETTE (ABCG) transporters were identified to be involved in long distance transport (Zhang et al., 2014; Ko et al., 2014) and PURINE PERMEASES (PUPs) are cytokinin importers, rather involved in short-distance signalling. Cytokinins are perceived by membrane bound ARABIDOPSIS HISTIDINE KINASEs (AHKs). Upon binding, autophosporylation of a conserved histidine in AHK leads to the activation of the two-component phosphorelay pathway, which is similar to the two-component signalling pathway in bacteria (Stock et al., 2000; Cheung and Hendrichson, 2011). The phosphate group is transferred from histidine to aspartate in the receiver

domain and subsequently relayed to the downstream components of ARABIDOPSIS HISTIDINE PHOSPHOTRANSFER PROTEINs (AHPs) (Riefler et al., 2006). AHPs1-5 are positive regulators in cytokinin signalling, shuttle to the nucleus where they transfer the phosphoryl group to the receiver domain of AUXIN RESPONSE REGULATORs (ARRs) (Hwang and Sheen, 2001). In Arabidopsis, two different types of ARRs exist: type-A ARRs are negative regulators of the cytokinin response and do not contain a DNA-binding domain, but are induced by type-B ARRs, which contain a DNA-binding domain and promote expression of cytokinin response genes upon activation by AHPs (Hwang and Sheen, 2001). Many phytohormone pathways display crosstalk to a certain extent depending on the signalling pathway and the type of tissue or developmental stage (Chandler et al., 2015; Liu et al., 2017). For auxin and cytokinin signalling pathways, crosstalk was identified for instance in the shoot apical meristem or the vasculature. For protoxylem development, the expression of *AHP6*, a pseudo-histidine transfer protein, is crucial to establish low cytokinin signalling. AHP6 competes with AHPs1-5, thereby negatively regulates cytokinin signalling in the protoxylem (Mähönen et al., 2006; Chandler and Werr, 2015). In turn, AHP6 is positively regulated by auxin via MP and TMO5-LHW in the vasculature (Bishopp et al., 2011; Ohashi-Ito et al., 2014). Interestingly, cross-talk of cytokinin signalling via type-A ARRs was identified with several members of CLAVATA3/ENDOSPERM SURROUNDING REGION (CLE) family members, which are small peptides involved in a plethora of developmental process in plants (Wang et al., 2016).

4.1.3 CLE signalling

In Arabidopsis, the CLAVATA3/ENDOSPERM SURROUNDING REGION (CLE) family, comprises 32 genes, some of them with redundant functionality (Strabala, 2006). They encode for small, pre-pro-peptides with a conserved 14 amino acid CLE domain and give rise to 27 distinct CLE peptides (Yamaguchi et al., 2016). Proteolytic processing yield the active CLE peptides, that are secreted and bind to their receptors, which are LRR receptor-like kinases (RLKs) (Gao et al., 2012). In each Arabidopsis tissue, at least one of the 32 CLE genes is expressed, indicating that CLE peptides might be involved in a vast number of biological processes during plant development (Jun et al., 2010). Although many CLE peptides have not been functionally characterized yet, for several of them, functions in regulating stem cell homeostasis in the SAM, RAM and cambium, vascular formation or lateral root establishment could be identified (Betsuyaku et al., 2011 a). *CLAVATA3* (*CLV3*), the founding member and best-studied peptide in the CLE family is expressed in stem cells in the shoot apical meristem and controls the size of the apical meristem (Brand et al., 2000; Rojo et al., 2002). Upon binding of CLV3 peptide to its

receptor CLV1, downstream signalling cascades are activated, which leads to transcriptional repression of *WUS* (Schoof et al., 2000). In turn, *WUS* expression is required to promote *CLV3* expression in the stem cells (Laux et al., 1996; Mayer et al., 1998). As a consequence, CLV3-CLV1-WUS regulate, in a negative feedback loop, the stem cell maintenance in the shoot apical meristem (Schoof et al., 2000; Brand et al., 2000).

CLE40 is the closest relative of CLV3 and regulates stem cell maintenance in the root apical meristem (Hobe et al., 2003; Jun et al., 2008; Stahl et al., 2009). In the RAM, *CLE40* is expressed in differentiating vascular cells in the stele and in columella cells. By diffusion, CLE40 migrates into RAM initals, where it promotes the expression of its putative receptor, the *RLK ARABIDOPSIS CRINKLY4* (*ACR4*) (De Smet et al., 2008; Stahl et al., 2009). ACR4 can form heterodimers with CLV1, which is also the receptor for CLV3 in the shoot apical meristem (Stahl et al., 2013), and negatively regulates the expression of the homeodomain transcription factor WUSCHEL RELATED HOMEOBOX 5 (WOX5) (Sarkar et al., 2007). WOX5 is expressed in the quiescent centre (QC), the stem cell niche in the root apical meristem, which is surrounded by stem cell initial cells for columella, epidermis, cortex/endodermis, and stele (Scheres, 2007). Thus, the promoting effect of CLE40 on *ACR4* expression restricts *WOX5* expression to the QC and thereby restricts distal root meristem stem cells (Stahl et al., 2013).

In the third meristem, the cambium, CLE41/44 control cell proliferation by binding to their receptor PHLOEM INTERCALATED WITH XYLEM (PXY). CLE41/44 are expressed in phloem tissues and diffuse into cambium stem cells, where they can bind to PXY (Hirakawa et al., 2008; Etchells and Turner, 2010). Analogous to WOX5 in the RAM and WUS in the SAM, WOX4 maintains stem cells of the cambium. Interaction of CLE41/44-PXY supports cambial stem cell maintenance by suppressing xylem differentiation (Ito et al., 2006). In addition, the receptor for CLE45, BARELY ANY MERISTEM 3 (BAM3), which represses phloem differentiation upon CLE45 perception, was recently identified (Depuydt et al., 2013; Rodriguez-Villalon et al., 2014; Hazak et al., 2017). It was considered as putative CLE45 receptor, because *bam3* mutants did not show root growth inhibition in a CLE45 bioassay (Depuydt et al., 2013). Recently, CLE25 was identified as a component of long-distance signalling, conveying water-deficiency signals from the vasculature to leaves, where they associate with BAM receptors, affecting stomatal closure and abscisic acid synthesis (Takahashi et al., 2018).

Although several of the CLE peptides and their receptors are well studied, many functions of CLEs and their receptors are still unknown. CLE root growth sensitivity bioassays are an effective tool, to screen for mutants that might be putative CLE receptors (Kondo et al., 2011). For this, 17 CLEs (CLV3, CLE8, 9/10, 11 12, 13, 14, 16, 18, 19, 20, 21, 22, 27, 40, 45), which are considered as

root-active and inhibit root growth and protoxylem formation, can be tested in combination with putative mutants in CLE perception or signalling (Kondo et al., 2011).

4.1.4 Cross-talk of cytokinin and CLE signalling

Phytohormones as well as peptide signalling pathways are crucial players for plant development. In the last years, more and more studies revealed cross-talk between different phytohormone pathways, for instance auxin and cytokinin signalling pathways controlling vasculature, root and shoot apical meristem maintenance (Bishopp et al., 2011; Liu et al., 2017; Xie et al., 2018). As previously stated, cytokinin and CLE peptides control diverse developmental processes in plants and are often involved in vascular development (Ito et al., 2006; Mähönen et al., 2006; Hirakawa et al., 2008; Ohashi-Ito et al., 2014; Bishopp et al., 2011; Kondo et al., 2011; Qian et al., 2018).

In vascular tissues, distinct levels of cytokinin signalling are required to determine cell fate and patterning. In the xylem, protoxylem cells are characterized by *AHP6* expression, a negative cytokinin signalling regulator, resulting in low cytokinin signalling (Mähönen et al., 2006). Metaxylem cells are in contrast characterized by elevated cytokinin signalling (Ohashi-Ito et al., 2014). In addition, many CLE peptides were identified being active in root tissues and being involved in vascular development (Ito et al., 2006; Hirakawa et al., 2008; Kondo et al., 2011; Qian et al., 2018). 17 CLE peptides are known to inhibit root growth and protoxylem formation at elevated concentrations, such as CLE9/10, CLE45, CLE21 and CLE27 (Kondo et al., 2011; Hazak et al., 2017; Qian et al., 2018). It is likely, that CLE9/10 and other root-active CLEs, can modulate cytokinin signalling locally by binding to their CLE receptors and activate downstream CLE signalling (Kondo et al., 2011). It was assumed, that activated CLE signalling can regulate type-A ARRs, thereby interfering with the cytokinin signalling pathway (Kondo et al., 2011). However, many of the CLE receptors are still unknown and how the cross-talk of CLEs and cytokinin signalling is achieved and regulated in detail, remains elusive.

In conclusion, CLE peptide signalling and phytohormone signalling pathways are involved in a plethora of developmental processes. In particular, these pathways are essential for stem cell maintenance in the three main meristems, the SAM, RAM and cambium, in Arabidopsis.

4.1.5 The shoot apical meristem (SAM)

The SAM harbours the stem cells, that give rise to all above ground tissues. In the RAM, the individual root tissues are defined in concentric layers around the vasculature. Almost all root tissues arise from specific initial or progenitor cells positioned adjacent to the quiescent centre (QC). Thus, cell identity and clonal identity largely overlap. However, in the SAM, descendants of transient amplifying cells acquire cell fate independent of lineage, but strictly dependent on positional information (Laufs et al., 1998; Gaillochet et al., 2017). Therefore, various signalling networks have to control proliferation and differentiation processes and restrict them to specific domains within the meristem. As mentioned before, the key regulators in maintaining stem cells and thereby proliferation are the homeodomain transcription factor WUS and the secreted peptide CLV3 in the centre of the meristem. *WUS* is expressed in the cell layers underneath the stem cells in the organizing centre (OC) and moves through plasmodesmata apically into the central zone (CZ) (Yadav et al., 2011; Daum et al., 2014). In the CZ, WUS directly represses or induces a plethora of genes, *CLV3* is one of the positively regulated WUS target genes (Laux et al., 1996; Mayer et al., 1998; Yadav et al., 2013; Miotk, 2015). From stem cells, CLV3 diffuses to the OC, where it can bind to several homo- and heteromultimeric complexes formed by the LRR-RLKs CLV1 and its homologues BARELY ANY MERISTEM 1 and 2 (BAM1 and 2), CLV2, CORYNE (CRN) and RECEPTOR-LIKE PROTEIN KINASE 2 (RPK2) (Brand et al., 2000; Schoof et al., 2000; Ogawa et al., 2008; Bleckmann et al., 2009; Nimchuk et al., 2015; Shinohara et al., 2015). CLV3 binding to its receptors activates a downstream signalling cascade which in turn repress *WUS* expression (Betsuyaku et al., 2011). Thus, stem cell maintenance is mainly controlled by the negative feedback loop of WUS and CLV3. In addition to the main WUS-CLV3 pathway, stem cell identities are maintained by elevated cytokinin signalling, because the cytokinin transcription factors type-B ARRs 1, 10 and 12, activate *WUS* expression (Leibfried et al., 2005; Gruel et al., 2016). Thus, cytokinin signalling promotes the proliferation of undifferentiated cells and represses their differentiation through the activation of WUS (Gordon et al., 2009; Gruel et al., 2016).

Besides the tightly controlled proliferation zone in the centre of the meristem, various factors also control the differentiation zone in the periphery of the meristem, where new lateral organs are initiated in a highly organized manner contributing to a regular arrangement, named phyllotaxis (Mirabet et al., 2012). A key factor for primordia initiation is auxin (Cheng, 2006; Vernoux et al., 2010; Bhatia et al., 2016). *MP* is upregulated upon auxin signalling and positively regulates the expression of *AHP6,* which in turn negatively regulates CK signalling and the establishement of CK inhibitory fields (Mähönen et al., 2006a; Besnard et al., 2014a/b; Bhatia et al., 2016). Furthermore, MP stabilizes the auxin maxima by redirecting the localization of *PIN FORMED 1* (*PIN1*), the auxin efflux transporter towards domains of elevated auxin levels (Bhatia et al., 2016),

forming a positive feedback loop. In parallel to the auxin signalling pathway, numerous other factors are involved in differentiation processes in the periphery of the apical meristem. *KANADI 1* (*KAN1*), *KAN*2, *ASYMMETRIC LEAVES 2* (*AS2*), and *YABBY3* encode key transcription factors that are involved in the determination of lateral organs (Yadav et al., 2013). These genes were also identified as being directly repressed by WUS, to prevent differentiation in the centre of the meristem (Yadav et al., 2009; Yadav et al., 2013). The group of HD-ZIP III transcription factors *HOMEOBOX GENE8 (ATHB-8), CORONA (CNA)*, *PHABULOSA* (*PHB*), *PHAVOLUTA* (*PHV*) and *REVOLUTA* (*REV*) (Landau et al., 2015) specify the adaxial side of leaves and form together with the abaxial *KANADI* (*KAN1-4*) group the dorsiventral patterning of the vascular system in leaves (Ramachandran et al., 2016).

Proliferation and differentiation processes in the shoot apical meristem are thereby tightly controlled to enable cell growth, expansion and differentiation, while stem cell identities are maintained in the centre of the meristem.

4.1.6 The floral meristem (FM)

In the reproductive stage of Arabidopsis, the shoot apical meristem shifts from initiating lateral organ/leaf primordia to flower primordia. In the SAM, cells are pushed from the centre towards the periphery, where they can acquire flower primordia fates. The floral meristem (FM) is initiated in young primordia by re-establishing of WUS-CLV3 and elevated cytokinin levels (Chandler, 2012). In contrast to the indeterminate SAM, stem cells are no longer maintained after initiation of carpels in the FM (Lenhard et al., 2001). Termination of the FM is controlled by a second negative feedback loop, the interplay of WUS and the MADS-box transcription factor AGAMOUS (AG) (Lohmann et al., 2001). Together with the transcription factor LEAFY (LFY), WUS activates the expression of *AG* in the centre of the flower at stage 3, which in turn directly and indirectly represses WUS (Smyth et al., 1990; Lohmann et al., 2001; Sun et al., 2009). When carpel primordia form in stage 6 flowers, *WUS* mRNA is already undetectable (Sun et al., 2009; Liu et al., 2011). Besides the two crucial negative feedback loops, that establish and terminate the floral meristem, many other signalling cascades are involved in fine-tuning the stem cell population, floral patterning and organogenesis (Thomson et al., 2016). *LFY* is expressed throughout the floral meristem and is crucial for floral meristem initiation but also promotes the expression of four classes of floral homeotic genes: A, B, C and E (Winter et al., 2011). The homeotic genes define the four concentric whorls that give rise to flower organs (Coen et al., 1991). From the most outer whorl (whorl one) to the inner whorl (whorl four), the whorls develop to four sepals, four petals,

six stamens and two carpels and are forming the later flower (Coen and Meyerowitz, 1991). Each letter represents a class of transcription factors that are active in two adjacent whorls (Winter et al., 2011). Class A comprises APETALA1 (AP1) and 2 (AP2), which are active in whorl one and two, class B contains AP3 and PISTILLATA (PI), which are active in whorl two and three. Class C comprises AG and is essential to establish whorls three and four and to terminate the floral meristem (Lohmann et al., 2001). Class E transcription factors SEPALLATA 1 (SEP1), SEP2, SEP3 and SEP4, function in identity determination of the four flower organs (Pelaz et al., 2000). Additionally, genes apart of the flower homeotic genes are crucial for flower patterning such as *UNUSUAL FLOWER ORGANS* (*UFO*), or boundary genes such as *CUP SHAPED COTELYDONS* (*CUC*s) and genes involved in organ differentiation such as the aforementioned KANADI and HD-ZIP III transcription factors *ATHB-8, CNA, PHB, PHV and REV* (Landau et al., 2015).

4.1.7 The root apical meristem (RAM)

The root meristem is composed of concentric layers of specific tissues, whose development is tightly controlled and can be spatially traced back to the first transient amplifying tissue-specific stem cells (Dolan et al., 1993; Wachsman et al., 2015). In the centre of the RAM, four largely mitotically arrested cells form the organizing centre also termed Q of the root meristem (Dolan et al., 1993). The QC is surrounded by initial/progenitor cells of the different root tissues: Columella initials, epidermis initials, cortex/endodermis initials and stele initials (Scheres, 2007; Sozzani and Iyer-Pascuzzi, 2014). *WUS-RELATED HOMEOBOX 5* (*WOX5*) is expressed in the QC and diffuses into the adjacent cells repressing their differentiation (De Smet et al., 2008; Stahl et al., 2009). *CLE40*, the closest relative of *CLV3*, is expressed in the stele, can migrate into the initials, where it promotes expression of *ACR4*, which in turn represses *WOX*5 and restricts it to the QC (Sarkar et al., 2007). The stem cells for the different tissues divide asymmetrically by producing one stem cell and a daughter cell, also called transit-amplifying cell (Scheres, 2007). Auxin and cytokinin are crucial for stem cell maintenance in the root meristem (Bishopp et al., 2011a; Schaller et al., 2015). High auxin response signals are found in the area of proliferating cells, like columella stem cells, but also in the QC, and in xylem cells (Liao et al., 2015; Liu et al., 2017), whereas cytokinin response signals are strong in the stele, procambial initials and in the columella, but not in xylem precursor cells (Zurcher et al., 2013; Ohashi-Ito et al., 2014).

4.1.8 The cambium

Vascular elements are a key innovation during the evolution from water to land plants. These conducting tissues transport water, nutrients and small molecules and provide the mechanical support for upright growth (De Rybel et al., 2016). The cambium is a secondary meristem and harbours the stem cells for secondary phloem and xylem cells, thus contributes to lateral growth in many plants (Greb and Lohmann, 2016; Tonn and Greb, 2017). In the primary root of *A. thaliana*, xylem cells are located in the centre of the stele in a single-cell-wide axis containing three to four metaxylem cells and one protoxylem cell on each end of the xylem axis. Phloem tissues comprise four cells in each of the two phloem poles perpendicular to the xylem axis with procambium cells located between xylem and phloem cells (De Rybel et al., 2015). Early in embryogenesis, the vascular tissues are established by various factors such as phytohormones, transcription factors or small peptides (De Rybel et al., 2016). Xylem tissues are mainly specified through three important processes that involve several pathways: 1. Establishing corresponding phytohormone tissue patterns by cross-talk of auxin and cytokinin signalling and 2. Establishment of tissue boundaries and 3. Non-cell autonomous functions of HD-ZIP III and miR165/166 gradients in proto- and metaxylem formation.

Early in embryogenesis, the four provascular cells are already patterned by asymmetric auxin distribution. High auxin expression in two of the four provascular cells, leads to expression of MONOPTEROS (MP/ARF5), which is critical for vascular tissue formation (Hardtke et al., 1998). Subsequently, MP directly activates TMO5 which forms a complex with LHW (Ohashi-Ito et al., 2013; De Rybel et al., 2013). Upon this interaction, cells divide in a periclinal manner and thereby increase the vasculature cell number during development from four to around 30 cells in the mature root (Ohashi-Ito et al., 2007; Ohashi-Ito et al., 2013; De Rybel et al., 2013). In addition, TMO5-LHW activate local CK biosynthesis by directly activating the transcription of *LONELY GUY 3* and its homologue *4* (*LOG3* and *4*) (Kuroha et al., 2009). High cytokinin (CK) levels are on the one hand important for procambial identity and cell divisions in the vasculature, on the other hand they inhibit the differentiation of protoxylem (Mähönen et al., 2006a). The *wooden leg* mutant (*wol*) has a dominant negative mutation in *AHK4*/*CRE1*, which is a CK receptor localized mostly in the ER. This mutant depicts reduced periclinal divisions in the vasculature and additionally only differentiated protoxylem cells, whereas treatment with CK inhibits this increased protoxylem formation (Scheres et al., 1995; Mähönen et al., 2000). In contrast, high auxin levels specify protoxylem cells and the expression of *AHP6*, a negative CK signalling regulator, represses CK signalling in the protoxylem (Mähönen et al., 2006; Bishopp et al., 2011) (Figure 24A).

In addition to mutually inhibitory auxin and cytokinin response domains, *AT-HOOK MOTIF NUCLEAR LOCALIZED 3* (*AHL3*) and *AHL4* were identified as central genes in establishing a boundary between procambium and xylem cells (Zhou et al., 2013). Knockout of *AHL3* and/or *AHL4* leads to establishment of more proto- and metaxylem cells (Zhou et al., 2013) Figure 24B).

Furthermore, xylem patterning is also controlled by non-cell-autonomous function of SHR-SCR-miR165/166 (Greenham, 2010). The transcription factor *SHORT ROOT* (*SHR*) is expressed in the stele, moves into the endodermis where it activates the expression of the transcription factor SCARECROW (SCR) and induces the expression of the microRNA 165/166 (miR156/166) (Greenham, 2010). In turn, miR156/166 diffuse towards the centre of the root establishing a gradient with high levels in the periphery of vasculature tissues and low levels in the centre (Greenham, 2010). Direct targets of miR165/166 are the HOMEODOMAIN-LEUCINE ZIPPER

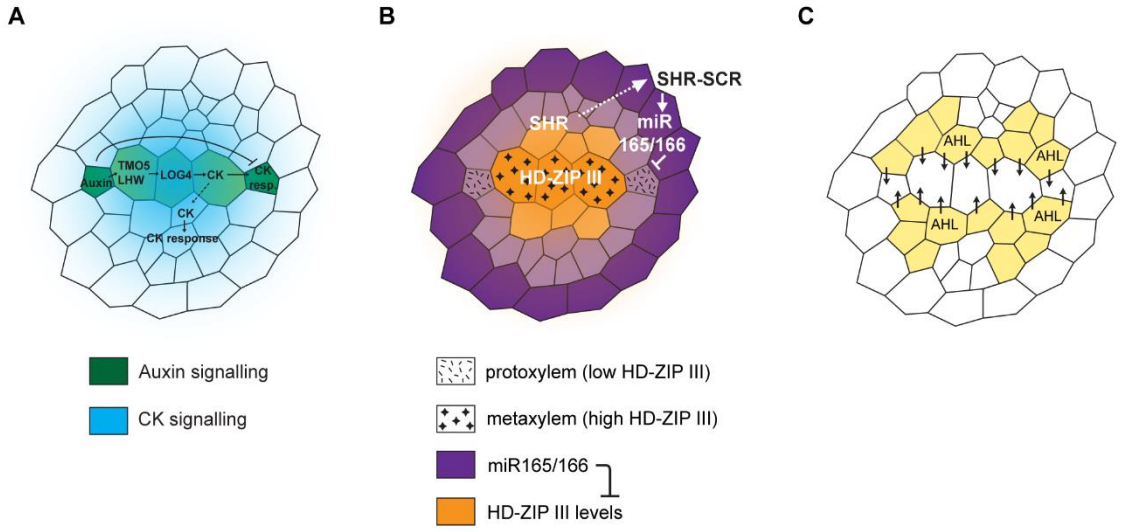

Figure 24. Networks involved in vascular development. (A) Auxin and cytokinin (CK) gradients establish proto- and metaxylem cells in the vasculature. Protoxylem cells are marked by elevated auxin levels, leading to expression of TARGET OF MONOPTEROS (TMO5), LONESOME HIGHWAY (LHW) and LONELY GUY 4 (LOG4). LOG4 synthesizes CK and establishes a cytokinin gradient in the metaxylem cells and the surrounding procambium. Elevated cytokinin levels trigger periclinal divisions in the procambium. ARABIDOPSIS HISTIDINE PHOSPHOTRANSFER PROTEIN6 (AHP6) is negatively regulated by cytokinin. (B) The transcription factors SHORT ROOT (SHR) and SCARECROW (SCR) promote expression of miRNA165/166 in the endodermis. miRNA165/166 diffuses towards the centre of the root and represses HD-ZIP IIIs in the outer xylem cells, leading to protoxylem formation. Higher HD-ZIP III concentration in the inner xylem cells differentiate into metaxylem cells. (C) AT-HOOK MOTIF NUCLEAR LOCALIZED (AHL) transcription factors are expressed in the procambium and establish the boundary between procambial and xylem cells. Modified after De Rybel et al., 2015.

Class III (HD-ZIP III) transcription factors *PHB*, *PHV*, *REV*, *CNA* and *ATHB-8* that are expressed in the root and shoot apical meristem (Prigge et al., 2004). In the outermost xylem cells, miR165/166 levels are still high enough to repress HD-ZIP III genes, which leads to the establishment of protoxylem cells (Du et al., 2015). In the centre of the stele, miR165/166 levels are too low to suppress genes leading to metaxylem cells (Du et al., 2015). Higher order mutants of HD-ZIP III genes depict ectopic protoxylem cells suggesting a default protoxylem differentiation programme in xylem cells (Greenham, 2010). Recent studies revealed putative downstream targets of *HD-ZIP III* genes, which are involved in xylem differentiation or secondary cell wall synthesis (Kubo et al., 2005; Yamaguchi et al., 2011; Liu et al., 2014; Taylor-Teeples et al., 2015) (Figure 24C).

Once specified, xylem cells have to differentiate into tracheary elements to be able to function as conductive tissues (De Rybel et al., 2015). Here, the NAC transcription factors VASCULAR-RELATED NAC-DOMAIN 6 (*VND6* and 7) control the differentiation into proto- and metaxylem cells and upregulate genes which are required for secondary cell wall biogenesis and programmed cell death (Ohashi-Ito et al., 2010; Yamaguchi et al., 2011). Activation of secondary cell wall synthesis results in lignin-rich cell walls in xylem cells with the characteristic ladder-like cell wall thickenings in the protoxylem or pits in the secondary cell wall of metaxylem cells (Schuetz et al., 2013 b).

4.1.9 Aims

Phenotypic and genetic characterizations of an originally derived CRISPR/Cas9 attempt to generate *rlp4 r4l1* double mutants exhibited severe phenotypes. These phenotypes were independent of the mutations in *RLP4* and *R4L1* mutations and comprised an increased shoot apical meristem, flower developmental permutations and alterations of vascular cell numbers, which were not reported so far. Analysis of the mutant by performing a CLE root growth bioassay, revealed a function in CLE perception or signalling, leading to the mutant name *cle signalling component1* (*csc1*). In this study, we aimed to attain the following goals:

A) Reveal the function of CSC1 in the shoot and the root apical meristem

B) Elucidate the role of CSC1 in CLE and cytokinin signalling

C) Identify the mutation/s in *csc1*

4.2 Results

4.2.1 CSC1 is required for normal growth in the shoot and the root

The *csc1* mutant was originally discovered in an approach to generate a *rlp4 r4l1* double mutant using the CRISPR/Cas9 technique where three independent alleles were identified for *rlp4 r4l1* (Figure 17C). Line #32-11 did not exhibit an obvious developmental phenotype, whereas lines #6-13 and #25-17 had enlarged shoot apical meristems in inflorescences and defects in flower development compared to Col-0 wild type (Figure 25). Initially, we assumed that mutations in *RLP4* and *R4L1* were causing the developmental phenotype in lines #6-13 and #25-17 and selected line #6-13 for experiments. While analysing segregating F_2 plants of line #6-13 with marker lines, we realized, that the shoot apical meristem and flower developmental phenotype was segregating independently of the *rlp4 r4l1* mutations. Thus, mutations in *RLP4* and *R4L1* were not causative for the developmental phenotype. However, due to the unique phenotype of the lines #6-13 and #25-17, we decided to unravel the mutation that was causing the developmental phenotype. To distinguish the different mutant lines, *rlp4 r4l1* #6-13 was named *cle signalling component 1* (referred to as *csc1*), because it depicted root growth insensitivity on CLE21 and CLE27 containing media. These results, described in 4.2.2, suggest a function of *CSC1* in CLE perception or signalling (Figure 28). It has to be mentioned that all phenotypic characterizations, CLE sensitivity assays and vasculature analysis of *csc1* were performed with the line *csc1* #6-13 still carrying the mutations in *RLP4* and *R4L1*. Experiments with *csc1* #6-13 crossed with marker lines were analysed in the F_3 generation and only plants wild type for RLP4 and R4L1 were used for experiments (Figure 34, Figure 36, Figure 35, Figure 38, Figure 39, Figure 40). Recently analysed plants of *csc1* backcrosses with Col-0 wild type revealed that mutation of *RLP4* and *R4L1* does not contribute to the *csc1* phenotype in a detectable manner.

csc1 mutant plants exhibited no obvious developmental phenotype in the vegetative stage compared to Col-0 wild type (data not shown). In the reproductive stage, 40-45-day-old plants with shoot lengths of around 15-20 cm had enlarged shoot apical meristems compared to Col-0 and defects in flower development (Figure 25). Defects in flower development did not occur in all flowers but appeared unregularly indicated by delays in fruit development or un-opened buds (Figure 25A-C). Furthermore, *csc1* plants also showed flower organ permutation based on the position of the siliques at the stem (white arrow heads, Figure 25B). Dissected un-opened buds revealed various defects in floral organ development such as presence of only two sepals or completely missing whorls for petals, stamens and carpels (Figure 25C, left). Some flowers had all four whorls but were not properly elongated, resulting in a small, underdeveloped gynoecium (white arrow head, Figure 25C, right). The most severe defects in flower development were

depicted by pedicels and completely missing flower whorls (white arrow heads, Figure 25D). Shoot apical meristems of c*sc1* seemed to be enlarged and encompass more primordia compared to Col-0 wild type (Figure 25E). *csc1* opened flowers often exhibited five to six petals instead of four (Figure 25F). The un-opened bud phenotype is reminiscent of the severe *clv3-10* phenotype, which additionally depicts a massively enlarged SAM, club-like siliques and a fasciated stem (Figure 25G). Although the other *clv3-10* phenotypes are not present in *csc1*, all phenotypes hint towards a function of CSC1 in the SAM.

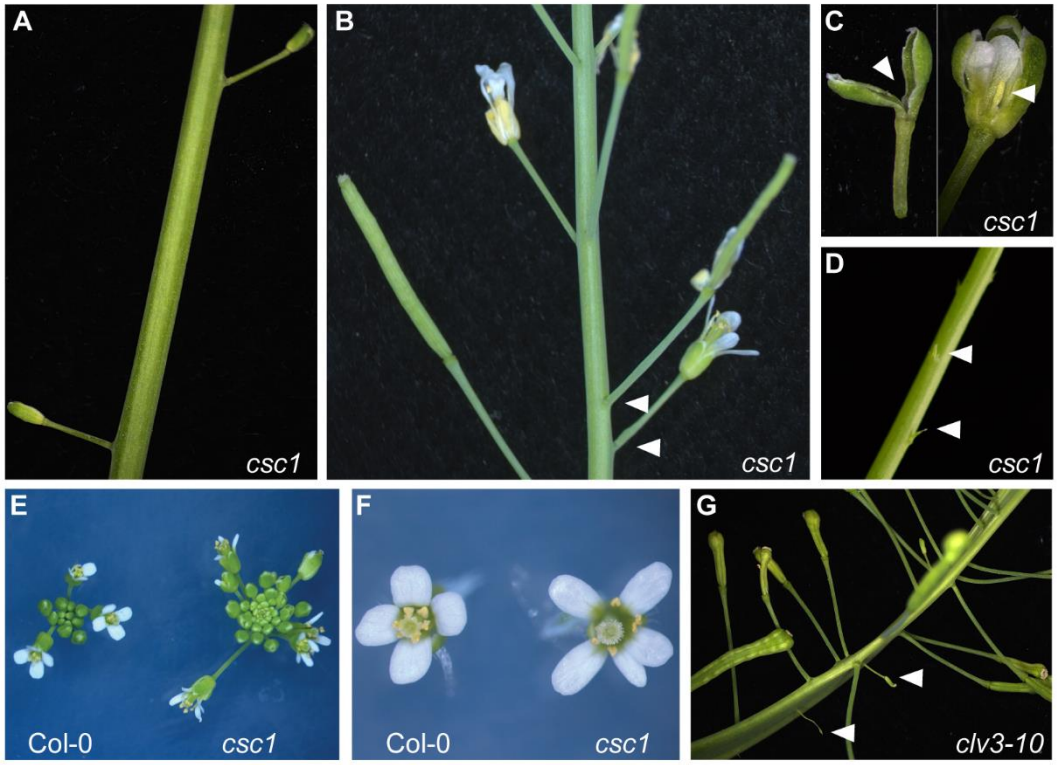

Figure 25. *csc1* depicts an enhanced SAM and defects in phyllotaxis and flower development. (A) Stem of *csc1* with un-opened flower buds. (B) Phyllotaxis defects in c*sc1* and delays in fruit development (white arrow heads). (C) Flower bud with missing petals, anthers and gynoecium (left, white arrow head) and flower bud with sepals and petals, but defects in anthers and gynoecium development (right, white arrow head). (D) Completely missing flower, only development of pedicels (white arrow heads). (E) Representative inflorescences of Col-0 and *csc1*. *csc1* depicts enlarged SAM with elevated primordia numbers. (F) Representative flowers of Col-0 and *csc*1, with elevated petal numbers in *csc1*. (G) *clv3-10* with similar flower phenotype as *csc1* (white arrow heads). *csc1* and *clv3-10*, 43-day-old plants.

To explore the possible CSC1 function in the SAM, we decided to analyze the *csc1* phenotypes in detail by dissecting and imaging using CLSM, *csc1* and Col-0 wild type shoot apical meristems of inflorescences. Representative 3D images of Col-0 and *csc1* revealed an increased shoot apical meristem size in *csc1* plants (Figure 26A,B). In addition, *csc1* seemed to have more organ primordia than Col-0 (Figure 26B). Quantifications of meristem size and epidermal cell number using the image analysis tool MorphoGraphX (Barbier de Reuille et al., 2015), exhibited a significant increase in meristem size and cell number of *csc1* compared to Col-0 wild type (Figure 26C,D). In contrast, cells in the epidermis of *csc1* had a smaller mean cell size as Col-0 (Figure 26E). These results support the macroscopic phenotypes of *csc1* and suggests a function of CSC1 in restricting the shoot apical meristem size.

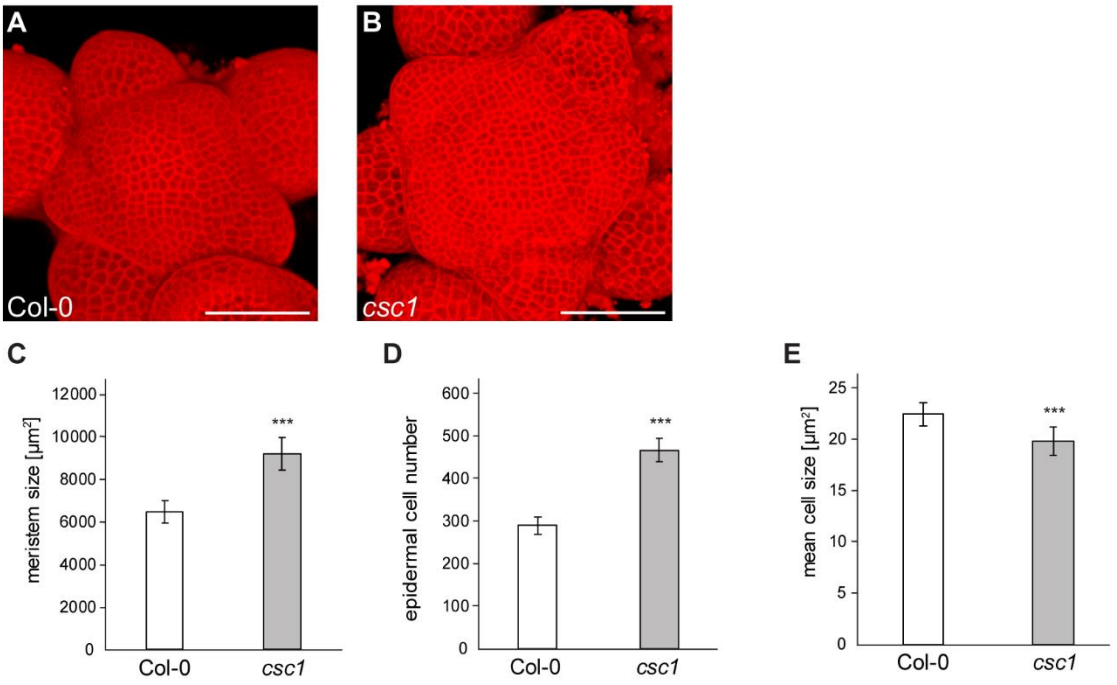

Figure 26. CSC1 regulates size and number of cells in the SAM. (A-B) Representative 3D views of shoot apical meristems of (A) Col-0 wild type and (B) *csc1* mutant. Scale bars: 50 µm. (C-E) Quantification of (C) meristem size, (D) epidermal cell numbers and (E) mean cell size in Col-0 wild type (n=10) and *csc1* (n=10) shoot apical meristems (37-day-old plants). Statistically significant difference from Col-0 based on pairwise t-test (*** p< 0.001).

We further wanted to investigate if *csc1* may also displayed defects in the development of below-ground tissues. Therefore, six-day-old seedlings of *csc1* and Col-0 were stained with basic fuchsin (Dharmawardhana et al., 1995) and calcofluor white (Waaland and Waaland, 1975). Basic fuchsin stains lignin in secondary cell walls of differentiated cells such as the endodermis (casparian strip) or proto- and metaxylem cells in the vasculature (Figure 27A,B).

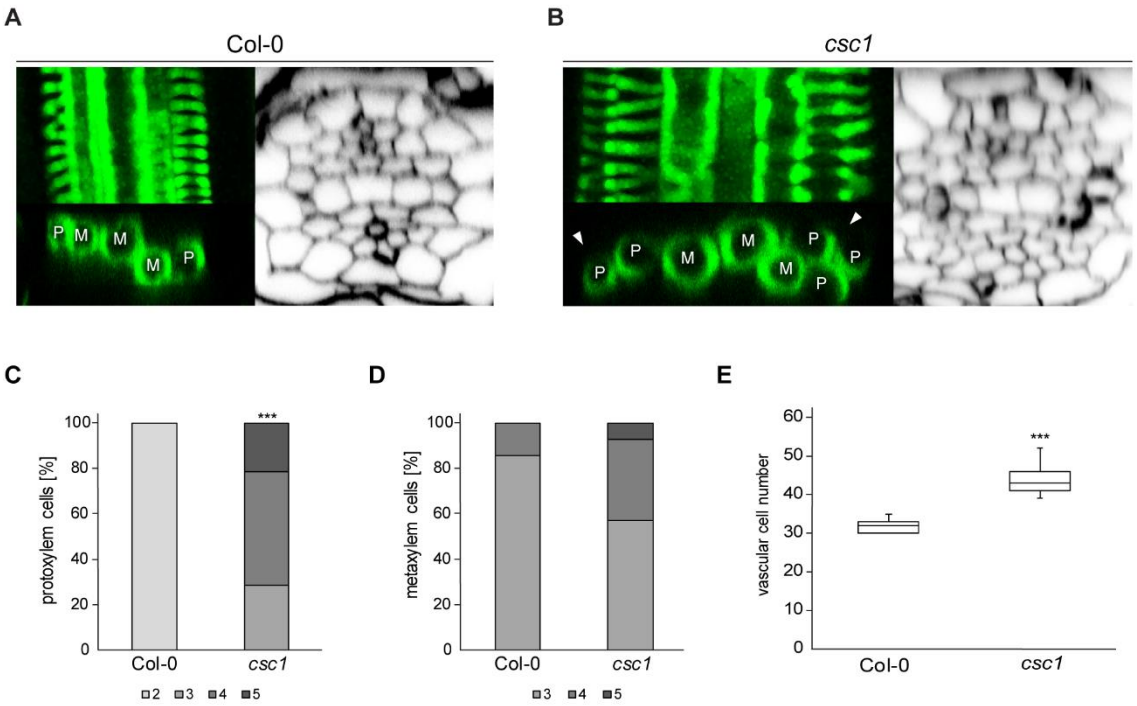

Figure 27. CSC1 regulates xylem and vascular cell number in the primary root. (A-B) Basic fuchsin and calcofluor white staining of six-day-old roots. Basic fuchsin labels lignified secondary cell walls in protoxylem (P) and metaxylem (M) cells (left). Calcofluor white labels cellulose in all cells (right). (A) Representative longitudinal (left) and orthogonal (left bottom, right) views (maximum projection) of vascular cells in the differentiation zone of the root in (A) Col-0 wild type and (B) *csc1* mutant. Note ectopic protoxylem cells (white arrow heads). (C-D) Quantification of (C) protoxylem and (D) metaxylem cells in Col-0 wild type (n=14) and *csc1* (n=14). Squares with different shades of grey represent numbers of protoxylem or metaxylem cells, respectively. (E) Quantification of total vascular cell number in Col-0 wild type (n=5) and *csc1* (n=5). Statistically significant difference from Col-0 based on Kruskal-Wallis test (*** $p<0.001$).

Calcofluor white stains cellulose, enabling counting of total cells in the root vascular tissues. In longitudinal microscopic sections, differentiated protoxylem cells were distinguishable from metaxylem cells by their characteristic ladder-like cell wall thickenings. Metaxylem cells depicted circular pits in the secondary cell walls (Figure 27A,B, left). Six-day-old seeding roots were imaged in the differentiation zone. Col-0 exhibited three to four metaxylem cells in one axis in the centre of the root with two protoxylem cells, one on each side of the metaxylem cells. For *csc1*, we observed elevated protoxylem numbers of three to five (Figure 27C). Furthermore, additional protoxylem cells often occurred in the procambial position, outside of the primary xylem axis (Figure 27B, white arrow head). Intriguingly, also metaxylem cells were elevated in *csc1* mutants, often depicting four or five metaxylem cells (Figure 27Figure 26D).

Next, we analysed if the increase in cell numbers was restricted to xylem or if enhanced proliferation in the vasculature resulted in increased total vascular cell numbers. For total vascular quantification, six-day-old seedling roots were stained with calcofluor white and imaged using CLSM cross-sections in the early differentiation zone. A significant increase in total vascular cell number was observed in *csc1* compared to Col-0 (Figure 27E). Taken together, the results of the cell number quantification in the shoot apical meristem and the vasculature, suggests that CSC1 functions in regulating cell proliferation.

4.2.2 CSC1 functions in CLE21 and CLE27 perception or signalling

Macroscopic and microscopic characterization of the *csc1* phenotype revealed severe developmental defects in the shoot apical meristem as well as in the vasculature of the root. Strikingly, *csc1* exhibited elevated vasculare cell numbers, presumably due to enhanced cytokinin signalling, which promotes cell proliferation (Kieber et al., 2018). Previous studies assumed a cross-talk of cytokinin signalling and the CLAVATA3/ENDOSPERM-SURROUNDING REGION-RELATED (CLE) peptides of which 17 have been distinguished as inhibitors of root growth (Kondo et al., 2011). Therefore, we used a CLE root sensitivity assay to gain further information about the function of CSC1 in vascular cell development.

We analysed the response of Col-0, *csc1* and *bam3-1* seven-day-old seedling roots growth on standard media containing concentrations from 0-100 nM of 14 root-active CLEs (CLE1/3/4, CLE9/10, CLE11, CLE13, CLE14, CLE18, CLE21, CLE25, CLE26, CLE27, CLE40, CLE41/44, CLE45 and CLV3) (Kondo et al., 2011). We chose *bam3-1* as a positive control for CLE45, because BAM3 is the receptor for CLE45 and mutants in *BAM3* showed a strong root growth insensitivity towards CLE45 (Depuydt et al., 2013; Rodriguez-Villalon et al., 2014; Hazak et al.,

2017). CLE root sensitivity assays were repeated four times and concentrations for the various CLEs were adjusted dependent on their effect on root growth. Among all tested CLE peptides, all four repetitions showed reduced sensitivity of *csc1* to the growth-inhibiting effects of CLE11, CLE21 and CLE27 with stronger effects on plates containing CLE21 and CLE27 (Figure 28). Graphs in Figure 28 show representative results of one of four independent experiment. Root growth on standard medium is slightly enhanced in *csc1* and *bam3-1* compared to Col-0 (Wolf et al., 2014). On 50 nM CLE21, *csc1* displayed a significant insensitivity in root growth compared to Col-0, whereas *bam3-1* was only slightly insensitive (Figure 28A). On elevated CLE21 concentrations (100 nM), both mutant genotypes depicted significantly longer roots than Col-0 (Figure 28A). Strongest root growth insensitivity could be detected on media containing 50 nM and 100 nM CLE27 for *csc1* and *bam3-1*. Col-0 showed on both CLE27 concentrations the same root growth reduction (Figure 28B). Compared to Col-0, *csc1* also showed a mildly increased root growth on 50 nM and 100 nM CLE11 (Figure 28C). *bam3-1* did not exhibit root growth insensitivity on CLE11 (Figure 28C). The strong root growth insensitivity of *csc1* towards CLE21 and CLE27 suggests a function of CSC1 in CLE perception or CLE signalling.

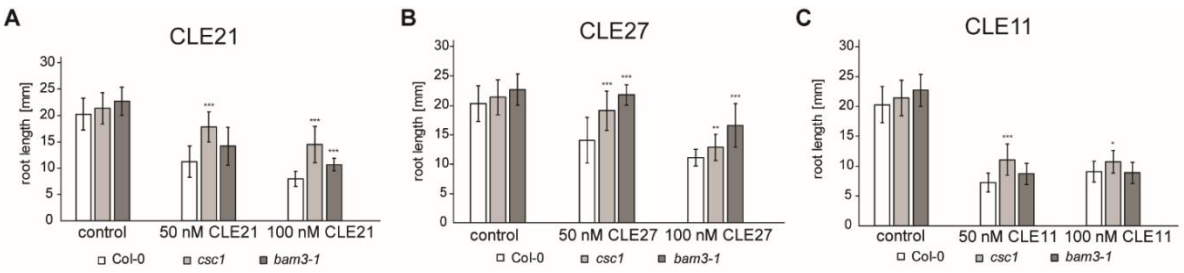

Figure 28. CSC1 might function in CLE21 and CLE27 perception or signalling. CLE root sensitivity assay with different Arabidopsis genotypes on medium containing various concentrations of CLE21, CLE27 and CLE11. Root length was measured from seven-day-old seedlings. (A-C) Quantification of root length of Col-0 wild type, *csc1* and *bam3-1* grown on media containing 50 nM and 100 nM (A) CLE21, (B) CLE27 and (C) CLE11. Asterisks indicate statistically difference from Col-0 per condition based on Kruskal-Wallis test (*p < 0.05, **p < 0.01, ***p < 0.001), (mean ± SD) (n=10-20). Experiments performed by Nabila El Arbi, supervised by A.-K. Schürholz.

Unfortunately, most of the CLE peptides are not well-studied so far and only for a few of them, the receptors have been identified. For CLE27, a putative receptor, the LRR-RLK ARABIDOPSIS THALIANA FASCIATED EAR 3 (AtFEA3, AT3G25670) was identified (Je et al., 2016), but for CLE21 no putative receptor is yet revealed.

Based on previous characterizations of c*sc1* mutant plants, we expected a function of CSC1 in the shoot and root apical meristems and the vasculature. If CSC1 might function in CLE21 and CLE27 perception or signalling, we would expect that CLE21 and CLE27 were expressed in the SAM and in the root vasculature, in similar tissues where we observed *csc1* phenotypes. We analysed *pCLE21:GUS* and *pCLE27:GUS* by analysing GUS expression in seven-day-old seedlings and in the shoot apical meristem of 35-day-old plants expressing *pCLE27:GUS* (Figure 29 and Figure 30) (Jun et al., 2010). *CLE21* activity was observed in the whole vascular tissues and the primary RAM, but not in the shoot apical meristem (Figure 29).

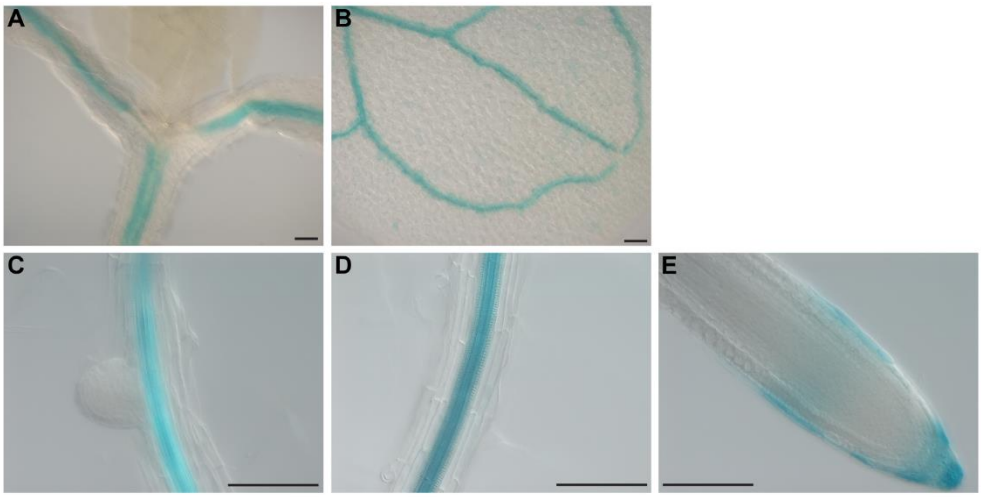

Figure 29. CLE21 is expressed in the vasculature. Six-day-old seedlings expressing *pCLE21:GUS* in (A) hypocotyl and petiole vasculature and (B) vasculature in the cotyledons. (C) *pCLE21* is not active in lateral root primordia, but in (D) the root vasculature. (E) *CLE21* promoter activity in the primary root columella and slightly in the RAM. Scale bars: 100 µm.

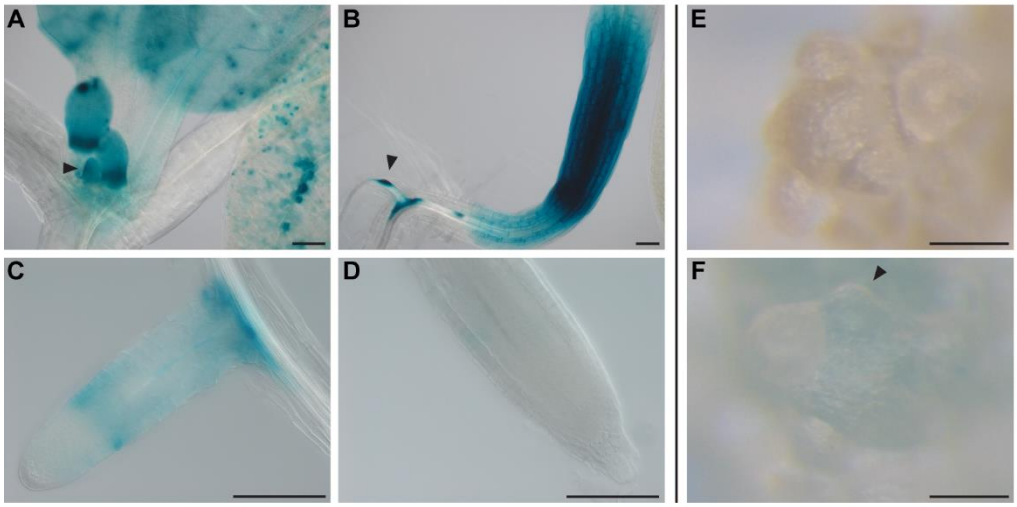

Figure 30. CLE27 is expressed in root and shoot primordia. (A-D) Six-day-old seedlings expressing *pCLE27:GUS* in young leaves, (B) the hypocotyl and lateral roots and primordia (black arrow heads). (C) *pCLE27* activity in elongation and differentiation zone in the lateral root. (D) *CLE27* promoter is not active in the primary root RAM. Scale bars: 100 µm. (E-F) Shoot apical meristems of 35-day-old plants. (E) Col-0 and (F) *pCLE27:GUS*. Note the slightly blue GUS staining of a young primordia in the SAM. Scale bar: 500 µm.

Analysis of *CLE27* promoter activity revealed expression in the hypocotyl, lateral root primordia and the RAM in lateral roots, but not in the primary RAM (Figure 30A-D). Additionally, *CLE27* was expressed in leaves and young primordia in the SAM (Figure 30A,F). *CLE2*1 and *CLE27* promoters are either active in the vasculature in the whole plant or in young primordia in the shoot apical meristem. Although *pCLE21* and *pCLE27* do not show the same expression pattern, CSC1 still might be involved in CLE21 and CLE27 perception or signalling. Dependent on how far CLE peptides are transported, they can also function away from cells/tissues, where they are expressed and synthesised (Stahl et al., 2009; Hazak et al., 2017).

4.2.3 Mutations in *CLE21* and *CLE27* do not resemble *csc1* phenotype

The most severe developmental defects in *csc1* plants were identified in the vasculature, the SAM and the flower organs. We therefore wanted to analyse if mutants in CLE21, CLE27 and CLE11, which shows a similar expression pattern as CLE21, depict a *csc1* related phenotype (Jun et al., 2010). CRISPR/Cas9 derived *cle11 cr3* (+53 bp, referred to as *cle11*), *cle21 cr1* (-1bp, referred to as *cle21*) and *cle27 cr1* (+1bp, referred to as *cle27*) mutants carried insertions or deletions creating frame shifts which led to knock-out lines (Yamaguchi et al., 2017). Seeds of single mutant

lines were kindly provided by Takashi Ishida (Yamaguchi et al., 2017). We generated *cle11 cle21* and *cle21 cle27* double mutants to overcome potential functional redundancy mainly in CLE11 and CLE21. However, CLE single and double mutants did not show any developmental phenotype compared to Col-0 (data not shown). Therefore, we next assessed if CLE single and double mutants exhibited a vascular phenotype in the root.

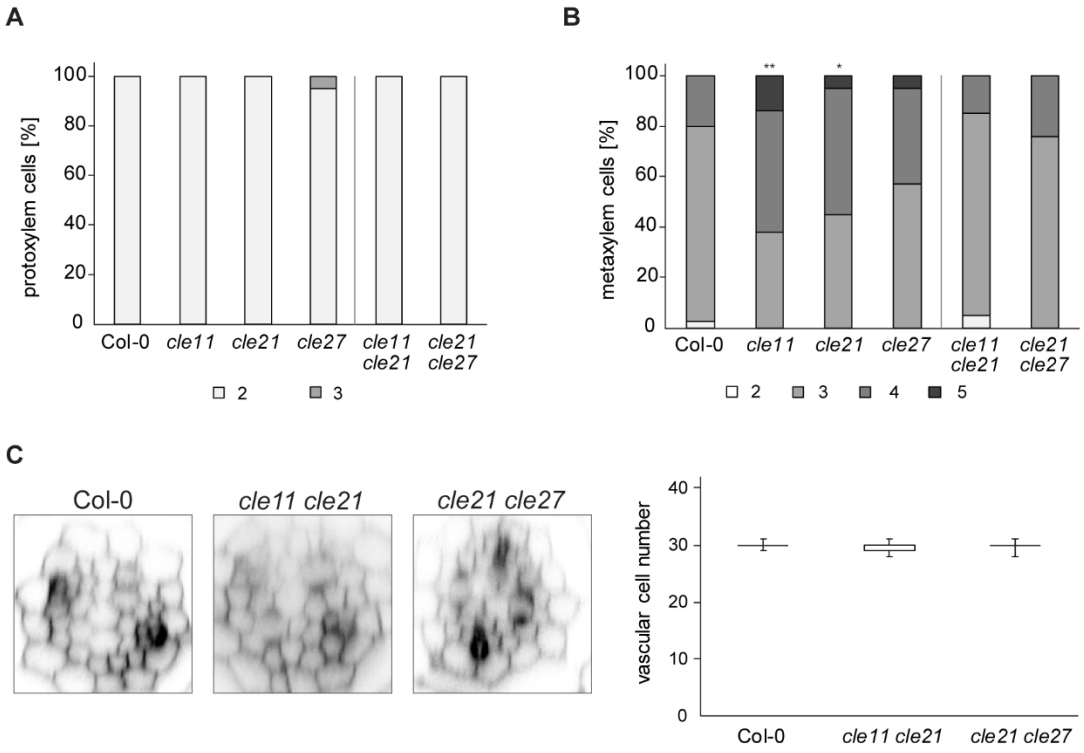

Figure 31. *cle* mutants do not exhibit *csc1* similar phenotypes in the vasculature. (A-B) Basic fuchsin staining of six-day-old roots. Basic fuchsin labels lignified secondary cell walls in protoxylem and metaxylem cells. Quantification of (A) protoxylem and (B) metaxylem cells in Col-0 (n=40), *cle11* (n=21), *cle21* (n=22), *cle27* (n=21), *cle11 cle21* (n=20) and *cle21 cle27* (n=17) roots. (C) Basic fuchsin and calcofluor white staining of six-day-old roots, confocal stacks, orthogonal views (left). Calcofluor white labels cellulose in all cell walls and allows quantification of vascular cell number in Col-0 (n=21), *cle11 cle21* (n=20), *cle21 cle27* (n=13) (right). Statistically significant difference from Col-0 based on Kruskal-Wallis test (*p < 0.05, **p < 0.01).

Lignified secondary cell walls of protoxylem and metaxylem cells were stained with basic fuchsin and cross-sections of six-day-old seedling roots in early differentiation zone were imaged for xylem cell quantifications (Figure 31). Col-0 roots had three to four metaxylem cells and always two protoxylem cells. For protoxylem cell numbers, no significant differences could be identified in *cle* single and double mutants compared to Col-0 (Figure 31A). Counts for metaxylem cell numbers revealed a significant increase of metaxylem cells in *cle11* and *cle21* single mutants compared to Col-0 (Figure 31B). Intriguingly, double mutants of *cle11 cle21* and *cle21 cle27* depicted Col-0-like metaxylem cell numbers (Figure 31B). In addition, total vascular cell numbers in Col-0, *cle11 cle21* and *cle21 cle27* double mutants were quantified by cellulose staining of cell walls with calcofluor white (Figure 31C). However, no alterations in cell numbers or cell positions in procambium, phloem or xylem cells were visible in the transverse cross-sections of the double mutants compared to Col-0 (Figure 31C, left). Counts for total vascular cell numbers neither revealed any differences compared to Col-0 (Figure 31C, right).

Taken together, *cle11* and *cle21* single mutants depict a slight increase in metaxylem cells, but not in protoxylem cells. Additionally, CLE single and double mutants do not show elevated cell numbers in the vasculature, which suggests that, assuming the *cle* mutants are null, the *csc1* phenotype cannot be explained by the CLEs.

4.2.4 CLE21 treatment enhances cytokin responses in the RAM

A previous study could reveal a connection between CLE and cytokinin signalling in the root of Arabidopsis (Kondo et al., 2011). CLE9/10 treatment inhibited the expression of type-A ARRs which are negative regulators of cytokinin signalling, thereby enhancing cytokinin signalling and expression of CK target genes (Kondo et al., 2011).

In order to test, if the application of CLE21 can also interfere with cytokinin signalling in the root, we imaged the expression of the *pTCSn:GFPer* cytokinin signalling reporter, kindly provided by Christophe Gaillochet (Jan Lohmann Lab, originally from Bruno Müller), in five-day-old seedlings grown on control media and media containing 50 nM CLE21 (Figure 32) (Zurcher et al., 2013). The seedling roots were stained with propidium iodide (PI) to counterstain cell wall. Fire projection of *pTCSn:GFPer* revealed highest fluorescence intensity in the lateral root cap, in pericycle initials and stele initials (sieve element-procambium precursor) and weaker expression in further differentiated protophloem, metaphloem and procambium files (Figure 32, top).

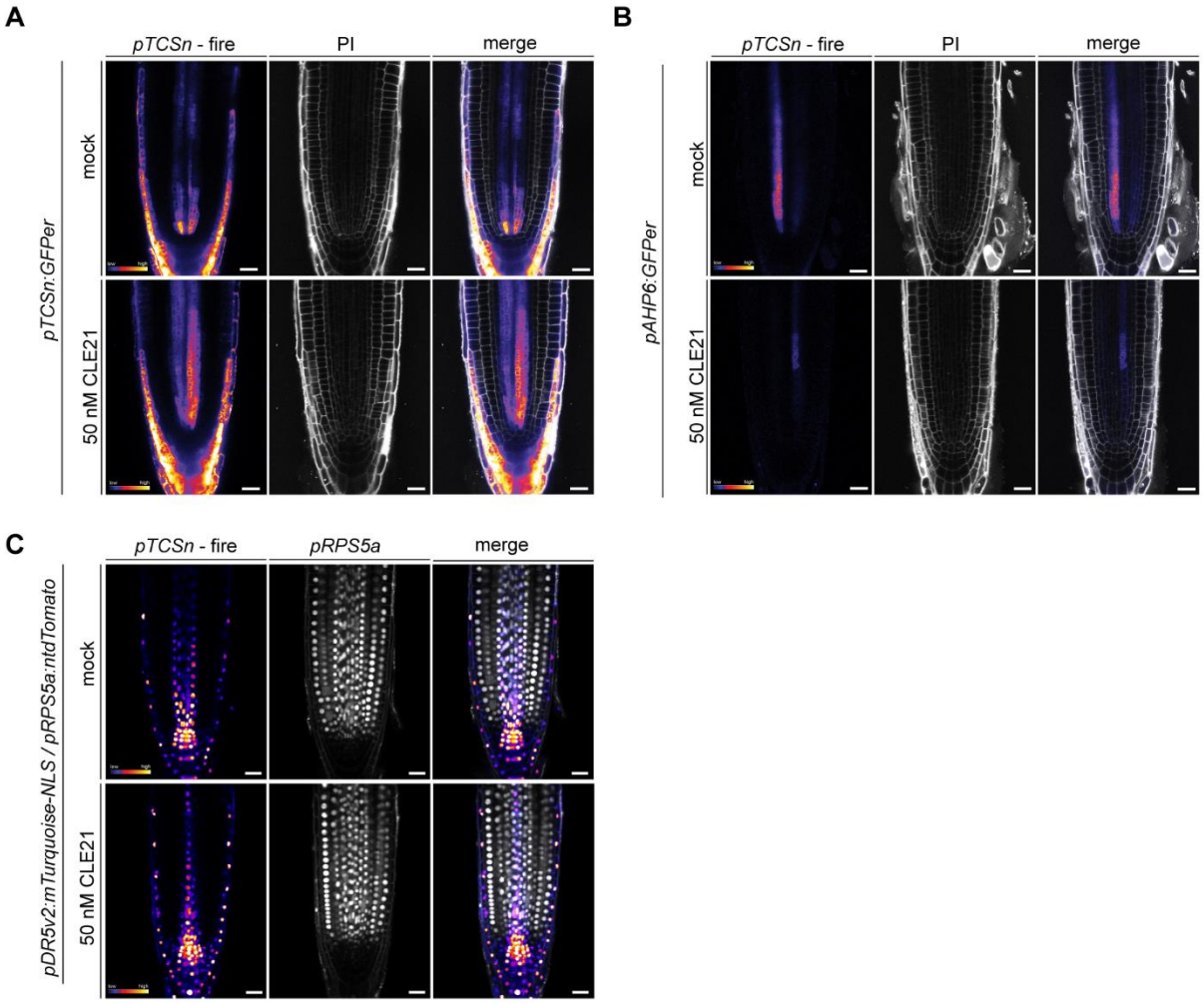

Figure 32. CLE21 treatment affects expression of *pTCSn* and *pAHP6* in the RAM. (A) Representative cytokinin response (*pTCSn:GFPer*) in the RAM after mock (top) and 50 nM CLE21 treatment in five-day-old seedling roots, grown for five days on plates containing control media or CLE21 media (bottom). Fire projection, propidium iodide (PI) and merged channels. (B) Representative *pAHP6:GFPer* expression in the RAM after mock (top) and 50 nM CLE21 treatment (bottom). Fire projection, propidium iodide (PI) and merged channels. (C) Representative auxin response (*pDR5v2:mTurquoise-NLS*) in the RAM after mock (top) and 50 nM CLE21 treatment (bottom). Fire projection, *pRPS5a:ntdTomato* and merged channels. Five-day-old seedlings. Scale bars = 20 µm, n=5-6. Experiment performed by Sebastian Wolf, analysed by A.-K. Schürholz.

CLE21 treatment enhanced the expression of *TCSn* in the lateral root cap, but led to decreased signal in the pericycle and stele initials. However, the *TCSn* signal clearly expanded further towards inner stele cell files and shootwards (Figure 32A, bottom). The cytokinin signalling reporter *pAHP6:GFPer*, kindly provided by Ari Pekka Mähönen, was showing weak activity in pericycle and sieve element-procambium precursor cells, but depicted an increased activity in young pericycle and sieve element precursor cells (Figure 32B, top) (Mähönen et al., 2006 a). CLE21 treatment led to weakening of *pAHP6:GFPer* signal, which was only detectable in one cell strand in the more mature vasculature (Figure 32B, bottom). Fire projections of fluorescence signal derived from the auxin signalling marker *pDR5v2:mTurquoise-NLS*, kindly provided by Marion (Maizel Lab), did not reveal severe differences between control conditions and CLE21 treatment (Figure 32C). CLE21 treatment lead to a mild decrease in *DR5v2* signal in the stele of the root (Figure 32, bottom).

These data suggest a cross-talk of CLE21 and cytokinin signalling by positively regulating cytokinin signalling. CLE21 does not seem to affect auxin signalling in the root apical meristem. Based on these results and the fact, that cytokinin is important for cell proliferation and represses protoxylem differentiation, we wanted to explore, if exogenous cytokinin affects vascular cell numbers in *csc1* (Mähönen et al., 2006a).

4.2.5 CSC1 seems to buffer elevated cytokinin levels in the root

Cytokinin is a crucial plant hormone for vascular development, enhancing procambial proliferation, whereas it suppresses on the other hand protoxylem formation (Mähönen et al., 2006; Hejatko et al., 2009). Exogenous application of the cytokinin derivate 6-benzylaminopurine (BA), was shown to promote proliferation in the stele of the root in the *ahp6-1* mutant, leading to elevated vascular cell numbers (Mähönen et al., 2006a). Furthermore, increased cytokinin signalling led to a reduction in protoxylem cell files (Mähönen et al., 2006a).

Taking this into account together with increased total vascular cell numbers in *csc1* seedling roots, we tested the effect of cytokinin treatment on the total vascular cell number in *csc1* and Col-0. Cell walls of seedling roots were stained with basic fuchsin to visualize lignified secondary cell walls and calcofluor white to visualize cellulose in primary cell walls. In control conditions, five-day-old Col-0 wild type roots exhibited an average of 32 cells in the vasculature in the early differentiation zone, whereas *csc1* displayed an average of 45 cells (Figure 33A,B). Treatment with 0.1 µM BA resulted in a mild increase of vascular cells from an average of 32 to 33 in Col-0, but in a significant increase in *csc1* from an average of 45 to 52 cells (Figure 33A,B). Treatment

with higher BA concentrations of 1 µM BA increased the vascular cell number in Col-0 to an average of 39 cells, in *csc1* to an average of 69, almost twice as many as untreated Col-0 (Figure 33A,B).

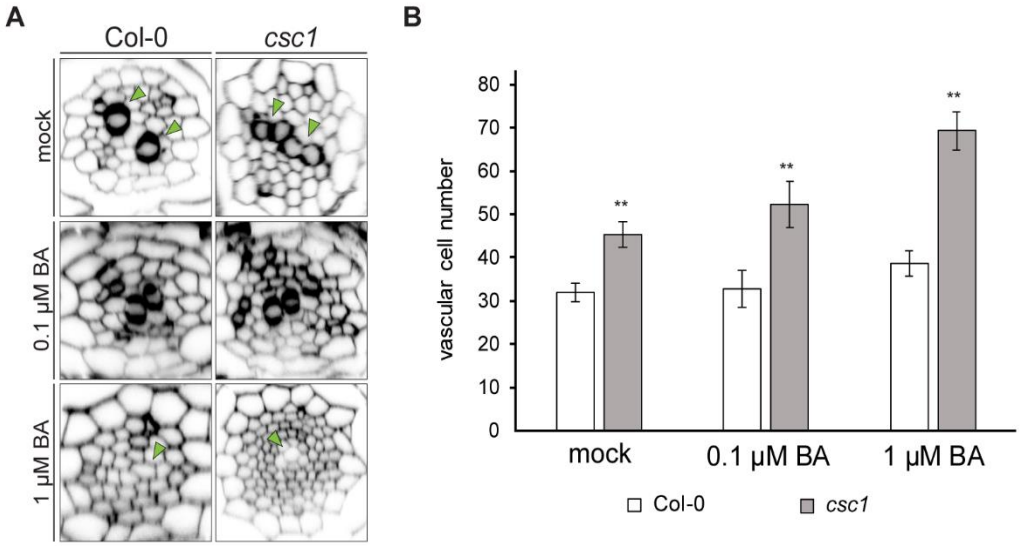

Figure 33. *csc1* is affected in the response to elevated cytokinin levels. (A) Basic fuchsin and calcofluor white staining in five-day-old seedling roots to visualise lignified secondary cell walls (green arrow heads, mock) and cellulose in cell walls, respectively. Transverse cross-sections obtained by confocal imaging depict vascular cells in Col-0 and *csc1* mock conditions (top) and treated with 0.1 µM (middle) and 1 µM BA (bottom). Note absence of lignified secondary cell walls in the xylem axis in Col-0 and *csc1* treated with 1 µM BA (green arrow heads, bottom). (B) Quantification of vascular cells in Col-0 and *csc1* in mock conditions and treated with 0.1 µM and 1 µM BA. Statistically significant difference from Col-0 based on Kruskal-Wallis test (**p < 0.01). Mean ± SD, n = 5/condition and genotype. Experiment performed by Sebastian Wolf, analysed by A.-K. Schürholz.

The elevated cytokinin levels resulted not only in enhanced proliferation, but also in repression of protoxylem cell formation, as reported in previous studies (Mähönen et al., 2006a; Mähönen et al., 2006b). Intriguingly, enhanced CK signalling, did not only repress protoxylem formation and differentiation, but also metaxylem formation and differentiation, indicated by the absence of basic fuchsin stained xylem cells at 1 µM BA treatments in Col-0 and *csc1* (Figure 33A, green arrow heads, top and bottom).

The strong effect of cytokinin treatment on the vascular cell number in *csc1* plants suggests, that CSC1 functions in buffering the response to cytokinin. It might also be possible, that cytokinin

levels are already elevated in *csc1* compared to Col-0 and increasing cytokinin levels cannot be buffered anymore.

To distinguish between these two hypotheses, we analysed the expression of the cytokinin signalling marker *pTCSn* in combination with an ubiquitous nuclei marker *pUBQ10:3xGFP-NLS* for cell counting. Expression of *pTCSn:GFP-NLS/pUBQ10:3xmCherry-NLS,* kindly provided by Christian Wenzl (Jan Lohmann Lab), was analysed in Col-0 and *csc1* mutant backgrounds in the RAM of seven-day-old seedlings. Similar to the *pTCSn:GFPer* marker (Figure 32A),

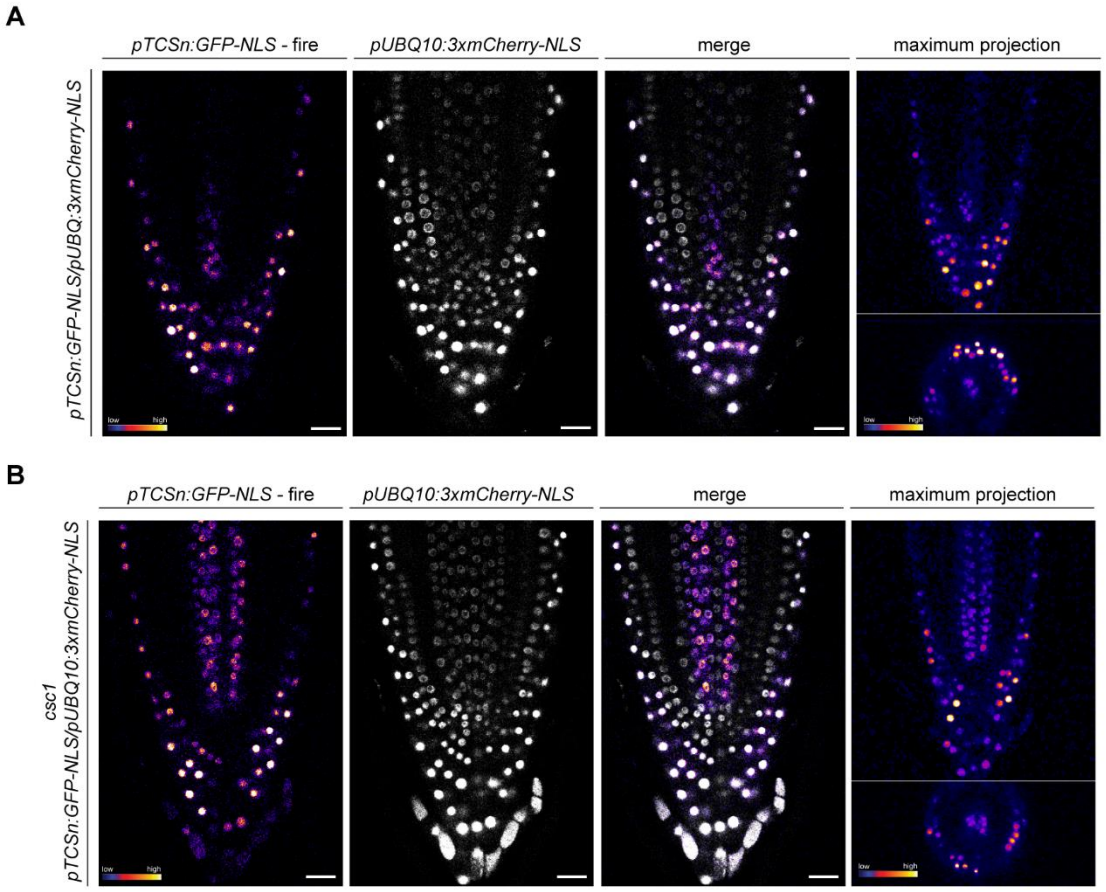

Figure 34. CSC1 represses cytokinin response levels in the RAM. (A-B) Cytokinin response (*pTCSn:GFP-NLS*) in root apical meristems of seven-day-old seedlings in (A) Col-0 and (B) *csc1* backgrounds. Representative images of *pTCSn:GFP-NLS* signals (fire), *pUBQ10:3xmCherry-NLS* signals (grey), merge and maximum projection (fire) in longitudinal and transverse sections from left to right. Col-0 (n=5) and *csc1* (n=5). Scale bars: 20 µm.

pTCSn:GFP-NLS marker also depicted strong cytokinin response in the lateral root cap and in the stele, close to the QC, in Col-0 (Figure 34A). However, no precise statement regarding the type of cell in the stele could be done, because cell outlines were not visible, which made it difficult

to distinguish the different cell types. The cross section of a maximum projection also depicted the cytokinin response in the stele (Figure 34A; right-bottom). Expression of *pTCSn:GFP-NLS* in *csc1* revealed cytokinin response in the lateral root cap and in the stele (Figure 34B). Compared to Col-0, *pTCSn* expression in *csc1* was broader and slightly stronger in vascular cells, close to the QC and in further differentiated vascular cells in more mature cells shootwards (Figure 34B). Maximum projection of longitudinal and transverse root sections depicted a wider *pTCSn* signal in the stele of *csc1* compared to Col-0, which is presumably due to more vascular cell files in *csc1* (Figure 34A,B; right-bottom). Together, the analysis of cytokinin treatment in the root vasculature and the cytokinin response in the RAM in Col-0 and *csc1*, suggested that CSC1 might function in regulating cytokinin signalling.

4.2.6 CSC1 controls cytokinin response in the SAM

Based on the data that *csc1* showed an enhanced cytokinin response in the RAM, we wanted to test, if this holds true for the SAM using the same line, *pTCSn:GFP-NLS/pUBQ10:3xmCherry-NLS* in Col-0 and *csc1* mutant backgrounds.

To investigate the CSC1 function in cytokinin response in more detail in the shoot meristems, we applied the image analysis pipeline developed by Christian Wenzl for our imaged z-stacks of *csc1* and Col-0 SAMs, to quantify cell numbers and expression domains in the SAM (Jan Lohmann Lab) (Berthold et a., 2008). 3D views of representative shoot meristems revealed an increased SAM in *csc1* plants compared to Col-0 and an additional increment of *pTCSn* expression domain (Figure 36A,B; top and bottom). Quantifications of TCSn signals in the shoot meristems revealed a significant increase (+116 %) in *TCSn* positive cells in *csc1* compared to Col-0 (Figure 36C). In addition, *csc1* exhibited almost twice as many cells (+87 %) in the total meristem as Col-0 (Figure 36D).

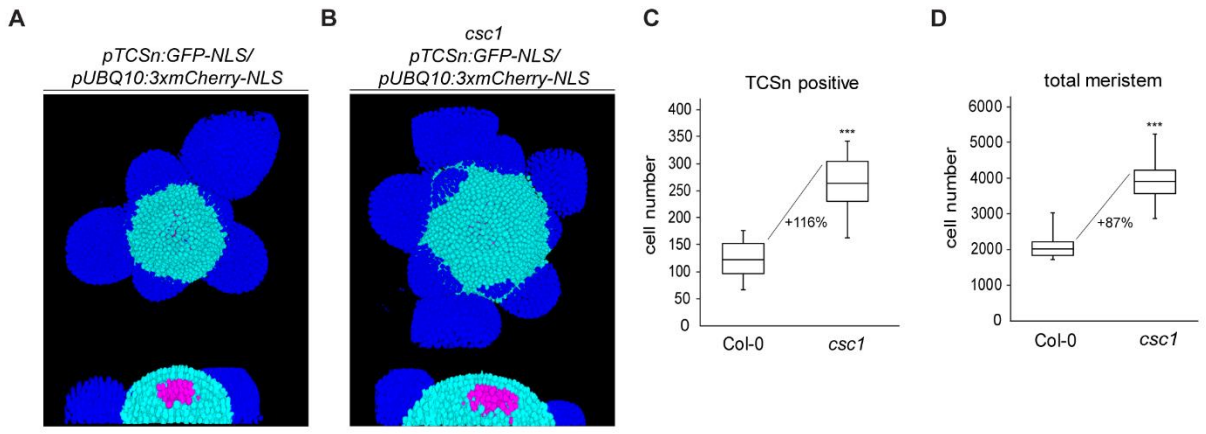

Figure 36. CSC1 function regulates cytokinin response in the SAM. (A-B) Representative views of 3D-reconstructed SAMs after nuclei segmentation from (A) Col-0 and (B) *csc1* in the *pTCSn:GFP-NLS /pUBQ10:GFP-NLS* reporter. Dark blue: primordia cells, cyan: SAM cells, magenta: TCSn positive cells. (C-D) Quantification of (C) TCSn positive cells and (D) total cell numbers in the SAM. Percentage values depict increase of cells from Col-0 to *csc1* Shoot meristems of 35-day-old plants. Statistically significant difference from Col-0 based on Kruskal-Wallis test (***p < 0.001). Col-0 (n=14), *csc1* (n=16).

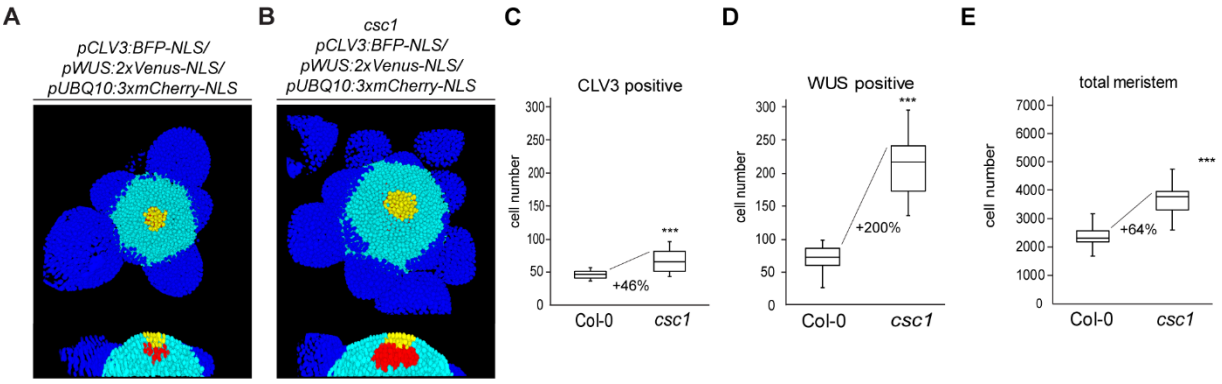

Figure 35. CSC1 functions in restricting *WUS* domain in the SAM. (A-B) Representative views of 3D-reconstructed SAMs after nuclei segmentation from (A) Col-0 and (B) *csc1* in the *pCLV3:BFP-NLS/pWUS:2xVenus-NLS/pUBQ10:3xmCherry-NLS* triple reporter. Dark blue: primordia cells, cyan: SAM cells, yellow: *CLV3* positive, red: *WUS* positive cells. (C-E) Quantification of (C) *CLV3* positive cells, (D) *WUS* positive cells and (E) total cell numbers in the SAM. Percentage values depict increase of cells from Col-0 to *csc1*. Shoot meristems of 35-day-old plants. Statistically significant difference from Col-0 based on Kruskal-Wallis test (***p < 0.001). Col-0 (n=18) *csc1* (n=16).

Second, we analysed the expression of *WUS* in the organising centre (OC) and *CLV3* in the central zone (CZ) of Col-0 and *csc1* shoot meristems using the *pCLV3:BFP-NLS/pWUS:2xVenus-NLS/pUBQ10:3xmCherry-NLS* triple reporter, kindly provided by Christian Wenzl (Jan Lohmann Lab). Cross-sections of 3D views of representative shoot meristems exhibited an expanded *WUS* distribution domain in *csc1* plants compared to Col-0 (Figure 35A,B). Quantifications of *CLV3* positive cells revealed a slight, but significant increase in *csc1* (+46 %) (Figure 35C). *WUS* positive cells were dramatically increased (+200 %) and the *WUS* domain expanded further into the rib meristem in *csc1* than in Col-0 (Figure 35B,D). The total cell number in the SAM also increased in *csc1* (+64 %) compared to Col-0 (Figure 35E). To identify, if this dramatic increase in the *WUS* domain is due to the general increase of the meristem size, we calculated the ratios of for instance *WUS* positive cells and total cells in the meristem for *csc1* and Col-0 (Figure 37). The ratios for *CLV3* depicted a smaller ratio for CLV3 in *csc1* compared to Col-0. This means, that in relation to the total cell number in the meristem, there are fewer *CLV3* positive cells in *csc1* than in Col-0 (Figure 37). In contrast to *CLV3*, the ratio of *WUS* positive cells in relation to total cell number is dramatically bigger in *csc1* compared to Col-0 (Figure 37). The difference of the ratio between *TCSn* positive and total cell number in Col-0 and *csc1* is almost the same, implying that the elevated *TCSn* positive cells might correlate with the increased meristem size (Figure 37).

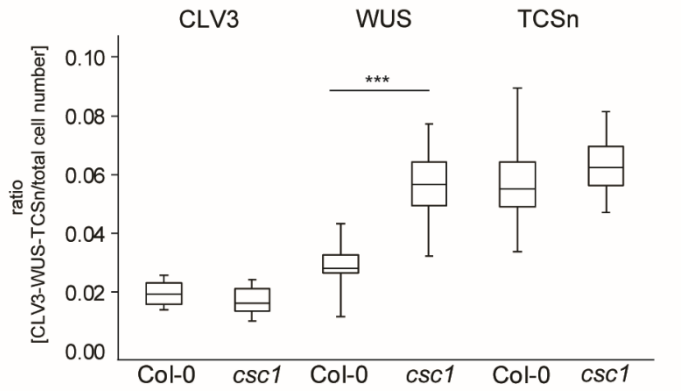

Figure 37. WUS domain increases independently of shoot apical meristem size in *csc1*. Ratios of CLV3-WUS-pTCSn positive cells/total cell number in Col-0 or *csc1*. Statistically significant difference from Col-0 based on pairwise t-test (***p < 0.001). Col-0 (n=14-18) *csc1* (n=14-15).

Taken together, we could identify a drastically increase in the WUS domain in *csc1* SAMs, whereas the CLV3 domain only slightly increased compared to Col-0, resulting in a reduction of the CLV3 domain in relation to the total cell number. These findings imply that CSC1 might uncouple the WUS-CLV3 feedback loop.

4.2.7 CSC1 might regulate auxin response via WUS

After identifying, that CSC1 might function in regulating cytokinin responses in the root and shoot apical meristem, we wanted to investigate, if auxin, the second important phytohormone signalling pathway in root and shoot meristems, is also altered in *csc1* mutants (Leyser, 2018). Therefore, we crossed the auxin response marker *pDR5v2:YFPer*, kindly provided by Jiyan Qi (Thomas Greb Lab), into *csc1*. Shoot apical meristems of 35-40-day-old plants with *csc1* phenotypes of a segregating F_2 population of this cross, were imaged (Figure 38).

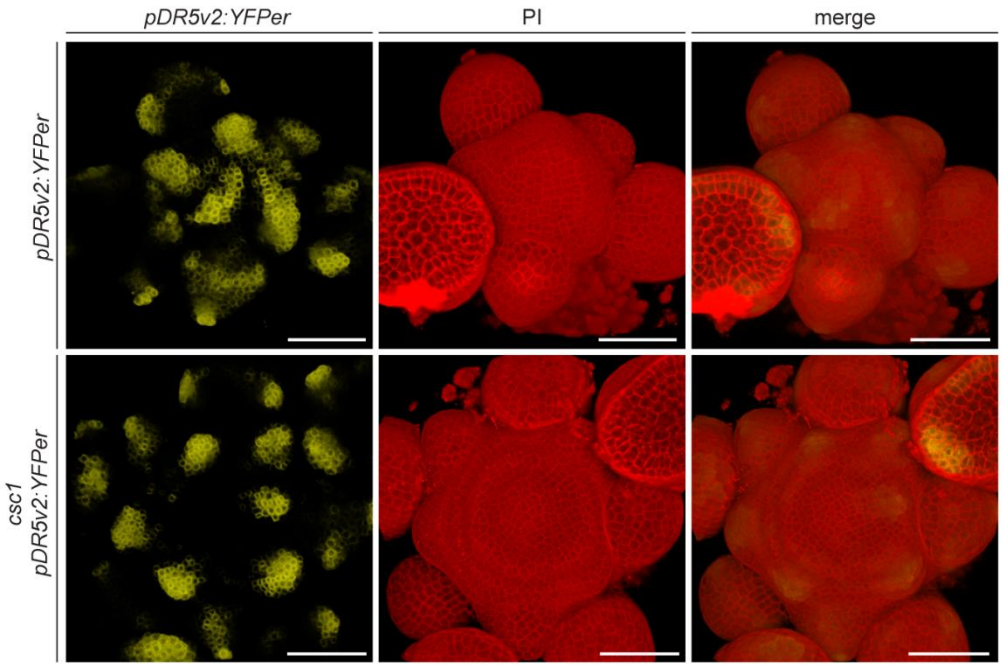

Figure 38. *csc1* depicts smaller auxin response domains. Representative 3D views of SAMs expressing auxin response marker *pDR5v2:YFPer* in Col-0 (top) and *csc1* (bottom) backgrounds of 35-40-day-old plants. Left to right: *pDR5v2:YFPer* channel, PI channel, merge. Col-0 (n=4), *csc1* (n=5), scale bar: 50 µm.

In the Col-0 background, the *pDR5v2* depicted a weak signal in the centre of the meristem (CZ) with increasing signals in spiral shaped zones towards the periphery (Figure 38, top). Auxin maxima define the loci of primordia initiation and can be directly used as read out for where and how many primordia are initiated (Heisler et al., 2005). Auxin response domains in *csc1* seemed to be smaller and they did not exhibit a spiral shaped zone from the centre of the meristem towards the periphery like Col-0, consistent with more WUS in the SAM (Figure 38, bottom) (Ma et al., 2018). In addition, no *pDR5v2:YFP* signal was detected in *csc1* plants in the centre of the SAM (Figure 38, bottom). However, the number of *pDR5v2* positive domains might be elevated in *csc1* compared to Col-0, which would support the assumption that *csc1* exhibited more primordia in the shoot apical meristem (Figure 26B). Compared to Col-0, the single domains were more constraint and presumably harboured less cells in each domain, which might also explain defects in flower development.

4.2.8 Genetic interaction of *CSC1* and *CLV3* in the SAM

Analysis of WUS and CLV3 markers in the *csc1* mutant background revealed that the mutation in *CSC1* resulted in an increased WUS domain but only a slight increase in the *CLV3* domain, suggesting, that in *csc1* mutants WUS-CLV3 feedback is uncoupled. Previous studies of *clv3* mutants revealed, that the absence of the CLV3 peptide results in a massive increase in the *WUS* and the *CLV3* domain in the shoot apical meristem (Schoof et al., 2000; Muller et al., 2008).

We wanted to investigate if *CSC1* might genetically interact with *CLV3* to gather more information where and how CSC1 functions in the shoot apical meristem. We crossed *csc1* with the TALEN derived *clv3-10* mutant (Forner et al., 2015). *csc1 clv3-10* double mutants in the F_3 generation, wild type for *RLP4* and *R4L1* mutations, were phenotypically characterized. The *clv3-10* mutant displayed a strong developmental phenotype with a fasciated stem, a massively increased SAM and club-like siliques (Figure 25G, Figure 39). As previously mentioned, *csc1* depicted un-opened flower buds, presumably due to defects in flower development, reminiscent of *clv3-10* (Figure 25A-D,G). During vegetative stage and early reproductive stage of *csc1 clv3-10* double mutants, it seemed as if *csc1* could repress the severe *clv3-10* phenotype (data not shown). Around 30-35 days after germination, *csc1 clv3-10* double mutants started developing a severe developmental phenotype. Around the same developmental stage, *csc1* also started depicting flower developmental phenotypes. *csc1 clv3-10* double mutants exhibited either one thick round stem or a thick fasciated stem, that often started splitting (Figure 39A-E, white arrow heads). Compared

to *csc1* or *clv3-10* single mutants, it is striking, that *csc1 clv3-10* double mutants did not develop side shoots at the primary shoot and only in rare occasions siliques (Figure 39A-C).

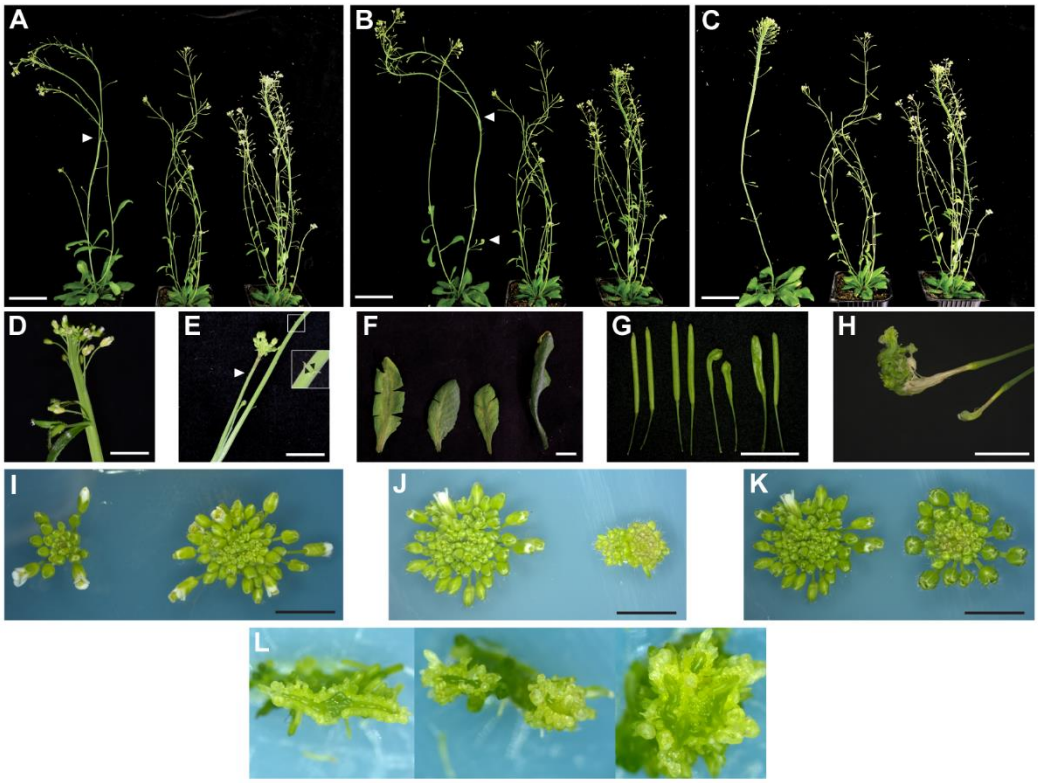

Figure 39. CSC1 and CLV3 seem to genetically interact in controlling shoot apical meristem. (A-C) Three representative phenotypes of *csc1 clv3-10* with *csc1* and *clv3-10* single mutants (left to right). Scale bars: 50 mm. Note splitting of primary stem and outgrowth of silique (white arrow heads). (D-E) Representative images of *csc1 clv3-10* inflorescences and (D) fasciated primary stem or (E) split stem with pedicels and missing flower whorls. Note white and black arrow heads. Scale bars: 10 mm (F) Rosette leaves of Col-0, *csc1*, *clv3-10* and *csc1 clv3-10,* left to right. Scale bar: 10 mm. Note the radialzed rosette leaf of *csc1 clv3-10*. (G) Siliques in pairs of Col-0, *csc1*, *clv3-10* and *csc1 clv3-10*, left to right. Scale bar: 10 mm. (H) Siliques of *csc1 clv3-10* with outgrowth, presumable non-terminated flower meristem, scale bar: 10 mm. (I) Inflorescences of *csc1* (left) and *clv3-10* (right), scale bar: 5 mm (J-K) Inflorescences of *clv3-10* (Left) and *csc1 clv3-10* #33 (right), scale bar: 5 mm (K) Inflorescences of *clv3-10* (left) and *csc1 clv3-10* #34 (right), scale bar: 5 mm. (L) Dissected SAMs of *clv3-10* (left) and two representative SAMs of *csc1 clv3-10* (middle, right) depicting either a split meristem (middle) or a circular meristem. For all phenotypic characterizations, 35-50-day-old plants were analysed.

Double mutants exhibited severe flower developmental phenotypes only developing pedicels and completely missing flower whorls (Figure 39E). Furthermore, *csc1 clv3-10* double mutants had also a rosette leaf phenotype in which the leaves had a darker green colour, were more rigid, exhibited downward curled and radialized leaves (Figure 39F) (Williams et al., 2005). In comparison to Col-0 or *csc1* siliques, siliques of double mutants were often reminiscent of *clv3-10*, exhibiting more than two carpels and a club-like shape (Figure 39G). On the other hand, double mutants also displayed Col-0 or *csc1*-like siliques (Figure 39G). Intriguingly, club-like shaped siliques of *csc1 clv3-10* double mutants occasionally increased in size and aberrant structures did grow out of the siliques probably due to non-terminated floral meristems (Figure 39H). Inflorescences of *csc1* and *clv3-10* single mutants depicted an enhanced shoot apical meristem of *clv3-10* with elevated numbers of flower buds (Figure 39I). Comparison of representative inflorescences of *csc1 clv3-10* double mutant lines #33 and #34 with *clv3-10*, revealed often smaller, but split inflorescences or similar sizes with increased flower buds (Figure 39J,K). These inflorescences were dissected and *clv3-10* depicted an increased sausage-like meristem (Figure 39L, left). The two representative *csc1 clv3-10* inflorescences exhibited an increased, but split meristem and an increased meristem with a circular structure (Figure 39L, middle and right).

Taken together, these phenotypic analyses of *csc1 clv3-10* revealed, that *csc1* seems to repress the *clv3-10* phenotype in the vegetative stage, but exacerbates it in the reproductive stage, suggesting a function of CSC1 and CLV3 in regulating stem cell maintenance in the inflorescence SAM.

4.2.9 *csc1 clv3-10* does not depict exaggerated phenotype in the root vasculature

Although CLV3 is only expressed by stem cells in the shoot apical meristem, we wanted to analysed if *csc1 clv3-10* plants might depict as well an exaggerated phenotype in the vasculature as in the SAM due to long distance effects. Six-day-old seedlings were stained with basic fuchsin and calcofluor white to counterstain lignin in secondary cell walls in xylem cells and cellulose in primary cell walls, respectively. Analysis of protoxylem cell numbers in the early differentiation zone of seedling roots revealed no differences in *clv3-10* compared to Col-0, whereas *csc1 clv3-10* had elevated protoxylem cell numbers like *csc1* (Figure 40A).

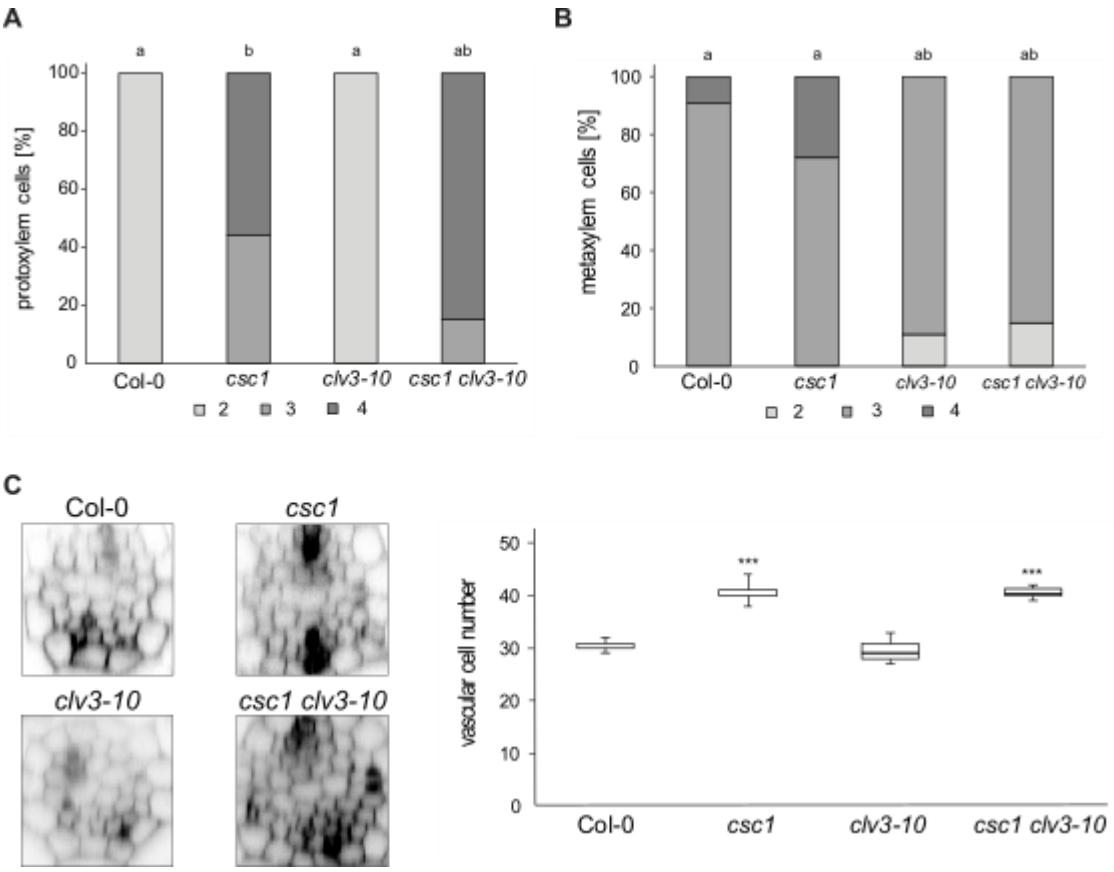

Figure 40. *csc1 clv3-10* does not depict enhanced phenotypes in root vasculature. Basic fuchsin and calcofluor white staining of six-day-old seedling roots. (A-B) Basic fuchsin staining enables counting of (A) protoxylem and (B) metaxylem cells. Squared greyish boxes depicts numbers of proto- or metaxylem cells, respectively. Col-0 wild type (n=21), *csc1* (n=18), *clv3-10* (n=19) and *csc1 clv3-10* (n=20). Statistically significant differences based on ANOVA and post-hoc Tukey. (C) Calcofluor white staining enables counting of vascular cells in the root. Representative orthogonal views of Col-0, *csc1*, *clv3-10* and *csc1 clv3-10* vascular cells in the early differentiation zone in the root. (D) Quantification of vascular cell numbers in Col-0 wild type (n=14), *csc1* (n=13), *clv3-10* (n=17) and *csc1 clv3-10* (n=12). Statistically significant difference from Col-0 based on Kruskal-Wallis test (***p < 0.001).

However, in 10 % of the counted metaxylem cells, only two metaxylem cells were counted in *clv3-10* and the double mutant *csc1 clv3-10*, instead of three to four in Col-0 (Figure 40B). The analysis of total vascular cell numbers in Col-0 and the three mutant genotypes revealed that *clv3-10* depicted a slightly decrease with an average of 29 cells in the vasculature compared to Col-0 with around 30 (Figure 40D). The double mutant and *csc1* revealed a similar vascular cell number with around 40 cells (Figure 40D).

4.2.10 RNA-Sequencing of *csc1* and Col-0

To gain further inside of the function of CSC1, we wanted to analyse which genes are down- or upregulated in the *csc1* mutant in the shoot and in the root apical meristems compared to Col-0. To perform this experiment, 20 SAMs of 35-day-old *csc1,* in *rlp4 r4l1* mutant background, and Col-0 plants with shoots around 10 cm, were dissected, primordia until flower stage 2 (Smyth et al., 1990) were removed, and triplicates were collected. For collection of root apical meristems, *csc1* and Col-0 seeds were sown out on nylon meshes which were placed on standard medium plates. Root apical meristems of six-day-old seedlings were collected in triplicates by cutting of the root apical meristems of *csc1* and Col-0, respectively. The RNA was extracted using a kit with additional DNase digestion and RNA concentrations of 350 - 750 ng/µL were sent for RNA sequencing. RNA sequencing was performed by next generation sequencing at the Deep sequencing platform at the University of Heidelberg by David Ibberson.

Using a NextSeq 550 sequencing platform and 75 bp single end read length, we obtained 30 – 60 Mio reads per sample. Reads were aligned to the Arabidopsis reference sequence (TAIR10) using RNA-Star software and over 90 % of reads could be aligned. Read counts were assinged by FeatureCounts and differentially expressed transcripts were calculated by DeSeq2. Adaptors were not removed from reads, due to the short sequencing length.

For further analysis, we analysed genes, that were significantly up- or downregulated, with a log2fold change (log2FC) of <-0.5 for downregulated genes and >0.5 for upregulated genes (Figure 41A). We utilized a VENN diagram to represent the significantly up- and down regulated genes in *csc1* in SAM and RAM (Figure 41A). In total, 2916 genes were differentially regulated in *csc1* in the RAM and the SAM. In the SAM, 2399 genes are either up- or downregulated, in the RAM 576 (Figure 41A). Of the 2916 genes, 24 were downregulated in SAM and RAM and 35 genes were upregulated in the both meristems (Figure 41A). Due to the fact, that *csc1* depicts a striking phenotype in the SAM and the RAM/vasculature, we further analysed genes that were significantly up- or downregulated in both. GO term analysis could not be computed, because of the small number common differentially expressed genes. In the list of down regulated genes in SAM and RAM, *RLP4* and *R4L1* are present, because *csc1* is still in the *rlp4 r4l1* double mutant background (Figure 41B). Furthermore, *ORA47* (AT1G74930) is downregulated in *csc1*.

ORA47 encodes a transcription factor which is proposed to act in ethylene, jasmonic acid (JA) and abscisic acid (ABA) signalling in response to wounding (Chen et al., 2016). Recent studies identified ORA47 as a putative actor in developmental processes based on the fact, that ORA47 binds to the promoter region of *WUS* and overexpression of ORA47 seems to decrease the WUS

domain in the SAM (personal conversation; Dan Zhang and Yanling Yu, Rosa Lozano Durán Lab). The increased WUS domain in *csc1* plants might be in response to downregulation of ORA47.

Among up regulated genes in SAM and RAM two genes are involved in secondary cell wall biosynthesis (Figure 41C). *TRACHEARY ELEMENT DIFFERENTIATION-RELATED 6* (*TED6*, AT1G43790), which is crucial for the differentiation of protoxylem and metaxylem cells (Endo et al., 2009) and *ALTERED XYLOGLUCAN 4* (*AXY4* or *TBL27*, AT1G70230), which is a member of the *TRICHOME BIREFRINGENCE-LIKE* (*TBL*) gene family and a putative xyloglucan (XyG) O-acetyltransferase, therefore presumably essential for the cell wall composition and properties (Gille et al., 2011; Zhu et al., 2014). Both genes are also expressed in the root and the shoot (eFP Browser; Zhu et al., 2014) and upregulation of these two genes might correlate with the increased numbers of vascular cells with elevated proto- and metaxylem cells in *csc1*.

A

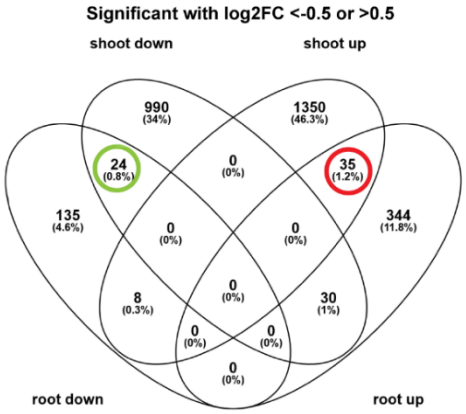

B

Down regulated genes in SAM and RAM

Accession number [TAIR]	gene name/description
AT1G28340	RLP4
AT1G14730	Cytochrome b561/ferric reductase transmembrane protein family;
AT3G01670	Encodes a protein localized to phloem filaments that is required for phloem filament formation.
AT4G04223	other_RNA
AT5G38005	other_RNA
AT5G67550	transmembrane protein
AT1G25570	R4L1
AT4G27654	transmembrane protein
AT1G74930	**ORA47**
AT3G01680	ARABIDOPSIS THALIANA SIEVE ELEMENT OCCLUSION-RELATED 1, ATSEOR1, SEOB
AT1G29380	Carbohydrate-binding X8 domain superfamily protein
AT2G44840	ERF13 (ETHYLENE-RESPONSIVE ELEMENT BINDING FACTOR 13)
AT1G15330	Cystathionine beta-synthase (CBS) protein
AT2G38470	WRKY33
AT4G24250	ATMLO13, MILDEW RESISTANCE LOCUS O 13, MLO13
AT3G10930	IDA-LIKE7, IDL7
AT2G13360	AGT, AGT1, ALANINE:GLYOXYLATE AMINOTRANSFERASE,
AT4G24450	GWD3, PHOSPHOGLUCAN, WATER DIKINASE, PWD
AT5G04680	Ankyrin repeat family protein
AT4G28703	RmlC-like cupins superfamily protein
AT3G29644	antisense_long_noncoding_rna, SHORT OPEN READING FRAME 29, SORF29
AT1G28330	ATDRM1, DORMANCY-ASSOCIATED PROTEIN 1, DORMANCY-ASSOCIATED PROTEIN-LIKE 1
AT4G23810	WRKY53
AT1G69890	actin cross-linking protein

C

Up regulated genes in SAM and RAM

Accession number [TAIR]	gene name/description
AT3G16520	UDP-GLUCOSYL TRANSFERASE 88A1
AT5G22460	alpha/beta-Hydrolases superfamily protein
AT3G21560	BRIGHT TRICHOMES 1, BRT1, UDP-GLUCOSYL TRANSFERASE 84A2, UGT84A2
AT5G59920	UV-B LIGHT INSENSITIVE 3
AT3G23150	ETHYLENE RESPONSE 2, ETR2
AT5G45650	subtilase family protein
AT4G15480	UGT84A1, encodes a protein that might have sinapic acid:UDP-glucose glucosyltransferase activity.
AT1G43790	**TED6, TRACHEARY ELEMENT DIFFERENTIATION-RELATED 6, plant 2nd cell wall biogenesis**
AT3G60720	PDLP8, PLASMODESMATA-LOCATED PROTEIN 8
AT1G26820	RIBONUCLEASE 3, RNS3
AT5G17860	CALCIUM EXCHANGER 7, CAX7, CCX1
AT2G46340	SPA1, SUPPRESSOR OF PHYA-105 1
AT1G13600	ATBZIP58, BASIC LEUCINE-ZIPPER 58, BZIP58
AT5G53590	SAUR30, SMALL AUXIN UPREGULATED RNA 30
AT4G08755	small_nuclear_rna
AT5G54270	LHCB3, LHCB3*1, LIGHT-HARVESTING CHLOROPHYLL B-BINDING PROTEIN 3
AT5G13930	ATCHS, CHALCONE SYNTHASE, CHS, TRANSPARENT TESTA 4, TT4
AT5G45630	senescence regulator
AT5G08640	ATFLS1, FLAVONOL SYNTHASE, FLAVONOL SYNTHASE 1, FLS, FLS1
AT1G62935	transmembrane protein
AT1G70230	**ALTERED XYLOGLUCAN 4, AXY4, TBL27, TRICHOME BIREFRINGENCE-LIKE 27,**
AT1G80760	NIP6, NIP6;1, NLM7, NOD26-LIKE INTRINSIC PROTEIN 6;1, boron transport
AT2G14095	hypothetical protein
AT3G25620	ABCG21, ATP-BINDING CASSETTE G21
AT4G14650	hypothetical protein
AT3G17790	ATACP5, ATPAP17, PAP17, PURPLE ACID PHOSPHATASE 17,
AT4G28720	CKRC2, CYTOKININ INDUCED ROOT CURLING 2, YUC8, YUCCA 8
AT3G26290	CYTOCHROME P450, FAMILY 71, SUBFAMILY B, POLYPEPTIDE 26", CYP71B26
AT1G48670	auxin-responsive GH3 family protein
AT5G64940	A. THALIANA OXIDATIVE STRESS-RELATED ABC1-LIKE PROTEIN 1, ABC1K8,
AT5G64170	LNK1, NIGHT LIGHT-INDUCIBLE AND CLOCK-REGULATED 1
AT1G34440	transmembrane protein
AT3G47420	ATG3PP1, ATPS3, G3PP1, GLYCEROL-3-PHOSPHATE PERMEASE 1
AT5G67390	glycosyltransferase-like protein
AT2G01422	other_rna

Figure 41. VENN diagramme shows more differentially expressed genes in the shoot apical meristem of *csc1*. (A) VENN diagram of significant up- (log2FC>0.5) or downregulated (log2FC<-0.5) genes (2916) in shoot and root of *csc1* compared to Col-0. (B) Table of 24 genes, that are significantly down regulated in SAM and RAM in *csc1* compared to Col-0, indicated by green circle (data from A). (C) Table of 35 genes, that are significantly up regulated in SAM and RAM in *csc1* compared to Col-0, indicated by red circle (data from A).

Additionally, we performed GO-enrichment analysis with all significantly up- and downregulated genes in the RAM and SAM samples, respectively. GO-enrichments for molecular function were calculated by Panther. 3770 genes were differentially expressed in the RAM and of these genes, 3238 genes could be classified depending on their molecular function (Table 3). Three different classes were highlighted, either because of a high fold enrichment in *csc1* compared to the reference genome or many genes were classified into one molecular function. The green group comprised genes involved in ATP/nucleotide binding, the yellow group genes, involved in protein kinase activity and the blue group depicted the highest fold enrichment compared to the reference and comprised genes involved in RNA binding/ribosomal complexes (Table 3). Based on this data, *CSC1* might regulate signalling cascades, which often contain protein kinases and phosphorylation and de-phosphorylation events. Downstream of activated signalling cascades, transcriptional and translational machineries are activated, which might be indicated by the overrepresentation of genes involved in RNA binding/ribosomal complexes. The GO-enrichment analysis of significantly up- and downregulated genes in SAM samples revealed similar results. 5942 genes were differentially expressed in the SAM and of these genes, 5054 genes could be classified depending on their molecular function (Table 4). However, only the blue and green groups with genes involved in RNA binding/ribosomal complexes and ATP/nucleotide binding could be assigned, respectively.

Table 3. GO-enrichment for molecular function of significantly up- and downregulated genes in the RAM. Genes involved in translation (rRNA) (blue), in kinase activity (yellow) and nucleotide binding (green) are highlighted.

	Arabidopsis thaliana (REF)	csc1			
GO molecular function complete	#	#	expected	Fold Enrichment	P value
structural constituent of ribosome	358	236	49.17	4.8	4.91E-64
structural molecule activity	502	265	68.95	3.84	1.59E-57
rRNA binding	102	56	14.01	4	3.75E-11
RNA binding	1136	342	156.02	2.19	9.40E-31
nucleic acid binding	3324	624	456.52	1.37	1.73E-10
organic cyclic compound binding	5689	1080	781.33	1.38	1.20E-23
binding	10024	1787	1376.71	1.3	5.11E-34
heterocyclic compound binding	5667	1077	778.31	1.38	1.02E-23
mRNA binding	420	160	57.68	2.77	4.03E-21
copper ion binding	239	74	32.82	2.25	2.16E-05
transition metal ion binding	1325	244	181.98	1.34	4.83E-02
metal ion binding	2586	472	355.16	1.33	9.70E-06
cation binding	2609	475	358.32	1.33	1.30E-05
ion binding	4455	800	611.85	1.31	1.43E-10
UDP-glucosyltransferase activity	171	52	23.49	2.21	4.09E-03
transferase activity	3725	637	511.59	1.25	1.18E-04
catalytic activity	8868	1485	1217.94	1.22	2.19E-14
glucosyltransferase activity	211	62	28.98	2.14	1.38E-03
calmodulin binding	231	62	31.73	1.95	2.02E-02
protein binding	4527	808	621.74	1.3	3.39E-10
identical protein binding	290	77	39.83	1.93	1.78E-03
cofactor binding	756	158	103.83	1.52	5.39E-03
protein serine/threonine kinase activity	931	188	127.86	1.47	3.72E-03
protein kinase activity	1070	221	146.95	1.5	9.68E-05
kinase activity	1390	268	190.9	1.4	7.51E-04
transferase activity, transferring phosphorus-containing groups	1595	292	219.06	1.33	1.00E-02
phosphotransferase activity, alcohol group as acceptor	1219	239	167.42	1.43	1.22E-03
ATP binding	1547	298	212.47	1.4	1.76E-04
drug binding	1908	355	262.05	1.35	1.94E-04
adenyl ribonucleotide binding	1569	302	215.49	1.4	1.43E-04
adenyl nucleotide binding	1576	303	216.45	1.4	1.52E-04
purine nucleotide binding	1807	331	248.18	1.33	2.01E-03
nucleotide binding	2231	411	306.41	1.34	4.46E-05
nucleoside phosphate binding	2231	411	306.41	1.34	4.46E-05
small molecule binding	2605	469	357.77	1.31	5.75E-05
purine ribonucleotide binding	1798	330	246.94	1.34	1.89E-03
ribonucleotide binding	1822	334	250.24	1.33	1.84E-03
carbohydrate derivative binding	1860	335	255.45	1.31	7.30E-03
purine ribonucleoside triphosphate binding	1777	326	244.05	1.34	2.34E-03
anion binding	2254	422	309.57	1.36	5.84E-06
Unclassified	5713	532	784.63	0.68	0.00E+00

Table 4. GO-enrichment for molecular function of significantly up- and downregulated genes in the SAM. Genes involved in translation (rRNA) (blue), and nucleotide binding (green) are highlighted.

	Arabidopsis thaliana (REF)	csc1			
GO molecular function complete	#	#	expected	Fold Enrichment	P value
structural constituent of ribosome	358	205	77.58	2.64	8.00E-23
structural molecule activity	502	259	108.79	2.38	3.12E-24
rRNA binding	102	57	22.1	2.58	9.40E-05
RNA binding	1136	438	246.18	1.78	1.81E-20
nucleic acid binding	3324	975	720.33	1.35	6.34E-15
organic cyclic compound binding	5689	1616	1232.85	1.31	2.40E-23
binding	10024	2755	2172.27	1.27	4.96E-41
heterocyclic compound binding	5667	1609	1228.08	1.31	4.26E-23
DNA-dependent ATPase activity	87	45	18.85	2.39	1.04E-02
ATPase activity, coupled	493	167	106.84	1.56	2.05E-03
ATPase activity	639	213	138.48	1.54	1.67E-04
nucleoside-triphosphatase activity	875	290	189.62	1.53	1.35E-06
pyrophosphatase activity	920	313	199.37	1.57	2.03E-08
hydrolase activity, acting on acid anhydrides, in phosphorus-containing anhydrides	922	314	199.8	1.57	1.66E-08
hydrolase activity, acting on acid anhydrides	928	317	201.1	1.58	1.12E-08
hydrolase activity	3162	832	685.23	1.21	2.90E-04
catalytic activity	8868	2254	1921.76	1.17	3.85E-13
protein transporter activity	146	62	31.64	1.96	3.92E-02
mRNA binding	420	178	91.02	1.96	1.02E-09
isomerase activity	256	98	55.48	1.77	7.97E-03
protein binding	4527	1325	981.03	1.35	6.09E-22
ATP binding	1547	424	335.25	1.26	2.68E-02
drug binding	1908	508	413.48	1.23	4.48E-02
adenyl ribonucleotide binding	1569	434	340.01	1.28	8.89E-03
adenyl nucleotide binding	1576	437	341.53	1.28	6.98E-03
purine nucleotide binding	1807	512	391.59	1.31	9.15E-05
nucleotide binding	2231	638	483.47	1.32	4.60E-07
nucleoside phosphate binding	2231	638	483.47	1.32	4.60E-07
small molecule binding	2605	712	564.52	1.26	2.37E-05
purine ribonucleotide binding	1798	508	389.64	1.3	1.57E-04
ribonucleotide binding	1822	515	394.84	1.3	1.18E-04
carbohydrate derivative binding	1860	525	403.08	1.3	9.84E-05
purine ribonucleoside triphosphate binding	1777	498	385.09	1.29	4.52E-04
anion binding	2254	628	488.46	1.29	1.89E-05
ion binding	4455	1162	965.43	1.2	1.99E-06
metal ion binding	2586	668	560.4	1.19	4.51E-02
cation binding	2609	678	565.39	1.2	2.07E-02
Unclassified	5713	888	1238.05	0.72	0.00E+00

4.2.11 *csc1* corresponds to an unknown mutation in chromosome five

4.2.11.1 Bulked segregant analysis identifies mutation on chromosome five

First, we attempted to narrow down the mutation to a chromosomal region by bulked segregant analysis. Thus, we crossed *csc1* (Col-0 background), still carrying mutations in *RLP4* and *R4L1*, with the Landsberg *erecta* (L*er*) ecotype (Figure 42). These two ecotypes contain repetitive regions interspersed on all chromosomes, that differ in lengths and thereby can be used as marker regions for PCR based amplifications (James et al., 2013).

F_1 hybrids of *csc1* and L*er* crosses depicted a phenotype similar to Col-0 (Figure 42A), consistent with a recessive mutation. Due to recombination events from F_1 to F_2 populations, the descendants of the F_1 plants are carrying chromosomes with a diverse *csc1* (Col-0) and L*er* region pattern. 200 F_2 plants were phenotypically characterized and genomic DNA (gDNA) was extracted from plants with *csc1* (+) and without *csc1* (-) phenotypes. Bulked gDNA of plants with *csc1* phenotypes (+) was analysed with a set of markers for all five chromosomes. As the mutation originates from plants with Col-0 background, we would expect only Col-0 DNA in the chromosomal region close to the mutation. Amplified PCR fragments of markers will show one strong band for Col-0 in this area. In areas further upstream or downstream of the mutation, recombination events occurred, leading to a higher percentage of L*er*, which will be depicted by a strong Col-0 band and a weak L*er* band. In chromosome areas, where Col-0 and L*er* are equally distributed, Col-0 and L*er* will depict bands with the same intensity.

PCRs of all markers in the five Arabidopsis chromosomes were performed with a Col-0 and L*er* gDNA control, the bulked gDNA of F_2 plants with the *csc1* phenotype (+) and as a negative control, bulked gDNA of F_2 plants without *csc1* phenotype (-). Gel electrophoresis revealed a characteristic Col-0/L*er* band pattern for the bottom of chromosome five, highlighted by the red frame (Figure 42B). For marker K6M13ind33 (~20 Mio bp), only one band at the size of the Col-0 band, was visible (Figure 42B). The flanking markers (~17.6 Mio bp and ~24.5 Mio bp) still depicted a weak band for L*er*, meaning that the mutation of *csc1* is localized in this area (Figure 42B). Additionally markers in this area could further narrowed down the region of the *csc1* mutation to a region from ~18 Mio bp to ~20 Mio bp (Figure 42B).

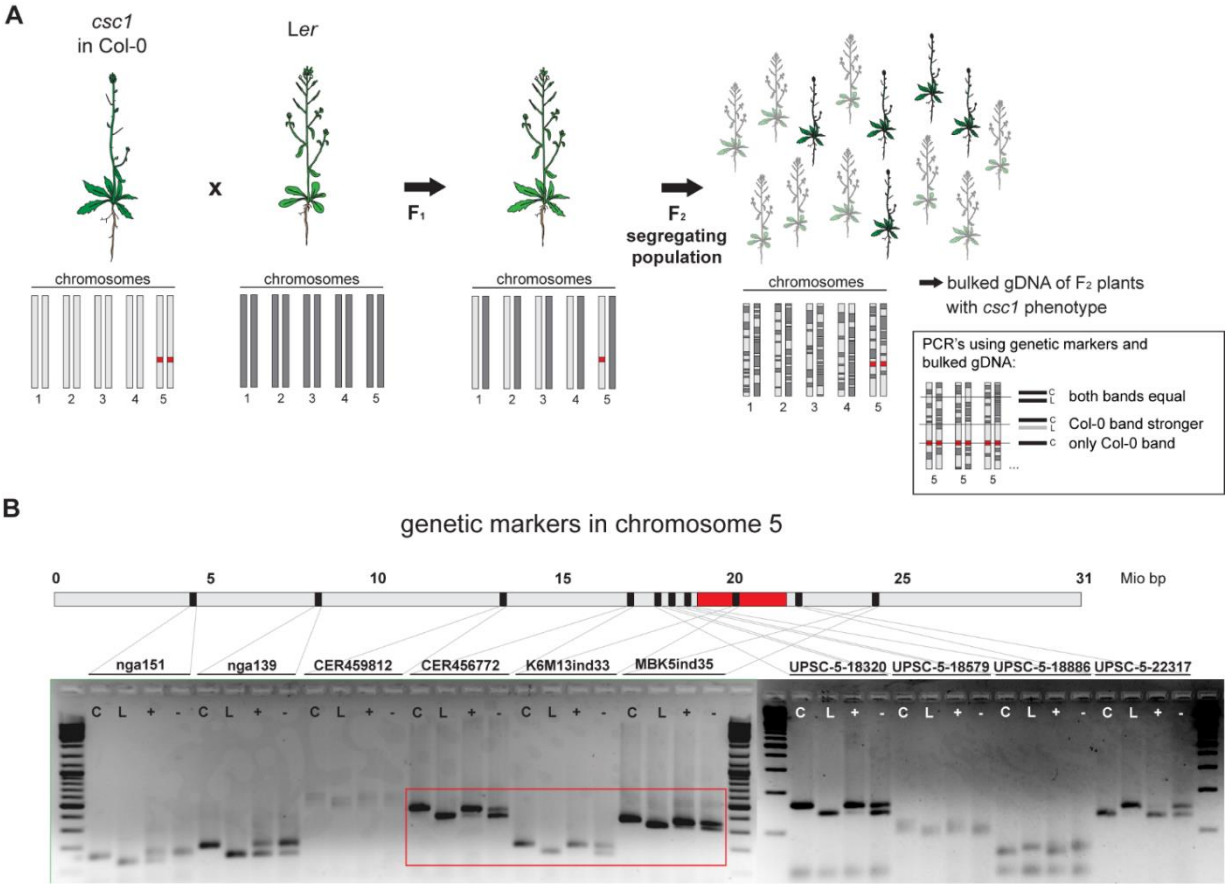

Figure 42. Mutation in *csc1* is localized on chromosome five. Bulked segregant analysis of a F_2 population of *csc1* in Col-0 crossed with L*er*. (A) Overview of establishing the bulked segregant population with *csc1* and L*er*. Pooled gDNA of F_2-plants with a *csc1* phenotypes was used for PCR reactions with genetic markers for the five chromosomes. (B) The mutation was identified on chromosome five using genetic markers that are amplifying the depicted areas on the chromosome and reveal different PCR amplified fragments depending on the ecotype background. Samples of Col-0 (C), L*er* (L) and bulked gDNA of plants with *csc1* (+) and without (-) phenotype were analysed. Red frame depicts the three genetic markers, where shifts in the intensity of band patterns occurred. In marker K6M13ind35 (~20.3 Mio bp), only a Col-0 band was detected.

4.2.11.2 Whole Genome Sequencing identifies three mutations in *csc1*

To identify the mutation in the *csc1* mutant, we sent samples for whole genome sequencing (WGS). Therefore, cauline leaves of a segregating *csc1* Col-0 F_2 population were collected. Plant material of around 50 plants (40 DAG) with *csc1* phenotype (+) and without *csc1* phenotype (-), were harvested. Additionally, around 50 seedlings of the same F_2 population were also screened and collected for the protoxylem *csc1* phenotype (+) and without *csc1* phenotype (-). Plant material from adult plants (F_2) and seedlings (F_2) with the *csc1* phenotype were bulked as one sample (+), the same was done for the samples without *csc1* phenotyppes (-). As a third sample, *csc1* seedlings and cauline leaves of adult plants were collected and bulked. Of all three plant samples gDNA was extracted using the CTAB-gDNA extraction protocol. Concentrations of 450 – 850 ng/µL gDNA were sent for sequencing (StarSeq, Mainz).

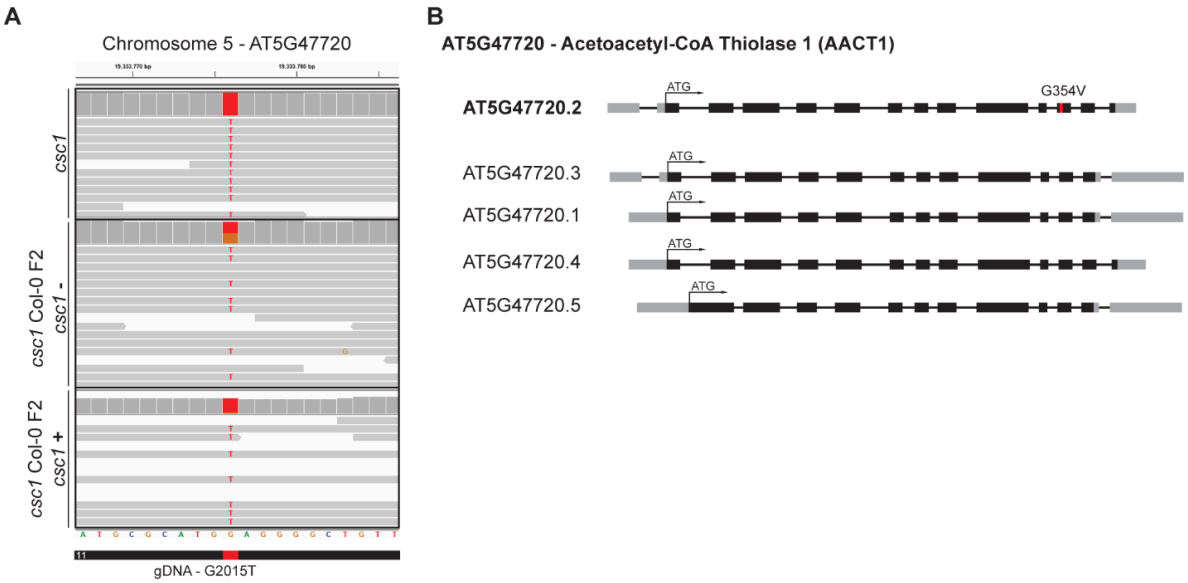

Figure 43. Identification of a SNP in Acetoacetyl-CoA Thiolase 1 (AACT1) in *csc1* plants. (A) Overview of mapping populations and position of identified SNP in exon eleven of AT5G47720 – Acetoacetyl-CoA Thiolase 1 (AACT1). SNP was identified in all reads in *csc1*, in around one third of reads of a segregating *csc1* Col-0 F_2 population, from plants without *csc1* phenotype (-), and in all reads of a segregating *csc1* Col-0 F2 population, from plants with *csc1* phenotype (+). The mutation is located 2015 bp downstream of the ATG (gDNA), exchange from guanine to thymine. (B) Overview of gene structure with exons (black boxes), introns (black lines), UTRs (grey boxes) and ATG codon. All five splice variants of AACT1 are listed. The position of the SNP is marked in red in exon eleven and is based on the splice variant 2 CDS sequence (AT5G47220.2). Base exchange from guanine to thymine leads to an exchange of amino acids from glycine (G) to valine (V) at amino acid sequence position 354 (G354V). Alignment was performed by IGV_2.5.0

Sequenced reads with a length of 150 bp were aligned to the *Arabidopsis thaliana* reference genome. Reads of *csc1*, *csc1* Col-0 F_2 (+) and *csc1* Col-0 F_2 (-) were aligned with the reference genome and analyzed using IGV_2.5.0. We could identify three SNPs on chromosome five, supporting the results from the bulked segregant analysis (Figure 42). The first SNP was located in AT5G47720 which encodes for ACETOACETYL-COA THIOLASE 1 (AACT1). In all three samples, the point mutation with an exchange of guanine to thymine was visible (Figure 43A). The mutation was found in 100 % of the *csc1* and *csc1* Col-0 F_2 (+) reads, and in around 35 % of the *csc1* Col-0 F_2 (-) samples. We expected around one third of mutations in the *csc1* Col-0 F_2 (-) population due to heterozygous plants. The SNP is situated in exon eleven, 2015 bp downstream of the ATG (gDNA) which leads to an exchange in the amino acids sequence from glycine to valine G354V. This position of amino acids exchange is based on the amino acid sequence of splice variant AT5G47720.2 (Figure 43B). AACT1 is located in the cytoplasm and chloroplasts, were it catalyzes the condensation of two acetyl-CoAs to form acetoacetyl-CoA (Jin et al., 2012). This is the initial step in the mevalonate (MVA) pathway, which includes also the synthesis of brassinosteroids (Jin et al., 2012). RNA-Seq data showed a significant downregulation of *AACT1* in the *csc1* mutant in the SAM, but in the RAM it was not differentially regulated (Appendix A2).

The second SNP was discovered in AT5G43810, better known as *ZWILLE* or *ARGONAUTE 10* (*ZLL*/*AGO10*). The point mutation depicted an almost 100 % penetration in *csc1* and *csc1* Col-0 F_2 (+) samples with an exchange of guanine to adenine 1333 bp downstream of ATG (gDNA) (Figure 44A). This point mutation is leading to an amino acid exchange from glutamic acid to lysine at position E444K in exon six both splice variants (Figure 44B). AGO10 is required to establish the central-peripheral organization of the embryo apex and controls together with WUS and CLV3 the organization of central and peripheral zone by sequestering miR165/166 to regulate SAM development (Manavella et al., 2011; Tucker et al., 2013; Xue et al., 2017). RNA-Seq data showed a significant upregulation of *AGO10* in the RAM of the *csc1* mutant, but in the SAM it was not differentially expressed (Appendix A2).

The third SNP was discovered either in the presumed terminator region of AT5G51560 or the predicted promoter region of the downstream gene AT5G51570. In 100 % of *csc1* and *csc1* Col-0 F_2 (+) reads, the point mutation showed an exchange of adenine to cytosine and is located 3328 bp downstream of the ATG in AT5G51560 (Figure 46A). The negative control showed the point mutation only in two reads (Figure 46A). AT5G51560 encodes for a LRR-RLK, thus being a putative candidate for *CSC1* as a receptor for CLE21 or CLE27. However, RNA-Seq data did not reveal a significant downregulation of At5G51560 in *csc1* in the RAM nor in the SAM compared to Col-0. AT5G51570 encodes for a SPFH/Band 7/PHB domain-containing membrane-associated

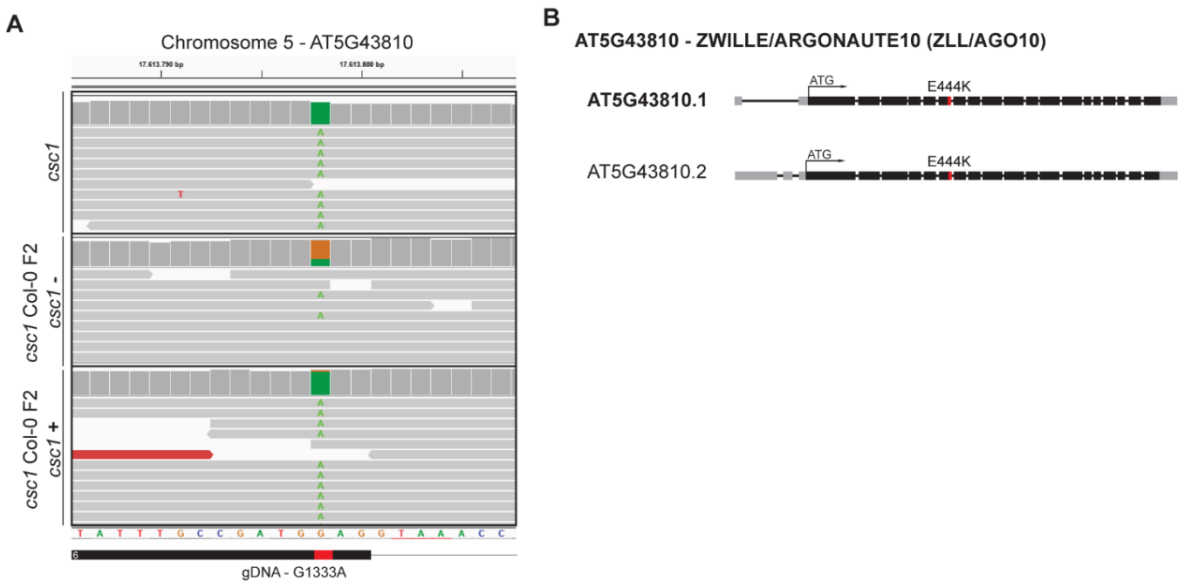

Figure 44. Identification of SNP in ZWILLE/ARGONAUTE10 (ZLL/AGO19) in *csc1* plants. (A) Overview of mapping populations and position of identified SNP in exon six of AT5G43810 – ZWILLE/ARGONAUTE10 (ZLL/AGO10). SNP was identified in all reads in *csc1*, only in two reads of a segregating *csc1* Col-0 F_2 population, from plants without *csc1* phenotype (-), and in almost all reads of a segregating *csc1* Col-0 F_2 population, from plants with *csc1* phenotype (+). The mutation is located 1333 bp downstream of the ATG (gDNA) with a base exchange from guanine to adenine. (B) Overview of gene structure with exons (black boxes), introns (black lines), UTRs (grey boxes) and ATG codon. Position of the identified SNP is marked in red at the end of exon six. Base exchange from guanine to adenine leads to an exchange of amino acids from glutamic acid (E) to lysine (K) at amino acid sequence position 444 (E444K). Both splice variants of ZLL/AGO10 are listed. Alignment was performed by IGV_2.5.0.

protein, but was not further characterized. RNA-Seq data neither revealed differentially expression of AT5G51570 in *csc1*.

In summary, results of phenotypic characterizations, phytohormonal and peptide responses, transcriptional and genetic analysis of CSC1 can be depicted in a preliminary scheme (Figure 45). We could reveal that CSC1 might regulate proliferation by negatively regulating cytokinin response in the shoot and root apical meristem. CSC1 is presumably involved in CLE21/CLE27 signalling which seems to cross-talk with cytokinin signalling. In the SAM, the regulation of proliferation is presumably controlled either via a direct or indirect interaction with WUS. In addition, CSC1 seems to positively regulate CLV3 signalling depicted by uncoupling the WUS-CLV3 feedback loop in the csc1 mutant.

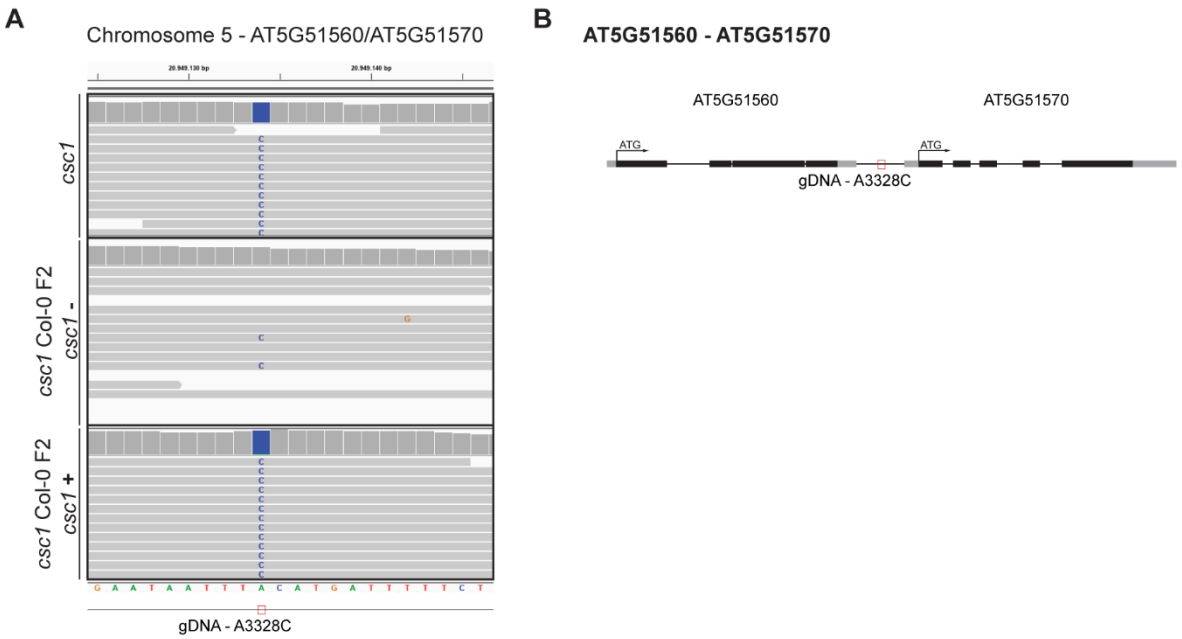

Figure 46. Identification of SNP in terminator or promoter region of AT5G51560/AT5G51570 in *csc1* plants. (A) Overview of a SNP in the terminator region of AT5G51560, encodes for a LRR-RLK or the promoter region of AT5G51570, encodes for SPFH/Band7/PHB domain-containing membrane-associated protein family. Replacement of an adenosine by cytosine, 3328 bp (A3328C) downstream of the AT5G51560 ATG. SNP was identified in all reads in *csc1*, only in two reads of a segregating *csc1* Col-0 F_2 population, from plants without *csc1* phenotype (-), and in all reads of a segregating *csc1* Col-0 F_2 population, from plants with *csc1* phenotype (+). (B) Overview of gene structure with exons (black boxes), introns (black lines), UTRs (grey boxes) and ATG codon. Position of the identified SNP is marked by a red box between AT5G51560 and AT5G51570. Alignment was performed by IGV_2.5.0

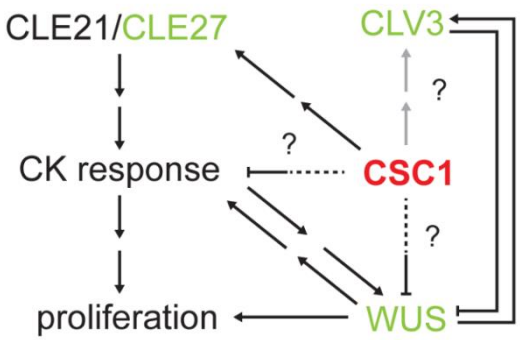

Figure 45. Overview of putative functions of CSC1 in maintaining stem cells in the SAM and controlling CLE and cytokinin signalling in shoot and root. The factors in green are specifically expressed in the shoot apical meristem, all other factors are expressed in shoot and root.

4.3 Discussion

4.3.1 CSC1 controls meristem size in the SAM through WUS

In this study, we could identify CSC1 as a new player in regulating meristem size presumably through regulating the cytokinin signalling pathway. *csc1* displayed severe defects in flower development, an enlarged SAM and more vascular cell numbers, which suggested a function of CSC1 in the SAM and the RAM.

The size of the SAM is mainly controlled by the negative feedback loop of the homeodomain transcription factor WUSCHEL (WUS) and the small secreted CLV3 peptide. Mutations in the CLV3 peptide or in the CLV3 receptors and co-receptors CLV1/CLV2/CRN/BAMs result in the disruption of the core WUS-CLV3 feedback loop and lead to severe stem cell over-proliferation, causing an increased SAM (Fletcher et al., 1999; Muller et al., 2008). *csc1* mutant plants also showed an increased apical meristem with more initiated primordia, reminiscent of the aforementioned mutants (Figure 25, Figure 26). We assessed if the increase in SAM size might be due to altered *WUS* and/or *CLV3* expression in the *csc1* mutant, analysing the *pCLV3:BFP-NLS/pWUS:2xVenus-NLS* marker. Analysis revealed a strong increase in the WUS domain in *csc1* plants and ratios of *pWUS* positive cells and total cell numbers in the SAM compared to Col-0 showed an increase independent of meristem size (Figure 37). Furthermore, the *CLV3* domain was slightly increased in the *csc1* mutant, which might be sufficient to increase the number of highly proliferating cells and to increase overall apical meristem size. Intriguingly, analysis of *CLV3*/total meristem size ratios in Col-0 and *csc1* plants revealed, that the *CLV3* domain was slighty reduced in relation to the meristem size in *csc1* plants (Figure 37). These findings are contradictory to previous studies, which showed that interferring with one player of the tightly controlled WUS-CLV3 feedback loop, affected all players, mainly leading to an increase of WUS and CLV3 domains (Fletcher et al., 1999; Muller et al., 2008; Je et al., 2016). Thus, these findings suggest, that CSC1 might interfere and modulate the WUS-CLV3 feedback loop.

4.3.2 CSC1 might control auxin signalling through the expression of WUS

In addition to a severe vascular and shoot apical meristem phenotype, *csc1* exhibited flower developmental defects. These defects did not occur from the early reproductive stage, but in plants approximately 40-45 days old with shoots around 15-20 cm. All degrees of developmental severity in flower development were visible along the primary shoot, mostly depicted by missing organs in the single whorls or completely missing flowers, elucidated by pedicels (Figure 25).

Strikingly, wild type-like flowers were still able to form and siliques of these flowers were also wild type-like. Thus, the *csc1* flower phenotype is presumably a secondary effect due to volatile concentrations of signal peptides or phytohormones and their signalling pathways, because wild type-like flowers and siliques could still be formed. We identified a similar phenotype in *clv3-10* mutant plants, either depicting too many organs, mainly in stamens and carpels, or exhibited the *csc1* phenotype with missing flower organs. It was previously reported, that increased shoot apical meristem size can result in flower development defects due to the initiation of too many primordia and/or the failure of establishing inhibitory fields by cytokinin signalling in between the initiated primordia (Mirabet et al., 2012; Besnard et al., 2014b; Landrein et al., 2015b). Primordia are initiated by establishing fields with elevated auxin signalling output, which can be visualized by the *pDR5v2* marker (Liao et al., 2015). In wild type conditions, *pDR5v2:YFP* is weakly expressed in the centre of the meristem and increases in a wedged shape towards the periphery, marking the area of primordia initiation (Figure 38). A recent study identified that low auxin signalling levels in the centre of the shoot apical meristem, mediated by WUS, are essential to maintain stem cell identities (Ma et al., 2018). Intriguingly, *csc1* plants did not show *pDR5v2* signal in the centre of the meristem and *Dr5v2* positive areas are smaller represented by a roundish shape (Figure 38). However, we identified an increased WUS domain in *csc1* that might compensate the missing auxin signalling domain in the centre. Smaller *pDR5v2* positive domains might signify less cells that are primed as primordia cells, which are missing in establishing a functional floral meristem and will lead to flower defects. Once cells are recruited and primed in the *pDR5v2* domain, the absence of *csc1* might also lead to increased cytokinin and WUS expression in the establishing floral meristem. Resulting either in wild type-like flowers or, if the WUS domain expands too much, in flowers with elevated organ numbers. The *csc1* flower developmental phenotype is also reminiscent of the FILAMENTOUS FLOWER (FIL) mutant phenotype. FIL on the one hand terminates floral meristem and is involved in specifying abaxial cell types, on the other hand *fil* mutants also depict increased shoot apical meristems, similar to *csc1* (Sawa et al., 1999; Lugassi et al., 2010; Bonaccorso et al., 2012). However, RNA-Seq data did not reveal differentially transcribed *FIL* in *csc1* (Appendix A2).

In conclusion, CSC1 seems to regulate auxin signalling by repressing *WUS* and constraining its activity to the centre of the meristem. The expanded cytokinin signalling domain in the centre of *csc1* meristems also forms an increased inhibitory field for auxin signalling and the initiation of primordia, pushing them towards the boundary zone (Besnard et al., 2014a, b). Probably due to the increased meristem size in *csc1*, phyllotaxis is altered and several primordia seemed to be initiated at the same time. It would be important for future analysis, to test if the application of CLV3 peptide might restore the *csc1* apical meristem and flower phenotypes.

4.3.3 CSC1 controls meristem size through cytokinin signalling

Cytokinin signalling is, together with auxin signalling, a crucial phytohormone in meristem maintenance in the SAM and the RAM. In the SAM, cytokinin levels in the organizing centre (OC) and the positive transcriptional regulators type-B ARRs (such as ARR10 and 12) promote WUS transcription and WUS in turn represses the cytokinin repressors type-A ARRs (Leibfried et al., 2005; Gordon et al., 2009; Xie et al., 2018). Thus, stem cell maintenance and meristem size is, apart from the WUS-CLV3 feedback loop, tightly controlled by cytokinin signalling which is also in cross-talk with other signalling pathways (Kondo et al., 2011; Uchida et al., 2013; Besnard et al., 2014a; Xie et al., 2018).

As mentioned before, cytokinin signalling can promote WUS expression via the transcriptional regulators type-B ARRs. Therefore, we analysed the cytokinin response in the shoot apical meristem of *csc1* mutants with the synthetic type-A ARR cytokinin reporter *pTCSn:GFP-NLS*. *csc1* plants showed a strong increase in the *pTCSn* domain, but ratios of *pTCSn* positive cells and total cell numbers in the SAM revealed almost the same ratios in Col-0 and *csc1*, assuming that the increase in *pTCSn* positive cells might be correlated with the increase of total meristem size and seems to be uncoupled from WUS, which showed a stronger increase in the expression domain (Figure 37). Wild type plants almost display the same amount of cells, that are positive for *pTCSn* and *pWUS* (Figure 34, Figure 36), displaying the tight control of cytokinin signalling and WUS. Recently, a publication could show, that the application of nitrate led to an increased SAM and affected to the most extent the cytokinin response (*pTCSn*) and to a lesser extent *WUS* and *CLV3* expression, suggesting a buffered system. In addition, it implies that *WUS* expression is only regulated via cytokinin signalling (Landrein et al., 2018). Furthermore, it could be identified, that elevated cytokinin signalling and an increase in *WUS* expression contributes more to the size of the SAM, than the expression of *CLV3* (Landrein et al., 2018). In our study, we revealed, that the mutation in *CSC1* had the strongest effect on *WUS* and to a lesser extent on cytokinin signalling and *CLV3*. This suggests, that CSC1 regulates (directly) WUS and cytokinin signalling, thereby maintaining stem cells in the apical meristem.

In addition to the severe *csc1* phenotype in the SAM, phenotypic characterization of *csc1* showed an increase in total root vascular cell numbers compared to Col-0 (Figure 27). Interestingly, procambium and xylem cell numbers were elevated, but phloem cell numbers did not seem to be affected. In the xylem, more metaxylem and protoxylem cells were counted already in the early differentiating zone of the root, likely due to a function of CSC1 in the root apical meristem, as ectopic xylem cells in *rlp44*, *bri1* and *pskr1 pskr2* occurred much later, because of cell fate shift (Holzwart et al., 2018). Especially the high numbers of four to five protoxylem numbers in *csc1*

compared to two in Col-0 were striking (Figure 27). Patterning and establishment of xylem identities is a highly controlled process in plants and involves interplay of phytohormonal and transcriptional networks as well as spatio-temporal patterning in the early embryo (De Rybel et al., 2016). Previously reported mutants with elevated protoxylem cell numbers were either involved in cytokinin perception/signalling or in tissue patterning in the root vasculature (Mähönen et al., 2000; Mähönen et al., 2006; Zhou et al., 2013). Reductions in cytokinin signalling levels in the vasculature due to mutations in cytokinin receptors *cre1 ahk3* or *wol* (*ahk4*), results in fewer vascular cells but in turn also fewer metaxylem cells and ectopic protoxylem (Mähönen et al., 2000; Mähönen et al., 2006). High levels of cytokinin maintain the vascular stem cells and repress differentiation into phloem and xylem cells. On the other hand, downregulation of cytokinin and upregulation of *AHP6* by auxin is crucial, to establish protoxylem cells (De Rybel et al., 2016). We hypothesised, that increased cytokinin levels in *csc1* might be causative for this effect and tested if exogenous cytokinin application may enhance the vascular cell number in *csc1*. In fact, exogenous cytokinin revealed a slight increase in total vascular cells, but a dramatic increase in *csc1* (Figure 33). These results indicate, that CSC1 might function in buffering cytokinin levels or is balancing cytokinin signalling to repress increased proliferation.

A second phenotype we identified in Col-0 and *csc1* plants treated with cytokinin, is the absence of protoxylem cells, depicted by the absence of secondary cell walls (Figure 33). These findings are supported by previous studies (Mähönen et al., 2006a). In higher concentrations even metaxylem cells were absent. These results suggest, that enhanced cytokinin signalling promotes proliferation of procambial cells and leads to reduction of cell differentiation, depicted by the absence of proto- and metaxylem cells. Contradictory, *csc1* mutants in standard conditions exhibits more vascular stem cells, but also more differentiated meta- and protoxylem cells. Because elevated cytokinin levels lead to enhanced proliferation but also inhibition of differentiation, additional factors have to be involved in xylem differentiation. AT-HOOK (AHL) transcriptions factors regulate tissue patterning in the vasculature and are crucial in establishing a boundary between procambium and xylem. In a recent study it is hypothesised, that these transcription factors are in a cross-talk with cytokinin (Zhou et al., 2013). Enhanced cytokinin signalling seems to positively regulate AHL3 and AHL4. Increased AHL3 and AHL4 activity might explain, why *csc1* still has differentiated xylem cells, although presumably elevated cytokinin levels promote proliferation. However, based on RNA-Seq data, upregulation of *AHL3* and *AHL4* could only be identified in the SAM of *csc1* (Appendix A2).

On grounds of the previous results, investigations of cytokinin responses (*pTCSn:GFP-NLS*) in the root apical meristem vasculature in Col-0 and *csc1* revealed, that the cytokinin response in *csc1* was slightly increased, but much broader and also in more mature cells in the vasculature

compared to Col-0 (Figure 34). The extensive response in the vasculature in *csc1* is presumably due to more procambium cells than in Col-0. In light of the phenotypes of *csc1* in the shoot and the root, CSC1 might function in repressing cytokinin signalling in both meristems, which has to be further investigated.

4.3.4 CSC1 might be involved in CLE21 and CLE27 perception or signalling

Phenotypical characterization of *csc1* phenotypes revealed an increased number of vascular cells, in particular more protoxylem cells, compared to Col-0. The CLE root bioassay is based on the growth-inhibitory effect of 17 root-active CLE peptides and a useful test to reveal putative new CLE receptors (Ito et al., 2006; Strabala, 2006). Mutations in putative receptors or downstream signalling components depict insensitivity to CLEs, illustrated by longer roots compared to Col-0 (Kondo et al., 2011). Therefore, we tested the *csc1* mutant root growth on root-active CLEs and identified an insensitivity towards CLE21 and CLE27 and a mild insensitivity towards CLE11. We have to mention, that *csc1* was still in the *rlp4 r4l1* double mutant background, hence we tested in parallel the root growth of *rlp4 r4l1* #32-11 double mutant on all CLEs, which behaved wild type-like. Thus, we hypothesized that CSC1 might function in direct CLE21 and CLE27 perception or downstream in CLE signalling (Figure 28). Several CLE peptides with their corresponding receptors could be identified over the last years, such as CLV3-CLV1/CLV2/CRN, CLE41/44-PXY or BAM1 serving as a receptor for many CLEs, but the receptors for several CLE peptides are still unknown. Expression analysis of CLE21 and CLE27 in this study could show, that CLE21 is mainly expressed in the vasculature in the shoot and the root and, to a lesser extent, in the primary root meristem (Figure 29). CLE27 is expressed in root primordia and meristems of lateral roots, in young leaves and in early primordia of the inflorescence meristem (Figure 30). This data supports the hypothesis, that CSC1 might be a receptor of CLE21 and CLE27, because we identified the severe phenotypes in *csc1* mainly in the tissues where CLE21 and CLE27 are expressed.

Based on the hypothesis, that CSC1 might function in perceiving CLE21 and CLE27 or being involved in CLE-activated downstream signaling cascades, we assumed, that *cle21* and *cle27* mutants presumably depicts elevated protoxylem cells, similar to *csc1* (Yamaguchi et al., 2017). Therefore, we investigated *cle21*, *cle27* and also *cle11* single mutants, because *csc1* depicted a slight insensitivity to CLE11 and CLE11 is also expressed in the vasculature (Jun et al., 2010). Several CLE peptides are functionally redundant, therefore we obtained *cle11 cle21* and *cle21 cle27* double mutants (Yamaguchi et al., 2017; Gregory et al., 2018). Single as well as *cle11 cle21*

and *cle21 cle27* double mutants did not show an above ground phenotype in comparison to Col-0. However, *cle11* and *cle21* single mutants depicted more metaxylem rather than protoxylem cells in the vasculature (Figure 31). We expected, that knock-out of root-active CLEs such as CLE11, CLE21 or CLE27 would increase the number of protoxylem cells, based on a previous study, that revealed, that CLE application inhibits protoxylem formation (Kondo et al., 2011). It has to be taken in consideration, that these experiments were performed with artificial CLE concentrations. Therefore, it is possible that root-active CLEs do not inhibit protoxylem formation. Another explanation might be that CLE11 and CLE21, which are expressed in the root vasculature, function similar as CLE9/10 in defining the periclinal cell division in the outer most xylem cell, to produce one metaxylem and one protoxylem cell (Qian et al., 2018). BAM1 was identified as the main CLE9/10 receptor in the vasculature. Upon binding of CLE9/10 to the receptor, the periclinal division is suppressed and protoxylem differentiation is presumably inhibited, supported by phenotypes after exogenous CLE treatment (Qian et al., 2018). Intriguingly, *cle11 cle21* and *cle21 cle27* double mutants displayed meta- and protoxylem cell numbers similar to Col-0. Single *cle27* mutants showed a slight increase in metaxylem cells but no differences were visible in the *cle21 cle27* double mutants compared to Col-0. Based on the strong activity of *pCLE27* only in root primordia, young leaves and inflorescence primordia, CLE27 signalling pathways may be only functional in these tissues, therefore no phenotypic differences compared to Col-0 were depicted in the vasculature of single and double mutants. Furthermore, analysis of the total vascular cell numbers in CLE single and double mutants did not show differences compared to Col-0 (Figure 31). Due to the functional redundancy of CLEs, as shown for CLE16, CLE17 and CLE27 in the SAM (Gregory et al., 2018), it would be necessary to generate *cle11 cle21 cle27* triple mutants and to identify protein-protein interactions.

To date only a putative receptor for CLE27 was identified, but receptors for CLE21 and CLE11 are still unknown. A recent study in maize could discover FASCIATED EAR3 (FEA3) and its Arabidopsis orthologue AtFEA3 (AT3G25670), an LRR-RLK, as a putative receptor for CLE27 (Je et al., 2016). In maize, *FEA3* is expressed in the organizing centre of the shoot apical meristem and the orthologue of CLE27, ZmFCP1 is expressed in differentiating primordia. ZmFCP1 diffuses towards the shoot apical meristem where it can bind to FEA3 and represses *WUS* expression and stem cell proliferation (Je et al., 2016). Mutation of the FEA3 receptor leads to an increased meristem size in maize and mutations in AtFEA3 in Arabidopsis revealed a similar meristem increase (Je et al., 2016). Albeit the direct binding of ZmFCP1 to FEA3 or CLE27 to AtFEA3 was not shown, AtFEA3 thus is a putative receptor for CLE27. These findings conclude, that the well-known WUS-CLV3 feedback loop is not the only CLE peptide signalling pathway, that controls stem cell maintenance in the SAM (Je et al., 2016). However, we could not find mutations in

*AtFEA*3 in the *csc1* mutant and RNA-Seq data did not reveal differentially expressed *AtFEA3* in *csc1* (Appendix A2). Based on our previous results, CSC1 might function downstream of CLE27 perception, negatively regulating WUS expression. In addition, RNA-Seq data illustrated, that the transcription factor ORA47 is downregulated in the SAM of *csc1*. ORA47 was identified as a transcriptional repressor of WUS, maybe downstream of *CSC1* (personal communication, Yanling Yu, Rosa Lozano Durán Lab and Dan Zhang, now Michael Raissig Lab). Future analysis should focus on the detailed analysis of RNA-Seq results and GO-enrichments, to identify putative target genes of CSC1. Preliminary analysis suggests a function of CSC1 in translation.

4.3.5 CLE21 might cross-talk with cytokinin signalling

As previously mentioned, CLE peptide signalling and cytokinin signalling might cross-talk to regulate eclectic developmental processes. However, neither many CLE receptors nor their downstream signalling members are identified to date. Application of exogenous CLE9/10 led to a repression of cytokinin negative regulators, the type-A ARRs. Thereby, the cytokinin signalling pathway is elevated and can repress the expression of *AHP6*, a negative cytokinin regulator, which is active in protoxylem cells (Mähönen et al., 2006 a). By now, the interaction of CLE and cytokinin signalling pathways was only reported for CLE9/10, although it is possible, that all root-active CLEs might inhibit the differentiation of protoxylem cells via the upregulation of cytokinin levels in the root vasculature or this effect is due to artificial CLE concentrations (Kondo et al., 2011).

To further test the hypothesis, that root-active CLEs might cross-talk with cytokinin signalling, we analysed the effect of exogenous applied CLE21 on a cytokinin response marker (*pTCSn:GFPer*), a reporter for the negative cytokinin regulator (*pAHP6:GFPer*) and an auxin response marker (*pDR5v2:mTurquoise*) in the root apical meristem. Interestingly, CLE21 decreases the cytokinin response signal in the stele initials, but broadens and extends it in the vasculature of the RAM (Figure 32). *pCLE21:GUS* expression revealed *pCLE21* activity in a similar domain as the *pTCSn* reporter in the root apical meristem. Elevated CLE21 treatment could therefore result in increased cytokinin response downstream of CLE21-receptor perception and would support the hypothesis of CLE21 and cytokinin signalling cross-talk. Consequently, CLE21 treatment leads to a decrease of the *pAHP6* signal in the vasculature (Figure 32). However, CLE21 treatment of *pDR5v2* only slightly decreased the signal in the vasculature, indicating no effect of CLE21 on auxin signalling in the root apical meristem (Figure 32). These results support our hypothesis, that elevated CLE21 can activate the cytokinin signalling pathway represented by increased activity of the *pTCSn*

marker in the vasculature and a decrease of *pAHP6* activity, which might lead to reduced protoxylem differentiation. With these findings, we partially disagree with previous finding, showing that CLE9/10 activate the cytokinin signalling pathway via the downregulation of type-A ARRs (Kondo et al., 2011). However, dependent on the CLE peptide, they might activate and cross-talk with CK signalling via type-A or type-B ARRs. Albeit the exact cross-talk mechanism of CLE21 and CK signalling could not be deciphered, it can be assumed, that AHP6 was repressed upon CLE21 treatment, which resulted in increased CK signalling or vice versa. To test the cross-talk of CLE21 and CK signalling, the dynamics of the two transcriptional reporters have to be studied in detail. Furthermore, experiments with the *pTCSn:GFPer* marker treated with cytokinin in Col-0 and *csc1* backgrounds, or with CLE21 in the *csc1* background would be crucial experiments, to identify, if and how CSC1 might modulate cytokinin and CLE signalling.

4.3.6 CSC1 might regulate CLV3 signalling

Based on previous results, we attempted to identify if CSC1 and CLV3 might interact in regulating the shoot apical meristem. The combination of *csc1* and *clv3-10* mutants results in a dramatic phenotype in the reproductive stage. The absence of CSC1 seems to repress the *clv3-10* mutant phenotype until the reproductive stage in which *csc1* starts depicting flower developmental defects (Figure 39). The primary shoots of *csc1 clv3-10* double mutants did not establish side shoots and flower developmental defects were increased illustrated by almost only pedicels at the primary shoot. Radialized rosette leaves and un-determined floral meristems were not visible in single *csc1* or *clv3-10* mutants. These findings suggest a function of CSC1 in a similar pathway as CLV3, due to the increased developmental phenotype of the *csc1 clv3-10* double mutant. In combination with the results of the *pCLV3*, *pWUS* and *pTCSn* marker lines in the SAM of *csc1*, CSC1 might be a positive regulator of CLV3 signalling within the WUS-CLV3 feedback loop. Additional analysis of vasculature cells revealed, that *csc1 clv3-10* double mutants depict the *csc1* phenotype. This is in line with the expression and function of CLV3 only in the SAM and is neither functional in the vasculature via a long-distance effect. However, no further conclusions can be considered due to the missing supporting data and putative multiple undefined background mutations in the mutants' genomes.

4.3.7 Identifying putative *CSC1* candidates

By using next generation sequencing, three SNPs on chromosome five in the region of 17.6 Mio bp to 20.9 Mio bp were revealed in *csc1*, which is supported by results of the bulked segregant analysis (Figure 42). The first SNP was identified in AT5G43810 which encodes for ZWILLE/ARGONAUTE (ZLL/AGO10) (Figure 44). AGO10 is a member of ELONGATION INITIATION FACTOR 2C (EIF2C) and controls together with WUS and CLV3 the organization of central and peripheral zones in the SAM by sequestering miR165/166, which in turn cannot interact with the HD-ZIP III target genes *REV*, *PHB*, *PHV*, *ATHB-8* and *CNA* (Manavella et al., 2011; Tucker et al., 2013; Xue et al., 2017). A recent study unravelled, that AGO10-miR165/166 interaction leads to upregulation of *PHB* and *REV* genes, which are regulating SAM formation and pattern the adaxial side of leaf and flower primordia (Zhou et al., 2015). A miR166g overexpressing mutant, *jba-1D*, depicts an enlarged SAM, vascular defects and radialized leaves (Williams et al., 2005). This phenotype is reminiscent of *csc1* and RNA-Seq analysis revealed, that AGO10 is upregulated in the root. In the vasculature, miR165/166 represses HD-ZIP III target genes in the outer xylem axis cells, leading to differentiation into protoxylem cells(Carlsbecker et al., 2010; Du et al., 2015; Ramachandran et al., 2016). Thus, more AGO10 could sequester miR165/166 which would lead to a reduced repression of HD-ZIP III genes in the vasculature and thereby to fewer protoxylem cells. This regulation would be contrary to our *csc1* phenotype with elevated protoxylem cells. Intriguingly, the miR166g overexpressing *jba-1D* plant depicts ectopic xylem cells close to the periphery and by forming extra vascular bundles in the inflorescence stem (Williams et al., 2005). Moreover, radialized leaves were identified in *jba-1D* plants, similar as depicted in *csc1 clv3-10* double mutants. ChIP-Seq analysis performed by Andrej Miotk (Miotk, PhD Thesis, 2015), could identify a WUS peak close to the ATG, assuming a direct regulation of AGO10 by WUS. AGO10 might be a putative candidate for CSC1, because it could explain the expanded WUS domain, if HD-ZIP III did not establish properly SAM boundary domains (Xue et al., 2017).

The second SNP was located in AT5G47720 and encodes for ACETOACETYL-COA THIOLASE 1 (AACT1). AACT1 is catalyzing the first step of the mevalonate (MVA) pathway, the condensation of two acetyl-CoAs to form acetoacetyl-CoA either in the cytoplasm or in chloroplasts (Jin et al., 2012). Knock-down or knock-out of *AACT1* would lead to Acetyl-CoA accumulation, which has been shown to promote acetylation of histones, resulting in wide-spread gene expression changes (Cai et al., 2011; Chen et al., 2017). RNA-Seq analysis of csc1 reveald many differentially expressed genes in the RAM and the SAM, thus *AACT1* might be a putative *CSC1* candidate.

The third mutation was identified in the untranscribed genomic region between AT5G51560 and AT5G51570. Both genes are un-characterized and no further studies are available. ChIP-Seq analysis performed by Andrej Miotk (Miotk, PhD Thesis, 2015), could identify a WUS peak upstream of AT5G51560, indicating a direct regulation of AT5G51560 by WUS. AT5G51560 encodes for a LRR-RLK, which makes it to a putative *CSC1* candidate, because many LRR-RLKs are involved in ligand perceptions or protein-protein interactions (He et al., 2018).

Taken together, we could identify three point mutations in genes, that might cause the *csc1* mutant phenotype. One point mutation was located either in the terminator region of AT5G51560 or the promoter region of AT5G51570. However, RNA-Seq analysis did not show changes in the expression of these two genes, why they were not longer considered as putative mutations causing the *csc1* phenotype. However, the mutations for AACT1 and AGO10 are located in an exon, but the point mutation is only exchanging one amino acid and does not introduce a premature stop codon. It is still possible, that the exchange of an amino acid could lead to miss folding and degradation of the protein. Nevertheless, the RNA-Seq results of AACT1 and AGO10 did reveal contrary results. AACT1 was not differentially expressed in the RAM, but was downregulated in the SAM (-0.674 log2FC). AGO10 is slightly upregulated in the RAM (0.4862 log2FC) and not differentially expressed in the SAM. First, it is surprising, that the genes are not similar expressed in the two meristems. Because *csc1* depicts severe developmental phenotypes in the SAM and the RAM, we expected that the mutated gene, that is causing the phenotype is similarly expressed in both tissues. Secondly, the point mutation in AGO10 is resulting in an upregulation of the gene. This might be explained by a secondary effect, a compensatory upregulation of the gene, due to impaired function. Another question is how was the mutation introduced into *csc1* mutant? As mentioned before, the *csc1* phenotype was identified in a CRISPR/Cas9 generated *rlp4 r4l1* double mutant. Recent studies revealed, that the Cas9 we were using in our cloning system is not as precise as predicted and can cause unspecific background mutations (Zhang et al., 2018). However, this explanation is unlikely, because we discovered the same *csc1* phenotype in two plants of the T_1 population of transformed Col-0 plants with the CRISPR/Cas9 plasmid carrying the 2gRNA for *RLP4* and *R4L1*. Another explanation might be, that the CRISPR/Cas9 construct was not transformed into Col-0 plants. It is possible, that the Col-0 seeds were contaminated for instance with another ecotype albeit sequence analysis of *csc1* with the 1001 Arabidopsis genome programme did not reveal any result (https://1001genomes.org/). An additional explanation is, that the Col-0 seeds accumulated and fixed a spontaneous mutation creating a new Col-0 accession. This mutation in the Col-0 background can for instance cause the *csc1* phenotype. Eventually, the mutation in *csc1* is not

one of the mentioned before, but is still unknown and was not discovered yet, because of the relatively short reads that are produced by next generation sequencing.

To identify, if one the three point mutations is causative for the *csc1* phenotype, the next crucial experiments will be the complementation of *csc1* phenotypes with *AGO10*, because we assume, that it is the most promising SNP causing the *csc1* phenotype. Additionally, if expression of *ago10*^{csc1} in Col-0 will show the *csc1* phenotype, the actual *CSC1* gene would be unravelled.

5 Conclusion

The role of pectin methyl esterases (PMEs) in the SAM

The goal of our work was to identify the function of PMEs in differentiation in the SAM. We could show that pectin modification by overexpression of a PME, *VANGUARD*1 (*VGD1*), or the PME inhibitor, *PMEI5*, resulted in a decrease of SAM size, indicating the importance of the cell wall state in cells in the SAM. Furthermore, we could illustrate that the expression of *PME*s and *PMEI*s in the centre of the meristem seemed to negatively affect the morphology of the meristem, indicated by altered cell sizes and arbitrary cell morphologies. Previous studies revealed the (direct) repression of PMEs by WUS in the centre of the SAM, which we could support with the PME5 reporter that exhibits activity only in the periphery and boundary domains of the SAM. We were also able to generate a toolkit for inducible, tissue-specific expression in the three meristems of Arabidopsis through a trans-activation approach in combination with effectors, which enables the expression of *PME*s and *PMEI*s in specific tissues in the SAM.

RLP4 and subfamily RLP4-like as putative cell wall binding proteins

Within this work, we were able to identify a new class of putative cell wall signalling components in the group of receptor-like proteins, RLP4 and the three RLP4-likes, R4L1, R4L2 and R4L3. We could illustrate that all contain a malectin-like domain and are well conserved in the plant kingdom. Additionally, we showed, that RLP4 localizes in the epidermal plasma membrane in differentiating cells in the shoot and the root and presumably identified RLP4 as a new class of cell wall signalling components, exhibiting a polar localization to cell edges in the root epidermis. Furthermore, we revealed association of the extracellular domain of RLP4 to the cell wall with preferences to cell edges in the lateral root.

Unravelling the function of *CLE SIGNALLING COMPONENT1* (*CSC1*)

The newly identified *cle signalling component1* (*csc1*) mutant exhibited severe phenotypes in the shoot and the root apical meristems. Our experiments revealed, that CSC1 is a putative member of the CLE21/CLE27 signalling pathways and we could support the hypothesis, that CLE signalling, here CLE21, cross-talks with cytokinin signalling pathway (Kondo et al., 2011). Thereby, CSC1 is a negative regulator of CLE21/27 and cytokinin signalling, repressing enhanced cell proliferation in the shoot and the root apical meristems. For the SAM, we could identify, that CSC1 represses cytokinin responses and *WUS* expression, but might positively regulate CLV3 expression. Thus, CSC1 is a noteable new player in the maintenance of stem cell identities in the shoot apical meristem, orchestrating the WUS-CLV3 signalling pathway and additionally the CLE

and cytokinin signalling pathways, which might be directly or indirectly connected. Furthermore, we could localize the probably causative mutation in *csc1* on chromosome five, identifying three SNPs with the most promising one in *ARGONAUTE10* (*AGO10*), involved in domain specifications in the SAM and the RAM.

Taken together, we could identify new players and their function in regulating phytohormonal networks in cross-talk with peptide signalling, and the importance of cell wall signalling and cell wall properties in establishing cell identities. Within this work, we could elucidate a small part of the wiring networks that have to be spatio-temporally controlled to maintain developmental plasticity in plants.

6 Materials and Methods

6.1 Green Gate cloning

All constructs in this study were created by using the modular GreenGate (GG) cloning method (Lampropoulos et al., 2013; Schürholz et al., 2018).

6.2 Entry module creation

Genomic sequences of interest were amplified with GreenGate specific primers (Table 13) using the Q5® High-Fidelity DNA Polymerase (NEB #M0491). Internal Eco31I sites were mutated by site-directed mutagenesis taking care, that amino acids in the open reading frame are not changed (Table 13). PCR cycler conditions and reaction mix components are listed in (Table 5). The amplified PCR product was separated on a 1 – 2 % agarose gel depending on the fragment size, cut out of the gel and purified with GeneJET PCR Purification Kit (ThermoFisher #K0701). PCR product and the empty entry vector (pGGA000-pGGI000) were digested separately with Eco31I FD (Thermo Fisher #FD0294) for 1 h at 37 °C. The digested PCR product was column-purified with GeneJET PCR Purification Kit (ThermoFisher #K0701), the digested entry vector was separated on a 1 % agarose gel and the vector backbone was cut out of the gel and purified using the same kit as for the PCR product. Digested and purified PCR product and entry vector were ligated using either the Instant Sticky-end Ligase Master Mix (NEB #M0370) or the T4 Ligase (5 U/µL; Thermo Fisher #EL0011). Entry vectors were transformed into chemically competent *Escherichia coli* (*E. coli)*, colonies were tested for the presence of the entry vector and positive colonies were used for over night cultures (see also 6.6). The plasmids were purified and their sequence was verified by sequencing. Entry vectors were used for the final GreenGate reaction into the pGGZ001 vector. Entry modules used in this study are depicted in Table 6.

Table 5. PCR reaction mix and PCR cycler conditions.

25 µL reaction mix	1x [µL]	temperature [°C]	duration	number of cycles
10xPCR Buffer	2.5	95	5 min	
dNTPs (10 mM)	0.5	95	25 s	35
Primer A	0.25	54	25 s	
Primer B	0.25	72	1 min/ 1kb (TAQ Pol.)	
TAQ-Polymerase	0.25	72	5 min	
H_20	to 25	4	∞	
DNA	colony/ 2			

Table 6. Entry modules used for GreenGate constructs.

plasmid number	name	source of plasmid
pSW810	pAt5g47500	this study
pSW179	pML1 (pGGA022)	Jan Lohmann Lab
pSW177	pCASP1 (pAVB009)	Alexis Maizel Lab
pSW178	pXPP (pAVB017)	Andersen et al., 2017
pSW454	pUFO	Jan Lohmann Lab
pSW455	pCLV3	Jan Lohmann Lab
pSW597	pCUC2	Gaillochet et al., 2017
pSW377	pTMO5	Schürholz et al., 2018
pSW614	pREV	Schürholz et al., 2018
pSW615	pATHB-8	Schürholz et al., 2018
pSW618	pAHP6	Schürholz et al., 2018
pSW457	tCLV3	Jan Lohmann Lab
pSW185	Rbcs term (pGGE001)	Lampropoulos et al., 2013
pSW186	UBQ10 term (pGGE009)	Lampropoulos et al., 2013
pSW181	GR-LhG4 (pGGC018)	Jan Lohmann Lab
pSW610	GR-LHG4_BD	Schürholz et al., 2018
pSW180	pOp4 (pGGA016)	Jan Lohmann Lab
pSW180a	pOp6 (pGGA016)	Jan Lohmann Lab
pSW182	B-Dummy (pGGB003)	Lampropoulos et al., 2013
pSW184	D-Dummy (pGGD002)	Lampropoulos et al., 2013
pSW188	F-H adapter (pGGG001)	Lampropoulos et al., 2013
pSW189	H-A adapter (pGGG002)	Lampropoulos et al., 2013
pSW548	Signal Peptide (ER)	Lampropoulos et al., 2013
pSW550	HDEL	Lampropoulos et al., 2013
pSW596	mTurquoise2 (pGGC088)	Jan Lohmann Lab
pSW393	SulfR	Lampropoulos et al., 2013
pSW319	BastaR	Lampropoulos et al., 2013
pSW322	3xGFP (pGGC025)	Lampropoulos et al., 2013
pSW323	linker-NLS (pGGD007)	Lampropoulos et al., 2013
pSW549	YFP/VENUS (pGGC023)	Jan Lohmann Lab
pSW321	pRPS5a (pGGA012)	Lampropoulos et al., 2013
pSW842	GAGAGA-eGFP	Guido Großmann Lab
pSW459	t-RLP4	Sebastian Wolf Lab
pSW330	pRLP4	Sebastian Wolf Lab
pSW333	RLP4	Sebastian Wolf Lab
pSW183	linker-GFP (pGGD001)	Lampropoulos et al., 2013
pSW724	R4L1	Sebastian Wolf Lab

6.3 Intermediate module creation

Driver lines were created by making use of the intermediate module pGGM000 and pGGN000, that consists both of six entry modules, whereas the sixth entry module of pGGM000 is not carrying a resistance cassette, but an adaptor sequence (F-H adaptor), that can be ligated to the adaptor sequence in the first entry module of pGGN000 (H-A adaptor). The intermediate vectors can be combined by performing the standard GreenGate reaction (Table 7).

6.4 Destination module creation

For the final GreenGate reaction (Table 7), 1.5 µL of each entry module (pGGA000 – pGGF000), 1 µL of destination vector (pGGZ001), 2 µL 10x FD buffer, 1.5 µL 10 mM ATP, 1 µL T4 DNA Ligase (30 U/µL) and 1 µL Eco31I were added and mixed directly in a PCR tube. GreenGate reaction was performed as depicted in (Table 7) and generated final GreenGate constructs in this study are depicted in (Table 8) (Lampropoulos et al., 2013).

Table 7. GreenGate reaction programme.

temperature [°C]	duration [min]	number of cycles
37	2	30
16	2	
50	5	1
80	5	1

Table 8. GreenGate destination constructs

plasmid number	construct names
pSW919	**CRISPR_2gRNA at5g53370-PME3**
pHEE401E	backbone plasmid
pSW919a	**CRISPR_2gRNA PME41-PME44**
pHEE401E	backbone plasmid
pSW834	**pAt5g47500::3xGFP-NLS**
pSW810	pAt5g47500
pSW182	B-Dummy (pGGB003)
pSW322	3xGFP (pGGC025)
pSW323	linker-NLS (pGGD007)
pSW186	UBQ10 term (pGGE009)
pSW319	BastaR

plasmid number	construct names
pSW689	**CRISPR_RLP4_1**
pHEE401E	backbone plasmid
pSW745	**CRISPR 2gRNA RLP4-R4L1**
pHEE401E	backbone plasmid
pSW908	**CRISPR_R4L2_R4L3_exon2**
pHEE401E	backbone plasmid
pSW726	**pRLP4:RLP4:linkerGFP:tRLP4:BastaR**
pSW330	pRLP4
pSW182	B-Dummy (pGGB003)
pSW333	RLP4
pSW183	linker-GFP (pGGD001)

pGGZ001	destination vector
pSW609	**pOp4:ER-mTurq2-HDEL:tUBQ10:SulfR (N001)**
pSW189	H-A adapter (pGGG002)
pSW180	pOp4 (pGGA016)
pSW548	Signal Peptide, ER (pGGB006)
pSW596	mTurquoise2 (pGGC088)
pSW550	HDEL (pGGD008)
pSW186	UBQ10 term (pGGE009)
pSW393	SulfR (pGGF012)
pGGN000	intermediate vector
pSW699	**pOp6:ER-mTurq2-HDEL:tUBQ10:SulfR (N002)**
pSW189	H-A adapter (pGGG002)
pSW180a	pOp6 (pGGA016)
pSW548	Signal Peptide, ER (pGGB006)
pSW596	mTurquoise2 (pGGC088)
pSW550	HDEL (pGGD008)
pSW186	UBQ10 term (pGGE009)
pSW393	SulfR (pGGF012)
pGGN000	intermediate vector
pSW646	**pML1::GR-LhG4:tRbsc-pOp4::ER-mTurquoise2-HDEL:tUBQ10:SulfR**
pSW304	pML1::GR-LhG4:tRbsc (M003)
pSW609	pOp4:ER-mTurq2-HDEL:tUBQ10:SulfR (N001)
pGGZ001	destination vector
pSW648	**pREV::GR-LhG4:tRbsc-pOp4::ER-mTurquoise2-HDEL:tUBQ10:SulfR**
pSW614	pREV
pSW610	GR-LHG4_BD
pSW185	Rbcs term (pGGE001)
pSW188	F-H adapter (pGGG001)
pSW609	pOp4:ER-mTurq2-HDEL:tUBQ10:SulfR (N001)
pSW698	**pCLV3::GR-LhG4:tCLV3-pOp6::ER-mTurquoise2-HDEL:tUBQ10:SulfR**
pSW455	pCLV3 (pGGA033)
pSW459	t-RLP4
pSW319	BastaR
pGGZ001	destination vector
pSW878	**pRPS5a:RLP4:GAGAGA-GFP**
pSW321	pRPS5a (pGGA012)
pSW182	B-Dummy (pGGB003)
pSW333	RLP4
pSW842	GAGAGA-eGFP
pSW186	UBQ10 term (pGGE009)
pSW319	BastaR
pGGZ001	destination vector
pSW875	**pRPS5a:R4L1:GAGAGA-GFP**
pSW321	pRPS5a (pGGA012)
pSW182	B-Dummy (pGGB003)
pSW724	R4L1
pSW842	GAGAGA-eGFP
pSW186	UBQ10 term (pGGE009)
pSW319	BastaR
pGGZ001	destination vector
pSW710	**pCUC2::GR-LhG4:tRbsc-pOp6::ER-mTurquoise2-HDEL:tUBQ10:SulfR**
pSW597	pCUC2 (pGGA045)
pSW610	GR-LHG4_BD
pSW185	Rbcs term (pGGE001)
pSW188	F-H adapter (pGGG001)
pSW699	pOp6:ER-mTurq2-HDEL:tUBQ10:SulfR (N002)
pGGZ001	destination vector
pSW725	**pUFO::GR-LhG4:tRbsc-pOp6::ER-mTurquoise2-HDEL:tUBQ10:SulfR**
pSW454	pUFO (pGGA027)
pSW610	GR-LHG4_BD
pSW185	Rbcs term (pGGE001)
pSW188	F-H adapter (pGGG001)

pSW610	GR-LHG4_BD
pSW457	t-CLV3 (pGGE008)
pSW188	F-H adapter (pGGG001)
pSW699	pOp6:ER-mTurq2-HDEL:tUBQ10:SulfR (N002)
pGGZ001	destination vector

pSW665	**pAHP6::GR-LhG4:tRbsc (M013)**
pSW618	pAHP6
pSW610	GR-LHG4_BD
pSW185	Rbcs term (pGGE001)
pSW188	F-H adapter (pGGG001)
pGGM000	intermediate vector

pSW683	**pAHP6::GR-LhG4:tRbsc-pOp4::ER-mTurquoise2-HDEL:tUBQ10:SulfR**
pSW665	pAHP6::GR-LhG4:tRbsc (M013)
pSW609	pOp4:ER-mTurq2-HDEL:tUBQ10:SulfR (N001)
pGGZ001	destination vector

pSW697	**pTMO5::GR-LhG4:tRbsc-pOp6::ER-mTurquoise2-HDEL:tUBQ10:SulfR**
pSW377	pTMO5
pSW610	GR-LHG4_BD
pSW185	Rbcs terminator (pGGE001)
pSW188	F-H adapter (pGGG001)
pSW699	pOp6:ER-mTurq2-HDEL:tUBQ10:SulfR (N002)
pGGZ001	destination vector

pSW699	pOp6:ER-mTurq2-HDEL:tUBQ10:SulfR (N002)
pGGZ001	destination vector

pSW696	**pATHB-8::GR-LhG4:tRbsc-pOp6::ER-mTurquoise2-HDEL:tUBQ10:SulfR**
pSW615	pATHB-8
pSW610	GR-LHG4_BD
pSW185	Rbcs term (pGGE001)
pSW188	F-H adapter (pGGG001)
pSW699	pOp6:ER-mTurq2-HDEL:tUBQ10:SulfR (N002)
pGGZ001	destination vector

pSW682	**pCASP1::GR-LhG4:tRbsc-pOp4::ER-mTurquoise2-HDEL:tUBQ10:SulfR**
pSW302	pCASP1::GR-LhG4:tRbsc (M001)
pSW609	pOp4:ER-mTurq2-HDEL:tUBQ10:SulfR (N001)
pGGZ001	destination vector

pSW702	**pXPP::GR-LhG4:tRbsc-pOp6::ER-mTurquoise2-HDEL:tUBQ10:SulfR**
pSW178	pXPP (pAVB017)
pSW610	GR-LHG4_BD
pSW185	Rbcs term (pGGE001)
pSW188	F-H adapter (pGGG001)
pSW699	pOp6:ER-mTurq2-HDEL:tUBQ10:SulfR (N002)
pGGZ001	destination vector

6.5 CRISPR/Cas9

Suitable gRNAs for the target genes were designed by using the ChopChop webpage (https://chopchop.cbu.uib.no/), targeting the beginning of the gene. To create a single gRNA, the following forward primer (5' ATTGnnnnnnnnnnnnnnnnnn 3') was designed with the first four nucleotides that serve as adaptor for Greengate cloning, followed by the gRNA sequence. The reverse primer (5' nnnnnnnnnnnnnnnnnnGTTT 3') consists of the reverse complement sequence of the gRNA followed by four nucleotide adaptor sequence. The complement primers were annealed and ligated into the pHEE401E vector. For the creation of two different gRNAs in one vector, the two gRNA sequences were incorporated into forward and reverse primer, respectively. The primers also contain the Eco31I recognition site before the gRNA sequence and the pHEE2E-TRI specific sequence (Forward primer: 5' aacaGGTCTCaattgNNNNNNNNNNNNNNNNNNNgttttagagctagaaatagc; reverse primer: 5' aacaGGTCTCtaaacNNNNNNNNNNNNNNNNNNNcaatctcttagtcgactctac). pHEE2E-TRI is used as template to amplify the two gRNAs together with promoter and terminator regions, an approximately 600 bp fragment. The amplified PCR product was gel purified and ligated into pHEE401E using the GreenGate reaction (Table 7) (Xing et al., 2014; Wang et al., 2015).

6.6 Transformation of *E. coli* and *Agrobacterium tumefaciens*

Ligated entry vectors/intermediate vectors/destination vectors assessed by GreenGate cloning, were transformed into chemically competent *E. coli* bacteria (DH5α) with the required volume of plasmid. Bacteria were incubated 10 min on ice, heat-shock at 42 °C for 45 s, and after 2 min on ice, 1 mL liquid LB medium was added. After 2-5 h incubation, the bacteria were plated on a LB-agar plate with carbenicillin/ampicillin for entry vectors, kanamycin for intermediate vectors and spectinomycin for destination vectors, over night at 37 °C (Table 9). The next day, colonies were checked for the presence of the ligated PCR product in the entry vector or the different entry modules in the intermediate or the destination vector, by colony PCRs with primers binding in the backbone of the entry/intermediate/destination vector and PCR product specific primers (Table 13). After the PCR, products were separated on a 1-2 % agarose gel. Positive colonies were picked and incubated over night in 2-3 mL liquid LB medium with the according antibiotics in a 37 °C shaker. Plasmids were isolated using GeneJet Plasmid Miniprep Kit (Thermo Fisher #K0502). The correct plasmid sequence was further verified by sequencing at Eurofins Genomics.

For GreenGate-derived constructs, plasmids were transformed into the chemically competent ASE pSOUP^{+} *Agrobacterium tumefaciens* (*A. tumefaciens*) strain. 5-10 µl of plasmid were added and bacteria were frozen for 5 min in liquid nitrogen with subsequent incubation for 5 min at 37

°C. 1 mL of liquid B medium was added and bacteria were incubated for 3-4 hours at 28 °C. For selection, bacteria were plated on LB-agar with the following antibiotics: chloramphenicol, kanamycin, spectinomycin and tetracyclin (CKST) and incubated at 28 °C for two to three nights. The antibiotics were used as depicted in Table 9.

CRISPR/Cas9 constructs were transformed into chemically competent *E. coli* bacteria (DH5α) as mentioned before, but with kanamycin as selection antibiotic. Colonies were checked by performing colony PCRs with primers binding in the backbone of the vector and the gRNA/PCR product specific primers (Table 13). After the PCR, products were separated on a 1-2 % agarose gel. Positive colonies were picked and incubated overnight in 2-3 mL liquid LB medium with the according antibiotics in a 37 °C shaker. Plasmids were isolated using GeneJet Plasmid Miniprep Kit (Thermo Fisher #K0502). The correct plasmid sequence was further verified by sequencing at Eurofins Genomics. *A. tumefaciens* transformation was performed as mentioned above, but with the *A. tumefaciens* strain GV3101. Transformed bacteria were plated on LB-agar plates containing rifampecin, gentamycin and kanamycin (RGK) and incubated for two to three nights at 28 °C. The antibiotics were used as depicted in Table 9.

Table 9. Antibiotics for selection of bacteria.

antibiotics	final concentration [µg/mL]
ampicillin	100
carbenicillin	50
chloramphenicol	34
gentamycin	50
kanamycin	50
rifampicin	25
spectinomycin	50
tetracyclin	12.5

6.7 Plant material and growth conditions

Seeds were sterilised in a reaction tube using 1 mL of the sterilisation solution (70 % ethanol, 1:10 dilution of 1.3 % (v/v) sodium hypochlorite), mixed for 1 min, the solution was removed and seeds were washed twice with 100 % ethanol each time for 1 min and dried in a laminar flow cabinet.

The sterilsed seeds were grown on ½ MS (Murashige Skoog, Duchefa), 1 % Sucrose (Carl Roth) and 0.9 % phytoagar (Duchefa), adjusted with KOH to pH 5.8. After two days of stratification, the plates were put in a vertical position in growth chambers with long day conditions (16 h light/8 h dark, 60-70 % humidity, 100 $\mu mol \cdot m^{-2} \cdot s^{-1}$ light intensitiy, 22 °C, Polyclima or Conviron) for 6-7 days, afterwards the seedlings were transferred to soil (CLT-SM soil, Einheitserde Classic) and were grown in plant rooms with long day conditions (16/8 h, 65 % humidity; 100 µE light intensity; 22 °C). For different seedling experiments on plate, the growth conditions can vary and are listed in the following sections.

6.8 Transgenic lines in *A. thaliana*

Plants for transformation with *A. tumefaciens* were grown for four to five weeks in plant rooms with long day conditions. The first inflorescence was cut off to induce the development of multiple inflorescences. Before dipping, siliques were removed from stems.

For GreenGate constructs, a positive transformed *A. tumefaciens* (ASE+pSOUP) colony was plated on LB agar with chloramphenicol, kanamycin, spectinomycin and tetracyclin (CKST) and incubated for one day at 28 °C. For CRISPR/Cas9-derived constructs, a positive transformed *A. tumefaciens* (GV3101) colony was plated on LB agar with rifampecin, gentamycin and kanamycin (RGK) and incubated for one day at 28 °C. From this plate, bacteria material was transferred on two LB-CKST plates with the appropriate antibiotics and incubated for two days at 28 °C. To each plate, 15 mL LB medium was added and Agrobacteria were carefully removed and resuspended from the LB agar. The 30 mL Agrobacteria suspension was added to 120 mL H_2O containing 5 % sucrose and 45 µL Silwet L-77 (Lehle Seeds). Plants' inflorescences were dipped for 30 s into the Agrobacteria suspension. After dipping, they were placed in a tray, wrapped in an autoclaving bag, sprayed with water and were kept at a dark place overnight, to keep a humid environment. To increase the transformation efficiency, dipping was repeated after one week.

T_1 plants were selected on ½ MS, 0.9 % phytoagar and the corresponding concentration of the selection marker (BASTA/glufosinate ammonium: 7.5 µg/mL, sulfadiazine: 1.875-3.75 µg/mL, end concentrations in medium). Around 40 positive T_1 plants were selected and propagated on soil.

20-30 T_2 seedlings were further analysed on ½ MS, 1 % sucrose, 0.9 % phytoagar and the respective selection marker for single integration of the T-DNA. Around ten T_2 plants with a ratio of 3:1 (alive/dead) were transferred on soil. In the T_3 generation, seedlings were analysed on selection plates for homzygosity (100 % alive) and these stable Arabidopsis lines were used for experiments.

CRISPR/Cas9 T_1 plants were selected on ½ MS, 0.75 % phytoagar and 15 µg/mL hygromycin. Plates were covered with sheets of paper for four to six days until positive T_1 plants with an elongated hypocotyl could be distinguished and kept for another four days at full light. Around 40 T_1 plants were transferred to soil and analysed for a phenotype due to the CRISPR/Cas9 mutation and additionally genotyped for a mutation in the GOI, see 6.11. Plants with a mutation were analysed in the T_2 generation for the absence of the Cas9 T-DNA either by genotyping the T_2 population for Cas9 using Cas9 specific primers (Table 14) or the selection on ½ MS, 0.75 % phytoagar and hygromycin and recover seedlings that might not be resistance to hygromycin anymore. Experiments were done with stable T_3 Arabidopsis lines. All lines used for experiments are depicted in Table 10.

Table 10. Arabidopsis lines used in this study.

genotype	reference
Col-0	Arabidopsis biological resource centre
L*er*	Arabidopsis biological resource centre
pme41 pme44	this study
pPME5:3xGFP-NLS	this study
VGD1ox	Wolf et al., 2012c
PMEIox	Wolf et al., 2012a
pATHB-8>GR>mTurquoise2	Schürholz et al., 2018
pAHP6>GR>mTurquoise2	Schürholz et al., 2018
pCASP1>GR>mTurquoise2	Schürholz et al., 2018
pTMO5>GR>mTurquoise2	Schürholz et al., 2018
pXPP>GR>mTurquoise2	Schürholz et al., 2018
pCLV3>GR>mTurquoise2	Schürholz et al., 2018
pCUC2>GR>mTurquoise2	Schürholz et al., 2018
pML1>GR>mTurquoise2	Schürholz et al., 2018
pREV>GR>mTurquoise2	Schürholz et al., 2018
pUFO>GR>mTurquoise2	Schürholz et al., 2018
pCVLV3>GR>3xGFP-NLS	Schürholz et al., 2018
rlp4 #30-3	this study
r4l1#24-13	this study
rlp4 r4l1 #32-11	this study
rlp4 r4l1 r4l2 r4l3 #14-3	this study

rlp4 r4l1 r4l2 r4l3 #14-6	this study
rlp4 r4l1 r4l2 r4l3 #14-19	this study
rlp4 r4l1 r4l2 r4l3 #21-7	this study
rlp4 r4l1 r4l2 r4l3 #21-13	this study
rlp4 r4l1 r4l2 r4l3 #26-2	this study
rlp4 r4l1 r4l2 r4l3 #26-3	this study
p35S:mGFP-LTI6b	Cutler et al., 2000
pUBQ10:RLP4-ECD:mCherry	Sebastian Augustin, 2015
p35S:mGFP-LTI6b pUBQ10:RLP4-ECD:mCherry	this study
csc1 #6-13	this study
cle11	Yamaguchi et al., 2017
cle21	Yamaguchi et al., 2017
cle27	Yamaguchi et al., 2017
cle11 cle21	this study
cle21 cle27	this study
clv3-10	Forner et al., 2015
csc1 clv3-10	this study
bam3-1	SALK_44433
pCLE21:GUS	Jun et al., 2010
pCLE27:GUS	Jun et al., 2010
pTCSn:GFPer	Jan Lohmann Lab
pTCSn:GFP-NLS pUBQ10:3xmCherry-NLS	Jan Lohmann Lab
pAHP6:GFPer	Mähönen et al., 2006a
C3PO (**pDR5v2:mTurquoise-NLS** / pRPS5a:mDII:ntdTomato /pRPS5a:DII:n3xVenus)	Dolf Weijers, not published
pDR5v2:YFP / pPXY:CFP	Thomas Greb Lab
pCLV3:BFP-NLS / pWUS:2xVenus-NLS / pUBQ10:3xmCherry-NLS	Jan Lohmann Lab

6.9 Crossing

A. thaliana plants with inflorescences SAMs were used for crossing. Siliques and already opened flower buds were removed from one stem of the “mother plant” either by sciccors or a sharp forcep. Under a binoccular, the SAM, primordia and young flower buds were removed from the centre of the inflorescence, except four to five closed but fully developed flower buds. These buds were opened by a sharp forcep and sepals, petals and stamens were carefully dissected. Anthers of the “father plant” were swept over the pistil until it was covered with pollen. Crossed plants were kept separately from others in the plant room in long day conditions and were harvested once they were dry.

6.10 Genomic DNA extraction

Plant material was collected in a 2 mL reaction tube with one to two glass beads and immediately put into liquid nitrogen. The samples were ground using the tissue homogenizer (Retsch mill, QIAGEN) for 30 s and 30 rpm. 250 µL of gDNA extraction buffer (150 mM Tris-HCl (pH 8), 250 mM NaCl, 25 mM EDTA 0.5% (w/v) SDS) was added to the samples, mixed and centrifuged for 15 min at max. speed at RT. 150 µL of the supernatant were transferred to a 1.5 mL reaction tube and 150 µL isopropanol was added, mixed and centrifugated for 10 min at max. speead at RT. The supernatant was discarded and precipitated DNA pellet was washed with 500 mL of 70 % ethanol and centrifugated for 10 min. The supernatant was discarded and the samples were briefly centrifugated to remove the residual ethanol. The DNA pellet was air-dried and dissolved in 40 µL TlowE buffer (10 mM Tris-HCl (pH 8), 0.5 mM EDTA).

6.11 Genotyping

CRISPR/Cas9-derived mutations in the target gene/s were either validated by amplification of the loci of interest and subsequent sequencing, for example for mutations in *R4L2* and *R4L3* in *rlp4 r4l1 r4l2 r4l3* quadruple mutants, or by using cleaved amplified polymorphic sequences (CAPS). They are useful for mutants with a SNP or an insertion or deletion of one nucleotide. CAPS markers were designed for *rlp4 r4l1*, *cle21* and *cle27* mutants. Primers and restriction enzymes are listed in Table 13.

The T-DNA mutant *bam3-1* (SALK_44433) was genotyped for the presence of the T-DNA with a T-DNA specific primer, listed in Table 14.

All reporter lines (*pTCSn:GFP-NLS*, *pCLV3:BFP-NLS/pWUS:2xYFP-NLS/pUBQ10:3xmCherry-NLS*, *pDR5v2:YFPer*) in this study crossed with *csc1* were genotyped for mutations in *RLP4* and

R4L1. As *csc1* was derived from a CRISPR/Cas9-derived attempt to generate *rlp4 r4l*1 double mutants, *csc1* is still carrying these mutations. Only lines wild type for *RLP4* and *R4L1* were used for analysis. The triple reporter *pCLV3:BFP-NLS/pWUS:2xYFP-NLS/pUBQ10:3xmCherry-NLS* was additionally genotyped for the presence of the fluorophores, listed in Table 14.

6.12 Root and hypocotyl length measurments

Dependent on the experimental set up, seeds were either grown in light on vertical plates containing ½ MS, 0.9 % phytoagar and 1 % sucrose or in the dark on horizontal plates with ½ MS and 0.75 % phytoagar.

For root growth experiments, seedlings were grown on vertical plates with the standard medium, supplemented with sodium chloride (NaCl, Fisher chemicals). Root length was measured after six days in light. For the CLE root growth insensitivity assay, standard medium was supplemented with CLE peptides, either CLE11 (RVVPSGPNPLHH), CLE21 (RSIPTGPNPLHN) or CLE27 (RIVPSCPDPLHN) (GeneScript USA Inc.). Root length was measured after seven days in light.

For hypocotyl length experiments, seedlings were grown on horizontal plates with reduced phytoagar and no sugar and supplemented isoxaben (Sigma-Aldrich), see above. Plates with stratified seed were put in light for six hours and afterwards, plates were wrapped in aluminium foil to cover them completely from light. After four days, hypocotyl lengths were measured.

6.13 CLE21 and BA treatment

Col-0 and *csc1* seedlings were grown for five days on standard medium and supplemented with 0.1 and 1 µM 6-Benzylaminopurine (BA), respectively (Sigma-Aldrich). After five days, seedlings were stained with the combined basic fuchsin/calcofluor white protocol, see 6.17. Total vascular cell number was analysed by CLSM imagine, see 6.19.

pTCSn-GFPer, pAHP6:GFPer and pDR5v2:mTurquoise-NLS/pRPS5a:ntd:Tomato reporter lines were grown for five days on standard medium and supplemented with 50 nM CLE21, respectively. After five days, seedlings were stained with PI and imaged using CLSM, see 6.19.

6.14 RNA extraction for RNA-Seq

For RNA-Seq analysis, Col-0 and *csc1* plant material was collected from SAM and RAM. RAM material was collected from seedlings growing on a nylon mesh on ½ MS (Duchefa), 0.9 %

phytoagar (Duchefa) and 1 % sucrose (Carl Roth) in squared petri dishes in a vertical position. Seven days after gemination the root tip of the seedlings was cut off and approximatelly 70 – 80 mg plant material was collected. From both genotypes triplicates were collected and stored at -80 °C. For SAM material, plants of both genotypes were grown on soil in single pots. After 28 days on soil, SAMs of Col-0 and *csc1* plants with a shoot hight of 10 – 20 cm were dissected to remove flower buds and primordia. Per genotype, 20 SAMs were dissected and approxiametelly 70 – 80 mg of plant material was collected. From both genotypes, triplicates were collected and stored at – 80 °C. Plant material was ground with a metal bead using a tissue homogenizer (Retsch Mill, QIAGEN). For RNA isolation, the RNA plant purification kit (Roboklon) was used following manufacturer's instruction. The DNase digestion step was performed on the column, with the recommended enzyme from Roboklon. RNA was eluted in RNase-free H_2O and the concentration was measured with a nanodrop. Next generation sequencing was conducted at the Deep Sequencing Core Facility by David Ibberson, Bioquant, University of Heidelberg.

6.15 Whole genome sequencing (WGS)

For whole genome sequence analysis, plant material of three different populations of *csc*1 plants were sent for next generation sequencing (NGS). The *csc1* #6-13 mutant in the *rlp4 r4l1* Col-0 mutant background (#1 *csc1*), *csc1* crossed with Col-0 in F_2 generation showing the csc1 mutant phenotype (enlarged SAM in adult plants and more protoxylem cells for seedlings) (#2 *csc1* Col-0 F_2 +) and *csc1* crossed with Col-0 in F_2 generation without *csc1* phenotype (#3 *csc1* Col-0 F_2 -). Sample #1 comprised small pieces of rosette leaves of three adult *csc*1 #6-13 plants, sample #2 comprised pooled cauline leaves of ~ 50 adult plants with the *csc1* SAM phenotype and ~ 50 seedlings with *csc1* protoxylem phenotype. Sample #3 comprised also pooled cauline leaves of ~ 50 adult plants without the *csc1* SAM phenotype and ~ 50 seedlings without *csc1* protoxylem phenotype.

For gDNA extraction, the CTAB DNA preparation method was used. The samples were ground under liquid nitrogen using pistil and mortar and 70 – 100 mg plant material was collected in a 2 mL reaction tube. 600 µL CTAB buffer (2 % CTAB, 1 % PVP 4000, 1.4 M NaCl, 100 mM Tris-HCl, pH 8, 20 mM EDTA, pH 8) was added and vortexed until the samples were solubilized. After one hour incubation at 65 °C, samples were colled down for 10 min at RT and 1 µL RNaseA (1 mg/mL) was added. Samples were incubated for one hour at 37 °C. 60 µL CHCl3 were added, gently mixed by inverting the tubes and spin down at 5000 rpm for 10 min at RT. The polar phase (~ 500 µL) were transferred to a new 2 mL reaction tube and 2.5x the volume (1250 mL) of 100 % ethanol

(-20 °C) were added, gently mixed by inverting the tubes and followed by incubating the samples for 30 min at – 20 °C. Afterwards, the samples were centrifugated at full speed for 10 min at 4 °C. The supernatant was discarded and 500 µL of 70 % ethanol (- 20 °C) were added to wash the precipitated DNA. The samples were again centrifugated at full speed for 10 min at 4 °C. The supernatant was discarded and the DNA pellet was dried at 55 °C until residual ethanol evaporated. The DNA pellet was resuspended in 50 µL H2O (important for sequencing: no EDTA in DNA). Next generation sequencing for the whole genome was performed by Starseq (Mainz).

6.16 GUS staining

Whole seedlings and dissected shoot apical meristems were used for GUS staining. The plant material was collected in a 2 mL reaction tube and fixed with 90 % acetone for one hour at – 20 °C. Afterwards, the samples were twice washed with washing buffer (0.1 M phosphate buffer (Na_2HPO_4/NaH_2PO_4), pH 7, 10 mM EDTA and 2 mM $K_3Fe(CN)_6$ (K-Ferri)) under vacuum for 5 min. The washing buffer was removed and samples were infiltrated with staining buffer (0.1 M phosphate buffer, pH 7, 10 mM EDTA, 1 mM $K_3Fe(CN)_6$ (K-Ferri), 1 mM $K_4Fe(CN)_6 * 3H_2O$ (K-Ferro) and 2 mM X-Gluc) by a brief vacuum treatment and samples were incubated overnight at 37 °C. GUS stained tissues were fixed in a 3:1 mixture of ethanol (100 %) and acetic acid for two to three hours. Afterwards, the samples were cleared and mounted in clearing solution (chloral hydrate:water:glycerol, 8:3:1) for long term storage, kept at 4 °C. Images were acquired using the Zeiss microscope Axio Imager.M1.

6.17 Basic Fuchsin and Calcofluor White staining

Seedlings grown for six to seven days on vertical ½ MS, 0.9 % phytoagar and 1 % sucrose plates, were used for staining. Seedlings were placed in cell strainers (Corning) into six well plates (Sarstedt), covered with 1 M KOH (~ 5 mL/well) and incubated for four to six hours at 37 °C. After incubation, KOH was removed and seedlings were stained with 0.01 % basic fuchsin in H_2O for five min. After incubation, the basic fuchsin solution was removed and seedlings were washed in 70 % ethanol for 10 min with subsequently three washing steps with 50 mM Tris-HCl, pH 7.5. Neutral pH was verified with litmus paper strips. Afterwards, seedlings were stained with 100 µg/mL Calcofluor White in 50 mM Tris-HCl, pH 7.5 for 90 min with slight agitation on a benchtop shaker. Seedlings were de-stained by three washing steps with 50 mM Tris-HCl, pH 7.5. For storage, the buffer was replaced by 50 % glycerol and samples were kept at 4 °C. Secondary cell wall staining in the xylem and cellulose staining in the root cells was imaged using CLSM (Table 12).

6.18 Plasmolysis

Plasmolysis was performed with the stable Arabidopsis line carrying the plasma membrane marker *p35S:GFP-LTI6b* and *pUBQ10:RLP4-ECD:mCherry.* Seven day-old seedlings were incubated for 20 min in 0.6 M sorbitol solution and directly imaged using CLSM (Table 12).

6.19 Confocal laser scanning microscopy (CLSM)

Confocal images for the SAM were acquired on a Nikon A1 Confocal with a CFI Apo LWD 25x water immersion objective.

Inflorescence meristems were dissected by cutting the stem with and primordia were removed by a forcep or a canula up to flower stage 3-4. Shoot apical meristems were counter stained, if needed, with PI (200 µg/mL) dissolved in water for 5 min and mounted in a small petri dish with 3 % agarose and covered with water. Excitation wavelengths for imaged fluorophors and the according emission wavelength are depicted in (Table 11).

Table 11. Excitation and emission wavelengths used with Nikon microscope

fluorophore	excitation [nm]	emission [nm]
mTurquoise2	405	425-475
GFP	488	500-550
YFP	488	500-550
mCherry	561	570-620
PI	561	570-620

Confocal images for the root were acquired on a Leica TCS SP5 inverted confocal microscope with a 63x water objective. If needed, roots were incubated in PI (10 µg/mL) dissolved in water for 20 min and directly imaged. Excitation wavelengths for used fluorophores and their according emission wavelengths are depicted in Table 12.

Table 12. Excitation and emission wavelengths used with Leica microscope

fluorophore	excitation [nm]	emission [nm]
mTurquoise2	458	490-525
GFP	488	480-530
YFP	488	480-530
mCherry	561	560-610
PI	561	560-610
Basic Fuchsin	514	560-610
Calcofluor white	405	500-520

6.20 Bioinformatics

6.20.1 Phylogenetic tree – RLP4

Protein sequences for phylogenetic analysis were received from the NCBI data base. The alignment of all amino acids and the phylogenetic tree was done using the programme/software CLC Main Workbench 8.1 (QIAGEN). For phylogenetic tree analysis, maximum likelihood phylogeny was performed using the 'neighbor joining' construction method and 'WAG' for the protein substitution model with a transition/transversion ratio of 2.0. Bootstrapping was performed with 1000 replicates.

6.20.2 Image analysis

All non-quantitative images were processed using ImageJ. MorphoGraphX was used to quantify cell surface area and cell numbers in the epidermis of the SAM (Barbier de Reuille et al., 2015). For the quantification of cells within a specific domain in the SAM, a customized workflow using KNIME Image Processing platform was established by Dr. Christian Wenzl (Berthold et al., 2008). Ubiquitiously expressed nuclear mCherry marked each nucleus in the SAM. CLV3 and WUS positive cells in the reporter *pCLV3:BFP-NLS/pWUS:2xYFP-NLS/pUBQ10:3xmCherry-NLS* and pTCSn positive cells in the pTCSn:GFP-NLS/*pUBQ10:3xmCherry-NLS* reporter line were assigned by using KNIME.

6.20.3 Statistical analysis

Significant differences between samples was either calculated by performing a one-factor analysis of variance (ANOVA) with Tukey's test as post-hoc analysis, a Student's t-test or Kruskal-Wallis test.

6.21 Primers

Table 13. Primers used for cloning.

primer name	stock name	sequence [5'-3]	gene
pAT5g47500_pPME5_GG_F	SW1871	aacaGGTCTCaACCTcatccgcaacgatagatat	AT5G47500
pAT5g47500_pPME5_GG_R	SW1872	aacaGGTCTCtTGTTTggcttgtgagaaaggaaac	AT5G47500
2gRNA_PME44_F	SW1876	atatatGGTCTCgATTGGGATCGCCGGCTGCAGAATGgttttagagctagaaatagc	AT4G33220
2gRNA_PME41_R	SW1877	attattGGTCTCgAAACCTTCTCCCTCCGCAAATCGCcaatctcttagtcgactctac	AT4G02330
2gRNA_at5g53370_F	SW1882	atatatGGTCTCgATTGGTGTAGTTCCGGGAGTGACGgttttagagctagaaatagc	AT5G53370
2gRNA_PME3_R	SW1883	attattGGTCTCgAAACCCGTAGCTTTGCTCTTCGTCcaatctcttagtcgactctac	AT3G14310
pREV_GGA_F	SW1337	AACAGGTCTCAACCTacacctctttctgattactag	AT5G60690
pREV_GGA_R	SW1338	AACAGGTCTCATGTTtttagctcgaccctcaaaaaaag	AT5G60690
pAtHB-8_GGA_F	SW1329	AACAGGTCTCAACCTggtcgaaaaatgtataacaatac	AT4G32880
pAtHB-8_GGA_R	SW1330	AACAGGTCTCtTGTTctttgatcctctccgatc	AT4G32880
pAtHB-8_in_F	SW1331	AACAGGTCTCAtccagTgaccagcgtgatcaaaaac	AT4G32880
pAtHB-8_in_R	SW1332	AACAGGTCTCAtggaagcaaaggaagatatag	AT4G32880
GGA_pAHP6_F	SW1477	AACAGGTCTCAACCTCACGGGGCGCAAAGAAG	AT1G80100
GGB_pAHP6_R	SW1478	AACAGGTCTCTTGTTCAACGGCACACCCGTCTT	AT1G80100
pTMO5_GGA_F	SW1223	AACAGGTCTCAACCTGTTGAACGTCGTGTGGGCTTC	AT3G25710
pTMO5_GGA_R	SW1224	AACAGGTCTCATGTTTTTTTGGTTTTTTTGGTTTTTTAGTTTTTGG	AT3G25710
GR-LHG4_GG_F_BD_adaptor	SW1469	AACAGGTCTCaAACAcaATGGCTAGTGAAGCTCGA	
GR-LHG4_GG_R_BD_adaptor	SW1470	AACAGGTCTCtGCAGTTACTCTTTTTTTGGGTTTG	
RLP4_1_2gRNA_F_1	SW1788	aacaGGTCTCaattgGTAAGTAGGCGTTGTTGCATgttttagagctagaaatagc	AT1G28340
R4L1_1_2gRNA_R_1	SW1789	aacaGGTCTCtaaacTCCTGGTCGTTACTATCTCCcaatctcttagtcgactctac	AT1G25570
R4L3_CRISPR_2gRNA_Exon2_F	SW2145	ATATATGGTCTCGATTGaacgagatagaatacacacGTTTTAGAGCTAGAAATAGC	AT3G19230

R4L2_CRISPR_2gRNA_Exon2_R	SW2146	ATTATTGGTCTCGAAACcctccgtaatcgacggccgCAATCTCTTAGTCGACTCTTAC	AT3G05990

Table 14. Primers used for genotyping.

primer name	stock name	sequence [5'-3]	gene	special remark
PME44_CRISPR_Geno_F	SW1878	TCATCGGAGGAGAATTTTCAAT	AT4G33220	
PME44_CRISPR_Geno_R	SW1879	ACTTTCCATATACCGGCAATA	AT4G33220	
PME41_CRISPR_Geno_F	SW1880	ATGCTATCTCTCAAACTCTTC	AT4G02330	
PME41_CRISPR_Geno_R	SW1881	GCAATGCGACACCGTTTC	AT4G02330	
at5g53370_CRISPR_Geno_F	SW1884	gtgatgcagtcgttatatatg	AT5G53370	
at5g53370_CRISPR_Geno_R	SW1885	ATCATCAAGTAACTCAAGGC	AT5G53370	
PME3_CRISPR_Geno_F	SW1886	ctgataacgacggtccag	AT3G14310	
PME3_CRISPR_Geno_R	SW1887	GCTTCTTCACGGTGAAGTA	AT3G14310	
CRISPR_Cas9_F	SW1861	AACCCCATTAATGCGTCAGGCG		
CRISPR_Cas9_R	SW1862	GTCAATGTACCCAGCGTAGCCG		
p6xOP_F	SW1777	TGCATATGTCGAGCTCAAGAA		
p6xOP_R	SW1778	CTTATATAGAGGAAGGGTCTT		
rlp4_r4l1_cr1_forRLP4_capsF	SW2063	GGATTAGTTGTGGAGCTAG	AT1G28340	HypCH4V
rlp4_r4l1_cr1_forRLP4_capsR	SW2064	TTGACTACTCCAACCAGATT	AT1G28340	
rlp4_r4l1_cr1_forR4L1_capsF	SW2065	aaactgaattcttcctctgtt	AT1G25570	BstNI
rlp4_r4l1_cr1_forR4L1_capsR	SW2066	ATCTCCAAGAGAAAACAAGAG	AT1G25570	
R4L2_at3g05990_F	SW2098	tatgctaacttcttctctacc	AT3G05990	
R4L2_at3g05990_R	SW2099	TCGTAATAAGAAGCGAGACC	AT3G05990	
R4L3_at3g19230_F	SW2100	ccattaacgacaatggaaagaa	AT3G19230	
R4L3_at3g19230_R	SW2101	GCTAGACAAACACTTAGTCTG	AT3G19230	

pCLE11_F_end	SW2030	ttactctatatcataatttgaa	AT1G49005	
CLE11_CDS_R	SW2031	cgcaacaaaaatctattgaaaca	AT1G49005	
cle21_caps_F	SW2164	ATGTTAATTTTATCTTCACGA	AT5G64800	XbaI
cle21_caps_R	SW2165	ACATATATACACCAAACGAAC	AT5G64800	
cle27_caps_F	SW2166	ATGACTCATGCTCGAGAATG	AT3G25905	RsaI
cle27_caps_R	SW2167	TATGAAATGGTTATAGATCAGT	AT3G25905	
mVenus_F	SW2084	cttccggatagcccagct		
mVenus_R	SW2085	aagggcgaggagctgttc		
mCherry_F	SW2086	aaggtgaagaggataatatgg		
mCherry_R	SW2087	cttcttcctcaccctcgttt		
BFP_F	SW2088	agggtgaagagcttatcaaag		
BFP_R	SW2089	agtcctgcgtatcttgcca		
SALK044433_bam3-1_F	SW2067	CTGCAACTTCTTCTCCGTTTG	AT4G20270	
SALK044433_bam3-1 R	SW2068	GATTCCTTCGAAACTCGGATC	AT4G20270	
LBb1.3	SW230	ATTTTGCCGATTTCGGAAC		

Table 15. Primers for bulked segregant analysis.

primer name	stock name	sequence [5'-3]	chromosome area
CER448567_F	SW675	ATA GAA AGG TTT GAG GGG GC	459000
CER448567_R	SW676	TGC GAA GAA CCA CTA AAC CC	
F9L1_F	SW677	CTC GGA AAT TCT TAG CTT TC	5022000
F9L1_R	SW678	TTA TAA CTT GCC CAA AGC GAA	
F1K23ind38_F	SW679	GGA TTG AAC ATA GGG AAG GGG	9893000
F1K23ind38_R	SW680	GAT CTG TAT CTG AAA CCT GGG	
CER464787-Indel-44_F	SW681	TTT GAA CTA ACC TTC TGA GG	13780000
CER464787-Indel-44_R	SW682	CAT GTT GAT GAT TCA ATT GC	

F6D8ind94_F	SW683	CCG TTA CCC CCA TAC GAA CG	19614000
F6D8ind94_R	SW684	TCG TGA GGT TAT GCC GAT CC	
F5I14_F	SW685	CTG CCT GAA ATT GTC GAA AC	23701000
F5I14_R	SW686	GGC ATC ACA GTT CTG ATT CC	
CER459153_F	SW687	TCG TGA CCA AAT CCT GAA CA	1562000
CER459153_R	SW688	TGT CCA AGT AAT GCC GTG AG	
CER466780_F	SW689	GAA CCC TTA TAA TAT GGC TGG C	6785000
CER466780_R	SW690	GGA AGT ATT CCC AAG ACA AGG	
MSAT2-36_F	SW691	GAT CTG CCT CTT GAT CAG C	8690000
MSAT2-36_R	SW692	CCA AGA ACT CAA AAC CGT T	
F3N11_F	SW693	GTT AAA GCG AGG ACG ATT GG	12107000
F3N11_R	SW694	AGA TAC TGT CGC CAT CAA GG	
T2P4_F	SW695	ACT AGT CCC ACT GTC GAT C	15011000
T2P4_R	SW696	GTT ACT TCG TAA GTC CCT AC	
MSAT2-9_F	SW697	TAA AAG AGT CCC TCG TAA AG	18150000
MSAT2-9_R	SW698	GTT GTT GTT GTG GCA TT	
nga172_F	SW699	AGC TGC TTC CTT ATA GCG TCC	790000
nga172_R	SW700	CAT CCG AAT GCC ATT GTT C	
CER455386_F	SW701	CTC TTT TGG CTC GGA CAA G	4590000
CER455386_R	SW702	GTT GTA ATC GGG AAA ATG C	
CER455914_F	SW703	GGA GCA GAG AAA GAG AC	7450000
CER455914_R	SW704	GAG GAA GGA CAA CAT GGC	
CER456071-Indel-35_F	SW705	AGC CAT AGG TAA TGT CCA CG	9170000
CER456071-Indel-35_R	SW706	CTC GCG GAT GAG TAT CAT CC	
CER470441_F	SW707	GCT AAC AGG GAT ATC AAA TGT GC	11886000

CER470441_R	SW708	CGG ACG AGC TGA CAC TTG TA	
CER470172_F	SW709	GTA AAA CTC CTC CTC TGG GG	18247000
CER470172_R	SW710	TGT AAT CGT GGC GGA ACG GG	
CER459609_F	SW711	TCG CTT TTG AAG ATT TGT GC	1997000
CER459609_R	SW712	GGG AGC TTC TCA GTG GTC TG	
nga8_F	SW713	GAG GGC AAA TCT TTA TTT CGG	5630000
nga8_R	SW714	TGG CTT TCG TTT ATA AAC ATC C	
FCA0ind25_F	SW715	AAG CCA ACT ATT GCC AAG GG	8101000
FCA0ind25_R	SW716	TCA CTG CCC TTT ACT CCG GT	
F7J7-47_F	SW717	TGG TGA AGA GCT TAG TTG ATG A	11293000
F7J7-47_R	SW718	TCA CTA GAT ATC TCT AGT GGC T	
CER451534_F	SW719	AGC TAC GGT GGA GTG TAA TTT CGT	14602000
CER451534_R	SW720	GCT GAT ACT TGC TTT CGC TTT GCA G	
CER459444_F	SW721	AGT AGC ATC GTA GCT CCT AGG	18000000
CER459444_R	SW722	GTT GTA TAC GTG CAC GTT CCC	
CER456519_F	SW723	TGC TAA AAT ATA AAA CTT CC	2247000
CER456519_R	SW724	TTA TGC AGA TGT ATG AGG CC	
nga151_F	SW725	GTT TTG GGA AGT TTT GCT GG	4670000
nga151_R	SW726	CAG TCT AAA AGC GAG AGT ATG ATG	
nga139_F	SW727	GGT TTC GTT TCA CTA TCC AGG	8430000
nga139_R	SW728	AGA GCT ACC AGA TCC GAT GG	
T26D22-IND52/CER459812_F	SW729	TCC CAC GAA GAG AGA AGT GC	13575000
T26D22-IND52/CER459812_R	SW730	CTA TTT GCT TAT GAA GGT GTC C	
CER456772_F	SW731	CCA TGT GAC ATG CAC TTA CAC	17610000
CER456772_R	SW732	ACC ATT CTC TAC CAC TCC AC	
K6M13ind33/CER454758_F	SW733	ATA GAT GAG ATC CAC TTG CC	20130000
K6M13ind33/CER454758_R	SW734	ACA AAC TGT TGC TGT GGG AG	

MBK5ind35/CER455203_F	SW735	ATT CTC GGA CCA GGC TTC AT	24544000
MBK5ind35/CER455203_R	SW736	AAA GAA CAG CTA CTG CGT GC	

References

Augustin, S., 2015: Structure-function analysis of the *Arabidopsis thaliana* Receptor-Like Protein 4 (AtRLP4). Master thesis

Antolín-Llovera, M.; Ried, M. K.; Parniske, M., 2014: Cleavage of the symbiosis receptor-like kinase ectodomain promotes complex formation with nod factor receptor 5. *Current Biology*., **24**, 422–427.

Band, L. R.; Wells, D. M.; Fozard, J. A.; Ghetiu, T.; French, A. P.; Pound, M. P.; Wilson, M. H.; Yu, L.; Li, W.; Hijazi, H. I.; Oh, J.; Pearce, S. P.; Perez-Amador, M. A.; Yun, J.; Kramer, E.; Alonso, J. M.; Godin, C.; Vernoux, T.; Hodgman, T. C. et al., 2014: Systems Analysis of Auxin Transport in the Arabidopsis Root Apex. *The Plant Cell*., **26**, 862–875.

Barbez, E.; Kubeš, M.; Rolčík, J.; Béziat, C.; Pěnčík, A.; Wang, B.; Rosquete, M. R.; Zhu, J.; Dobrev, P. I.; Lee, Y.; Zažímalovà, E.; Petrášek, J.; Geisler, M.; Friml, J.; Kleine-Vehn, J., 2012: A novel putative auxin carrier family regulates intracellular auxin homeostasis in plants. *Nature*., **485**, 119–122.

Barbier de Reuille, P.; Routier-Kierzkowska, A. L.; Kierzkowski, D.; Bassel, G. W.; Schüpbach, T.; Tauriello, G.; Bajpai, N.; Strauss, S.; Weber, A.; Kiss, A.; Burian, A.; Hofhuis, H.; Sapala, A.; Lipowczan, M.; Heimlicher, M. B.; Robinson, S.; Bayer, E. M.; Basler, K.; Koumoutsakos, P. et al., 2015: MorphoGraphX: A platform for quantifying morphogenesis in 4D. *eLife*., **4**, 1–20.

Bellande, K.; Bono, J. J.; Savelli, B.; Jamet, E.; Canut, H., 2017: Plant lectins and lectin receptor-like kinases: How do they sense the outside? *International Journal of Molecular Sciences*., **18**, 1164.

Besnard, F.; Rozier, F.; Vernoux, T., 2014a: The AHP6 cytokinin signaling inhibitor mediates an auxin-cytokinin crosstalk that regulates the timing of organ initiation at the shoot apical meristem, 4–7.

Besnard, F.; Refahi, Y.; Morin, V.; Marteaux, B.; Brunoud, G.; Chambrier, P.; Rozier, F.; Mirabet, V.; Legrand, J.; Lainé, S.; Thévenon, E.; Farcot, E.; Cellier, C.; Das, P.; Bishopp, A.; Dumas, R.; Parcy, F.; Helariutta, Y.; Boudaoud, A. et al., 2014b: Cytokinin signalling inhibitory fields provide robustness to phyllotaxis. *Nature*., **505**, 417–421.

Besson, S.; Dumais, J., 2011: Universal rule for the symmetric division of plant cells. *Proceedings of the National Academy of Sciences*., **108**, 6294–6299.

Betsuyaku, S.; Sawa, S.; Yamada, M., 2011a: The Function of the CLE Peptides in Plant Development and Plant-Microbe Interactions. *The Arabidopsis Book*., **9**.

Betsuyaku, S.; Takahashi, F.; Kinoshita, A.; Miwa, H.; Shinozaki, K.; Fukuda, H.; Sawa, S., 2011b: Mitogen-activated protein kinase regulated by the CLAVATA receptors contributes to shoot apical meristem homeostasis. *Plant and Cell Physiology*., **52**, 14–29.

Bhatia, N.; Bozorg, B.; Ohno, C.; Heisler, M. G.; Ohno, C.; Jo, H., 2016: Auxin Acts through MONOPTEROS to Regulate Plant Cell Polarity and Pattern Phyllotaxis, 1–7.

Bi, G.; Liebrand, T. W. H.; Cordewener, J. H. G.; America, A. H. P.; Xu, X.; Joosten, M. H. A. J., 2014: Arabidopsis thaliana receptor-like protein At RLP23 associates with the receptor-like kinase At SOBIR1. *Plant Signaling & Behavior*., **9**, e27937.

Bi, G.; Zhou, Z.; Wang, W.; Li, L.; Rao, S.; Wu, Y.; Zhang, X.; Menke, F. L. H.; Chen, S.; Zhou, J. M., 2018: Receptor-like Cytoplasmic Kinases Directly Link Diverse Pattern Recognition Receptors to the Activation of Mitogen-activated Protein Kinase Cascades in Arabidopsis. *The Plant Cell*., **30**, tpc.00981.2017.

Bishopp, A.; Help, H.; El-Showk, S.; Weijers, D.; Scheres, B.; Friml, J.; Benková, E.; Mähönen, A. P.; Helariutta, Y., 2011a: A Mutually Inhibitory Interaction between Auxin and Cytokinin Specifies Vascular Pattern in Roots. *Current Biology*., **21**, 917–926.

Bishopp, A.; Lehesranta, S.; Vatén, A.; Help, H.; El-Showk, S.; Scheres, B.; Helariutta, K.; Mähönen, A. P.; Sakakibara, H.; Helariutta, Y., 2011b: Phloem-Transported Cytokinin Regulates Polar Auxin Transport and Maintains Vascular Pattern in the Root Meristem. *Current Biology*., **21**, 927–932.

Bleckmann, A.; Weidtkamp-Peters, S.; Seidel, C. A. M.; Simon, R., 2009: Stem Cell Signaling in Arabidopsis Requires CRN to Localize CLV2 to the Plasma Membrane. *Plant Physiology*., **152**, 166–176.

Bohnert, H. J.; Nelson, D. E.; Jensen, R. G., 1995: Adaptations to Environmental Stresses. *The Plant*

Cell., **7**, 1099.

Boisson-Dernier, A.; Roy, S.; Kritsas, K.; Grobei, M. A.; Jaciubek, M.; Schroeder, J. I.; Grossniklaus, U., 2009: Disruption of the pollen-expressed FERONIA homologs ANXUR1 and ANXUR2 triggers pollen tube discharge. *Development*., **136**, 3279–3288.

Boisson-Dernier, A.; Kessler, S. A.; Grossniklaus, U., 2011: The walls have ears: The role of plant CrRLK1Ls in sensing and transducing extracellular signals. *Journal of Experimental Botany*., **62**, 1581–1591.

Bonaccorso, O.; Lee, J. E.; Puah, L.; Scutt, C. P.; Golz, J. F., 2012: FILAMENTOUS FLOWER controls lateral organ development by acting as both an activator and a repressor. *BMC plant biology*., **12**, 176.

Bosch, M.; Cheung, A. Y.; Hepler, P. K., 2005: Pectin Methylesterase , a Regulator of Pollen Tube Growth 1 [w], **138**, 1334–1346.

Braidwood, L.; Breuer, C.; Sugimoto, K., 2014: My body is a cage: Mechanisms and modulation of plant cell growth. *New Phytologist*., **201**, 388–402.

Brand, U.; Fletcher, J. C.; Hobe, M.; Meyerowitz, E. M.; Simon, R.; Brand, U.; Fletcher, J. C.; Hobe, M., 2000: Dependence of Stem Cell Fate in Arabidopsis on a Feedback Loop Regulated by CLV3 Activity, **289**, 617–619.

Braybrook, S. A.; Peaucelle, A., 2013: Mechano-Chemical Aspects of Organ Formation in Arabidopsis thaliana : The Relationship between Auxin and Pectin. *PloS one*., **8**, e57813.

Brutus, A.; Sicilia, F.; Macone, A.; Cervone, F.; Lorenzo, G. De, 2010: A domain swap approach reveals a role of the plant wall-associated kinase 1 (WAK1) as a receptor of oligogalacturonides, **1**.

Caffall, K. H.; Mohnen, D., 2009: The structure, function, and biosynthesis of plant cell wall pectic polysaccharides. *Carbohydrate Research*., **344**, 1879–1900.

Cai, L.; Sutter, B. M.; Li, B.; Tu, B. P., 2011: Acetyl-CoA Induces Cell Growth and Proliferation by Promoting the Acetylation of Histones at Growth Genes. *Molecular Cell*., **42**, 426–437.

Calderón Villalobos, L. I. A.; Lee, S.; De Oliveira, C.; Ivetac, A.; Brandt, W.; Armitage, L.; Sheard, L. B.; Tan, X.; Parry, G.; Mao, H.; Zheng, N.; Napier, R.; Kepinski, S.; Estelle, M., 2012: A combinatorial TIR1/AFB–Aux/IAA co-receptor system for differential sensing of auxin. *Nature Chemical Biology*., **8**, 477–485.

Carlsbecker, A.; Lee, J. Y.; Roberts, C. J.; Dettmer, J.; Lehesranta, S.; Zhou, J.; Lindgren, O.; Moreno-Risueno, M. A.; Vatén, A.; Thitamadee, S.; Campilho, A.; Sebastian, J.; Bowman, J. L.; Helariutta, Y.; Benfey, P. N., 2010: Cell signalling by microRNA165/6 directs gene dose-dependent root cell fate. *Nature*., **465**, 316–321.

Chandler, J. W., 2012: Floral meristem initiation and emergence in plants. *Cellular and Molecular Life Sciences*., **69**, 3807–3818.

Chandler, J. W.; Werr, W., 2015: Cytokinin – auxin crosstalk in cell type specification. *Trends in Plant Science*., **20**, 291–300.

Chen, C.; Li, C.; Wang, Y.; Renaud, J.; Tian, G.; Kambhampati, S.; Saatian, B.; Nguyen, V.; Hannoufa, A.; Marsolais, F.; Yuan, Z. C.; Yu, K.; Austin, R. S.; Liu, J.; Kohalmi, S. E.; Wu, K.; Huang, S.; Cui, Y., 2017: Cytosolic acetyl-CoA promotes histone acetylation predominantly at H3K27 in Arabidopsis. *Nature Plants*., **3**, 814–824.

Chen, H. Y.; Hsieh, E. J.; Cheng, M. C.; Chen, C. Y.; Hwang, S. Y.; Lin, T. P., 2016: ORA47 (octadecanoid-responsive AP2/ERF-domain transcription factor 47) regulates jasmonic acid and abscisic acid biosynthesis and signaling through binding to a novel cis-element. *The New phytologist*., **211**, 599–613.

Cheng, Y., 2006: Auxin biosynthesis by the YUCCA flavin monooxygenases controls the formation of floral organs and vascular tissues in Arabidopsis. *Genes & Development*., **20**, 1790–1799.

Cheung, J.; Hendrickson, W. A., 2011: Sensor Domains of Two-Component Regulatory Systems. *Curr Opin Microbiol.*, **13**, 116–123.

Clark, S. E.; Williams, R. W.; Meyerowitz, E. M., 1997: The CLAVATA1 gene encodes a putative receptor kinase that controls shoot and floral meristem size in Arabidopsis. *Cell*., **89**, 575–585.

Coen, E. S.; Meyerowitz, E. M., 1991: The war of the whorls: genetic interactions controlling flower development. *Nature*., **353**, 31–37.

Cosgrove, D. J., 2005: GROWTH OF THE PLANT, **6**, 850–861.

Cosgrove, D. J., 2014: Re-constructing our models of cellulose and primary cell wall assembly. *Current Opinion in Plant Biology*., **22**, 122–131.

Cosgrove, D. J., 2015: ScienceDirect Plant expansins : diversity and interactions with plant cell walls. *Current Opinion in Plant Biology*., **25**, 162–172.

Cosgrove, D. J., 2016a: Plant cell wall extensibility : connecting plant cell growth with cell wall structure , mechanics , and the action of wall- modifying enzymes, **67**, 463–476.

Cosgrove, D. J., 2016b: Catalysts of plant cell wall loosening [version 1 ; referees : 2 approved] Referee Status :, **5**, 1–13.

Cutler, S. R.; Ehrhardt, D. W.; Griffitts, J. S.; Somerville, C. R., 2000: Random GFP::cDNA fusions enable visualization of subcellular structures in cells of Arabidopsis at a high frequency. *Proceedings of the National Academy of Sciences*., **97**, 3718–3723.

Daher, F. B.; Braybrook, S. A., 2015: How to let go: pectin and plant cell adhesion. *Frontiers in Plant Science*., **6**, 1–8.

Daum, G.; Medzihradszky, A.; Suzaki, T.; Lohmann, J. U., 2014: A mechanistic framework for noncell autonomous stem cell induction in Arabidopsis, **2014**.

De Rybel, B.; Möller, B.; Yoshida, S.; Grabowicz, I.; Barbier de Reuille, P.; Boeren, S.; Smith, R. S.; Borst, J. W.; Weijers, D., 2013: A bHLH Complex Controls Embryonic Vascular Tissue Establishment and Indeterminate Growth in Arabidopsis. *Developmental Cell*., **24**, 426–437.

De Rybel, B.; Mähönen, A. P.; Helariutta, Y.; Weijers, D., 2016: Plant vascular development: from early specification to differentiation. *Nature Reviews Molecular Cell Biology*., **17**, 30–40.

De Smet, I.; Grunewald, W.; Damme, D. Van; Noorden, G. Van; Naudts, M.; Isterdael, G. Van; Clercq, R. De; Wang, J. Y.; Meuli, N.; Vanneste, S.; Friml, J.; Hilson, P.; Jürgens, G.; Ingram, G. C.; Inzé, D.; Benfey, P. N.; Beeckman, T., 2008: Receptor-like kinase ACR4 restricts formative cell divisions in the Arabidopsis Root. *Science*., **322**, 594–597.

Decreux, A.; Messiaen, J., 2005: Wall-associated kinase WAK1 interacts with cell wall pectins in a calcium-induced conformation. *Plant and Cell Physiology*., **46**, 268–278.

Depuydt, S.; Rodriguez-Villalon, A.; Santuari, L.; Wyser-Rmili, C.; Ragni, L.; Hardtke, C. S., 2013: Suppression of Arabidopsis protophloem differentiation and root meristem growth by CLE45 requires the receptor-like kinase BAM3. *Proceedings of the National Academy of Sciences*., **110**, 7074–7079.

Dharmawardhana, D. P.; Ellis, B. E.; Carlson, J. E., 1995: A [beta]-Glucosidase from Lodgepole Pine Xylem Specific for the Lignin Precursor Coniferin. *Plant Physiology*., **107**, 331–339.

Dinneny, J. R.; Long, T. A.; Wang, J. Y.; Jung, J. W.; Mace, D.; Pointer, S.; Barron, C.; Brady, S. M.; Schiefelbein, J.; Benfey, P. N., 2008: Arabidopsis Roots to Abiotic Stress. *Science*., **320**, 942–946.

Dolan, L.; Janmaat, K.; Willemsen, V.; Linstead, P.; Poethig, S.; Roberts, K.; Scheres, B., 1993: Cellular organisation of the Arabidopsis thaliana root. *Development (Cambridge, England)*., **119**, 71–84.

Dolzblasz, A.; Nardmann, J.; Clerici, E.; Causier, B.; van der Graaff, E.; Chen, J.; Davies, B.; Werr, W.; Laux, T., 2016: Stem Cell Regulation by Arabidopsis WOX Genes. *Molecular Plant*., **9**, 1028–1039.

Drisch, R. C.; Stahl, Y., 2015: Function and regulation of transcription factors involved in root apical meristem and stem cell, **6**, 1–8.

Du, Q.; Wang, H., 2015: The role of HD-ZIP III transcription factors and miR165/166 in vascular development and secondary cell wall formation. *Plant Signaling & Behavior*., **10**, e1078955.

Dünser, K.; Kleine-Vehn, J., 2015: Differential growth regulation in plants-the acid growth balloon theory. *Current Opinion in Plant Biology*., **28**, 55–59.

Efroni, I., 2018: A Conceptual Framework for Cell Identity Transitions in Plants. *Plant and Cell Physiology*., **59**, 691–701.

Endo, S.; Pesquet, E.; Yamaguchi, M.; Tashiro, G.; Sato, M.; Toyooka, K.; Nishikubo, N.; Udagawa-Motose, M.; Kubo, M.; Fukuda, H.; Demura, T., 2009: Identifying New Components Participating in the Secondary Cell Wall Formation of Vessel Elements in Zinnia and Arabidopsis. *the Plant Cell Online*., **21**, 1155–1165.

Etchells, J. P.; Turner, S. R., 2010: The PXY-CLE41 receptor ligand pair defines a multifunctional pathway that controls the rate and orientation of vascular cell division. *Development*., **137**, 767–774.

Feng, W.; Kita, D.; Peaucelle, A.; Cartwright, H. N.; Doan, V.; Duan, Q.; Liu, M. C.; Maman, J.;

Steinhorst, L.; Schmitz-Thom, I.; Yvon, R.; Kudla, J.; Wu, H. M.; Cheung, A. Y.; Dinneny, J. R., 2018: The FERONIA Receptor Kinase Maintains Cell-Wall Integrity during Salt Stress through Ca2+ Signaling. *Current Biology*., **28**, 666–675.e5.

Fleming, A. J.; McQueen-Mason, S.; Mandel, T.; Kuhlemeier, C., 1997: Induction of Leaf Primordia by the Cell Wall. *Science*., **276**, 1415–1419.

Fletcher, J. C.; Brand, U.; Running, M. P.; Simon, R.; Meyerowitz, E. M.; Fletcher, J. C.; Brand, U., 1999: Signaling of Cell Fate Decisions by CLAVATA3 in Arabidopsis Shoot Meristems. *Science*., **283**, 1911–1914.

Forner, J.; Pfeiffer, A.; Langenecker, T.; Manavella, P., 2015: Germline-Transmitted Genome Editing in Arabidopsis thaliana Using TAL-Effector- Nucleases. *PLOS ONE*., **10**, e0121056.

Franck, C. M.; Westermann, J.; Boisson-Dernier, A., 2018: Plant Malectin-Like Receptor Kinases: From Cell Wall Integrity to Immunity and Beyond. *Annual Review of Plant Biology*., **69**, 301–328.

Gaillochet, C.; Lohmann, J. U., 2015: The never-ending story: from pluripotency to plant developmental plasticity. *Development*., **142**, 2237–2249.

Gaillochet, C.; Stiehl, T.; Wenzl, C.; Ripoll, J. J.; Bailey-Steinitz, L. J.; Li, L.; Pfeiffer, A.; Miotk, A.; Hakenjos, J. P.; Forner, J.; Yanofsky, M. F.; Marciniak-Czochra, A.; Lohmann, J. U., 2017: Control of plant cell fate transitions by transcriptional and hormonal signals. *eLife*., **6**, 1–30.

Gao, X.; Guo, Y., 2012: CLE Peptides in Plants: Proteolytic Processing, Structure-Activity Relationship, and Ligand-Receptor Interaction. *Journal of Integrative Plant Biology*., **54**, 738–745.

Ge, Z.; Bergonci, T.; Zhao, Y., 2017: Arabidopsis pollen tube integrity and sperm release are regulated by RALF-mediated signaling. *Science*., **358**, 1596–1600.

Geisler, M.; Blakeslee, J. J.; Bouchard, R.; Lee, O. R.; Vincenzetti, V.; Bandyopadhyay, A.; Titapiwatanakun, B.; Peer, W. A.; Bailly, A.; Richards, E. L.; Ejendal, K. F. K.; Smith, A. P.; Baroux, C.; Grossniklaus, U.; Müller, A.; Hrycyna, C. A.; Dudler, R.; Murphy, A. S.; Martinoia, E., 2005: Cellular efflux of auxin catalyzed by the Arabidopsis MDR/PGP transporter AtPGP1. *Plant Journal*., **44**, 179–194.

Gille, S.; de Souza, A.; Xiong, G.; Benz, M.; Cheng, K.; Schultink, A.; Reca, I. B.; Pauly, M., 2011: O -Acetylation of Arabidopsis Hemicellulose Xyloglucan Requires AXY4 or AXY4L, Proteins with a TBL and DUF231 Domain . *The Plant Cell*., **23**, 4041–4053.

Goedhart, J.; Von, D.; Joosen, L.; Hink, A.; Weeren, L. Van; Jr, T. W. J. G.; Royant, A., 2012: structure-guided evolution of cyan fluorescent proteins towards a quantum yield of 93%. *Biochemistry*.

Gómez-Gómez, L.; Boller, T., 2000: FLS2: An LRR Receptor-like kinase involved in the perception of the bacterial elicitor flagellin in Arabidopsis. *Molecular Cell*., **5**, 1003–1011.

Gonneau, M.; Desprez, T.; Martin, M.; Doblas, V. G.; Bacete, L.; Miart, F.; Sormani, R.; Hématy, K.; Renou, J.; Landrein, B.; Murphy, E.; Van De Cotte, B.; Vernhettes, S.; De Smet, I.; Höfte, H., 2018: Receptor Kinase THESEUS1 Is a Rapid Alkalinization Factor 34 Receptor in Arabidopsis. *Current Biology*., **28**, 2452–2458.e4.

Gordon, S. P.; Chickarmane, V. S.; Ohno, C.; Meyerowitz, E. M., 2009: Multiple feedback loops through cytokinin signaling control stem cell number within the Arabidopsis shoot meristem. *Proceedings of the National Academy of Sciences*., **106**, 16529–16534.

Gou, J. Y.; Miller, L. M.; Hou, G.; Yu, X. H.; Chen, X. Y.; Liu, C. J., 2012: Acetylesterase-Mediated Deacetylation of Pectin Impairs Cell Elongation, Pollen Germination, and Plant Reproduction. *The Plant Cell*., **24**, 50–65.

Grant, G. T.; Morris, E. R.; Rees, D. A.; Smith, P. J. C.; Thom, D., 1973: Biological interactions between polysaccharides and divalent cations: The egg-box model. *FEBS Letters*., **32**, 195–198.

Gray, W. M.; Kepinski, S.; Rouse, D.; Leyser, O.; Estelle, M., 2001: Auxin regulates SCFTIR1-dependent degradation of AUX/IAA proteins. *Nature*., **414**, 271–276.

Greb, T.; Lohmann, J. U., 2016: Minireview Plant Stem Cells Minireview. *Current Biology*., **26**, R816–R821.

Grebe, M., 2011: Unveiling the Casparian strip. *Nature*., **473**, 294–295.

Greenham, D., 2010: Nature. In: Mott, W. (ed.), *Ralph Waldo Emerson in Context*. Cambridge University Press, Cambridge, Vol. 465pp. 84–91.

Gregory, E. F.; Dao, T. Q.; Alexander, M. A.; Miller, M. J.; Fletcher, J. C., 2018: The signaling peptide-encoding genes CLE16, CLE17 and CLE27 are dispensable for Arabidopsis shoot apical meristem

activity. *PLoS ONE*., **13**, 1–16.

Gruel, J.; Landrein, B.; Tarr, P.; Schuster, C.; Refahi, Y.; Sampathkumar, A.; Hamant, O.; Meyerowitz, E. M.; Jönsson, H., 2016: An epidermis-driven mechanism positions and scales stem cell niches in plants, 22–24.

Gu, Y.; Kaplinsky, N.; Bringmann, M.; Cobb, A.; Carroll, A.; Sampathkumar, A.; Baskin, T. I.; Persson, S.; Somerville, C. R., 2010: Identification of a cellulose synthase-associated protein required for cellulose biosynthesis. *Proceedings of the National Academy of Sciences*., **107**, 12866–12871.

Guo, H.; Li, L.; Ye, H.; Yu, X.; Algreen, A.; Yin, Y., 2009a: Three related receptor-like kinases are required for optimal cell elongation in Arabidopsis thaliana. *Proceedings of the National Academy of Sciences*., **106**, 7648–7653.

Guo, H.; Ye, H.; Li, L.; Yin, Y., 2009b: BES1 and involved in plant growth in Arabidopsis A family of receptor-like kinases are regulated by BES1 and involved in plant growth in Arabidopsis thaliana. *Plant signaling & behavior*., **4**, 784–786.

Gust, A. A.; Felix, G., 2014: Receptor like proteins associate with SOBIR1-type of adaptors to form bimolecular receptor kinases. *Current Opinion in Plant Biology*., **21**, 104–111.

Gutierrez, C., 2009: The Arabidopsis Cell Division Cycle. *The arabidopsis Book*., **7**, 1–19.

Gutierrez, R.; Lindeboom, J. J.; Paredez, A. R.; Emons, A. M. C.; Ehrhardt, D. W., 2009: Arabidopsis cortical microtubules position cellulose synthase delivery to the plasma membrane and interact with cellulose synthase trafficking compartments. *Nature Cell Biology*., **11**, 797–806.

Hamel, L. P.; Nicole, M. C.; Duplessis, S.; Ellis, B. E., 2012: Mitogen-Activated Protein Kinase Signaling in Plant-Interacting Fungi: Distinct Messages from Conserved Messengers. *The Plant Cell*., **24**, 1327–1351.

Hardtke, C. S., 1998: The Arabidopsis gene MONOPTEROS encodes a transcription factor mediating embryo axis formation and vascular development. *The EMBO Journal*., **17**, 1405–1411.

Hardtke, C. S.; Berleth, T., 1998: The Arabidopsis gene MONOPTEROS encodes a transcription factor mediating embryo axis formation and vascular development. *EMBO Journal*., **17**, 1405–1411.

Haruta, M.; Sabat, G.; Stecker, K.; Minkoff, B. B.; Sussman, M. R., 2014a: A Peptide Hormone and Its Receptor Protein Kinase Regulate Plant Cell Expansion. *Science*., **343**, 408–411.

Haruta, M.; Sabat, G.; Stecker, K.; Minkoff, B. B.; Sussman, M. R., 2014b: A Peptide Hormone and Its Receptor, **408**.

Haruta, M.; Gray, W. M.; Sussman, M. R., 2015: Regulation of the plasma membrane proton pump (H(+)-ATPase) by phosphorylation. *Curr Opin Plant Biol.*, **28**, 68–75.

Hazak, O.; Brandt, B.; Cattaneo, P.; Santiago, J.; Rodriguez-Villalon, A.; Hothorn, M.; Hardtke, C. S., 2017: Perception of root-active CLE peptides requires CORYNE function in the phloem vasculature. *EMBO reports*., **18**, 1367–1381.

He, Y.; Zhou, J.; Shan, L.; Meng, X., 2018: Plant cell surface receptor-mediated signaling – a common theme amid diversity. *Journal of Cell Science*., **131**, jcs209353.

Heim, D. R.; Skomp, J. R.; Tschabold, E. E.; Larrinua, I. M., 1990: Isoxaben Inhibits the Synthesis of Acid Insoluble Cell Wall Materials In Arabidopsis thaliana. *PLANT PHYSIOLOGY*., **93**, 695–700.

Heisler, M. G.; Ohno, C.; Das, P.; Sieber, P.; Reddy, G. V; Long, J. A.; Meyerowitz, E. M., 2005: Patterns of Auxin Transport and Gene Expression during Primordium Development Revealed by Live Imaging of the Arabidopsis Inflorescence Meristem, **15**, 1899–1911.

Hejatko, J.; Ryu, H.; Kim, G. T.; Dobesova, R.; Choi, S.; Choi, S. M.; Soucek, P.; Horak, J.; Pekarova, B.; Palme, K.; Brzobohaty, B.; Hwang, I., 2009: The Histidine Kinases CYTOKININ-INDEPENDENT1 and ARABIDOPSIS HISTIDINE KINASE2 and 3 Regulate Vascular Tissue Development in Arabidopsis Shoots. *THE PLANT CELL ONLINE*., **21**, 2008–2021.

Hématy, K.; Sado, P. etienne; Van Tuinen, A.; Rochange, S.; Desnos, T.; Balzergue, S.; Pelletier, S.; Renou, J. pierre; Höfte, H., 2007: A Receptor-like Kinase Mediates the Response of Arabidopsis Cells to the Inhibition of Cellulose Synthesis. *Current Biology*., **17**, 922–931.

Hirakawa, Y.; Shinohara, H.; Kondo, Y.; Inoue, A.; Nakanomyo, I.; Ogawa, M.; Sawa, S.; Ohashi-ito, K.; Matsubayashi, Y.; Fukuda, H., 2008: Non-cell-autonomous control of vascular stem cell fate by a CLE system_PNAS_Hirakawa, Fukuda.pdf, **105**.

Hobe, M.; Müller, R.; Grünewald, M.; Brand, U.; Simon, R., 2003: Loss of CLE40, a protein functionally equivalent to the stem cell restricting signal CLV3, enhances root waving in Arabidopsis.

Development Genes and Evolution., **213**, 371–381.

Hocq, L.; Pelloux, J.; Lefebvre, V., 2017a: Connecting Homogalacturonan-Type Pectin Remodeling to Acid Growth. *Trends in Plant Science*., **22**, 20–29.

Hocq, L.; Pelloux, J.; Lefebvre, V., 2017b: Connecting Pectin Remodeling to Acid Growth. *Trends in Plant Science*., **22**, 20–29.

Hok, S.; Danchin, E. G. J.; Allasia, V.; Panabières, F.; Attard, A.; Keller, H., 2011: An Arabidopsis (malectin-like) leucine-rich repeat receptor-like kinase contributes to downy mildew disease. *Plant, Cell and Environment*., **34**, 1944–1957.

Hok, S.; Allasia, V.; Andrio, E.; Naessens, E.; Ribes, E.; Panabieres, F.; Attard, A.; Ris, N.; Clement, M.; Barlet, X.; Marco, Y.; Grill, E.; Eichmann, R.; Weis, C.; Huckelhoven, R.; Ammon, A.; Ludwig-Muller, J.; Voll, L. M.; Keller, H., 2014: The Receptor Kinase IMPAIRED OOMYCETE SUSCEPTIBILITY1 Attenuates Abscisic Acid Responses in Arabidopsis. *PLANT PHYSIOLOGY*., **166**, 1506–1518.

Holzwart, E.; Huerta, A. I.; Glöckner, N.; Garnelo Gómez, B.; Wanke, F.; Augustin, S.; Askani, J. C.; Schürholz, A. K.; Harter, K.; Wolf, S., 2018: BRI1 controls vascular cell fate in the Arabidopsis root through RLP44 and phytosulfokine signaling. *Proceedings of the National Academy of Sciences*., **115**, 11838–11843.

Hwang, I.; Sheen, J., 2001: Two-component circuitry in Arabidopsis cytokinin signal transduction. *Nature*., **413**, 383–389.

Igarashi, D.; Tsuda, K.; Katagiri, F., 2012: The peptide growth factor, phytosulfokine, attenuates pattern-triggered immunity. *Plant Journal*., **71**, 194–204.

Ito, Y.; Nakanomyo, I.; Hiroyasu, M.; Iwamoto, K.; Sawa, S.; Dohmae, N.; Fukuda, H., 2006: Dodeca-CLE Peptides as Suppressors. *Science*., **313**, 842–845.

James, G. V.; Patel, V.; Nordström, K. J. V.; Klasen, J. R.; Salomé, P. A.; Weigel, D.; Schneeberger, K., 2013: User guide for mapping-by-sequencing in Arabidopsis. *Genome Biology*., **14**, R61.

Janocha, D.; Lohmann, J. U., 2018: From signals to stem cells and back again. *Current Opinion in Plant Biology*., **45**, 136–142.

Je, B. Il; Gruel, J.; Lee, Y. K.; Bommert, P.; Arevalo, E. D.; Eveland, A. L.; Wu, Q.; Goldshmidt, A.; Meeley, R.; Bartlett, M.; Komatsu, M.; Sakai, H.; Jönsson, H.; Jackson, D., 2016: Signaling from maize organ primordia via FASCIATED EAR3 regulates stem cell proliferation and yield traits.

Jeong, S.; Trotochaud, A. E.; Clark, S. E., 1999: The Arabidopsis CLAVATA2 Gene Encodes a Receptor-Like Protein Required for the Stability of the CLAVATA1 Receptor-Like Kinase. *The Plant Cell*., **11**, 1925.

Jiang, L.; Yang, S. L.; Xie, L. F.; Puah, C. S.; Zhang, X. Q.; Yang, W. C.; Sundaresan, V.; Ye, D., 2005: VANGUARD1 Encodes a Pectin Methylesterase That Enhances Pollen Tube Growth in the Arabidopsis Style and Transmitting Tract. *THE PLANT CELL ONLINE*., **17**, 584–596.

Jin, H.; Song, Z.; Nikolau, B. J., 2012: Reverse genetic characterization of two paralogous acetoacetyl CoA thiolase genes in Arabidopsis reveals their importance in plant growth and development. *Plant Journal*., **70**, 1015–1032.

Jinek, M.; Chylinski, K.; Fonfara, I.; Hauer, M.; Doudna, J. A.; Charpentier, E., 2012: A Programmable Dual-RNA-Guided DNA Endonuclease in Adaptive Bacterial Immunity. *Science*., **337**, 816–821.

Jones, A. R.; Forero-Vargas, M.; Withers, S. P.; Smith, R. S.; Traas, J.; Dewitte, W.; Murray, J. A. H., 2017: Cell-size dependent progression of the cell cycle creates homeostasis and flexibility of plant cell size. *Nature Communications*., **8**, 1–13.

Jun, J.; Fiume, E.; Roeder, A. H. K.; Meng, L.; Sharma, V. K.; Osmont, K. S.; Baker, C.; Ha, C. M.; Meyerowitz, E. M.; Feldman, L. J.; Fletcher, J. C., 2010: Comprehensive Analysis of CLE Polypeptide Signaling Gene Expression and Overexpression Activity in Arabidopsis. *PLANT PHYSIOLOGY*., **154**, 1721–1736.

Jun, J. H.; Fiume, E.; Fletcher, J. C., 2008: The CLE family of plant polypeptide signaling molecules. *Cellular and Molecular Life Sciences*., **65**, 743–755.

Keinath, N. F.; Kierszniowska, S.; Lorek, J.; Bourdais, G.; Kessler, S. A.; Shimosato-Asano, H.; Grossniklaus, U.; Schulze, W. X.; Robatzek, S.; Panstruga, R., 2010: PAMP (Pathogen-associated Molecular Pattern)-induced Changes in Plasma Membrane Compartmentalization Reveal Novel Components of Plant Immunity. *Journal of Biological Chemistry*., **285**, 39140–39149.

Kieber, J. J.; Schaller, G. E., 2014: Cytokinins. *Hormone Metabolism and Signaling in Plants*. Elsevier,

pp. 77–106.

Kieber, J. J.; Schaller, G. E., 2018: Cytokinin signaling in plant development. *Development*., **145**, dev149344.

Kierzkowski, D.; Routier-Kierzkowska, A. L., 2019: Cellular basis of growth in plants: geometry matters. *Current Opinion in Plant Biology*., **47**, 56–63.

Kimura, Y.; Tasaka, M.; Torii, K. U.; Uchida, N., 2018: ERECTA-family genes coordinate stem cell functions between the epidermal and internal layers of the shoot apical meristem. *Development*., **145**, dev156380.

Kirchhelle, C.; Chow, C. M.; Foucart, C.; Neto, H.; Stierhof, Y. D.; Kalde, M.; Walton, C.; Fricker, M.; Smith, R. S.; Jérusalem, A.; Irani, N.; Moore, I., 2016a: The Specification of Geometric Edges by a Plant Rab GTPase Is an Essential Cell-Patterning Principle During Organogenesis in Arabidopsis. *Developmental Cell*., **36**, 386–400.

Kirchhelle, C.; Moore, I.; Smith, R. S.; Chow, C. M.; Irani, N.; Fricker, M.; Kalde, M.; Neto, H.; Foucart, C.; Stierhof, Y. D.; Jérusalem, A.; Walton, C., 2016b: The Specification of Geometric Edges by a Plant Rab GTPase Is an Essential Cell-Patterning Principle During Organogenesis in Arabidopsis. *Developmental Cell*., **36**, 386–400.

Klis, F. M.; Boorsma, A.; De Groot, P. W. J., 2006: Cell wall construction in Saccharomyces cerevisiae. *Yeast*., **23**, 185–202.

Ko, D.; Kang, J.; Kiba, T.; Park, J.; Kojima, M.; Do, J.; Kim, K. Y.; Kwon, M.; Endler, A.; Song, W. Y.; Martinoia, E.; Sakakibara, H.; Lee, Y., 2014: Arabidopsis ABCG14 is essential for the root-to-shoot translocation of cytokinin. *Proceedings of the National Academy of Sciences*., **111**, 7150–7155.

Kohorn, B. D.; Kohorn, S. L., 2012: The cell wall-associated kinases, WAKs, as pectin receptors. *Frontiers in Plant Science*., **3**, 1–5.

Kondo, Y.; Hirakawa, Y.; Kieber, J. J.; Fukuda, H., 2011: CLE peptides can negatively regulate protoxylem vessel formation via cytokinin signaling. *Plant and Cell Physiology*., **52**, 37–48.

Kosuta, S.; Held, M.; Hossain, M. S.; Morieri, G.; MacGillivary, A.; Johansen, C.; Antolín-Llovera, M.; Parniske, M.; Oldroyd, G. E. D.; Downie, A. J.; Karas, B.; Szczyglowski, K., 2011: Lotus japonicus symRK-14 uncouples the cortical and epidermal symbiotic program. *Plant Journal*., **67**, 929–940.

Kubicek, C. P.; Starr, T. L.; Glass, N. L., 2014: Plant Cell Wall–Degrading Enzymes and Their Secretion in Plant-Pathogenic Fungi. *Annual Review of Phytopathology*., **52**, 427–451.

Kubo, M.; Udagawa, M.; Nishikubo, N.; Horiguchi, G.; Yamaguchi, M.; Ito, J.; Mimura, T.; Fukuda, H.; Demura, T., 2005: Transcription switches for protoxylem and metaxylem vessel formation. *Genes & Development*., **19**, 1855–1860.

Kumar, M.; Campbell, L.; Turner, S., 2016: Secondary cell walls: Biosynthesis and manipulation. *Journal of Experimental Botany*., **67**, 515–531.

Kuroha, T.; Tokunaga, H.; Kojima, M.; Ueda, N.; Ishida, T.; Nagawa, S.; Fukuda, H.; Sugimoto, K.; Sakakibara, H., 2009: Functional Analyses of LONELY GUY Cytokinin-Activating Enzymes Reveal the Importance of the Direct Activation Pathway in Arabidopsis. *The Plant Cell*., **21**, 3152–3169.

Lampropoulos, A.; Sutikovic, Z.; Wenzl, C.; Maegele, I.; Lohmann, J. U.; Forner, J., 2013: GreenGate - A Novel, Versatile, and Efficient Cloning System for Plant Transgenesis. (Janssen, P. J., Ed.)*PLoS ONE*., **8**, e83043.

Landau, U.; Asis, L.; Eshed Williams, L., 2015: The ERECTA, CLAVATA and class III HD-ZIP pathways display synergistic interactions in regulating floral meristem activities. *PLoS ONE*., **10**, 1–11.

Landrein, B.; Kiss, A.; Sassi, M.; Chauvet, A.; Das, P.; Cortizo, M.; Laufs, P.; Takeda, S.; Aida, M.; Traas, J.; Vernoux, T.; Boudaoud, A.; Hamant, O., 2015a: Mechanical stress contributes to the expression of the STM homeobox gene in Arabidopsis shoot meristems. *eLife*., **4**, 1–27.

Landrein, B.; Refahi, Y.; Besnard, F.; Hervieux, N.; Mirabet, V.; Boudaoud, A.; Vernoux, T.; Hamant, O., 2015b: Meristem size contributes to the robustness of phyllotaxis in Arabidopsis. *Journal of Experimental Botany*., **66**, 1317–1324.

Landrein, B.; Formosa-Jordan, P.; Malivert, A.; Schuster, C.; Melnyk, C. W.; Yang, W.; Turnbull, C.; Meyerowitz, E. M.; Locke, J. C. W.; Jönsson, H., 2018: Nitrate modulates stem cell dynamics in Arabidopsis shoot meristems through cytokinins. *Proceedings of the National Academy of Sciences*., **115**, 1382–1387.

Laufs, P.; Grandjean, O.; Jonak, C.; Kieu, K.; Traas, J., 1998: Cellular Parameters of the Shoot Apical

Meristem in Arabidopsis. *The Plant Cell*., **10**, 1375.

Laux, T.; Mayer, K. F.; Berger, J.; Jürgens, G., 1996a: The WUSCHEL gene is required for shoot and floral meristem integrity in Arabidopsis. *Development (Cambridge, England)*., **122**, 87–96.

Laux, T.; Mayer, K.; Berger, J.; Jurgens, G., 1996b: The WUSCHEL gene is required for shoot and floral meristem integrity in Arabidopsis. *Development*., **122**, 87–96.

Leibfried, A.; To, J. P. C.; Busch, W.; Stehling, S.; Kehle, A.; Demar, M.; Kieber, J. J.; Lohmann, J. U., 2005: WUSCHEL controls meristem function by direct regulation of cytokinin-inducible response regulators. *Nature*., **438**, 1172–1175.

Lenhard, M.; Bohnert, A.; Ju, G.; Laux, T.; Morgenstelle, A. Der; Tu, D., 2001: Termination of Stem Cell Maintenance.pdf, **105**, 805–814.

Leyser, O., 2018: Auxin Signaling. *Plant physiology*., **176**, 465–479.

Li, C.; Wu, H.; Cheung, A. Y., 2016a: Update on Receptor-Like Kinases FERONIA and Her Pals : Functions and Mechanisms 1 [OPEN], **171**, 2379–2392.

Li, J.; Chory, J., 1997: A Putative Leucine-Rich Repeat Receptor Kinase Involved in Brassinosteroid Signal Transduction. *Cell*., **90**, 929–938.

Li, J.; Wen, J.; Lease, K. A.; Doke, J. T.; Tax, F. E.; Walker, J. C., 2002: BAK1 , an Arabidopsis LRR Receptor-like Protein Kinase , Interacts with BRI1 and Modulates Brassinosteroid Signaling, **110**, 213–222.

Li, S.; Bashline, L.; Lei, L.; Gu, Y., 2014: Cellulose Synthesis and Its Regulation. *The Arabidopsis Book / American Society of Plant Biologists*., **12**, e0169.

Li, S. B.; Xie, Z. Z.; Hu, C. G.; Zhang, J. Z., 2016b: A Review of Auxin Response Factors (ARFs) in Plants. *Frontiers in Plant Science*., **7**, 1–7.

Lian, G.; Ding, Z.; Wang, Q.; Zhang, D.; Xu, J., 2014: Origins and Evolution of WUSCHEL-Related Homeobox Protein Family in Plant Kingdom. *The Scientific World Journal*., **2014**, 1–12.

Liao, C. yang; Smet, W.; Brunoud, G.; Yoshida, S.; Vernoux, T.; Weijers, D., 2015: Reporters for sensitive and quantitative measurement of auxin response, **12**.

Liao, H.; Tang, R.; Zhang, X.; Luan, S.; Yu, F., 2017: FERONIA Receptor Kinase at the Crossroads of Hormone Signaling and Stress Responses. *Plant and Cell Physiology*., **58**, 1143–1150.

Lidell, M. E.; Hansson, G. C., 2006: Cleavage in the GDPH sequence of the C-terminal cysteine-rich part of the human MUC5AC mucin. *Biochemical Journal*., **399**, 121–129.

Lin, G.; Zhang, L.; Han, Z.; Yang, X.; Liu, W.; Li, E.; Chang, J.; Qi, Y.; Shpak, E. D.; Chai, J., 2017: A receptor-like protein acts as a specificity switch for the regulation of stomatal development. *Genes and Development*., **31**, 927–938.

Lin, W.; Tang, W.; Anderson, C. T.; Yang, Z., 2018: FERONIA's sensing of cell wall pectin activates ROP GTPase signaling in Arabidopsis. *BioRchiv*., 269647.

Lipka, E.; Herrmann, A.; Mueller, S., 2015: Mechanisms of plant cell division. *Wiley Interdisciplinary Reviews: Developmental Biology*., **4**, 391–405.

Liu, J.; Moore, S.; Chen, C.; Lindsey, K., 2017: Crosstalk Complexities between Auxin, Cytokinin, and Ethylene in Arabidopsis Root Development: From Experiments to Systems Modeling, and Back Again. *Molecular Plant*., **10**, 1480–1496.

Liu, X.; Kim, Y. J.; Muller, R.; Yumul, R. E.; Liu, C.; Pan, Y.; Cao, X.; Goodrich, J.; Chen, X., 2011: AGAMOUS Terminates Floral Stem Cell Maintenance in Arabidopsis by Directly Repressing WUSCHEL through Recruitment of Polycomb Group Proteins. *The Plant Cell*., **23**, 3654–3670.

Liu, Y.; You, S.; Taylor-Teeples, M.; Li, W. L.; Schuetz, M.; Brady, S. M.; Douglas, C. J., 2014: BEL1-LIKE HOMEODOMAIN6 and KNOTTED ARABIDOPSIS THALIANA7 Interact and Regulate Secondary Cell Wall Formation via Repression of REVOLUTA . *The Plant Cell Online*., **26**, 4843–4861.

Lohmann, J. U.; Hong, R. L.; Hobe, M.; Busch, M. A.; Parcy, F.; Simon, R.; Weigel, D., 2001: A Molecular Link between Stem Cell Regulation and Floral Patterning in Arabidopsis. *Cell*., **105**, 793–803.

Louveaux, M.; Julien, J. daniel; Mirabet, V.; Boudaoud, A.; Hamant, O., 2016: Cell division plane orientation based on tensile stress in Arabidopsis thaliana.

Lugassi, N.; Nakayama, N.; Bochnik, R.; Zik, M., 2010: A novel allele of FILAMENTOUS FLOWER reveals new insights on the link between inflorescence and floral meristem organization and flower

morphogenesis. *BMC Plant Biology*., **10**, 131.

Ma, Y.; Miotk, A.; Sutikovic, Z.; Medzihradszky, A.; Wenzl, C.; Ermakova, O.; Gaillochet, C.; Forner, J.; Utan, G.; Brackmann, K.; Galvan-Ampudia, C. S.; Vernoux, T.; Greb, T.; Lohmann, J. U., 2018: WUSCHEL acts as a rheostat on the auxin pathway to maintain apical stem cells in Arabidopsis. *bioRxiv*., 468421.

Mähönen, A. P.; Bonke, M.; Kauppinen, L.; Riikonen, M.; Benfey, P. N.; Helariutta, Y., 2000: A novel two-component hybrid molecule regulates vascular morphogenesis of the Arabidopsis root. *Genes and Development*., **14**, 2938–2943.

Mähönen, A. P.; Bishopp, A.; Higuchi, M.; Nieminen, K. M.; Kinoshita, K.; Törmäkangas, K.; Ikeda, Y.; Oka, A.; Kakimoto, T.; Helariutta, Y., 2006a: Cytokinin signaling and its inhibitor AHP6 regulate cell fate during vascular development. *Science*., **311**, 94–98.

Mähönen, A. P.; Higuchi, M.; Törmäkangas, K.; Miyawaki, K.; Pischke, M. S.; Sussman, M. R.; Helariutta, Y.; Kakimoto, T., 2006b: Cytokinins Regulate a Bidirectional Phosphorelay Network in Arabidopsis. *Current Biology*., **16**, 1116–1122.

Manavella, P. A.; Weigel, D.; Wu, L., 2011: Argonaute10 as a miRNA locker. *Cell*., **145**, 173–174.

Martinière, A.; Gayral, P.; Hawes, C.; Runions, J., 2011: Building bridges: Formin1 of Arabidopsis forms a connection between the cell wall and the actin cytoskeleton. *Plant Journal*., **66**, 354–365.

Mayer, K. F.; Schoof, H.; Haecker, A.; Lenhard, M.; Jürgens, G.; Laux, T., 1998: Developments in automated reflectance microscopy of coal. *Cell Press*., **95**, 3–12.

Mcfarlane, H. E.; Anett, D., 2014: The Cell Biology of Cellulose Synthesis.

Milani, P.; Gholamirad, M.; Traas, J.; Arnéodo, A.; Boudaoud, A.; Argoul, F.; Hamant, O., 2011: In vivo analysis of local wall stiffness at the shoot apical meristem in Arabidopsis using atomic force microscopy. *Plant Journal*., **67**, 1116–1123.

Miotk, A., 2015: Das WUSCHEL abhängige transkriptionelle Netzwerk und der molekulare Regulationsmechanismus in der pflanzlichen Stammzellkontrolle. PhD Thesis

Mirabet, V.; Das, P.; Boudaoud, A.; Hamant, O., 2011: The Role of Mechanical Forces in Plant Morphogenesis. *Annual Review of Plant Biology*., **62**, 365–385.

Mirabet, V.; Besnard, F.; Vernoux, T.; Boudaoud, A., 2012: Noise and Robustness in Phyllotaxis, **8**.

Miyawaki, K.; Tarkowski, P.; Matsumoto-Kitano, M.; Kato, T.; Sato, S.; Tarkowska, D.; Tabata, S.; Sandberg, G.; Kakimoto, T., 2006: Roles of Arabidopsis ATP/ADP isopentenyltransferases and tRNA isopentenyltransferases in cytokinin biosynthesis. *Proceedings of the National Academy of Sciences*., **103**, 16598–16603.

Miyazaki, S.; Murata, T.; Sakurai-Ozato, N.; Kubo, M.; Demura, T.; Fukuda, H.; Hasebe, M., 2009: ANXUR1 and 2, Sister Genes to FERONIA/SIRENE, Are Male Factors for Coordinated Fertilization. *Current Biology*., **19**, 1327–1331.

Moussu, S.; Augustin, S.; Roman, A. O.; Broyart, C.; Santiago, J., 2018: Crystal structures of two tandem malectin-like receptor kinases involved in plant reproduction. *Acta Crystallographica Section D Structural Biology*., **74**, 671–680.

Muller, R.; Bleckmann, A.; Simon, R., 2008: The Receptor Kinase CORYNE of Arabidopsis Transmits the Stem Cell-Limiting Signal CLAVATA3 Independently of CLAVATA1. *the Plant Cell Online*., **20**, 934–946.

Nadeau, J. A.; Sack, F. D., 2002: Control of Stomatal Distribution on the Arabidopsis Leaf Surface. *Science*., **296**, 1697–1700.

Nam, K. H.; Li, J., 2002: BRI1/BAK1, a receptor kinase pair mediating brassinosteroid signaling. *Cell*., **110**, 203–212.

Ngo, Q. A.; Vogler, H.; Lituiev, D. S.; Nestorova, A.; Grossniklaus, U., 2014: A calcium dialog mediated by the FERONIA signal transduction pathway controls plant sperm delivery. *Developmental Cell*., **29**, 491–500.

Nimchuk, Z. L.; Zhou, Y.; Tarr, P. T.; Peterson, B. A.; Meyerowitz, E. M., 2015: Plant stem cell maintenance by transcriptional cross-regulation of related receptor kinases. *Development*., **142**, 1043–1049.

Nissen, K. S.; Willats, W. G. T.; Malinovsky, F. G., 2016: Understanding CrRLK1L Function: Cell Walls and Growth Control. *Trends in Plant Science*., **21**, 516–527.

Niu, X.; Bressan, R. A.; Hasegawa, P. M.; Pardo, J. M., 1995: Ion Homeostasis in NaCl Stress

Environments. *Plant physiology*., **109**, 735–742.

O'Neill, M. A.; Ishii, T.; Albersheim, P.; Darvill, A. G., 2004: RHAMNOGALACTURONAN II: Structure and Function of a Borate Cross-Linked Cell Wall Pectic Polysaccharide. *Annual Review of Plant Biology*., **55**, 109–139.

Ogawa, M.; Shinohara, H.; Sakagami, Y.; Matsubayashi, Y., 2008: Arabidopsis CLV3 peptide directly binds CLV1 ectodomain. *Science*., **319**, 294–294.

Ohashi-Ito, K.; Bergmann, D. C., 2007: Regulation of the Arabidopsis root vascular initial population by LONESOME HIGHWAY. *Development*., **134**, 2959–2968.

Ohashi-Ito, K.; Oda, Y.; Fukuda, H., 2010: Arabidopsis VASCULAR-RELATED NAC-DOMAIN6 Directly Regulates the Genes That Govern Programmed Cell Death and Secondary Wall Formation during Xylem Differentiation . *The Plant Cell*., **22**, 3461–3473.

Ohashi-Ito, K.; Matsukawa, M.; Fukuda, H., 2013: An atypical bHLH transcription factor regulates early xylem development downstream of auxin. *Plant and Cell Physiology*., **54**, 398–405.

Ohashi-Ito, K.; Saegusa, M.; Iwamoto, K.; Oda, Y.; Katayama, H.; Kojima, M.; Sakakibara, H.; Fukuda, H., 2014: A bHLH complex activates vascular cell division via cytokinin action in root apical meristem. *Current Biology*., **24**, 2053–2058.

Osička, R.; Procházková, K.; Šulc, M.; Linhartová, I.; Havlíček, V.; Šebo, P., 2004: A novel 'clip-and-link' activity of repeat in toxin (RTX) proteins from gram-negative pathogens: Covalent protein cross-linking by an Asp-Lys isopeptide bond upon calcium-dependent processing at an Asp-Pro bond. *Journal of Biological Chemistry*., **279**, 24944–24956.

Pagnussat, G. C.; Yu, H. J.; Ngo, Q. A.; Rajani, S.; Mayalagu, S., 2005: Genetic and molecular identification of genes required for female gametophyte development and function in Arabidopsis. *Development*., **132**, 603–614.

Park, J.; Lee, Y.; Martinoia, E.; Geisler, M., 2017: Plant hormone transporters: What we know and what we would like to know. *BMC Biology*., **15**, 1–15.

Pattathil, S.; Avci, U.; Baldwin, D.; Swennes, A. G.; McGill, J. A.; Popper, Z.; Bootten, T.; Albert, A.; Davis, R. H.; Chennareddy, C.; Dong, R.; O'Shea, B.; Rossi, R.; Leoff, C.; Freshour, G.; Narra, R.; O'Neil, M.; York, W. S.; Hahn, M. G., 2010: A Comprehensive Toolkit of Plant Cell Wall Glycan-Directed Monoclonal Antibodies. *Plant Physiology*., **153**, 514–525.

Peaucelle, A.; Louvet, R.; Johansen, J. N.; Höfte, H.; Laufs, P.; Pelloux, J.; Mouille, G., 2008: Arabidopsis Phyllotaxis Is Controlled by the Methyl-Esterification Status of Cell-Wall Pectins. *Current Biology*., **18**, 1943–1948.

Peaucelle, A.; Braybrook, S. A.; Guillou, L. Le; Bron, E.; Kuhlemeier, C., 2011: Report Pectin-Induced Changes in Cell Wall Mechanics Underlie Organ Initiation in Arabidopsis, 1720–1726.

Peaucelle, A.; Braybrook, S.; Höfte, H., 2012: Cell wall mechanics and growth control in plants: the role of pectins revisited. *Frontiers in Plant Science*., **3**, 1–6.

Peaucelle, A.; Wightman, R.; Höfte, H., 2015: The Control of Growth Symmetry Breaking in the Arabidopsis Hypocotyl. *Current Biology*., **25**, 1746–1752.

Pelaz, S.; Ditta, G. S.; Baumann, E.; Wisman, E.; Yanofsky, M. F., 2000: B and C floral organ identity functions require SEPALLATA MADS-box genes. *Nature*., **405**, 200–203.

Pelletier, S.; Jaillard, D.; Ho, H., 2004: Interaction between Wall Deposition and Cell Elongation in Dark-Grown Hypocotyl Cells in Arabidopsis 1, **135**, 959–968.

Peret, B.; Swarup, K.; Ferguson, A.; Seth, M.; Yang, Y.; Dhondt, S.; James, N.; Casimiro, I.; Perry, P.; Syed, A.; Yang, H.; Reemmer, J.; Venison, E.; Howells, C.; Perez-Amador, M. A.; Yun, J.; Alonso, J.; Beemster, G. T. S.; Laplaze, L. et al., 2012: AUX/LAX Genes Encode a Family of Auxin Influx Transporters That Perform Distinct Functions during Arabidopsis Development. *The Plant Cell*., **24**, 2874–2885.

Petrasek, J.; Friml, J., 2009: Auxin transport routes in plant development. *Development*., **136**, 2675–2688.

Prigge, M. J.; Otsuga, D.; Alonso, J. M.; Ecker, J. R.; Drews, G. N.; Clark, S. E., 2004: Class III Homeodomain-Leucine Zipper Gene Family Members Have Overlapping, Antagonistic, and Distinct Roles in Arabidopsis Development. *the Plant Cell Online*., **17**, 61–76.

Qi, J.; Wang, Y.; Yu, T.; Cunha, A.; Wu, B.; Vernoux, T.; Meyerowitz, E., 2014: Auxin depletion from leaf primordia contributes to organ patterning, **111**, 18769–18774.

Qi, J.; Wu, B.; Feng, S.; Lü, S.; Guan, C.; Zhang, X.; Qiu, D.; Hu, Y.; Zhou, Y.; Li, C.; Long, M.; Jiao, Y., 2017: Mechanical regulation of organ asymmetry in leaves. *Nature Plants*., **3**, 724–733.

Qian, P.; Song, W.; Yokoo, T.; Minobe, A.; Wang, G.; Ishida, T.; Sawa, S.; Chai, J.; Kakimoto, T., 2018: The CLE9/10 secretory peptide regulates stomatal and vascular development through distinct receptors. *Nature Plants*., **4**, 1071–1081.

Ramachandran, P.; Carlsbecker, A.; Etchells, J. P.; Turner, S., 2016: Class III HD-ZIPs govern vascular cell fate: An HD view on patterning and differentiation. *Journal of Experimental Botany*., **68**, 55–69.

Rasmussen, C. G.; Wright, A. J.; Müller, S., 2013: The role of the cytoskeleton and associated proteins in determination of the plant cell division plane. *Plant Journal*., **75**, 258–269.

Rayle, D. L.; Cleland, R., 1970: Enhancement of wall loosening and elongation by Acid solutions. *Plant physiology*., **46**, 250–253.

Rayle, D. L., 1973: Auxin-induced hydrogen-ion secretion in Avena coleoptiles and its implications. *Planta*., **114**, 63–73.

Reinhardt, D.; Frenz, M.; Mandel, T.; Kuhlemeier, C., 2003a: Microsurgical and laser ablation analysis of interactions between the zones and layers of the tomato shoot apical meristem. *Development*., **130**, 4073–4083.

Reinhardt, D.; Pesce, E. R.; Stieger, P.; Mandel, T.; Baltensperger, K.; Bennett, M.; Traas, J.; Friml, J.; Kuhlemeier, C., 2003b: Regulation of phyllotaxis by polar auxin transport. *Nature*., **426**, 255–260.

Riefler, M.; Novak, O.; Strnad, M.; Schmülling, T., 2006: Arabidopsis Cytokinin Receptor Mutants Reveal Functions in Shoot Growth, Leaf Senescence, Seed Size, Germination,Root Development, and Cytokinin Metabolism. *Plant Cell*., **18**, 40–54.

Robatzek, S.; Somssich, I. E., 2002: Targets of AtWRKY6 regulation during plant senescence and pathogen defense. *Genes & development*., **16**, 1139–1149.

Rodriguez-Villalon, A.; Gujas, B.; Kang, Y. H.; Breda, A. S.; Cattaneo, P.; Depuydt, S.; Hardtke, C. S., 2014: Molecular genetic framework for protophloem formation. *Proceedings of the National Academy of Sciences*., **111**, 11551–11556.

Rojo, E.; Sharma, V. K.; Kovaleva, V.; Raikhel, N. V.; Fletcher, J. C., 2002: CLV3 Is Localized to the Extracellular Space, Where It Activates the Arabidopsis CLAVATA Stem Cell Signaling Pathway. *THE PLANT CELL ONLINE*., **14**, 969–977.

Sarkar, A. K.; Luijten, M.; Miyashima, S.; Lenhard, M.; Hashimoto, T.; Nakajima, K.; Scheres, B.; Heidstra, R.; Laux, T., 2007: Conserved factors regulate signalling in Arabidopsis thaliana shoot and root stem cell organizers. *Nature*., **446**, 811–814.

Sassi, M.; Ali, O.; Cloarec, G.; Abad, U.; Cellier, C.; Chen, X.; Gilles, B.; Milani, P., 2014: Report An Auxin-Mediated Shift toward Growth Isotropy Promotes Organ Formation at the Shoot Meristem in Arabidopsis, 2335–2342.

Sauter, M., 2015: Phytosulfokine peptide signalling. *Journal of Experimental Botany*., **66**, 5161–5169.

Savatin, D. V.; Gramegna, G.; Modesti, V.; Cervone, F., 2014: Wounding in the plant tissue: the defense of a dangerous passage. *Frontiers in Plant Science*., **5**, 1–11.

Sawa, S.; Watanabe, K.; Goto, K.; Liu, Y. G.; Shibata, D.; Kanaya, E.; Morita, E. H.; Okada, K., 1999: FILAMENTOUS FLOWER, a meristem and organ identity gene of Arabidopsis, encodes a protein with a zinc finger and HMG-related domains [published erratum appears in Genes Dev 1999 Sep 1;13(17):2337]. *Genes Dev*., **13**, 1079–1088.

Schaller, G. E.; Bishopp, A.; Kieber, J. J., 2015: The Yin-Yang of Hormones: Cytokinin and Auxin Interactions in Plant Development. *The Plant Cell Online*., **27**, 44–63.

Schallus, T.; Jaeckh, C.; Fehér, K.; Palma, A. S.; Liu, Y.; Simpson, J. C.; Mackeen, M.; Stier, G.; Gibson, T. J.; Feizi, T.; Pieler, T.; Muhle-Goll, C., 2008: Malectin: a novel carbohydrate-binding protein of the endoplasmic reticulum and a candidate player in the early steps of protein N-glycosylation. *Molecular biology of the cell*., **19**, 3404–3414.

Schallus, T.; Fehér, K.; Sternberg, U.; Rybin, V.; Muhle-Goll, C., 2010: Analysis of the specific interactions between the lectin domain of malectin and diglucosides. *Glycobiology*., **20**, 1010–1020.

Scheible, W. R.; Eshed, R.; Richmond, T.; Delmer, D.; Somerville, C., 2001: Modifications of cellulose synthase confer resistance to isoxaben and thiazolidinone herbicides in Arabidopsis Ixr1 mutants . *Proceedings of the National Academy of Sciences* ., **98**, 10079–10084.

Scheller, H. V.; Ulvskov, P., 2010: Hemicelluloses. *Annual Review of Plant Biology*., **61**, 263–289.

Scheres, B.; Di Laurenzio, L.; Willemsen, V.; Hauser, M. T.; Janmaat, K.; Weisbeek, P.; Benfey, P. N., 1995: Mutations affecting the radial organisation of the Arabidopsis root display specific defects throughout the embryonic axis. *Development*., **121**, 53–62.

Scheres, B., 2007: Stem-cell niches: Nursery rhymes across kingdoms. *Nature Reviews Molecular Cell Biology*., **8**, 345–354.

Schoof, H.; Lenhard, M.; Haecker, A.; Mayer, K. F. .; Jürgens, G.; Laux, T., 2000: The Stem Cell Population of Arabidopsis Shoot Meristems Is Maintained by a Regulatory Loop between the CLAVATA and WUSCHEL Genes. *Cell*., **100**, 635–644.

Schuetz, M.; Smith, R.; Ellis, B., 2013a: Xylem tissue specification, patterning, and differentiation mechanisms. *Journal of Experimental Botany*., **64**, 11–31.

Schuetz, M.; Smith, R.; Ellis, B.; Bitonti, M. B.; Smith, M., 2013b: Xylem tissue oceanica specification , patterning , and differentiation In Posidonia cadmium induces changes in DNA mechanisms and chromatin patterning methylation, **64**, 11–31.

Schulz, P.; Herde, M.; Romeis, T., 2013: Calcium-Dependent Protein Kinases: Hubs in Plant Stress Signaling and Development. *Plant Physiology*., **163**, 523–530.

Schulze-Muth, P.; Irmler, S.; Schröder, G.; Schröder, J., 1996: Novel Type of Receptor-like Protein Kinase from a Higher Plant (Catharanthus roseus). *Journal of Biological Chemistry*., **271**, 26684–26689.

Schürholz, A. K.; López-Salmerón, V.; Li, Z.; Forner, J.; Wenzl, C.; Gaillochet, C.; Augustin, S.; Barro, A. V.; Fuchs, M.; Gebert, M.; Lohmann, J. U.; Greb, T.; Wolf, S., 2018: A Comprehensive Toolkit for Inducible, Cell Type-Specific Gene Expression in Arabidopsis. *Plant Physiology*., **178**, 40–53.

Sénéchal, F.; Wattier, C.; Rustérucci, C.; Pelloux, J., 2014a: Homogalacturonan-modifying enzymes: Structure, expression, and roles in plants. *Journal of Experimental Botany*., **65**, 5125–5160.

Sénéchal, F.; Graff, L.; Surcouf, O.; Marcelo, P.; Rayon, C.; Bouton, S.; Mareck, A.; Mouille, G.; Stintzi, A.; Höfte, H.; Lerouge, P.; Schaller, A.; Pelloux, J., 2014b: Arabidopsis PECTIN METHYLESTERASE17 is co-expressed with and processed by SBT3.5, a subtilisin-like serine protease. *Annals of Botany*., **114**, 1161–1175.

Shih, H. wei; Miller, N. D.; Dai, C.; Spalding, E. P.; Monshausen, G. B., 2014: Report The Receptor-like Kinase FERONIA Is Required for Mechanical Signal Transduction in Arabidopsis Seedlings. *Current Biology*., **24**, 1887–1892.

Shinohara, H.; Matsubayashi, Y., 2015: Reevaluation of the CLV3-receptor interaction in the shoot apical meristem: Dissection of the CLV3 signaling pathway from a direct ligand-binding point of view. *Plant Journal*., **82**, 328–336.

Shiu, S. H.; Bleecker, A. B., 2002: Receptor-like kinases from Arabidopsis form a monophyletic gene family related to animal receptor kinases. *Proceedings of the National Academy of Sciences*., **98**, 10763–10768.

Singh, S. K.; Fischer, U.; Singh, M.; Grebe, M.; Marchant, A., 2008: Insight into the early steps of root hair formation revealed by the procuste1 cellulose synthase mutant of Arabidopsis thaliana. *BMC Plant Biology*., **8**, 1–12.

Smakowska-Luzan, E.; Mott, G. A.; Parys, K.; Stegmann, M.; Howton, T. C.; Layeghifard, M.; Neuhold, J.; Lehner, A.; Kong, J.; Grünwald, K.; Weinberger, N.; Satbhai, S. B.; Mayer, D.; Busch, W.; Madalinski, M.; Stolt-Bergner, P.; Provart, N. J.; Mukhtar, M. S.; Zipfel, C. et al., 2018: An extracellular network of Arabidopsis leucine-rich repeat receptor kinases. *Nature*., **553**, 342–346.

Smith, L. G., 2001: Plant cell division: Building walls in the right places. *Nature Reviews Molecular Cell Biology*., **2**, 33–39.

Smyth, D. R.; Bowman, J. L.; Meyerowitz, E. M., 1990: Early Flower Development in Arabidopsis. *The Plant Cell*., **2**, 755.

Somssich, M.; Khan, G. A.; Persson, S., 2016: Cell Wall Heterogeneity in Root Development of Arabidopsis, **7**, 1–11.

Sorensen, I.; Domozych, D.; Willats, W. G. T., 2010: How Have Plant Cell Walls Evolved? *Plant Physiology*., **153**, 366–372.

Sozzani, R.; Iyer-Pascuzzi, A., 2014: Postembryonic control of root meristem growth and development. *Current Opinion in Plant Biology*., **17**, 7–12.

Stahl, Y.; Wink, R. H.; Ingram, G. C.; Simon, R., 2009: A Signaling Module Controlling the Stem Cell

Niche in Arabidopsis Root Meristems. *Current Biology*., **19**, 909–914.

Stahl, Y.; Grabowski, S.; Bleckmann, A.; Kühnemuth, R.; Weidtkamp-Peters, S.; Pinto, K. G.; Kirschner, G. K.; Schmid, J. B.; Wink, R. H.; Hülsewede, A.; Felekyan, S.; Seidel, C. A. M.; Simon, R., 2013: Moderation of Arabidopsis Root Stemness by CLAVATA1 and ARABIDOPSIS CRINKLY4 Receptor Kinase Complexes. *Current Biology*., **23**, 362–371.

Stegmann, M.; Monaghan, J.; Smakowska-Luzan, E.; Rovenich, H.; Lehner, A.; Holton, N.; Belkhadir, Y.; Zipfel, C., 2017: The receptor kinase FER is a RALF-regulated scaffold controlling plant immune signaling. *Science*., **355**, 287–289.

Stepanova, A. N.; Robertson-Hoyt, J.; Yun, J.; Benavente, L. M.; Xie, D. Y.; Doležal, K.; Schlereth, A.; Jürgens, G.; Alonso, J. M., 2008: TAA1-Mediated Auxin Biosynthesis Is Essential for Hormone Crosstalk and Plant Development. *Cell*., **133**, 177–191.

Stock, A. M.; Robinson, V. L.; Goudreau, P. N., 2000: Two-Component Signal Transduction. *Annual Review of Plant Biology*., **69**, 183–215.

Strabala, T. J., 2006: Gain-of-Function Phenotypes of Many CLAVATA3/ESR Genes, Including Four New Family Members, Correlate with Tandem Variations in the Conserved CLAVATA3/ESR Domain. *PLANT PHYSIOLOGY*., **140**, 1331–1344.

Stracke, S.; Kistner, C.; Yoshida, S.; Mulder, L.; Sato, S.; Kaneko, T.; Tabata, S.; Sandal, N.; Stougaard, J.; Szczyglowski, K.; Parniske, M., 2002: A plant receptor-like kinase required for both bacterial and fungal symbiosis. *Nature*., **417**, 959–962.

Sun, B.; Xu, Y.; Ng, K. H.; Ito, T., 2009: A timing mechanism for stem cell maintenance and differentiation in the Arabidopsis floral meristem. *Genes & development*., **23**, 1791–1804.

Takahashi, F.; Suzuki, T.; Osakabe, Y.; Betsuyaku, S.; Kondo, Y.; Dohmae, N.; Fukuda, H.; Yamaguchi-shinozaki, K.; Shinozaki, K., 2018: Abscisic Acid in Long-Distance Signalling. *Nature*., **25**.

Takahashi, K.; Hayashi, K. i.; Kinoshita, T., 2012: Auxin Activates the Plasma Membrane H+-ATPase by Phosphorylation during Hypocotyl Elongation in Arabidopsis. *Plant Physiology*., **159**, 632–641.

Taylor-Teeples, M.; Lin, L.; De Lucas, M.; Turco, G.; Toal, T. W.; Gaudinier, A.; Young, N. F.; Trabucco, G. M.; Veling, M. T.; Lamothe, R.; Handakumbura, P. P.; Xiong, G.; Wang, C.; Corwin, J.; Tsoukalas, A.; Zhang, L.; Ware, D.; Pauly, M.; Kliebenstein, D. J. et al., 2015: An Arabidopsis gene regulatory network for secondary cell wall synthesis. *Nature*., **517**, 571–575.

Thomson, B.; Zheng, B.; Wellmer, F., 2016: Floral Organogenesis: When Knowing Your ABCs Is Not Enough. *Plant Physiology*., **173**, 56–64.

Tian, H.; Niu, T.; Yu, Q.; Quan, T.; Ding, Z., 2013: Auxin gradient is crucial for the maintenance of root distal stem cell identity in Arabidopsis. *Plant Signaling and Behavior*., **8**, 8–10.

Tonn, N.; Greb, T., 2017: Radial plant growth. *Current Biology*., **27**, R878–R882.

Tör, M.; Lotze, M. T.; Holton, N., 2009: Receptor-mediated signalling in plants: Molecular patterns and programmes. *Journal of Experimental Botany*., **60**, 3645–3654.

Tucker, M. R.; Roodbarkelari, F.; Truernit, E.; Adamski, N. M.; Hinze, A.; Lohmüller, B.; Würschum, T.; Laux, T., 2013: Accession-specific modifiers act with ZWILLE/ARGONAUTE10 to maintain shoot meristem stem cells during embryogenesis in Arabidopsis. *BMC Genomics*., **14**, 809.

Uchida, N.; Shimada, M.; Tasaka, M., 2013: ERECTA-family receptor kinases regulate stem cell homeostasis via buffering its cytokinin responsiveness in the shoot apical meristem. *Plant and Cell Physiology*., **54**, 343–351.

van den Berg, C.; Willemsen, V.; Hage, W.; Weisbeek, P.; Scheres, B., 1995: Cell fate in the Arabidopsis root meristem determined by directional signalling. *Nature*., **378**, 62–65.

Van Holle, S.; Van Damme, E. J. M., 2019: Messages From the Past: New Insights in Plant Lectin Evolution. *Frontiers in Plant Science*., **10**, 1–14.

Vernoud, V.; Horton, A. C.; Yang, Z.; Nielsen, E., 2003: Analysis of the Small GTPase Gene Superfamily of Arabidopsis. *PLANT PHYSIOLOGY*., **131**, 1191–1208.

Vernoux, T.; Besnard, F.; Traas, J., 2010: Auxin at the shoot apical meristem. *Cold Spring Harbor perspectives in biology*., **2**, 1–14.

Waaland, S. D.; Waaland, J. R., 1975: Analysis of cell elongation in red algae by fluorescent labelling. *Planta*., **126**, 127–138.

Wachsman, G.; Sparks, E. E.; Benfey, P. N., 2015: Genes and networks regulating root anatomy and architecture. *New Phytologist*., **208**, 26–38.

Wang, G.; Ellendorff, U.; Kemp, B.; Mansfield, J. W.; Forsyth, A.; Mitchell, K.; Zipfel, C.; Wit, P. J. G. M. De; Bastas, K.; Liu, C. ming; Woods-to, A., 2008: A Genome-Wide Functional Investigation into the Roles of Receptor-Like Proteins in Arabidopsis 1 [W][OA], **147**, 503–517.

Wang, G.; Fiers, M., 2010: Receptor-like proteins, **5**, 540–542.

Wang, G.; Zhang, G.; Wu, M., 2016: CLE Peptide Signaling and Crosstalk with Phytohormones and Environmental Stimuli. *Frontiers in Plant Science*., **6**, 1–7.

Wang, M.; Yuan, D.; Gao, W.; Li, Y.; Tan, J.; Zhang, X., 2013: A Comparative Genome Analysis of PME and PMEI Families Reveals the Evolution of Pectin Metabolism in Plant Cell Walls. (Zabotina, O. A., Ed.)*PLoS ONE*., **8**, e72082.

Wang, Z. P.; Xing, H. L.; Dong, L.; Zhang, H. Y.; Han, C. Y.; Wang, X. C.; Chen, Q. J., 2015: Egg cell-specific promoter-controlled CRISPR/Cas9 efficiently generates homozygous mutants for multiple target genes in Arabidopsis in a single generation. *Genome Biology*., **16**, 1–12.

Weijers, D.; Wagner, D., 2016: Transcriptional Responses to the Auxin Hormone. *Annual Review of Plant Biology*., **67**, 539–574.

Werner, T., 2003: Cytokinin-Deficient Transgenic Arabidopsis Plants Show Multiple Developmental Alterations Indicating Opposite Functions of Cytokinins in the Regulation of Shoot and Root Meristem Activity. *THE PLANT CELL ONLINE*., **15**, 2532–2550.

Willats, W. G. T.; Orfila, C.; Limberg, G.; Buchholt, H. C.; van Alebeek, G. J. W. M.; Voragen, A. G. J.; Marcus, S. E.; Christensen, T. M. I. E.; Mikkelsen, J. D.; Murray, B. S.; Knox, J. P., 2001: Modulation of the Degree and Pattern of Methyl-esterification of Pectic Homogalacturonan in Plant Cell Walls. *Journal of Biological Chemistry*., **276**, 19404–19413.

Williams, L.; Grigg, S.; Xie, M.; Christensen, S.; Fletcher, J. C., 2005: Regulation of Arabidopsis shoot apical meristem and lateral organ formation by microRNA miR166g and its AtHD-ZIP target genes. *Development*., **132**, 3657–3668.

Winter, C. M.; Austin, R. S.; Blanvillain-Baufumé, S.; Reback, M. A.; Monniaux, M.; Wu, M. F.; Sang, Y.; Yamaguchi, A.; Yamaguchi, N.; Parker, J. E.; Parcy, F.; Jensen, S. T.; Li, H.; Wagner, D., 2011: LEAFY Target Genes Reveal Floral Regulatory Logic, cis Motifs, and a Link to Biotic Stimulus Response. *Developmental Cell*., **20**, 430–443.

Wolf, S.; Mouille, G.; Pelloux, J., 2009a: Homogalacturonan Methyl-Esterification and Plant Development. *Molecular Plant*., **2**, 851–860.

Wolf, S.; Rausch, T.; Greiner, S., 2009b: The N-terminal pro region mediates retention of unprocessed type-I PME in the Golgi apparatus. *The Plant Journal*., **58**, 361–375.

Wolf, S.; Mravec, J.; Greiner, S.; Mouille, G.; Höfte, H., 2012a: Plant Cell Wall Homeostasis Is Mediated by Brassinosteroid Feedback Signaling. *Current Biology*., **22**, 1732–1737.

Wolf, S.; Hématy, K.; Höfte, H., 2012b: Growth Control and Cell Wall Signaling in Plants. *Annual Review of Plant Biology*., **63**, 381–407.

Wolf, S.; Greiner, S., 2012c: Growth control by cell wall pectins. *Protoplasma*., **249**, 169–175.

Wolf, S.; Hofte, H., 2014a: Growth Control: A Saga of Cell Walls, ROS, and Peptide Receptors. *The Plant Cell*., **26**, 1848–1856.

Wolf, S.; van der Does, D.; Ladwig, F.; Sticht, C.; Kolbeck, A.; Schürholz, A. K.; Augustin, S.; Keinath, N.; Rausch, T.; Greiner, S.; Schumacher, K.; Harter, K.; Zipfel, C.; Höfte, H., 2014b: A receptor-like protein mediates the response to pectin modification by activating brassinosteroid signaling. *Proceedings of the National Academy of Sciences*., **111**, 15261–15266.

Wolf, S.; van der Does, D.; Ladwig, F.; Sticht, C.; Kolbeck, A.; Schürholz, A. K.; Augustin, S.; Keinath, N.; Rausch, T.; Greiner, S.; Schumacher, K.; Harter, K.; Zipfel, C.; Höfte, H., 2014c: A receptor-like protein mediates the response to pectin modification by activating brassinosteroid signaling. *Proceedings of the National Academy of Sciences*., **111**, 15261–15266.

Wolf, S., 2017: Plant cell wall signalling and receptor-like kinases. *Biochemical Journal*., **474**, 471–492.

Wu, S. J.; Ding, L.; Zhu ' ', J. K., 1996: SOS1, a Genetic Locus Essential for Salt Tolerance and Potassi u m Acq u isi t ío n. *The Plant Cell American Society of Plant Physiologists*., **8**, 617–627.

Xiao, C.; Zhang, T.; Zheng, Y.; Cosgrove, D. J.; Anderson, C. T., 2016: Xyloglucan Deficiency Disrupts Microtubule Stability and Cellulose Biosynthesis in Arabidopsis, Altering Cell Growth and Morphogenesis. *Plant Physiology*., **170**, 234–249.

Xie, M.; Chen, H.; Huang, L.; O'Neil, R. C.; Shokhirev, M. N.; Ecker, J. R., 2018: A B-ARR-mediated

cytokinin transcriptional network directs hormone cross-regulation and shoot development. *Nature Communications*., **9**, 1–13.

Xing, H. L.; Dong, L.; Wang, Z. P.; Zhang, H. Y.; Han, C. Y.; Liu, B.; Wang, X. C.; Chen, Q. J., 2014: A CRISPR/Cas9 toolkit for multiplex genome editing in plants. *BMC Plant Biology*., **14**, 1–12.

Xue, T.; Dai, X.; Wang, R.; Wang, J.; Liu, Z.; Xiang, F., 2017: ARGONAUTE10 inhibits in vitro shoot regeneration via repression of miR165/166 in arabidopsis thaliana. *Plant and Cell Physiology*., **58**, 1789–1800.

Yadav, R. K.; Girke, T.; Pasala, S.; Xie, M.; Reddy, G. V., 2009a: Gene expression map of the Arabidopsis shoot apical meristem stem cell niche. *Proceedings of the National Academy of Sciences*., **106**, 4941–4946.

Yadav, R. K.; Perales, M.; Gruel, J.; Girke, T.; Jönsson, H.; Venugopala Reddy, G., 2011: WUSCHEL protein movement mediates stem cell homeostasis in the Arabidopsis shoot apex. *Genes and Development*., **25**, 2025–2030.

Yadav, R. K.; Perales, M.; Gruel, J.; Ohno, C.; Heisler, M.; Girke, T.; Jönsson, H.; Venugopala Reddy, G., 2013: Plant stem cell maintenance involves direct transcriptional repression of differentiation program. *Molecular Systems Biology*., **9**, 654.

Yadav, R. K.; Tavakkoli, M.; Xie, M.; Girke, T.; Reddy, G. V., 2014: A high-resolution gene expression map of the Arabidopsis shoot meristem stem cell niche, **17**, 2735–2744.

Yadav, S.; Yadav, P. K.; Yadav, D.; Yadav, K. D. S., 2009b: Pectin lyase: A review. *Process Biochemistry*., **44**, 1–10.

Yamaguchi, M.; Mitsuda, N.; Ohtani, M.; Ohme-Takagi, M.; Kato, K.; Demura, T., 2011: VASCULAR-RELATED NAC-DOMAIN 7 directly regulates the expression of a broad range of genes for xylem vessel formation. *Plant Journal*., **66**, 579–590.

Yamaguchi, Y. L.; Ishida, T.; Sawa, S., 2016: CLE peptides and their signaling pathways in plant development. *Journal of Experimental Botany*., **67**, 4813–4826.

Yamaguchi, Y. L.; Ishida, T.; Yoshimura, M.; Imamura, Y.; Shimaoka, C.; Sawa, S., 2017: A Collection of Mutants for CLE-Peptide-Encoding Genes in Arabidopsis Generated by CRISPR/Cas9-Mediated Gene Targeting. *Plant and Cell Physiology*., **58**, 1848–1856.

Yang, W.; Schuster, C.; Beahan, C. T. T.; Charoensawan, V.; Peaucelle, A.; Bacic, A.; Doblin, M. S. S.; Wightman, R.; Meyerowitz, E. M. M., 2016: Regulation of Meristem Morphogenesis by Cell Wall Synthases in Arabidopsis. *Current Biology*., **26**, 1404–1415.

Yang, Y.; Hammes, U. Z.; Taylor, C. G.; Schachtman, D. P.; Nielsen, E., 2006: High-Affinity Auxin Transport by the AUX1 Influx Carrier Protein. *Current Biology*., **16**, 1123–1127.

Zabotina, O. A.; Avci, U.; Cavalier, D.; Pattathil, S.; Chou, Y. H.; Eberhard, S.; Danhof, L.; Keegstra, K.; Hahn, M. G., 2012: Mutations in Multiple XXT Genes of Arabidopsis Reveal the Complexity of Xyloglucan Biosynthesis. *Plant Physiology*., **159**, 1367–1384.

Zamil, M. S.; Geitmann, A., 2017: The middle lamella - More than a glue. *Physical Biology*., **14**, 015004.

Zhang, K.; Novak, O.; Wei, Z.; Gou, M.; Zhang, X.; Yu, Y.; Yang, H.; Cai, Y.; Strnad, M.; Liu, C. J., 2014: Arabidopsis ABCG14 protein controls the acropetal translocation of root-synthesized cytokinins. *Nature communications*., **5**, 3274.

Zhang, Q.; Xing, H. L.; Wang, Z. P.; Zhang, H. Y.; Yang, F.; Wang, X. C.; Chen, Q. J., 2018: Potential high-frequency off-target mutagenesis induced by CRISPR/Cas9 in Arabidopsis and its prevention. *Plant Molecular Biology*., **96**, 445–456.

Zhao, C.; Zayed, O.; Yu, Z.; Jiang, W.; Zhu, P.; Hsu, C. C.; Zhang, L.; Tao, W. A.; Lozano-Durán, R.; Zhu, J. K., 2018: Leucine-rich repeat extensin proteins regulate plant salt tolerance in Arabidopsis. *Proceedings of the National Academy of Sciences*., **115**, 13123–13128.

Zhou, J.; Wang, X.; Lee, J. Y.; Lee, J. Y., 2013: Cell-to-Cell Movement of Two Interacting AT-Hook Factors in Arabidopsis Root Vascular Tissue Patterning . *The Plant Cell*., **25**, 187–201.

Zhou, Y.; Honda, M.; Zhu, H.; Zhang, Z.; Guo, X.; Li, T.; Li, Z.; Peng, X.; Nakajima, K.; Duan, L.; Zhang, X., 2015: Spatiotemporal Sequestration of miR165/166 by Arabidopsis Argonaute10 Promotes Shoot Apical Meristem Maintenance. *Cell Reports*., **10**, 1819–1827.

Zhu, X. F.; Sun, Y.; Zhang, B. C.; Mansoori, N.; Wan, J. X.; Liu, Y.; Wang, Z. W.; Shi, Y. Z.; Zhou, Y. H.; Zheng, S. J., 2014: *TRICHOME BIREFRINGENCE-LIKE27* Affects Aluminum Sensitivity by Modulating the *O* -Acetylation of Xyloglucan and Aluminum-Binding Capacity in Arabidopsis. *Plant*

Physiology., **166**, 181–189.

Zipfel, C.; Kunze, G.; Chinchilla, D.; Caniard, A.; Jones, J. D. G.; Boller, T.; Felix, G., 2006: Perception of the Bacterial PAMP EF-Tu by the Receptor EFR Restricts Agrobacterium-Mediated Transformation. *Cell*., **125**, 749–760.

Zurcher, E.; Tavor-Deslex, D.; Lituiev, D.; Enkerli, K.; Tarr, P. T.; Muller, B., 2013: A Robust and Sensitive Synthetic Sensor to Monitor the Transcriptional Output of the Cytokinin Signaling Network in Planta. *PLANT PHYSIOLOGY*., **161**, 1066–1075.

List of abbreviations

aa	Amino acid
AACT1	Acetoacetyl-CoA Thiolase 1
AGO10/ZWILLE	ARGONAUTE10/ZWILLE
AHL	AT HOOK MOTIF NUCLEAR LOCALIZED
AHP6	ARABIDOPSIS HISTIDINE PHOSPHOTRANSFER PROTEIN 6
ARE	Auxin response element
ARF	Auxin response factor
ATHB-8	HOMEOBOX GENE8
BA	6-Benzylaminopurine
BAK1	BRI-ASSOCIATED KINASE 1
BAM	BARELY ANY MERISTEM
bp	Base pairs
BR	Brassinosteroid
BRI1	BRASSINOSTEROID RECEPTOR1
BZ	Boundary zone
CD	Cytoplasmic domain
CDS	Coding sequence
CESA	Cellulose synthase
ChIP	Chromatin immunoprecipitation
Col-0	Columbia-0
CK	Cytokinin
CNA	CORONA
CRISPR	Clustered regularly interspaced short palindromic repeats
CRN	CORYNE
CrRLK1L	Catharanthus roseus Receptor-like kinase1-like
CLE	CLAVATA3/ENDOSPERM-SURROUNDING (ESR)-RELATED
CLSM	Confocal laser scanning microscopy
CLV3	CLAVATA3
CPKs	Ca^{2+}-dependent kinase
CSC	Cellulose synthesis complex
CSC1	CLE SIGNALLING COMPONENT1
CUC2	CUP-SHAPED COTELYDON2
CWS	Cell wall signalling
CZ	Central zone
Dex	Dexamethasone
DMSO	Dimethyl sulfoxide
DNA	Deoxyribonucleic acid
ECD	Extracellular domain
FEA3	ARABIDOPSIS THALIANA FASCIATED EAR 3
FER	FERONIA
FM	Floral meristem
FIL	FILAMENTOUS FLOWER
GA	Giberrellic acid
gDNA	Genomic DNA
GO	Gene ontology
GOI	Gene of interest
GFP	Green fluorescent protein
GT	Glycosyltransferase
HG	Homogalacturonan
HMG	*HIGH MOBILITY GROUP*
JA	Jasmonic acid

KAN	KANADI
LAS	LATERAL SUPPRESSOR
L*er*	Landsberg *erecta*
LHW	LONESOME HIGHWAY
LOG4	LONELY GUY4
LRRs	Leucine rich repeats
LTI6b	LOW TEMPERATURE INDUCED PROTEIN 6B
M	Molar
MAPK	Mitogen-activated protein kinase
Mal	Malectin-like
MP	MONOPTEROS
MS	Murashige & Skroog
MT	Microtubule
NGS	Next-generation sequencing
NLS	Nuclear localization signal
OC	Organizing centre
OG	Oligogalacturonic acid
PAE	Pectin acetyl esterase
PCR	Polymerase chain reaction
PG	Poly galacturonase
PHB	PHABULOSA
PHV	PHAVOLUTA
PI	Propidium iodide
PL	Pectate lyase
PM	Plasma membrane
PME	Pectin methyl esterase
PMEI	Pectin methyl esterase inhibitor
PMEIox	PECTIN METHYL ESTERASE INHIBITOR5 over-expressing
PSK	Phytosulfokine
PSKR	Phytosulfokine receptor
PPB	Pre prophase band
pTS	Tissue specific promoter
PXY	PHLOEM INTERCALATED WITH XYLEM
PZ	Peripheral zone
QC	Quiescent centre
RALF	RAPID ALKALIZATION FACTOR1
RAM	Root apical meristem
REV	REVOLUTA
RGI/II	RhamnogalacturonanI/II
RLK	Receptor-like kinase
RLCK	Receptor-like cytoplasmic kinases
RLP	Receptor-like protein
RNA	Ribonucleic acid
R4L	RLP4-like
SAM	Shoot apical meristem
SBTs	Subtilisin-like serine protease
SCR	SCARECROW
SD	Standard deviation
SERK	SOMATIC EMBRYOGENESIS RECEPTOR-LIKE KINASE
SHR	SHORT ROOT
SNP	Single nucleotide polymorphism
T-DNA	Transfer DNA
TFs	Transcription factors
THE1	THESEUS1

TMD	Transmembrane domain
TMO5	TARGET OF MONOPTEROS5
UFO	UNUSUAL FLORAL ORGANS
UTR	Untranslated region
VGD1	VANGUARD1
VND	VASCULAR RELATED NAC DOMAIN
WAKs	WALL ASSOCIATED KINASE
WUS	WUSCHEL
XGA	Xylogalacturonan
X-Gluc	ß-Glucuronidase
XPP	XYLEM POLE PERICYCLE
YFP	Yellow fluorescent protein

Appendix

A1 Alignment of RLP4, R4L1, R4L2, R4L3 and CLV1: only on attached CD

A2 RNA-Seq data from *csc1*, significantly/non-significantly transcripts: only on attached CD

A3 eFP Browser data for RLP4

A4 eFP Browser data for R4L1

A5 eFP Browser data for R4L2

A6 eFP Browser data for R4L3

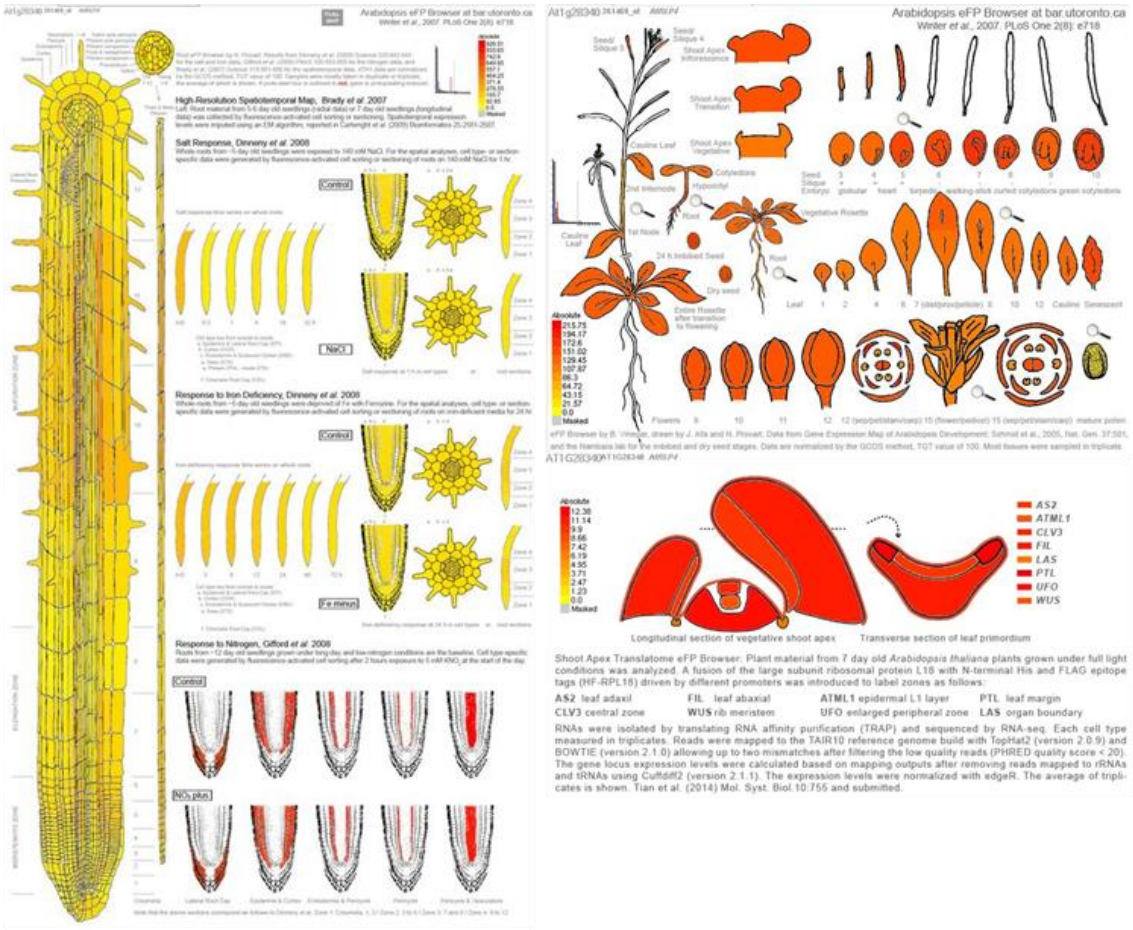

A3. Expression of RLP4 (AT1G28340) in Arabidopsis, eFP Browser data.

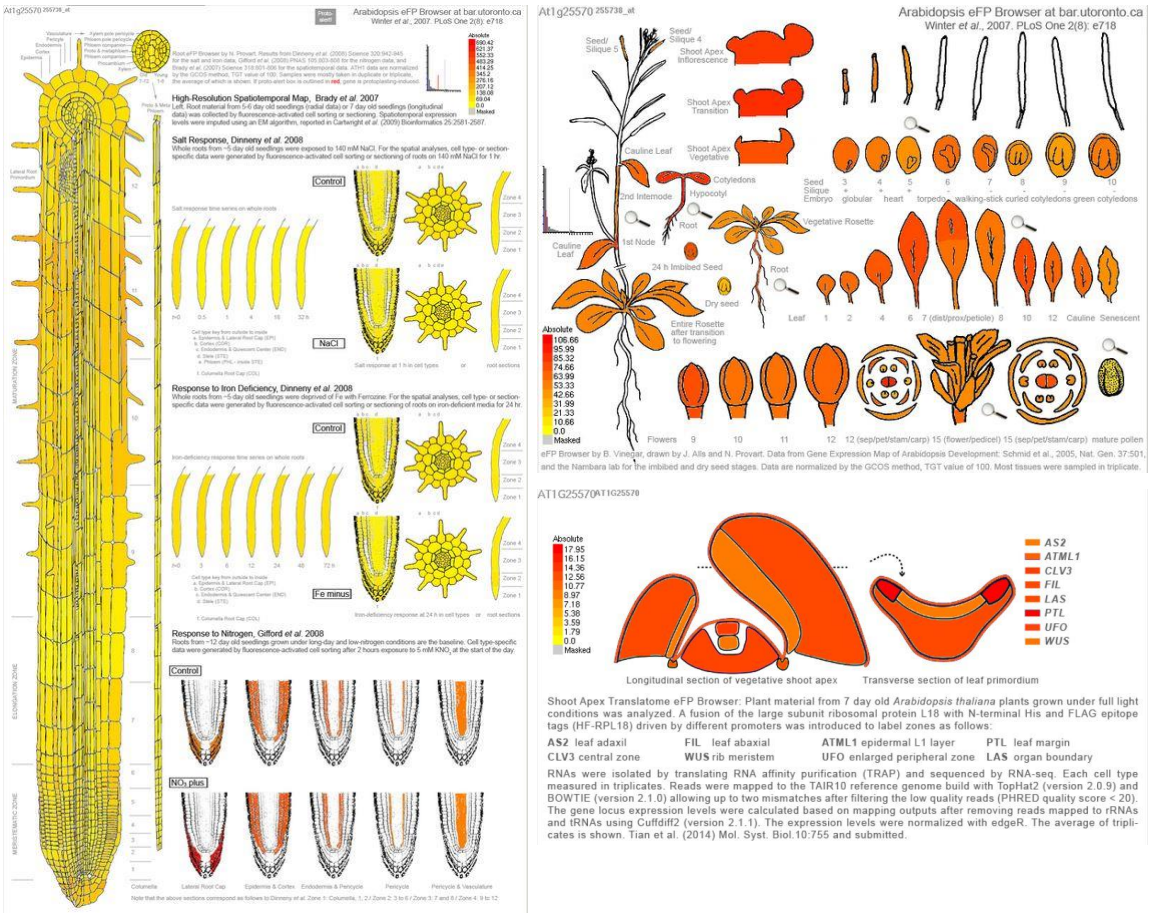

A4. Expression of R4L1 (AT1G25570) in Arabidopsis, eFP Browser data.

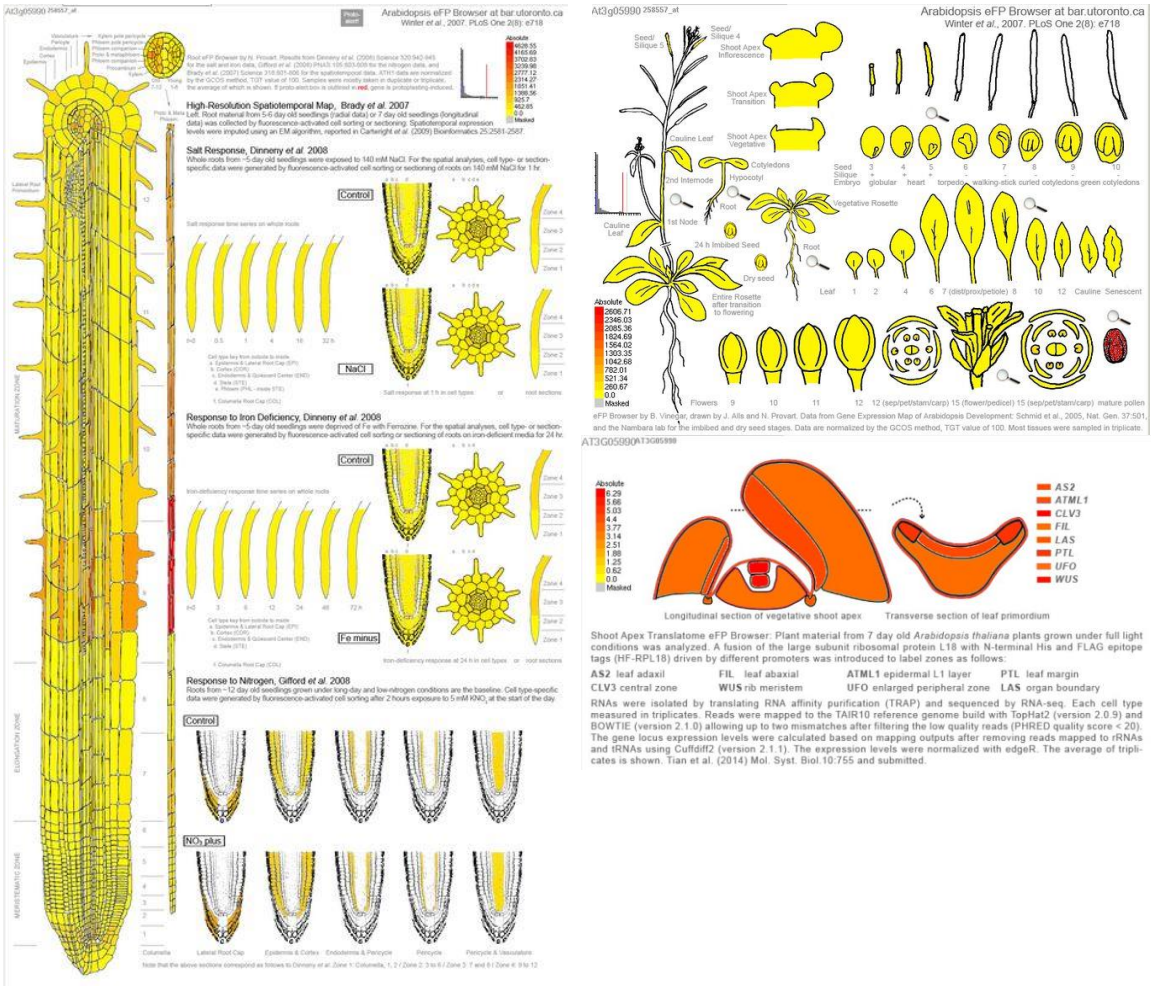

Shoot Apex Translatome eFP Browser: Plant material from 7 day old *Arabidopsis thaliana* plants grown under full light conditions was analyzed. A fusion of the large subunit ribosomal protein L18 with N-terminal His and FLAG epitope tags (HF-RPL18) driven by different promoters was introduced to label zones as follows:

AS2 leaf adaxil **FIL** leaf abaxial **ATML1** epidermal L1 layer **PTL** leaf margin
CLV3 central zone **WUS** rib meristem **UFO** enlarged peripheral zone **LAS** organ boundary

RNAs were isolated by translating RNA affinity purification (TRAP) and sequenced by RNA-seq. Each cell type measured in triplicates. Reads were mapped to the TAIR10 reference genome build with TopHat2 (version 2.0.9) and BOWTIE (version 2.1.0) allowing up to two mismatches after filtering the low quality reads (PHRED quality score < 20). The gene locus expression levels were calculated based on mapping outputs after removing reads mapped to rRNAs and tRNAs using Cuffdiff2 (version 2.1.1). The expression levels were normalized with edgeR. The average of triplicates is shown. Tian et al. (2014) Mol. Syst. Biol.10:755 and submitted.

A5. Expression of R4L2 (AT3G05990) in Arabidopsis, eFP Browser data.

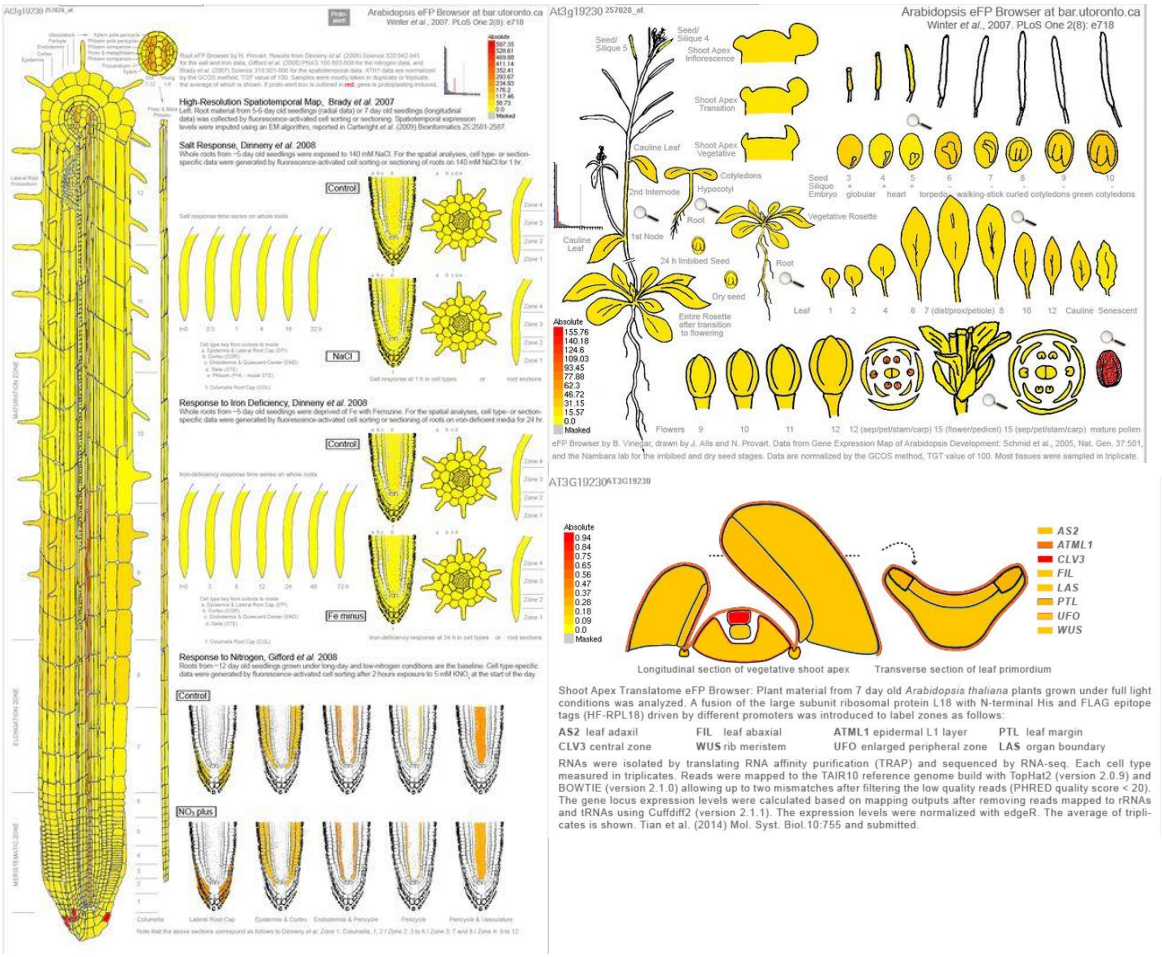

Shoot Apex Translatome eFP Browser: Plant material from 7 day old *Arabidopsis thaliana* plants grown under full light conditions was analyzed. A fusion of the large subunit ribosomal protein L18 with N-terminal His and FLAG epitope tags (HF-RPL18) driven by different promoters was introduced to label zones as follows:

AS2 leaf adaxil **FIL** leaf abaxial **ATML1** epidermal L1 layer **PTL** leaf margin
CLV3 central zone **WUS** rib meristem **UFO** enlarged peripheral zone **LAS** organ boundary

RNAs were isolated by translating RNA affinity purification (TRAP) and sequenced by RNA-seq. Each cell type measured in triplicates. Reads were mapped to the TAIR10 reference genome build with TopHat2 (version 2.0.9) and BOWTIE (version 2.1.0) allowing up to two mismatches after filtering the low quality reads (PHRED quality score < 20). The gene locus expression levels were calculated based on mapping outputs after removing reads mapped to rRNAs and tRNAs using Cuffdiff2 (version 2.1.1). The expression levels were normalized with edgeR. The average of triplicates is shown. Tian et al. (2014) Mol. Syst. Biol.10:755 and submitted.

A6. Expression of R4L3 (AT3G19230) in Arabidopsis, eFP Browser data.

Acknowledgments

First of all, I want to thank Dr. Sebastian Wolf. Since I have done my first lab rotation in your group, I knew I want to do my PhD here. Thanks Sebo, for giving me the opportunity to work on these interesting projects and always being supportive during all the years.

I would like to thank my PhD thesis committee members, Prof. Dr. Jan Lohmann, also for the great support as a TAC member, and Prof. Dr. Steffen Lemke and Dr. Michael Raissig. Many thanks also to Prof. Dr. Karin Schumacher and Prof. Dr. Thomas Greb, for their helpful scientifc discussions and advices in my TAC meetings.

Special thanks to Prof. Dr. Rüdiger Hell on behalf of the Schmeil Stiftung, for supporting me with the “PhD Completion Scholarship”.

After almost ten great years in Heidelberg, it’s time to say goodbye. The last years would not have been the same without all the people I met during the journey from bachelor student to (hopefully) PhD. Thanks to the whole Wolf group, the “wolvies”, being the best colleagues I could imagine. Eli, Paola, John, Hannah and all the students that joined our group during the last years. I want to thank my practical students Nabila, Enric and Dan, you helped me with my project and turned supervising to a great experience for me. My biggest thanks goes to the “core Wolvies” Eli, Zhenni and Borja. I will always remember the fun we had in the lab, the office, at beer hours, our retreat and also in rough times - frustration killer was always helpful ;).

Eli, I want to thank you for always being a helping hand, and being the base for the whole group and always being up for having fun.

Zhenni, my Chinese tomato, I want to thank you for all the years and great moments we shared together during my Master and PhD. Thanks to you I got to know the chinese culture better and fell in love with Chinese food.

Borja, mi guapo, since the beginning of my Master thesis I appreciated you as a great colleague and I’m happy to say that you are one of my best friends I found during my time in Heidelberg. When you left, you left a hole in our group … drama, crazy singing and dance choreographies, our sport sessions, concerts, and happiness bubbles. I’m missing all of that. Thanks for all these awesome memories and your support during the last weeks!

Zaida, mi guapa, many thanks for having you as a great colleague, but especially as an awesome friend. In the last years we shared so many great times together and I’m looking forward to more concerts, gossiping, fun, mud runs and game nights!

Andrea, my architect partner, together we created bombastic COS parties! Thanks for all the fun and craziness we shared together, exhausting discussions in the Spanish-Italian way, delicious Italian food and distracting me from lab life.

Raina, thanks a lot for your always open ear and your scientific support with improving cloning protocols, … and scientific discussions. I will miss our mornings walks to the lab and your valuable and open feedback.

Thanks Vadir, for your help in the lab and having you as an amazing colleague in the last years, together we rocked the “Driver line” paper! I’m happy that you are still “around” COS for interesting conversations about science and life outside of science.

Nina and Jana, thanks for the always welcomed coffee breaks and discussions about life.

Many thanks to the whole second floor for the nice working environment. Thanks to Barbara, Beate and Fabian, who took care of the lab basics, Melanie, for controlling and managing the lab and Ines, for all the paper work.

I want to thank the rest of the colleagues from the Maizel, Schumacher, Greb and Lohmann group and COS. Special thanks to Upendo, Paula, Amaya, Theresa, Jazmin, Paula, Zhaoxue, Rachel, Alyona, Michi, Christian, Denis, Christophe, Yanfei and Jiyan for all the scientific and non-scientific discussions. Many thanks to Christian who introduced me to the “SAM universe” with fancy microscopes and software.

Not to forget, the colleagues from 360 and AG Rausch. I started my first lab rotation as a Master student in your group and I think it was the best start I could have. Thanks to Thomas, Heike, Conny, Tanja, Katja, Angelika, Roland and Steffen for this great start and also the support during the last years.

Lea, Anikó, Robin, Lucas and Christian, we all got to know in the first semester of the bachelor studies and we stayed until the end. Thanks for your friendship and the awesome moments we had during our studies and beyond.

I want to thank my friends from school, that always reminded me of the good old school times and that life out of science exists ;)

Thanks to all the people who helped me proofreading my thesis.

In the end, I want to thank my family, my mom Birgit, Werner, my brother Max and “Öpp und Ömm”. They always believe in me and support me in fulfilling my goals. Thanks for everything! Special thanks to my boyfriend Andreas, who supported me during my studies/PhD and often had to step back for science.